3D Reconstruction and Modelling of the *Sierras Exteriores Aragonesas* (Southern Pyrenees, Spain)

Structural Evolution of the *Pico del Águila* anticline

Oskar Vidal Royo

GGAC
Grup de Geodinàmica i Anàlisi de Conques

UNIVERSITAT DE BARCELONA

geomodels
centre mixt d'investigació

3D Reconstruction and Modelling of the Sierras Exteriores Aragonesas (Southern Pyrenees, Spain): *Structural evolution of the Pico del Águila anticline*

Oskar Vidal Royo

Memòria de Tesi Doctoral
Abril de 2010

Institut de Recerca Geomodels
Grup de Recerca Consolidat de Geodinàmica i Anàlisi de Conques
Departament de Geodinàmica i Geofísica
Universitat de Barcelona

Institut de Recerca Geomodels
Grup de Recerca Consolidat de Geodinàmica i Anàlisi de Conques
Departament de Geodinàmica i Geofísica
Universitat de Barcelona

3D RECONSTRUCTION AND MODELLING OF THE SIERRAS EXTERIORES ARAGONESAS (SOUTHERN PYRENEES, SPAIN)

Structural Evolution of the Pico del Águila anticline

Memòria presentada per l'Oskar Vidal Royo per optar al grau de Doctor en Geologia. Aquesta memòria ha estat realitzada dins del Programa de Doctorat d'Exploració, Anàlisi i Modelització de Conques i Sistemes Orogènics (Bienni 2005-2006) i sota la direcció del Dr. Josep Anton Muñoz de la Fuente i del Dr. Stuart Hardy

Oskar Vidal Royo

Barcelona, Abril de 2010

Dr. Josep Anton Muñoz de la Fuente

Dr. Stuart Hardy

La recerca presentada en aquesta tesi s'ha realitzat en el si del Grup de Geodinàmica i Anàlisi de Conques de la Universitat de Barcelona (Grup de Recerca Consolidat reconegut per la Generalitat de Catalunya; referències 2005SGR-000397 i 2009SGR-1198) i l'Institut de Recerca Geomodels (finançat per la Generalitat de Catalunya, el Instituto Geológico y Minero de España i altres empreses privades de l'àmbit nacional i internacional). Així mateix, aquesta tesi ha estat recolzada econòmicament per l'Agència de Gestió d'Ajuts Universitaris i de Recerca (AGAUR) de la Generalitat de Catalunya, mitjançant una beca predoctoral per a la formació de investigadors (FI, referència 2005FI-00200) i tres beques per a estades curtes en centres d'investigació estrangers (beques BE, referència 2005 BE 00071, a l'Université de Rennes 1 de França, referència 2006 BE-2 00095, a la Uppsala Universitet de Suècia, i referència 2008 BE1 00348, a la Universitetet i Bergen de Noruega). Els treballs d'investigació s'emmarquen dins dels projectes nacionals *CONSTRUCCIÓN DE MODELOS ESTRUCTURALES 3D* (CGL2004-05816-C02-01) i *MODELIZACIÓN ESTRUCTURAL 4D* (CGL2007-66431-C02-01) i internacional *4D MODELLING BASED ON FIELD DESCRIPTIONS* (StatoilHydro). Agraïm a Midland Valley Exploration, Paradigm i IGEOSS per proveir llicències acadèmiques dels softwares emprats per la realització dels treballs presentats.

Al Josep Maria i la Mari Carmen, els meus pares,
per tants anys d'esforç incondicional

“Se me antojó un milagro que aparecieras ante mis ojos como un espejismo de piedra imbatible que no pide paso ni permiso para ocupar su lugar, para presidir el valle. Creí que te habrías disuelto, y te encontré resistiendo en soledad el envite del tiempo, manteniéndote terca, insolente y melancólica. Te comprendo, sé lo que significa sobrevivir al naufragio, que todos los que supieron de tus gozos y de tus penas ya no estén, y que solamente quedes tú para recordarlos...que alegría encontrarte.

Aún me parece ver a Mosen Martín llegando tarde a oficiar misa, y saliendo de ella con un trago de más, ¡como corríamos los zagales tras él y su mula parda, esperando verle caer! Y que inviernos más duros pasamos ¿verdad? Recuerdo como mi madre me sentaba en sus rodillas al calor del fogaril mientras me explicaba la imposible historia de amor entre Gratal y la dulce Gabardiella…cómo nos ardía el corazón al verlos reverdecer en primavera.

¿Y qué me cuentas de Herminia? Ella sí que nos hacía soñar... Seguro que la recuerdas, paseando por tus calles, inundándolas de ese olor a tierra húmeda que brotaba de sus cabellos, adornando las ventanas y las puertas de tus casas con su risa...yo la recuerdo cada día. Ella como todos fue a buscar otro porvenir ¿no es cierto? Dos vueltas de llave y nunca más supiste de ella... Yo tampoco, y tenía tantas cosas que decirle.

Ahora ya es tarde. Ella marchó y yo estoy viejo y cansado. No me queda más que mirarme en ti como en un espejo... mi vieja aldea, mi Lúsera…”

Y el viento silba entre las piedras, arrastrando desde otro tiempo las canciones de antaño en la voz fresca de la bella Herminia.

Agraïments / Agradecimientos / Acknowledgements

Després de tots aquests anys de treball a la Tesi sembla que això arriba al final, i cal fer un petita aturada per pensar en tot el que ha passat durant aquests últims cinc anys, en les persones que he conegut, i en les moltíssimes coses que he après i viscut gràcies a elles. Tot i que n'hi ha hagut de tots colors al llarg d'aquest temps, per mi aquest és l'apartat més agraït i emotiu d'escriure; és una forma de resumir part de les vivències que he passat durant aquesta etapa *pre-doctoral*. Moltes persones (i molts moments) em venen al cap, a les quals els hi dec un sentiment honest de gratitud que vull expressar en aqueste línies.

En primer lloc vull agrair tot l'enorme esforç, temps, dedicació i falta d'hores de son a una persona sense la qual aquesta Tesi mai hagués pogut veure la llum: jo mateix. Així doncs, gràcies Oskar.

Òbviament els meus directors de Tesi, el Josep Anton i l'Stuart, amb els que he après una enorme quantitat de coses molt més enllà de la geologia. Als dos els hi he d'agrair moltes coses, les discussions dels projectes, les revisions dels articles, la visió de la ciència i de la vida, i el més important: totes les coses que he après com a *científic* i persona mentre ells parlaven sense ser conscients de que en aquell moment també m'estaven formant. Del Josep Anton el gran coneixement que té de Pirineus i la geologia estructural (realment sembla que no té fi), la capacitat de trobar la millor solució i de donar serenor en moments d'estrés màxim, el saber posar-se en la pell de l'altre i poder comprendre'l i el donar-me total llibertat i confiança per fer les coses a la meva manera, sense qüestionar-ho. Del Stuart l'eficiència en el treball, aquest sentit de l'humor tan profundament sarcàstic amb el que tant he rigut, l'aprendre a no necessitar tres línies per escriure el que es pot dir en només una, la total llibertat i confiança en el meu treball, i la bellesa de corregir un article o discutir un projecte més enllà de les fronteres de la facultat. Per aquestes i tantes altres coses, moltíssimes gràcies!

Per descartat a tots els meus companys i amics del departament i de la facultat al llarg d'aquests anys, alguns dels quals ja han marxat a treballar a altres llocs però que segueixen estant igual de presents. És la infinitiat de moments que dóna el dia a dia la que em ve al cap, amb moments bons, dolents, de nervis, de relax, pero sobretot de riure, molt riure: a la hora dels cafès, els esmorzars, les calçotades, les paelles, les kartingades, les hores intempestives al Departament, els viatges i els congressos. També per donar-me suport i ajuda quan ho he necessitat, per fer que les coses fossin més fàcils, i per ajudar-me sense rebre res a canvi, per les discussions científiques, pseudo-científiques, in-científiques i anti-científiques. Per les *coffee & beer meeting sessions*, les bajanades dites, i les que queden per dir. Tot aquest trajecte ha estat ple de moments únics gràcies a ells i elles. El Marc Rubinat, el Jordi Bausà, l'Oriol Ferrer, l'Oriol Rosell, la Pati Cabello, la Ximena Moreno, el Daniel Bello, el Miki Marín, l'Óscar Gratacós, l'Àlex Amilibia, la Gemma Labraña, el Marco Snidero, la Joana Mencos, el Pau Arbués, l'Ana Carmona, l'Stefano Tavani, la Ylènia Almar, la Núria Carrera, el Bahman Soleimany, l'Angel Rodés, el Pablo Martínez, el Manoel Valcárcel, la Ruth Soto, la Teresa i la Bet Beamud (*the Beamud sisters*), la Berta López, el David Garcia Sellés, l'Oriol Falivene, l'Hector Perea, el Diego Iaffa, la Mireia Butillé, l'Anna Quintà, la Cristina Biete, l'Eduard Roca, el Juanjo Ledo i una llarga llista de persones que m'han acompanyat en algun moment del camí, per petit o curt que hagi estat. Sincerament, de veritat, moltíssimes gracies a tots/es vosaltres!

Als professors del departament que tant m'han ajudat al llarg d'aquests anys, i amb els que també he pogut gaudir de molts bons moments. Vull fer un agraïment especial tant al Francesc Sàbat com a la Pilar Queralt, directors del Departament en el moment en que jo vaig entrar-hi, i que em van donar la benvinguda i totes les facilitats necessàries per poder començar la meva formació *científica*.

I also wish to deeply thank to Professor Hemin Koyi the huge amount of things I learnt from and with him during my stay in the Hans Ramberg Tectonic Laboratory at Uppsala University. I have beautiful memories of my stay there, both in personal livings and working experiences. He has been, and still is, a reference scientist, professor and person in my short career. Also thanks to Zurab and Zuzanna, Faramarz and Osama for being there.

Many thanks also to Professor Jean Pierre Brun, who welcomed me at Géosciences Rennes in a very early stage of my research, and taught me many things about analogue modelling and encouraged me to go one step further. Thanks also to Xavier Fort for helping me in the analogue laboratory, and to all the friends I met there, who made my stay in Rennes an unforgettable experience.

I also wish to thank Dr Jan Tveranger for welcoming and helping me with my research at the Centre for Integrated Petroleum Researh of University of Bergen. Thanks also to the colleagues I met there.

Un gran muchas gracias es para Nestor Cardozo, quien se ocupó y preocupó de ayudarme y facilitarme mi estancia en Noruega, tanto en Bergen como en el Department of Petroleum Engineering de la University of Stavanger. Gracias a él me introduje en la restitución geomecánica y pude aprender muchas cosas tanto geológicas como personales. Gracias por todo el tiempo y la dedicación durante esos meses, y todos los meses que vinieron después cuando ya estaba de vuelta en Barcelona.

Por supuesto quiero también darles las gracias a mis amigos de toda la vida, justamente por eso, por estar ahí toda la vida. Por las risas, las cenas, el apoyo moral, y todo el tiempo que les debo y del que esta Tesis se ha apropiado en muchas ocasiones. Por ser personas tan importantes para mi, y por tenerlas mucho más presentes de lo que se piensan. A la familia Salida de Emergencia: a Roger, a Isaac, a Alfonso, por todo lo vivido y por todo lo que nos queda por vivir (este verano va a ser grande...). A Miquel y a los demás por las largas conversaciones alrededor de una cerveza en el Ceferino, una copa de vino, un vaso de zumo de melocotón, o un plato de Arroz tres delicias y Ternera en salsa de ostras del Mey-Mey, sobre la vida, la política, la música, y lo que saliera a colación.

Un enorme gracias va también para Miguel Ángel y el resto de los amigos y compañeros de Ta Ta For Now: Joan, Ian, Alex, Marc, y los miembros de la antigua formación con los que también he compartido buenos momentos. Muchas gracias a todos por darme la oportunidad de retomar algo de lo que jamás debería haberme alejado.

Un muchísimas gracias para mi familia, mis hermanos Jose, Virginia, Raul, Sandra y Javi, mis sobrinillos y sobrinilla Marco, Jan, Mario y Ainara, que son la alegría de la casa, y a los que también les debo mucho tiempo y muchos momentos que he dedicado a escribir este *capítulo* de mi vida. Espero a partir de ahora poder devolveros parte del tiempo que os debo, y poder empezar a disfrutar de vosotros de nuevo. Otro muchísimas gracias va también para mi tío y padrino, José Martín, que con tres décadas de experiencia docente en la universidad ha sabido entenderme y apoyarme a la perfección aun desde la distancia. Gracias también por ser un apoyo y referente para mi y una persona en la que puedo confiar a ciegas.

Un gracias muy especial para dos personas que para mi siguen y seguirán siendo pilares básicos de mi vida: mis padres. Realmente no soy capaz de imaginarme como hubiera sido todo sin su ayuda, comprensión, amor, abnegación y dedicación infinita. Realmente me supera con creces todo lo que les tengo que agradecer, y lo afortunado que me siento de haber tenido unos padres como ellos. Realmente sin ellos no seria yo. Porque también les he quitado, muy a mi pesar, muchos momentos que eran suyos y que he dedicado a un ritmo de vida ciclónico durante estos años. Porque realmente tengo ganas de poder volver a disfrutar de mi familia con tranquilidad, y de devolverles el tiempo que les pertenece. Muchas gracias de verdad, de corazón.

Finalmente otro gracias muy especial también para una persona que empezó y ha acabado la tesis conmigo, ironías de la vida, aunque no sea geóloga: Irene. Por aguantarme, ayudarme incondicionalmente, animarme y estar siempre de mi lado, apoyarme, pasar madrugadas enteras a mi lado ayudándome con la redacción de la tesis, tener esas manos de oro que han pintado el cuadro de la cubierta de la tesis, mimarme y estar a todas conmigo. Creo que tampoco podré agradecer lo suficiente toda su ayuda y comprensión, el tiempo y los mimos que le debo. Sin embargo, gracias infinitas.

Qué buena suerte he tenido. A tod@s, ¡muchísimas gracias!

CONTENTS

Index of Contents

RESUM EXTENS

Evolució estructural de l'anticlinal del Pico del Águila mitjançant modelització estructural 3D, analògica i numèrica

En aquest apartat es presenta un resum extens de la Tesi traduït al català, el qual recull les raons que motivaren la realització d'aquesta Tesi, els objectius establerts, l'estructura en la que s'organitza la memòria, la metodologia aplicada, els principals resultats i una discussió general sobre aquests. Finalment es presenten una llista de consideracions globals respecte els aspectes geològics i metodològics més rellevants, i diverses perspectives d'investigacions que s'han plantejat de portar a terme després de la finalització d'aquesta Tesi. Cal esmentar que el resum dels resultats i la discussió general presentats en aquest apartat han estat extrets del **Capítol V** d'aquesta memòria. Les consideracions finals i les perspectives d'avenç, en canvi, han estat extretes del **Capítol VI**.

R.1 SINOPSI

La present Tesi té com a finalitat elaborar un model conceptual unificat de l'evolució estructural de l'anticlinal del Pico del Águila (Sierras Exteriores Aragonesas, Pirineus Meridionals) a partir de la integració de diverses tècniques de modelització geològica. El Pico del Águila és un exemple ben conegut de plec de desenganxament, caracteritzat per una orientació N-S, paral·lela a la direcció de transport tectònic als Pirineus Meridionals.

S'ha construït un model tridimensional de l'estructural del Pico del Águila a partir de dades de camp i interpretació de perfils sísmics, posant de manifest els trets geomètrics de l'anticlinal, amb especial èmfasi en la interferència entre les estructures N-S i les E-W, així com en la geometria dels estrats de creixement.

En base a observacions de camp d'una distribució irregular del nivell basal de desenganxament es realitzaren una sèrie de models analògics que mostren com es poden generar estructures perpendiculars a l'orogen que poden finalment donar lloc a anticlinals perpendiculars a la tendència estructural general de la serralada.

Els models numèrics presentats investiguen l'efecte d'una estratigrafia mecànica complexa, caracteritzada per la intercalació de unitats amb marcades diferències de competència, així com el rol de la sedimentació sin-cinemàtica en el creixement d'un plec de desenganxament.

A partir del model 3D anteriorment esmentat es presenta també una restitució seqüencial geomecànica de l'estructura que suggereix la coexistència de múltiples mecanismes de plegament produint-se simultàniament en diferents unitats i dominis estructurals del plec. Aquesta superposició de mecanismes produeix una distribució complexa de la deformació que difícilment pot ser avaluada mitjançant models cinemàtics bidimensionals.

Integrant els models presentats amb dades prèvies de la regió, hom discuteix els beneficis i inconvenients de cadascuna de les tècniques de modelització i es presenta un model integrat d'evolució estructural de l'anticlinal del Pico del Águila, el qual ens permet una millor comprensió de l'estructura així com dels processos que menaren l'evolució dels plecs de desenganxament N-S de les Sierras Exteriores Aragonesas.

R.2 MOTIVACIÓ, OBJECTIUS I ORGANITZACIÓ DE LA TESI

R.2.1 MOTIVACIÓ

Una de les principals motivacions per realitzar aquesta Tesi va ser la d'investigar els mecanismes que governen la formació de plecs de desenganxament en 3D. A més, es disposava del que pot ser considerat un dels millors laboratoris naturals del planeta per estudiar la geologia estructural en contextos compressius: les Sierras Exteriores Aragonesas dels Pirineus Meridionals. La geologia de les Sierras Exteriores es caracteritza per trets ben particulars que després de dècades d'estudi segueixen sent objecte de treballs i discussions geològiques quant als processos que menaren la seva formació i evolució es refereix. En aquest sentit, els anticlinals N-S de les Sierras Exteriores tenen una gran rellevància geològica i requerien de noves metodologies d'estudi per abordar els aspectes que romanien (i alguns d'ells encara romanen) poc coneguts. Les excel·lents condicions d'aflorament, l'alt grau de preservació de les estructures i la fàcil accessibilitat van fer d'aquesta àrea el lloc adient per provar i aplicar les tècniques de reconstrucció estructural i modelització més noves desenvolupades en el si de l'Institut de Recerca Geomodels i del Grup de Geodinàmica i Anàlisi de Conques (GGAC-UB) de la Universitat de Barcelona. En aquest estadi primerenc de la memòria de Tesi es creu necessari reconèixer emfàticament el gran esforç, el treball dur i l'entusiasme de tot el personal del GGAC, en especial dels professors J.A Muñoz i Stuart Hardy, que van obrir camí en les tècniques de Modelització Estructural 4D i Modelització Mecànica d'estructures, de les quals aquesta Tesi se n'ha beneficiat en gran mesura. Es pot dir que aquesta tessitura inicial va ser un punt de partida prometedor que va constituir, per si mateix, una important motivació addicional.

Com s'ha dit, els processos que originaren els anticlinals N-S de les Sierras Exteriores són encara objecte d'estudi i discussió. L'estructura és complexa, i els mecanismes que hi van tenir lloc són múltiples i difícils d'abordar per mètodes senzills. Tanmateix, les Sierras Exteriores presenten immillorables facilitats per quant a grau d'exposició i accessibilitat es refereix. Això significa que els anticlinals N-S de les Sierras Exteriores, i en particular el

Pico del Águila, poden ser considerats exemples aflorants de primer ordre mundial de plecs de desenganxament. Per tant, una bona comprensió dels processos, mecanismes i paràmetres que van tenir lloc en l'evolució d'aquestes estructures conduirà a una millor comprensió sobre la formació i evolució d'estructures formades sota condicions similars en altres parts de la Terra, en les que la pobre qualitat de les dades o la difícil accessibilitat poden comprometre la veracitat dels resultats i portar a error en la interpretació dels trets geològics que caracteritzen l'estructura. A més, si aquestes estructures són altament preuades per contenir hidrocarburs o altres recursos naturals explotables comercialment, una bona comprensió de la seva geometria, evolució i trets característics pot tenir un gran impacte econòmic en termes d'exploració i producció dels possibles reservoris. Aquest podria ser el cas, per citar uns pocs exemples, dels cinturons de plecs i encavalcaments d'aigües profundes del Mississipi fan i Perdido (Mitra, 2002; Camerlo & Benson, 2006), o del cinturó de Papua Nova Guinea (Hill, 1991; Mitra, 2002), entre d'altres.

R.2.2 OBJECTIUS

La present Tesi se centra en investigar la generació, evolució estructural i relacions tecto-sedimentàries dels anticlinals N-S de les Sierras Exteriores Aragonesas, i més precisament, de l'anticlinal del Pico del Águila. Aplicant diferents tècniques de modelització es dóna resposta a diverses preguntes nascudes de l'observació dels trets geològics de les Sierras Exteriores, i que poden ser esteses a altres exemples de plecs de desenganxament descrits en altres parts del món. Els objectius específics són:

1) Conèixer els mecanismes que poden donar lloc a la generació d'estructures perpendiculars a l'orogen tals com l'anticlinal del Pico del Águila, en absència de cap altre esdeveniment d'escurçament que no sigui la compressió de l'orogènia alpina, de direcció de transport tectònic N-S.
2) Millorar la comprensió de com es distribueix la deformació al llarg d'una seqüència estratigràfica heterogènia com la descrita a les Sierras Exteriores i, per tant, com s'acomoda la deformació depenent de les propietats mecàniques de cada unitat.

3) Comprendre el paper de la sedimentació sin-cinemàtica (estrats de creixement) en l'evolució del plec i com acomoda la deformació.
4) Conèixer els mecanismes que governen la formació dels plecs de desenganxament en 3D i entendre com es distribueixen al llarg i ample de l'estructura. Al mateix temps, comprendre com la distribució dels mecanismes de plegament afecta la geometria de l'anticlinal i les taxes de sedimentació i aixecament que, al seu torn, també influencien el creixement de l'anticlinal.
5) Presentar un model unificat d'evolució estructural d'acord amb les observacions i estudis previs i amb els resultats obtinguts a partir de diferents eines de modelització.
6) Contribuir a un millor coneixement sobre la cinemàtica i la mecànica dels plecs de desenganxament per aconseguir una millor interpretació i comprensió d'altres estructures anàlogues al llarg del planeta que no exhibeixin unes condicions d'aflorament i accessibilitat tant favorables com les de l'anticlinal del Pico del Águila.

R.2.3 ORGANITZACIÓ DE LA TESI

Aquesta Tesi es presenta com una compilació de quatre publicacions científiques, i s'ha estructurat en sis capítols principals, organitzats de la següent manera:

El **Capítol I** presenta una descripció general de la geologia de les Sierras Exteriores Aragonesas dels Pirineus Meridionals. Els articles científics tenen una extensió limitada dins la qual només es pot encabir una breu descripció dels trets més essencials de la geologia de la regió. Tanmateix, l'àrea d'estudi es caracteritza per nombrosos trets geològics d'importància que no van ésser esmentats a les publicacions, o que es troben disseminats en l'apartat del marc geològic de cadascun dels articles. En aquesta secció es presenta una descripció global d'aquests aspectes per tenir un millor coneixement global de l'àrea d'estudi. Es posa especial èmfasi en la descripció de l'estratigrafia, donada la

seva importància en l'evolució dels anticlinals N-S, i en els trets estructurals generals de la regió.

El **Capítol II** conté el primer article científic de la Tesi: **Vidal-Royo, O., Koyi, H.A., Muñoz, J.A., 2009. Formation of orogen-perpendicular thrusts due to mechanical contrasts in the basal décollement in the Central External Sierras (Southern Pyrenees, Spain). Journal of Structural Geology, 31 (5), 523-539.**

Aquest article presenta dues sèries de models analògics (Sèries A i B) que s'han utilitzat per investigar l'efecte de les irregularitats mecàniques en el nivell basal de desenganxament (fàcies Muschelkalk i Keuper) en la formació d'estructures obliqües i perpendiculars a l'orogen, tals com els anticlinals N-S de les Sierras Exteriores Aragonesas. La sèrie A de models investiga la proporció de gruix estratigràfic entre la cobertora i el nivell de desenganxament, mentre que la sèrie B de models analitza l'amplada (perpendicular a la direcció d'escurçament) del desenganxament friccional.

El **Capítol III** conté el segon article científic que constitueix aquesta Tesi: **Vidal-Royo, O., Hardy. S., Muñoz, J.A., 2010. The roles of complex mechanical stratigraphy and syn-kinematic sedimentation in fold development: Insights from discrete-element modelling and application to the Pico del Águila anticline (External Sierras, Southern Pyrenees). A: Poblet, J., Lisle, R.J. (Eds.). Kinematic Evolution and Structural Styles of Fold-and-Thrust Belts, Special Publication of the Geological Society, v.330, doi: 10.1144/SP330.**

En aquest estudi es presenten dos models numèrics en 2D, basats en el mètode de Modelització d'Elements Discrets, per tal d'investigar l'efecte de una estratigrafia mecànica complexa com la descrita al camp, així com dels estrats de creixement en l'evolució de l'anticlinal del Pico del Águila. Es presenten dos models: el Model 1 explora la resposta d'aquesta estratigrafia mecànica

complexa a l'escurçament sota condicions que porten a la formació d'un plec de desenganxament; el Model 2 investiga l'efecte de la sedimentació sin-cinemàtica sota les mateixes condicions de contorn que el Model 1.

Al **Capítol IV** es presenta la tercera publicació científica d'aquesta Tesi: **Vidal-Royo, O., Cardozo, N., Muñoz, J.A., Hardy, S., Maerten, L., (en revisió). Multiple mechanisms driving detachment folding as deduced from 3D reconstruction and geomechanical restoration: The Pico del Águila anticline (External Sierras, Southern Pyrenees).** ***Enviat a Basin Research.***

Aquest estudi presenta una reconstrucció i restitució geomecànica tridimensionals de l'anticlinal del Pico del Águila. A partir de dades de camp (mesures de cabussament i cartografia de traces geològiques) i interpretació de perfils sísmics es presenta una reconstrucció acurada de la geometria de la seqüència pre-plegament i dels estrats de creixement. Mercès a la reconstrucció de quatre seqüències deposicionals dins del paquet sedimentari sin-plegament, es va poder realitzar una restitució seqüencial de l'estructura en la que es va poder establir una cronologia de la deformació. Basat en un mètode de Modelització d'Elements Finits, l'algoritme de restitució considera les propietats mecàniques de les roques per portar a terme una restitució en la que no s'assumeix ni s'imposa cap criteri cinemàtic previ. A partir d'aquesta restitució s'han pogut obtenir nous coneixements de l'evolució de l'anticlinal en 3D.

El **Capítol V** conté el quart article científic d'aquesta Tesi: **Vidal-Royo, O., Muñoz, J.A., Hardy, S., Koyi, H.A., Cardozo, N., (enviat). Structural evolution of the Pico del Águila anticline (External Sierras, Southern Pyrenees) derived from sandbox, numerical and 3D structural modelling techniques.** ***Enviat a Geologica Acta.***

Aquest capítol conté un resum dels resultats presentats en els capítols previs, així com la discussió general de la Tesi. En aquest capítol discutim sobre

els beneficis, desavantatges, limitacions i idoneïtat de les tècniques de modelització presentades, així com els resultats dels models i la seva integració en un model unificat d'evolució estructural.

Al **Capítol VI** es presenten les conclusions finals d'aquesta Tesi, així com una proposta de tasques futures a realitzar.

R.3 INTRODUCCIÓ

Els models geològics proporcionen explicacions i ajuden a un millor coneixement dels processos geològics que tenen lloc a la Terra. Tanmateix, en la majoria dels casos els models geològics no han de ser entesos com una rèplica de la natura sinó com una manera de simular i representar els processos geològics a una escala de temps observable per l'ésser humà.

La geologia estructural té ja una llarga tradició en l'ús de la modelització com a eina per millorar l'enteniment de la generació i evolució d'estructures. D'ençà els primers experiments de models analògics de sorra (Hall, 1815; Daudre, 1879; Cadell, 1888; entre d'altres) s'han creat i desenvolupat nombroses tècniques en resposta a la necessitat creixent dels geòlegs de donar explicació a nous problemes i situacions. Els models analògics han esdevingut més sofisticats, incorporant elements i dispositius que produeixen resultats quantitatius per comparar amb la natura (Koyi, 1997). Amb l'expansió de la informàtica van aparèixer els models numèrics, contribuint amb una ràpida solució d'algoritmes matemàtics que implicà grans avenços en la comprensió dels processos geològics (Krumbein and Graybill, 1965; Agterberg, 1967; Harbaugh and Merriam, 1968). En aquest sentit, els models numèrics afegiren un control quantitatiu de les lleis i paràmetres que governen els processos naturals.

Malgrat tots aquests avenços, cada tècnica de modelització presenta els seus propis punts forts, febleses i limitacions, portant doncs a una representació

de la natura relativament simplificada o incompleta. Això fa que cada tècnica sigui adient per determinades finalitats, tenint en compte que conèixer les limitacions de cada tècnica és essencial per comprendre correctament l'aportació dels models geològics. Per aquest motiu, darrera de cada model ha d'haver-hi una sèrie de paràmetres físics per testar, o un conjunt de processos copsables per esclarir, més que no pas un intent de reproduir detalladament el que s'ha descrit en la natura.

En aquesta Tesi es presenten tres tècniques de modelització per millorar el coneixement sobre l'evolució estructural dels anticlinals N-S de les Sierras Exteriores Aragonesas dels Pirineus Meridionals. Entre ells, el Pico del Águila ha estat l'objecte d'estudi donat que és una estructura àmpliament coneguda com a exemple de plec de desenganxament, és fàcilment accessible i té un excel·lent grau de preservació i aflorament. A més, el mapa geològic del Pico del Águila pot ser considerat una secció al llarg de l'eix del plec, mostrant la geometria i distribució de les unitats al llarg de l'estructura. Els plecs N-S de les Sierras Exteriores Aragonesas es caracteritzen per una interferència estructural amb les estructures E-W generals dels Pirineus, i mostren un alt grau de preservació dels estrats de creixement, fet que permet registrar de forma precisa l'evolució de la deformació a l'anticlinal. L'estructura és ben coneguda i s'ha estudiat des de moltes perspectives diferents. S'han fet contribucions sobre la cinemàtica i evolució estructural del plec a partir d'estudis sedimentològics (Millán et al., 1994; Castelltort et al., 2003), paleomagnetisme (Pueyo et al., 2002; Rodríguez-Pintó et al., 2008), models analògics (Nalpas et al., 1999, 2003), models cinemàtics 2D (Poblet and Hardy, 1995; Poblet et al., 1997), restitució de talls geològics (Novoa et al., 2000), i altres estudis multidisciplinaris (Huyghe, et al., 2009). Malgrat aquest nombre d'estudis previs, no existeix cap estudi integrat posant en comú els resultats derivats de diverses tècniques de modelització i anàlisi que es complementin i validin mútuament, construint així un model d'evolució més robust.

Aquests motius fan del Pico del Águila una estructura ideal per reconstruir en 3D. En aquest estudi es presenta en primer lloc el model 3D de l'anticlinal, a partir del qual s'ha obtingut la geometria del patró d'interferència entre les estructures N-S i E-W, així com la geometria dels estrats de

creixement. Més que proporcionar respostes sobre l'evolució del plec, el model 3D planteja noves preguntes sobre els processos geològics que van tenir-hi lloc. Per donar-hi resposta s'han emprat tres tècniques de modelització que es presenten a continuació de la reconstrucció 3D del plec. En conjunt, aquest treball presenta un model conceptual unificat d'evolució estructural basat en la integració dels resultats obtinguts a partir de models analògics (Vidal-Royo et al., 2009), models mecànics 2D (Vidal-Royo et al., 2010), i restitució geomecànica 3D de l'anticlinal del Pico del Águila (Vidal-Royo et al., *enviat*). Els models analògics presentats mostren la formació d'estructures perpendiculars a l'orogen en un únic esdeveniment compressiu, com a conseqüència d'importants contrastos mecànics en el nivell basal de desenganxament. Els models numèrics investiguen la importància de l'estratigrafia mecànica i la sedimentació sin-cinemàtica en el creixement d'un plec de desenganxament com el Pico del Águila. Finalment, la restitució geomecànica 3D mostra la complexitat de la interferència en l'estructura de l'anticlinal, així com la seva evolució seqüencial i la combinació de mecanismes de plegament produint-se simultàniament durant el creixement del plec.

R.4 MARC GEOLÒGIC

La geologia de les Sierras Exteriores Aragonesas és ben coneguda i ha estat objecte de nombrosos estudis al llarg dels anys. Una descripció detallada dels trets geològics de la regió va més enllà dels objectius d'aquest resum, tot i que el lector interessat podrà trobar bones i profundes descripcions en treballs clau com són Puigdefàbregas (1975), Millán et al. (1994), i Pueyo et al. (2002). Malgrat això, una descripció general de la regió es presenta també en aquesta secció.

L'anticlinal del Pico del Águila es localitza en les denominades Sierras Exteriores Aragonesas dels Pirineus Meridionals. Les Sierras Exteriores Aragonesas estan constituïdes per una sèrie de làmines d'encavalcament imbricades, desenganxades sobre les fàcies evaporítiques, calcàries i dolomítiques del Triàsic mig i superior (fàcies Muschelkalk i Keuper) (Soler &

Puigdefàbregas, 1970; IGME, 1992; Millán et al. 1994; Millán, 1995; Pueyo et al., 2002). Les Sierras Exteriores constitueixen la part frontal emergent de l'encavalcament sudpirinenc , i es troben desplaçades cap al sud sobre els sediments d'edat terciària de la conca d'avantpaís de l'Ebre.

Una de les peculiaritats de les Sierras Exteriores és la presència d'un conjunt d'anticlinals amb orientació axial N-S a NW-SE. Aquestes estructures són, doncs, perpendiculars a la tendència estructural general dels Pirineus (E-W, amb la direcció de transport tectònic cap al sud) i creen per tant un patró de interferència estructural complex (Fig. R1). Els anticlinals N-S són més joves i més petits cap a l'oest (Millán et al., 1994; Millán, 1995) i el seu creixement va ser sincrònic a la deposició del sediments de l'Eocè mig a l'Oligocè i al desenvolupament del front d'encavalcament sudpirinenc (actiu fins al Miocè inferior; Puigdefàbregas, 1975; Holl and Anastasio, 1993; Millán et al., 1994; Millán, 1995).

El Pico del Águila és un dels anticlinals N-S més estudiats de totes les Sierras Exteriores Aragonesas. Va créixer durant el període comprès entre 42.67 ± 0.02 Ma (Lutecià superior) i 34.8 ± 1.72 Ma (Priabonià mig) (Poblet & Hardy, 1995), i mostra una espectacular seqüència d'estrats de creixement (Figs. R3 i R4) (Millán et al., 1994; Millán, 1995, Poblet & Hardy, 1995; Pueyo et al., 2002; Castelltort et al., 2003; Vidal-Royo et al., 2010).

La seqüència estratigràfica de les Sierras Exteriores Aragonesas es caracteritza per ser una intercalació de materials competents i incompetents (Millán et al., 1994), cadascú dels quals mostra una diferent resposta a la deformació (Vidal-Royo et al., 2010). L'estratigrafia de la zona consisteix en unes centenes de metres de materials mesozoics coberta per una seqüència més gruixuda de materials terciaris (Fig. R2). La sèrie mesozoica està composada per calcàries, dolomies i argiles amb evaporites del Triàsic mig i superior, cobertes per les calcàries de plataforma soma del Cretàcic superior. El Terciari està composat pels gresos, limolites i calcàries lacustres de la transició Cretàcic-Terciari (fàcies del Garumnià), les calcàries de la plataforma marina soma de la Formació Guara (Lutecià), les margues, calcàries i gresos deltaics de plataforma marina i transicionals de les Formacions Arguis i Belsué-Atarés (Lutecià

superior a Priabonià mig), i les argiles, gresos i conglomerats fluvials de la Formació Campodarbe (Priabonià mig a Oligocè mig).

La seqüència pre-plegament comprèn materials que van del Triàsic al Lutecià, amb el límit superior al sostre de la seqüència deposicional 2 de la Formació Guara. Dins del nivell de desenganxament Triàsic, observacions de camp (IGME, 1992) indiquen que les calcàries i dolomies del Muschelkalk (Triàsic mig) són les roques més antigues que afloren al nucli de l'anticlinal (Fig. R1), trobant-se plegades, encavalcades i amb una gran deformació interna.

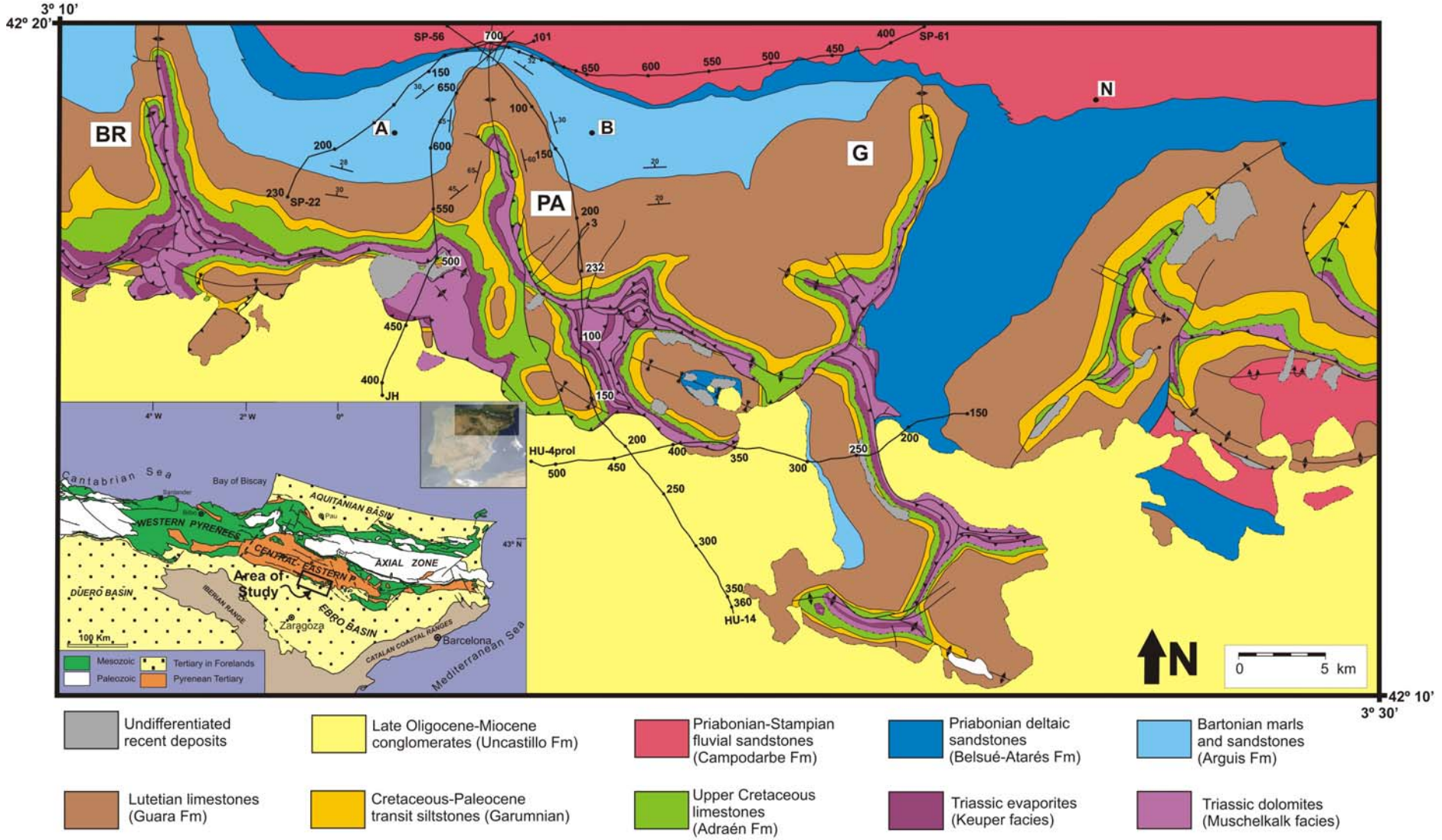
3º 10'
42º 20'
SP-56
SP-61
SP-22
BR
PA
G
A
B
N
JH
HU-4prol
HU-14
Cantabrian Sea
Bay of Biscay
AQUITANIAN BASIN
WESTERN PYRENEES
CENTRAL-EASTERN P.
AXIAL ZONE
Area of Study
DUERO BASIN
IBERIAN RANGE
EBRO BASIN
Zaragoza
Barcelona
CATALAN COASTAL RANGES
Mediterranean Sea
100 Km
Mesozoic
Paleozoic
Tertiary in Forelands
Pyrenean Tertiary
N
0
5 km
42º 10'
3º 30'
Undifferentiated recent deposits
Late Oligocene-Miocene conglomerates (Uncastillo Fm)
Priabonian-Stampian fluvial sandstones (Campodarbe Fm)
Priabonian deltaic sandstones (Belsué-Atarés Fm)
Bartonian marls and sandstones (Arguis Fm)
Lutetian limestones (Guara Fm)
Cretaceous-Paleocene transit siltstones (Garumnian)
Upper Cretaceous limestones (Adraén Fm)
Triassic evaporites (Keuper facies)
Triassic dolomites (Muschelkalk facies)

Fig. R1. **(PÀGINA ANTERIOR)** Mapa geològic del sector central de les Sierras Exteriores Aragonesas (modificat de IGME, 1992). BR: anticlinal de Bentué de Rasal; PA: anticlinal del Pico del Águila; G: anticlinal de Gabardiella. Les línies negres indiquen els perfils sísmics interpretats en la reconstrucció 3D de l'anticlinal del Pico del Águila.

Per altra banda, malgrat que les argiles i evaporites del Keuper (Triàsic superior) dibuixen la geometria del plec com la resta de la seqüència mesozoica, s'ha observat un notable decreixement del gruix estratigràfic cap a les parts internes de l'anticlinal, on les fàcies Keuper són pràcticament inexistents en el nucli de l'estructura (Fig. R1). D'aquesta manera, les fàcies Keuper són més gruixudes i estan millor exposades a les àrees entre els anticlinals N-S més que no pas al nucli d'aquestes estructures. La seqüència sin-plegament comprèn des de la seqüència deposicional 3 de la Formació Guara (Fig. R3) i la seqüència de somerització formada per les Formacions Arguis, Belsué-Atarés i Campodarbe. La base de la Formació Arguis defineix una discordança regional, indicant un canvi brusc cap a ambients deposicionals de talús (Figs R2 i R4). Millán et al., 1994 va definir quatre seqüències deposicionals principals dins de les Formacions Arguis i Belsué-Atarés. La seqüència I (anomenada GS-I a partir d'ara) està composada per margues blaves i margues sorrenques amb important contingut en glauconita, i té una edat compresa entre el Lutecià superior i el Bartonià inferior. Aquesta seqüència s'aprima cap a la cresta de l'anticlinal i desapareix sense arribar a cobrir-la. La seqüència II (anomenada GS-II a partir d'ara) té una edat de Bartonià mig a superior, i està composada per margues blaves lleugerament biotorbades. La seqüència III (anomenada GS-III a partir d'ara) correspon a una plataforma de pectínids d'edat Priabonià inferior formada per margues blaves riques en contingut fòssil marí i amb traces de biotorbació. La seqüència IV (anomenada GS-IV a partir d'ara) es d'edat priaboniana inferior i està composada per margues sorrenques deltaiques i nivells siliciclàstics purs formats per progradació deltaica. El límit inferior de la GS-IV correspon al contacte entre les Formacions Arguis i Belsué-Atarés. El límit superior és una discordança regional, reconeixible tot al llarg de la conca sudpirinenca, i que correspon al contacte entre les Formacions Belsué-Atarés i Campodarbe (Fig. R2). Aquesta discordança representa un trànsit brusc a ambients deposicionals continentals.

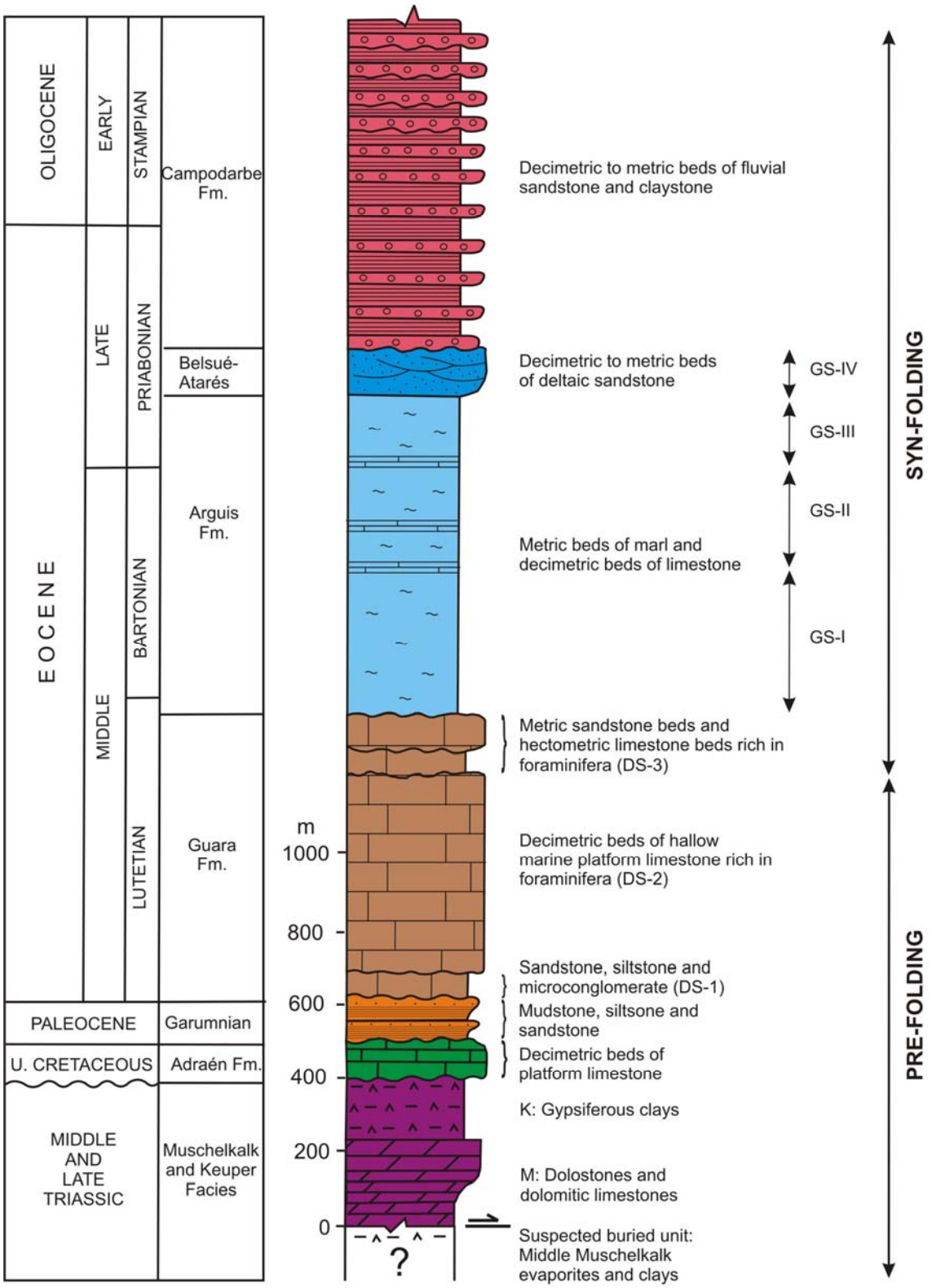

Fig. R2. Columna estratigràfica de la regió, descrivint les litologies i gruixos promig dels materials aflorants. M: fàcies Muschelkalk; K: fàcies Keuper. DS: seqüències deposicionals definides a la Formació Guara. GS: seqüències deposicionals definides als estrats de creixement. Modificada de Millán et al. (1994).

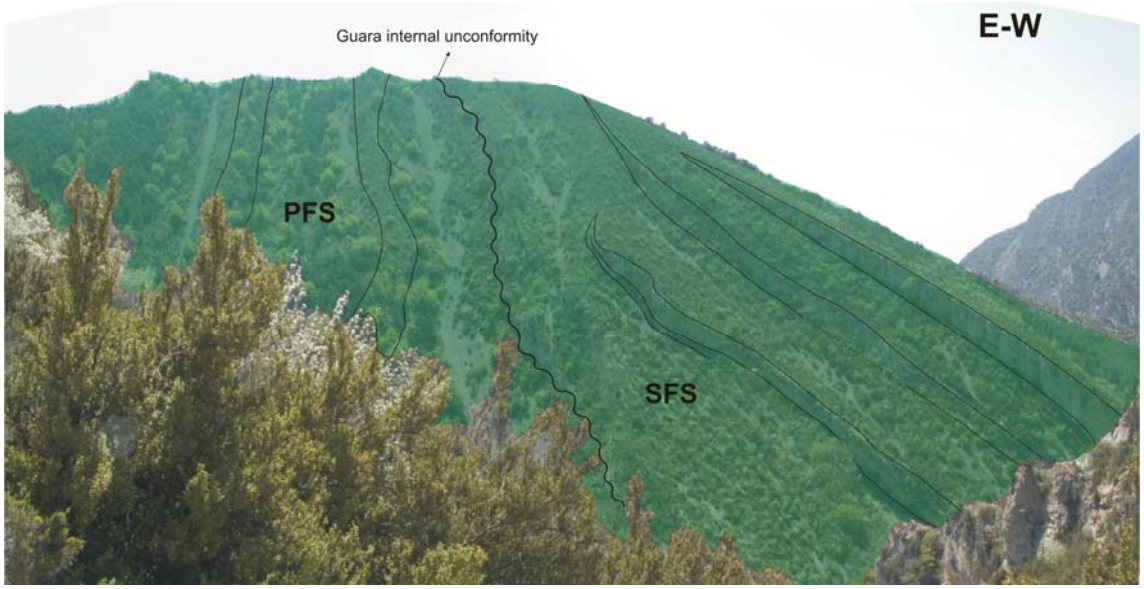

Fig. R3. Fotografia obliqua del flanc occidental de l'anticlinal del Pico del Águila mostrant una discordança interna a la Formació Guara que separa la seqüència pre-plegament (PFS) de la seqüència sin-plegament (SFS), la qual s'aprima clarament sobre l'anterior.

R.5 RECONSTRUCCIÓ 3D DE L' ANTICLINAL DEL PICO DEL ÁGUILA

R.5.1 METODOLOGIA DE RECONSTRUCCIÓ

La reconstrucció de l'anticlinal del Pico del Águila es basa en un acurat treball de camp amb recol·lecció de dades de superfície i en la interpretació de diversos perfils sísmics (veure Fig. R1 per identificació i localització dels perfils). Totes aquestes dades van ser posteriorment integrades en un entorn de treball GIS (3D) . Això va donar com a resultat un model més robust, que incorpora totes les dades i mesures disponibles. Les dades adquirides en superfície comprenen mesures de cabussament, traces cartogràfiques de falles i fractures i una acurada cartografia de traces d'estratificació de la seqüència d'estrats de creixement. Aquestes dades es van posicionar en 3D sobre un Model Digital del

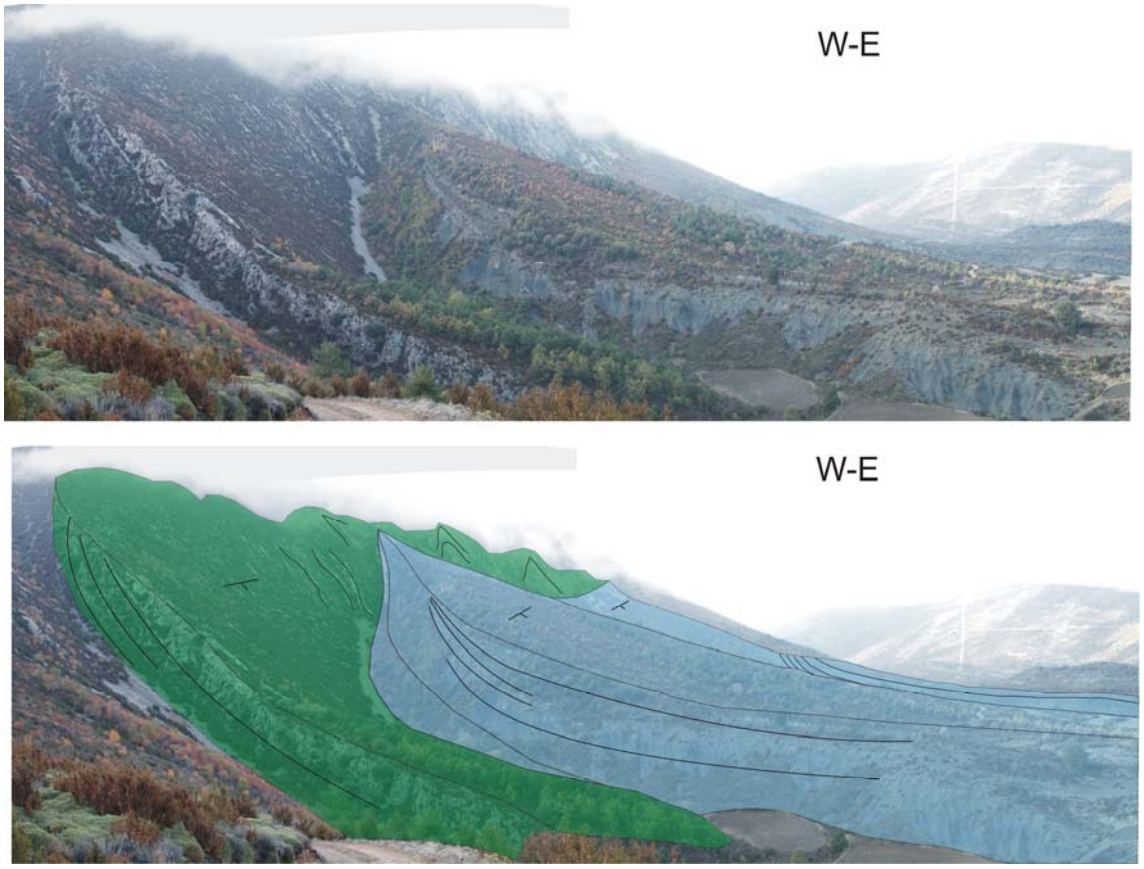

Fig. R4. Fotografia obliqua del flanc oriental del Pico del Águila. Es pot observar clarament com les margues de la Formació Arguis (en blau) s'aprimen i dibuixen *onlaps* sobre el sostre de la Formació Guara (en verd).

Terreny (MDT) de l'àrea amb una resolució de ±2.5 m (Fig. R5). L'anticlinal es va reconstruir aplicant el Mètode dels Dominis de Cabussament (Fernández et al., 2004 a i b), el qual enuncia que la geometria d'una estructura es pot simplificar en volums en els quals l'orientació de l'estratificació és constant (Fig. R6). Per aplicar el mètode s'ha d'establir prèviament un model geomètric a partir de les dades disponibles. Aquest model geomètric ha d'incloure: 1) una definició dels dominis de cabussament (orientació promig de l'estratificació del domini i polaritat, posició i extensió dels límits del domini); i 2) una definició de les geometries estratigràfiques en 3D (un model de separacions estratigràfiques entre diferents horitzons). En total es van definir 91 dominis de cabussament per la reconstrucció del sostre de la Formació Guara, assumint una variació de

±5º en l'azimut i ±3º en el valor del cabussament com a límits de tolerància entre dominis de cabussament. Intersectant els dominis de cabussament adjacents es va obtenir el mapa de contorns estructurals en 3D. A partir d'aquest es va realitzar una interpolació dels contorns estructurals a GOCAD (Paradigm™), obtenint una geometria més suavitzada de la superfície de referència que incorpora i respecta totes les dades d'entrada. La resta de les superfícies de la seqüència pre-plegament van ser reconstruïdes emprant una eina disponible a 3DMove (Midland Valley Exploration) que permet la creació de noves superfícies plegades a partir d'una superfície preexistent per plecs similars i paral·lels. Donat que el Pico del Águila és considerat un plec paral·lel d'escala quilomètrica (Millán , 1995), l'eina de creació de superfícies plegades va ser emprada per reconstruir la geometria de les superfícies del sostre del Triàsic, Cretaci superior i Garumnià. Les superfícies de la seqüència sin-plegament van ser reconstruïdes individualment, aplicant el Mètode dels Dominis de Cabussament. Per controlar la variació de gruix estratigràfic dels estrats de creixement es va aprofitar l'excel·lent grau d'afloració d'aquestes unitats al camp així com les columnes estratigràfiques detallades publicades a Millán et al. (1994).

Les dades de profunditat consisteixen en la interpretació de diversos perfils sísmics, la identificació i localització dels quals pot trobar-se a la Fig. R1. Aquests han permès conèixer la geometria de l'anticlinal en profunditat i validar les interpretacions a partir de dades de camp. Donada la pobra qualitat dels perfils sísmics, només s'han pogut interpretar els trets geomètrics generals de la seqüència pre-plegament, així com la geometria de l'encavalcament frontal sudpirinenc. Les interpretacions sísmiques es van convertir llavors a profunditat utilitzant la velocitat d'interval de cada unitat, deduïda a partir d'un pou d'exploració situat fora de l'àrea d'estudi i dels *Common Depth Points* (CDP's) dels perfils sísmics. Aquesta informació es va transferir a l'entorn de treball 3D, per tal de correlacionar els horitzons entre els diferents perfils interpretats. Es va generar llavors un mapa de contorns estructurals en 3D per cada falla o horitzó. En el cas dels horitzons estratigràfics pre-plegament, les noves dades es van afegir com a punts de control en profunditat a cada corresponent mapa de contorns.

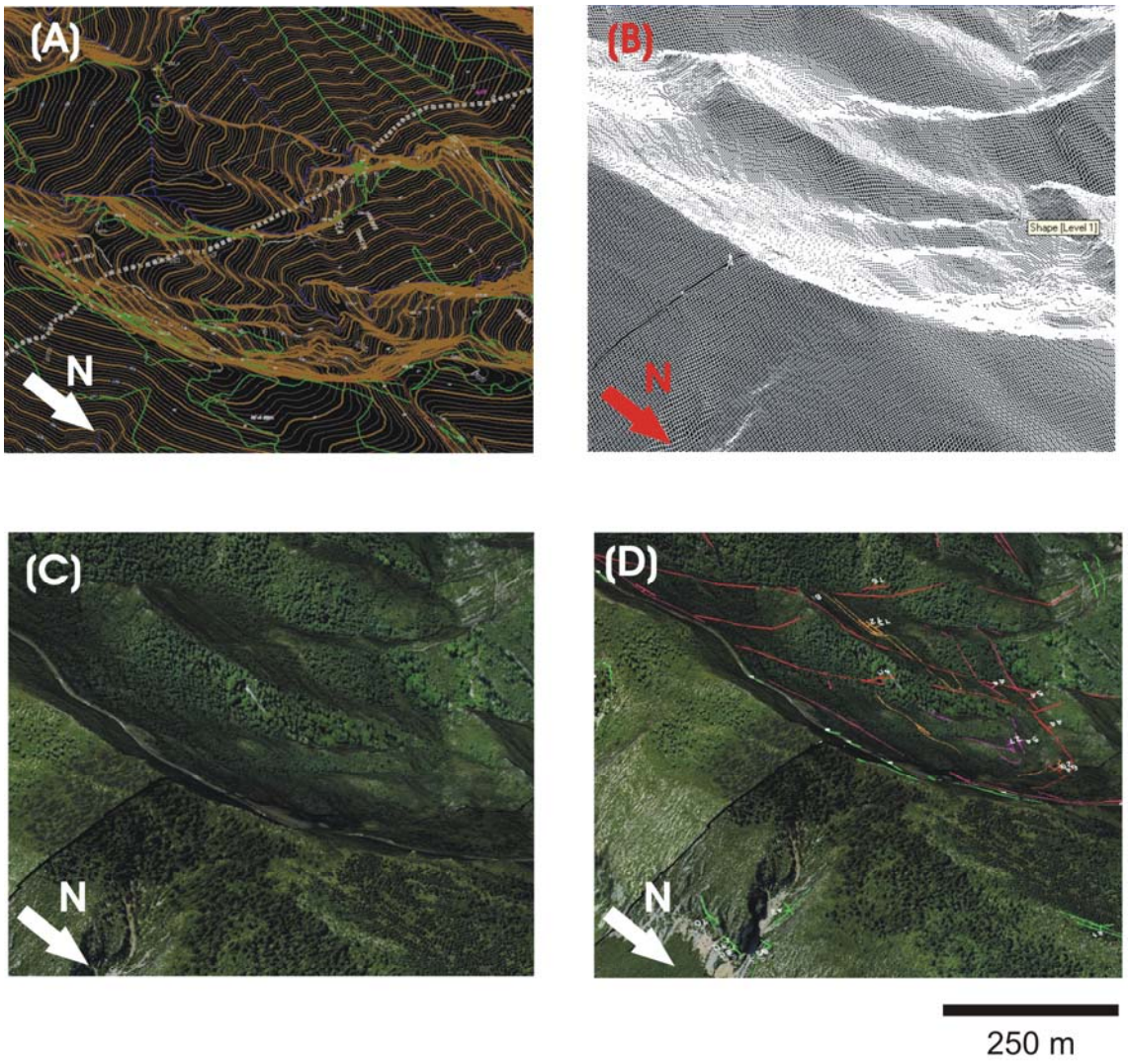

Fig. R5. Diferents etapes de la construcció del Model Digital del Terreny (DTM) i de la digitalització de les dades de camp. (A) Mapa topogràfic 1:5000 a partir del qual s'extreu un model d'elevació en XYZ. Després, es porta a terme una triangulació creant una malla feta de triangles. A partir d'aquesta es crea una malla regular de 5 x 5 m (B), sobre la qual s'entapissa la corresponent ortofotografia (C). Amb el MDT disponible ja es poden digitalitzar totes les dades, posicionant-les a les seves corresponents coordenades XYZ (D).

R.5.2 RESULTATS DE LA RECONSTRUCCIÓ

Mitjançant la metodologia exposada s'han reconstruït vuit horitzons estratigràfics i nou superfícies de falla. De la seqüència pre-plegament s'han reconstruït les superfícies corresponents al sostre de les següents unitats (Fig. R7): 1) Formació Guara (superfície de referència del plec); 2) les fàcies del Garumnià; 3) el Cretaci superior; i 4) els materials Triàsics. Vuit superfícies de falla, l'encavalcament intern N-S de l'anticlinal així com la geometria de

l'encavalcament frontal sudpirinenc han estat també reconstruïts. De la seqüència d'estrats de creixement s'ha reconstruït el sostre de quatre superfícies, corresponents a les quatre seqüències deposicionals principals de les Formacions Arguis i Belsué-Atarés (GS-I a GS-IV; Figs. R8 i R9).

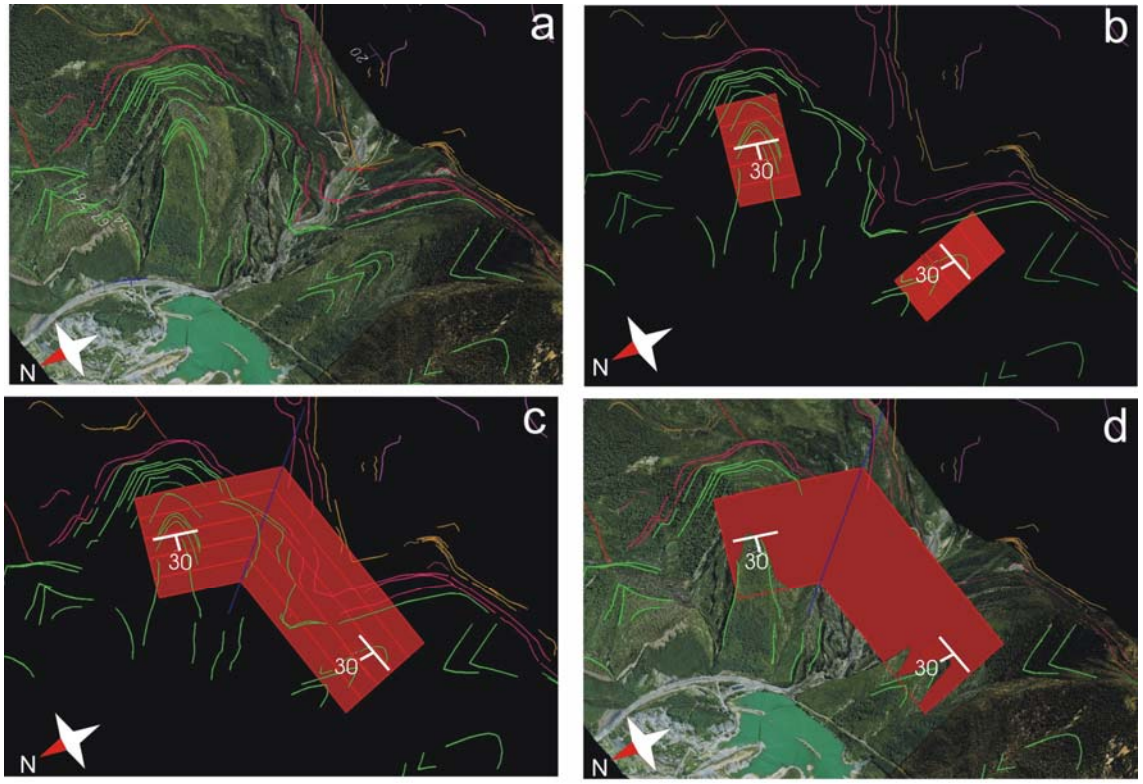

Fig. R6. Diferents passos resumint el procés seguit per generar els dominis de cabussament: a) posicionament de les mesures de cabussament; b) creació dels dominis de cabussament; c) definició de l'extensió, intersecció dels diferents dominis i creació del mapa de contorns estructurals; i d) generació de la superfície.

La geometria de l'encavalcament frontal sudpirinenc consisteix en una rampa que cabussa cap al nord, variant des de 15º a la part septentrional de l'anticlinal fins a 37º en la zona frontal emergent, i un replà subhorizontal que s'estén cap al nord. El sostre de la Formació Guara no es troba massa afectat per la presència de les falles internes, i fossilitza l'encavalcament intern N-S de l'anticlinal. Les unitats inferiors, en canvi, mostren un patró estructural complex

degut a la interferència entre les falles (d'orientació compresa entre E-W i NNE-SSW) i l'encavalcament N-S (Figs. R7 i R10a).

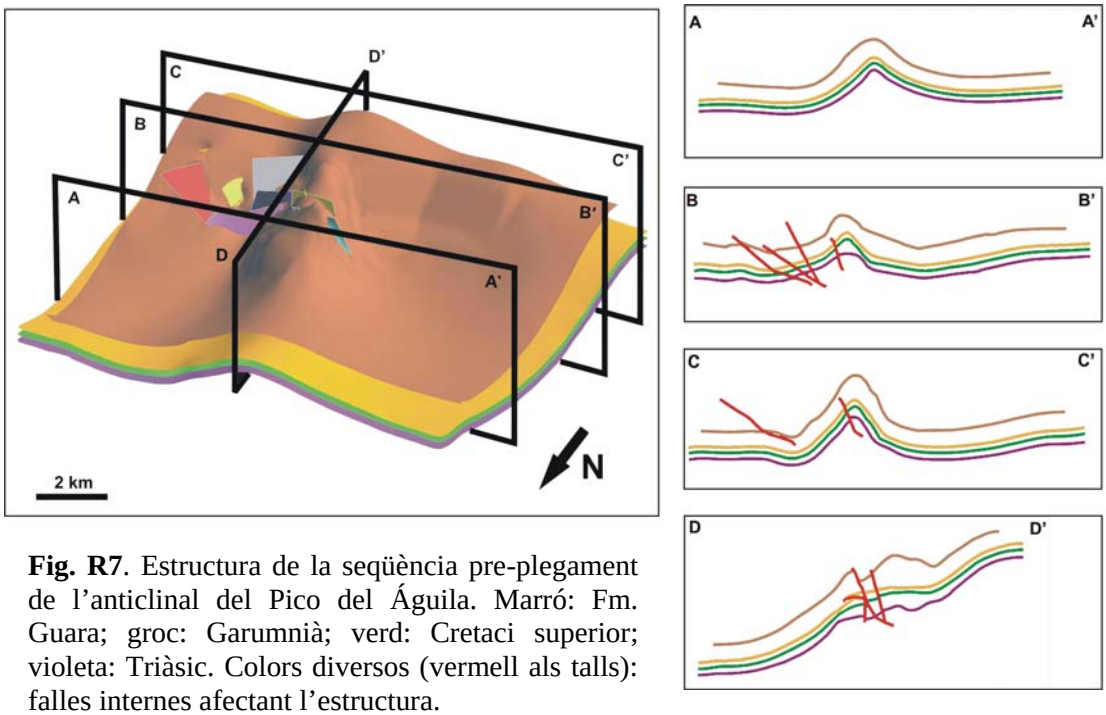

Fig. R7. Estructura de la seqüència pre-plegament de l'anticlinal del Pico del Águila. Marró: Fm. Guara; groc: Garumnià; verd: Cretaci superior; violeta: Triàsic. Colors diversos (vermell als talls): falles internes afectant l'estructura.

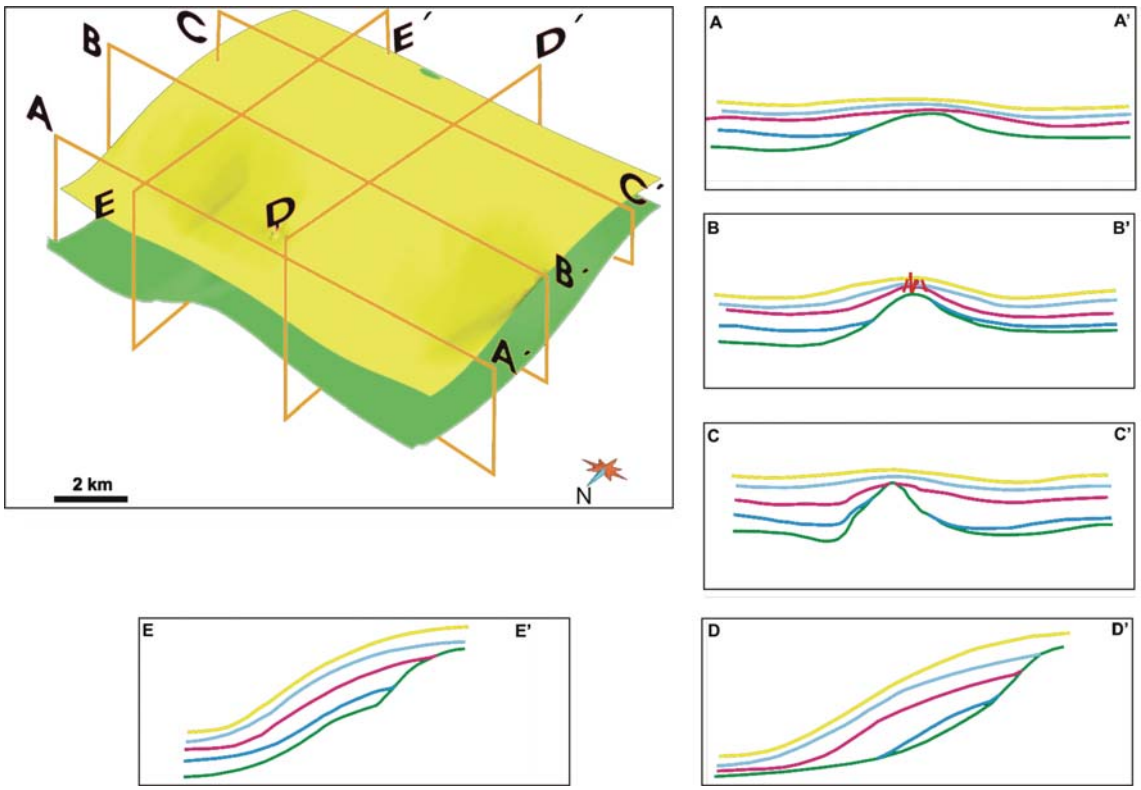

Fig. R8. **(PÀGINA ANTERIOR)** Estructura dels estrats de creixement de l'anticlinal del Pico del Águila, mostrant la geometria de les seqüències deposicionals reconstruïdes sobre el sostre de la Formació Guara (en verd). Observi's com les GS s'aprimen cap a la cresta de l'anticlinal i com la GS-I no assoleix la xarnera.

La seqüència sin-plegament mostra una geometria més suavitzada, caracteritzada per un aprimament cap a la cresta de l'anticlinal i un decreixement cap a sostre de la intensitat de la deformació (Figs. R8, R9 i R10b). La seqüència GS-I no arriba a cobrir la cresta de l'anticlinal, i descriu geometries en *onlap* sobre ambdós flancs de l'anticlinal. Les seqüències superiors cobreixen progressivament el sostre de la Formació Guara (Figs. R8 i R9).

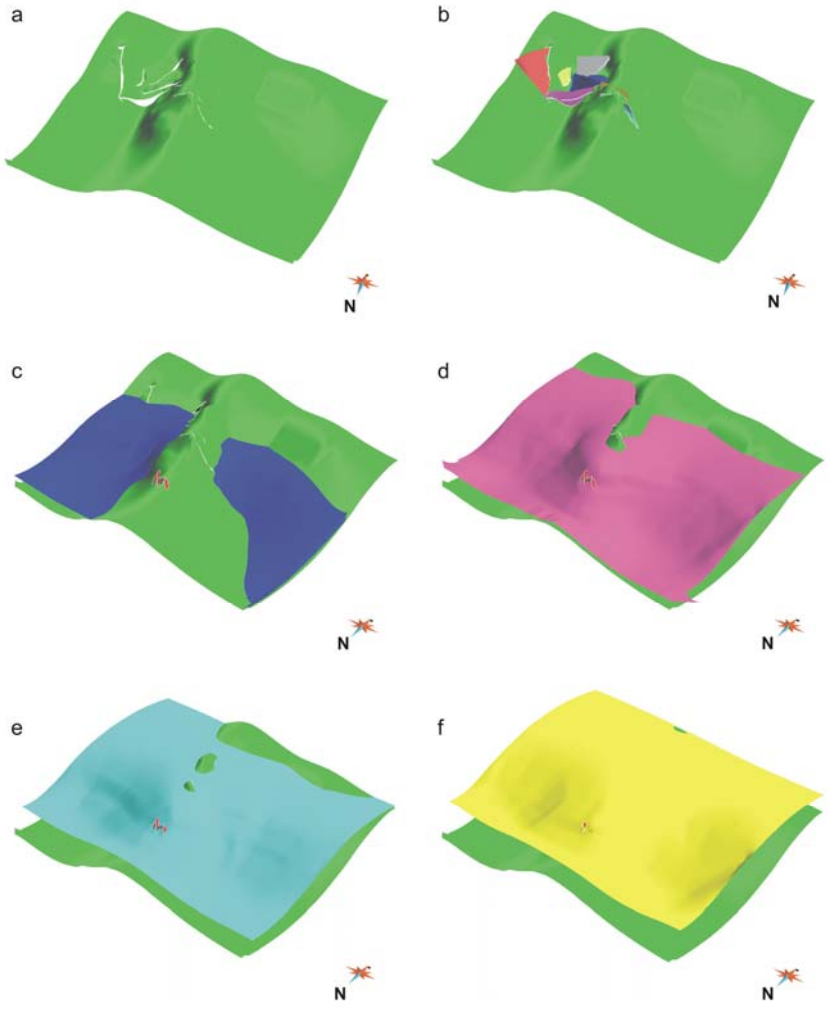

Fig. R9. Vistes 3D dels estrats de creixement: a) Sostre de la Formació Guara (en marró a la Fig. R7); b) Formació Guara amb les falles internes; c) GS-I; d) GS-II; e) GS-III; f) GS-IV.

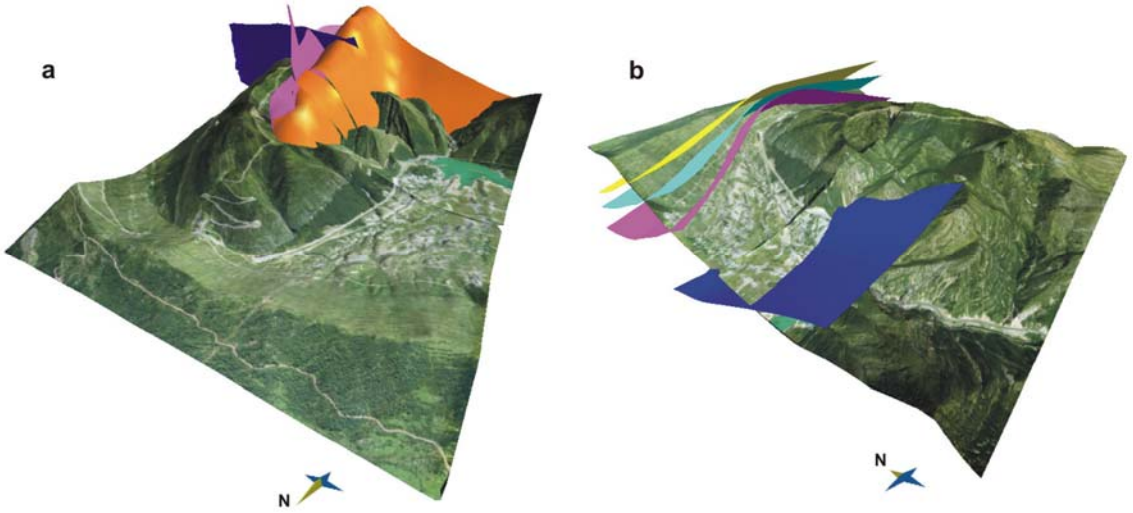

Fig. R10. Imatges obliqües de l'anticlinal del Pico del Águila: a) mostra la interferència entre l'anticlinal (superfície del sostre del garumnià, en taronja), el conjunt de falles internes d'orientació NNE-SSW a E-W (blau fosc) i l'encavalcament intern N-S (rosa); b) mostra la geometria dels estrats de creixement intersectant la topografia i aprimant-se cap al tancament periclinal del plec definit pel sostre de la Formació Guara.

R.6 MODELITZACIÓ ANALÒGICA: GENERACIÓ D'ESTRUCTURES PERPENDICULARS A L'OROGEN

Els models analògics presentats en aquest treball investiguen la geometria inicial del nivell basal de desenganxament com a possible factor de control en la generació estructures obliqües i perpendiculars a l'orogen tals com les descrites a les Sierras Exteriores Aragonesas. El disseny de l'experiment es basa en observacions de camp que indiquen una pràctica absència de les fàcies Keuper al nucli dels anticlinals N-S (p.ex. anticlinals del Pico del Águila i Gabardiella; Fig. R1), i un gruix més notable d'aquests materials a les zones intermèdies, on les estructures generals pirinenques E-W es formen (p.ex. el front d'encavalcament sudpirinenc). L'objectiu de simular aquest nivell basal de desenganxament distribuït heterogèniament va ser la de testar si els canvis laterals de fricció podien ser capaços o no de causar la generació d'estructures arquejades, obliqües i perpendiculars independentment de la orientació de la direcció d'escurçament.

R.6.1 CONFIGURACIÓ INICIAL

La configuració inicial de l'experiment es composa d'una seqüència de capes de sorra interestratificades i de diferents colors que cobreixen un nivell basal irregular format per tres cossos de silicona separats per sorra sense cohesió (Fig. R11). La cobertora sedimentària de materials del Cretaci superior fins al Lutecià, doncs, es va simular mitjançant sorra quarsítica de densitat 1700 kg m^{-3}, valor de cohesió C d'uns 140 Pa i garbellada a un mida de gra promig de 35 μm. El nivell de desenganxament irregular Triàsic es va simular mitjançant la silicona SGM36 (amb una densitat de 987 kg m^{-3} i viscositat efectiva η de 5 x 10^4 Pa s a temperatura ambient, manufacturada per Dow Corning Ltd.) intercalada lateralment amb sorra quarsítica seca i sense cohesió.

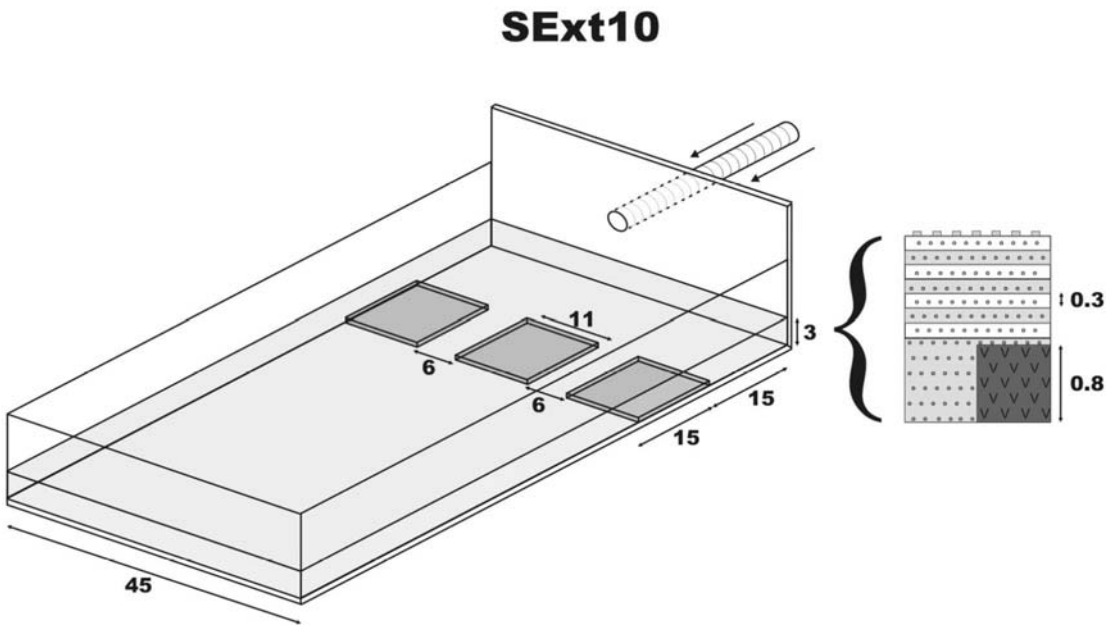

Fig. R11. Configuració inicial del model analògic Sext10 presentat en aquesta Tesi, mostrant la distribució dels desenganxaments dúctils (SGM-36) i fràgils (sorra) i l'orientació de l'escurçament. La seqüència estratigràfica del model es mostra a la dreta. Tots els valors són en cm.

L'aparell de deformació es trobava sobre una placa d'alumini a la qual se li van encolar grans de sorra. Els models tenien una amplada fixa de 45 cm, una longitud inicial de 60 cm i un gruix constant de nivell de desenganxament de 8

cm (Fig. R11). El motiu d'encolar sorra sobre la placa basal d'alumini va ser la de forçar un comportament altament friccional en el basament per tal d'accentuar el contrast entre el desenganxament dúctil (capes de silicona) i el desenganxament friccional (sorra). Es va aplicar compressió a una velocitat constant de 2 cm/h (5.56×10^{-6} m/s) des d'un únic costat utilitzant un pistó mobilitzat per un motor (Fig. R11). Els models es van comprimir fins a u 20% durant 6 hores.

R.6.2 RESULTATS DE LA MODELITZACIÓ ANALÒGICA

L'escurçament aplicat als models va causar la deformació tant en les capes de sorra com en les de silicona. El patró de deformació va ser diferent entre les zones desenganxades sobre un nivell friccional (sorra; àrees HF) i les zones desenganxades sobre un nivell dúctil (silicona; àrees LF). La deformació començà amb l'aparició de tres encavalcaments a grans trets rectilinis, donat que el front de deformació encara no havia assolit la posició de la silicona. Després d'un 9% d'escurçament (Fig. R12b) el front de deformació assoleix la posició de la silicona, creant així una diferència d'avenç entre les àrees desenganxades sobre la sorra i les desenganxades sobre la silicona. Les àrees HF mostren un aixecament addicional respecte les àrees LF, que ocasionalment s'expressa a través de petits encavalcaments oblics que s'uneixen a l'encavalcament frontal principal en la part posterior del model. Després d'un 16% d'escurçament (Fig. R12c) les estructures no poden acomodar més deformació i el front migra cap endavant. Com a conseqüència, es forma una segona generació d'estructures paral·leles a la direcció d'escurçament. Malgrat això, en aquesta segona generació la posició del front de deformació coincideix amb la línia d'acabament de les capes de silicona. Després d'un 20% d'escurçament (Fig. R12d) les àrees HF no avancen tanta distància com les àrees LF, creant un patró estructural constituït per encavalcaments de morfologia ondulada que transporten més lluny les àrees desenganxades sobre silicona que no pas les àrees desenganxades sobre sorra.

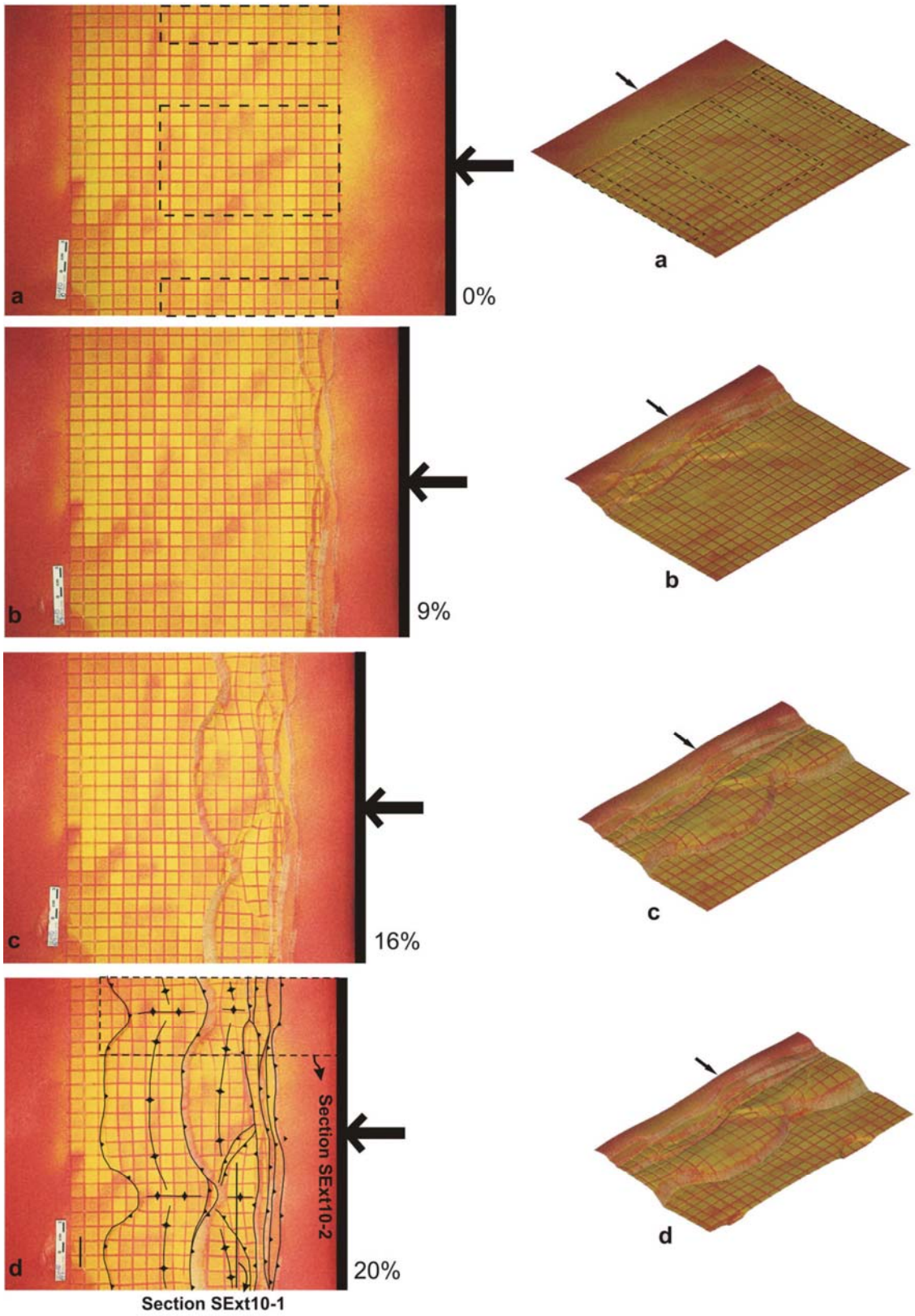

Fig. R12. Vistes en planta i en 3D del model analògic en diferents etapes d'escurçament: a) estadi no deformat; b) 9% d'escurçament; c) 16% d'escurçament; d) 20% d'escurçament. Les fletxes indiquen l'orientació i sentit de l'escurçament.

La deformació de les capes dúctils per flux i engruiximent dúctil i plegament es transfereix lateralment a les àrees HF, de forma que es generen rampes laterals dels encavalcaments que ascendeixen en la sèrie des de la terminació lateral de les capes de silicona. Aquestes rampes laterals s'uneixen en el nucli de les àrees HF, produint aixecament i suau deformació en les unitats superiors mentre que les unitats inferiors pateixen gran deformació interna per mitjans de falles (Fig. R13 a i b). Es produeix doncs una migració lateral de les capes dúctils cap a les àrees HF, així com un engruiximent al llarg del límit entre les àrees HF i LF, on les rampes laterals descrites es desenganxen (Fig. R13 a i b). Les seccions horitzontals mostren la geometria interna de les capes en profunditat, podent-se observar com les capes mostren encavalcaments dirigits cap a l'avantpaís en els que les unitats inferiors es troben encavalcades mentre que les superiors es troben suaument plegades. L'únic tancament periclinal observable es troba al costat més proper a l'orogen de les estructures transversals (Fig. R13), indicant així que aquestes estructures tenen una certa immersió cap a l'orogen degut al basculament creat per l'emplaçament de la làmina encavalcant.

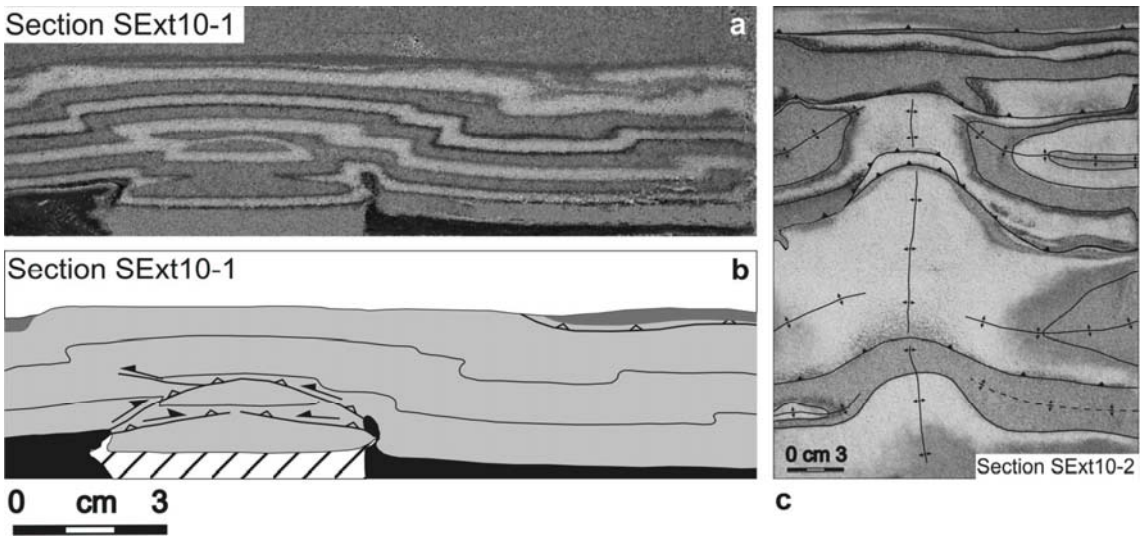

Fig. R13. Imatges i interpretacions de seccions perpendiculars a l'escurçament i seccions horitzontals preses del model SExt10 (veure Fig. R12 per localització de les seccions). La secció Sext10-1 mostra l'aixecament addicional de les zones HF respecte les LF, i com les capes dúctils es fan més gruixudes cap al centre de les zones HF. La secció Sext10-2 mostra la interferència estructural entre les estructures paral·leles a l'orogen i les perpendiculars, proporcionant una informació valuosa sobre com les unitats canvien de morfologia quan canvia el comportament mecànic del desenganxament basal.

Les àrees desenganxades sobre sorra, per tant, acomoden la deformació per mitjans d'un aixecament addicional respecte les àrees desenganxades sobre silicona, desenvolupant-se suaus anticlinals perpendiculars a l'orogen en el bloc superior dels encavalcaments. La localització de les crestes d'aquests anticlinals coincideix pràcticament amb el centre de les àrees HF. Aquest fet indica que el contrast de fricció entre la sorra i la silicona al llarg de la direcció d'escurçament ha permès la nucleació dels encavalcaments sobre la línia d'acabament lateral de les capes de silicona.

R.7 MODELITZACIÓ NUMÈRICA: EFECTE DE L'ESTRATIGRAFIA MECÀNICA I SEDIMENTACIÓ SIN-CINEMÀTICA

Aquest subcapítol presenta els resultats obtinguts a partir d'un model numèric, el qual s'ha utilitzat per millorar el coneixement sobre l'efecte de una estratigrafia mecànica complexa (no trivial) i de la sedimentació sin-cinemàtica en el creixement de l'anticlinal del Pico del Águila. Per tal de portar-ho a terme s'ha emprat una tècnica de modelització 2D coneguda com Modelització d'Elements Discrets (*Discrete Element Modelling, DEM*).

Aquest mètode tracta una massa de roca com un conjunt d'elements circulars connectats per parelles mitjançant enllaços que es trenquen per sobre de determinats llindars de deformació (Hardy & Finch, 2005, 2007). Assignant doncs diferents valors de llindar de trencament a cada parella d'elements és possible modelitzar diferents propietats mecàniques (p.ex. a una seqüència estratigràfica) en el conjunt d'elements que simulen la massa de roca. Això ens permet testar l'efecte d'una determinada estratigrafia mecànica sobre la geometria, la cinemàtica i els mecanismes que es produeixen al plec. D'aquesta manera, aquest mètode proporciona més informació que les tècniques de modelització cinemàtica prèvies. A més, permet una fàcil supervisió del desplaçament/localització dels elements durant la modelització. El trajecte de desplaçament, l'evolució cinemàtica i la distribució de la deformació dins del cos de roca pot ser fàcilment seguida a qualsevol estadi de la modelització. Donada

la intercalació de materials competents i incompetents que caracteritza l'estratigrafia de la zona d'estudi (Fig. R2) considerem aquest un mètode adient per modelitzar l'evolució de l'anticlinal del Pico del Águila.

Com s'ha esmentat prèviament, el Pico del Águila ofereix una bona secció al llarg de l'eix del plec de tota la seqüència estratigràfica, fins als materials Triàsics del nucli, així com una estratigrafia mecànica ben descrita i una excel·lent preservació i afloració dels estrats de creixement que enregistraren el creixement del plec. Això proporciona una excel·lent base per poder comparar com la estratigrafia mecànica es comporta tant en el model com en la natura, i com la sedimentació sin-cinemàtica va influenciar l'evolució del plec.

R.7.1 CONFIGURACIÓ INICIAL I PARÀMETRES EXPERIMENTALS

El comportament de la massa de roca modelitzada és a grans trets elastoplàstic i sense fricció (Place and Mora, 2001; Finch et al., 2003, 2004; Hardy and Finch, 2005, 2007), una aproximació que ja s'ha emprat prèviament en altres estudis per modelitzar deformació fràgil en roques sedimentàries a l'escorça superior. La deformació de la seqüència sedimentària modelitzada es produeix en resposta a l'escurçament per subducció de la base del model a través d'una ranura localitzada al centre de la caixa, en la qual la meitat dreta del model es mou cap a l'esquerra a una velocitat continua de 0.001 m per unitat de temps (Fig. R14). S'ha emprat una densitat homogènia de 2500 kg m^{-3} per tota la massa de roca, un valor comú en la modelització de roques sedimentàries en l'escorça superior. La constant elàstica K és de 5.5 x 10^9 N m^{-2}. L'experiment va córrer durant 2 x 10^6 unitats de temps amb entrega de resultats cada 10^5 unitats (és a dir, cada 100 m d'escurçament). Això va proporcionar un control precís sobre l'evolució estructural del plec i sobre la variació de la deformació, així com una geometria dels estrats de creixement ben delimitada. El desplaçament total de l'experiment va ser de 2 km.

En el marc de treball de la modelització una *Lattice Unit* (LU) equival a 250 metres. El conjunt inicial de partícules conté 10245 elements, agrupats en

quatre subconjunts de radis diferents: 0.125, 0.1, 0.075 i 0.05 LU (és a dir, 31.25, 25, 18.75, 12.5 m, respectivament). Aquests elements estan distribuïts aleatòriament en una caixa rectangular tancada. Considerem aquestes dimensions adients, donat que proporcionen suficient resolució per modelitzar una estructura d'escala quilomètrica com el Pico del Águila, evitant la generació de plans preferents de debilitat i permetent per tant una localització de la deformació no predefinida. Després de la generació inicial del conjunt d'elements, aquests es deixen reposar fins que arriben a un equilibri estable i se'ls deixa compactar sota l'efecte de la gravetat durant 2 x 10^6 unitats de temps fins a obtenir una configuració inicial d'elements estable, ben empaquetada, que minimitza l'espai entre partícules. La configuració inicial resultant d'aquest procés de sedimentació i compactació mesura 12.5 km de llarg i aproximadament 1.25 km de gruix estratigràfic, simulant una massa de roca continua que pot deformar-se per trencament progressiu dels enllaços entre partícules (fracturació/falles) i moviment massiu de parelles d'elements sense trencament d'enllaços (plegament).

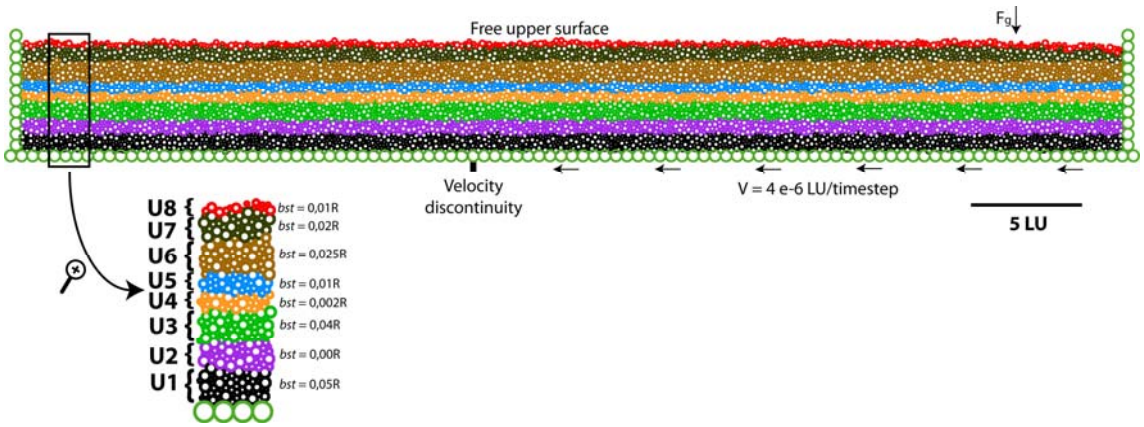

Fig. R14. Configuració inicial i condicions de contorn aplicades al model numèric d'elements discrets. EL conjunt inicial contenia 10245 elements de radi 31.25, 25, 18.75, i 12.5 m, posicionats aleatòriament dins de la caixa, la qual mesura 12.5 x 1.25 km. La massa de roca està composada de 32 capes inicialment horitzontals agrupades en vuit unitats de propietats mecàniques diferents. El desplaçament va ser de 0.001 m/unitat de temps. F_g correspon a la força de la gravetat.

La seqüència sedimentària sin-cinemàtica es va modelitzar afegint sediments incrementalment fins a un total de 11708 elements. La configuració inicial està formada per 32 capes horitzontals agrupades en unitats amb diferents propietats mecàniques per tal de crear una complexa estratigrafia mecànica (Fig. R14).

R.7.2 RESULTATS DE LA MODELITZACIÓ NUMÈRICA

L'evolució de la geometria i la deformació de cisalla del model es mostren a la Fig. R15.

Després d'un 4% d'escurçament (500 m; Fig. R15b) una petita estructura incipient, de poca amplitud, ha començat a formar-se sobre la discontinuïtat de velocitat (ranura al centre del model). Les unitats incompetents U2 i U4 mostren alta deformació de cisalla (abreujada com a "deformació" *sensu lato* a partir d'ara) tant en l'estructura com a certa distància de ella al llarg del model. La unitat més competent, U1, es troba ja molt deformada en el nucli de l'anticlinal. Les altres unitats pre-cinemàtiques mostren baixa deformació, lleugerament accentuada a la zona de l'anticlinal (Fig. R15b). Els estrats de creixement mostren gran deformació, tot i que variable, al llarg de l'estructura. Tanmateix, cal distingir dos tipus de deformació dins dels estrats de creixement: en primer lloc la deformació de cisalla deguda a la deposició i continua compactació de les unitats més recents (deformació restringida essencialment a les dues capes més superficials del conjunt; Fig. R15); en segon lloc la deformació mostrada per la pila sedimentària sin-cinemàtica deguda a l'escurçament i plegament de l'estructura. Un efecte de vora s'observa al límit dret del model degut al desplaçament de la paret de la caixa cap a l'esquerra. Després d'un escurçament del 8% (1000 m; Fig. R15c) l'estructura central ha crescut significativament, els flancs estan més inclinats i mostra una lleugera vergència cap a la dreta. S'observa disharmonia en el plegament: sota U4 s'han generat plecs menors, particularment entre U2 i U4 cap a la dreta del model. U1 mostra una complexa deformació al nucli de l'anticlinal. Per sobre de U4 la geometria de l'anticlinal es més suau, dibuixant un plec continu. Els estrats de

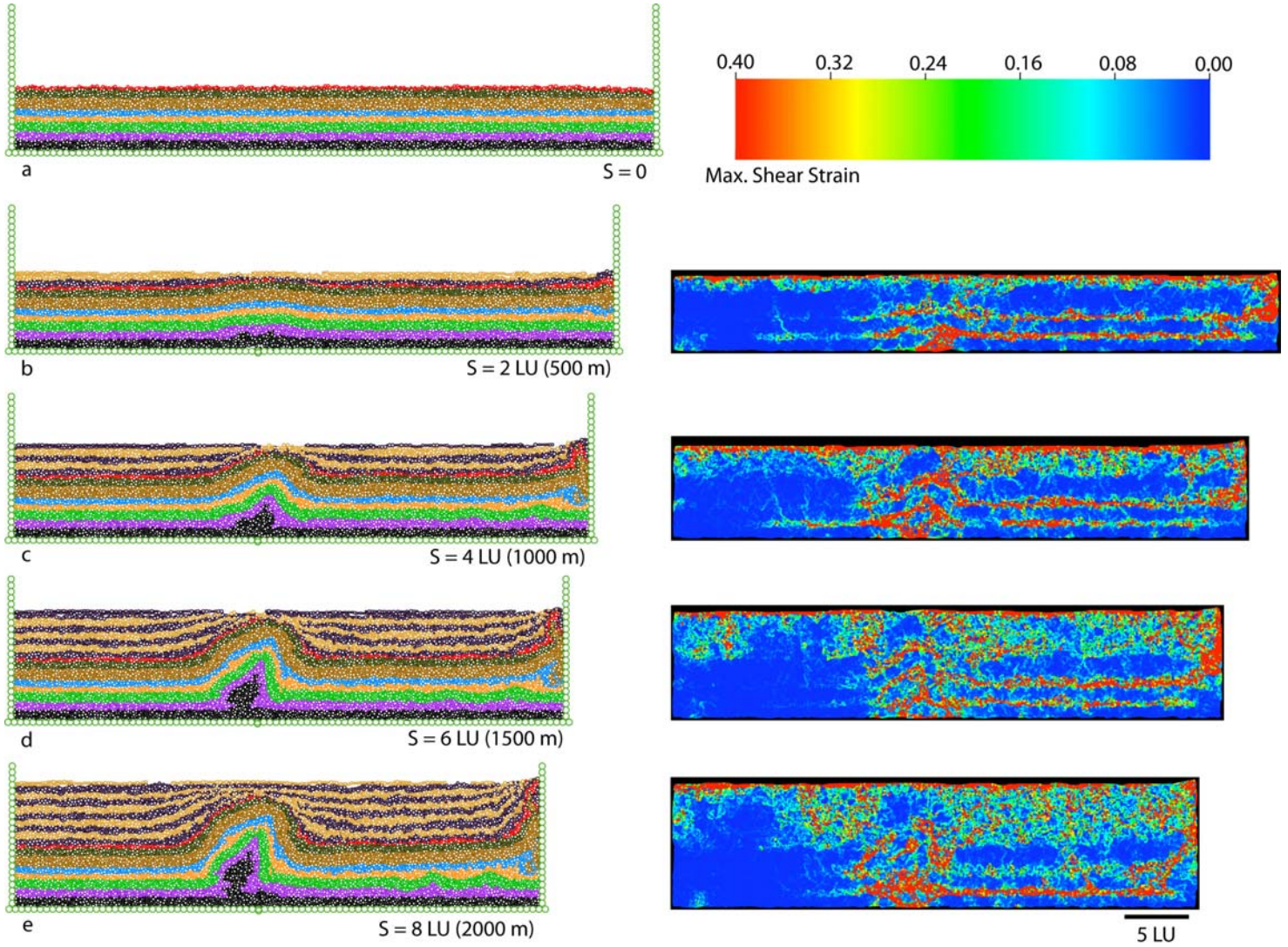
a
S = 0
0.40
0.32
0.24
0.16
0.08
0.00
Max. Shear Strain
b
S = 2 LU (500 m)
c
S = 4 LU (1000 m)
d
S = 6 LU (1500 m)
e
S = 8 LU (2000 m)
5 LU

Fig. R15. **(PÀGINA ANTERIOR)** Evolució del model numèric després de: a) 0m; b) 500 m; c) 1000 m; d) 1500 m; e) 2000 m d'escurçament. La columna de l'esquerra mostra l'evolució geomètrica de l'anticlinal, mentre que la columna dreta mostra la distribució de la deformació en cadascuna d'aquestes etapes. L'escala a dalt a la dreta mostra el rang de deformació considerat.

creixement mostren marcades diferències de gruix estratigràfic produint prismes sedimentaris que s'aprimen cap a la xarnera de l'anticlinal. En els estrats de creixement s'observa una deformació moderada a alta, amb un contrast distintiu de deformació localitzat a la base dels sediments sin-cinemàtics. Després d'un escurçament del 12% (1500 m; Fig. R15d) s'observa un clar engruiximent de les capes més incompetents a les zones de xarnera d'ambdós sinclinals associats a l'estructura central, així com una deformació molt complexa al nucli de l'anticlinal. En particular, U1 esdevé dramàticament deformada, mostrant una geometria de coll d'ampolla. Plecs menors creixen a U2 entre l'anticlinal i el límit dret del model. S'observa plegament disharmònic a la xarnera de l'anticlinal, amb grans contrastos en l'estil de plegament per sobre i per sota de U4. La major part de la deformació segueix concentrada en les unitats menys competents. Els estrats de creixement roten i s'aprimen cap al creixent anticlinal, exhibint una gran deformació interna. Després d'un escurçament del 16% (2000 m; Fig. R15e) el creixement vertical de l'anticlinal sembla aturar-se (els estrats de creixement cobreixen l'estructura) amb el plec estrenyent-se mitjançant rotació dels flancs. Malgrat això, el model mostra un desplaçament en la distribució de la deformació cap a la dreta, manifestat per la propagació del plegament des del límit dret i donant lloc a petits plecs de desenganxament que es generen sobre U2. En l'estructura central la deformació segueix concentrada al nucli, així com als flancs especialment en les unitats U4 i U5. Al nucli, U1 mostra una morfologia encara més accentuada de coll d'ampolla. En aquest estadi els estrats de creixement mostren un gruix màxim als sinclinals de 1.2 km, valor similar al descrit al camp a l'anticlinal del Pico del Águila.

R.8 RESTITUCIÓ GEOMECÀNICA 3D DE L'ANTICLINAL DEL PICO DEL ÁGUILA

La restitució geomecànica de l'anticlinal del Pico del Águila s'ha realitzat utilitzant un algoritme de Modelització d'Elements Finits (*Finite Element Modelling, FEM*), el qual considera propietats mecàniques de les roques per restituir l'estructura de l'anticlinal (el que s'ha anomenat recentment *restitució geomecànica*), en comptes de considerar qualsevol criteri de caire cinemàtic. En la majoria dels casos la cinemàtica d'una estructura és desconeguda o, si més no, no s'ha quantificat de forma precisa. D'aquesta manera la restitució geomecànica proporciona un resultat mecànicament estable basat en la geometria de l'estadi deformat i en les propietats mecàniques de les roques, tals com densitat, mòdul de Young i coeficient de Poisson (Maerten and Maerten, 2006; Guzofski et al., 2009).

R.8.1 METODOLOGIA I CONFIGURACIÓ INICIAL

La restitució seqüencial de l'anticlinal del Pico del Águila es va portar a terme amb el programa Dynel3D (igeoss. Maerten & Maerten, 2006). El codi implementat a Dynel3D està basat en un algoritme de tipus FEM, una tècnica de medis continus que permet l'estudi de la deformació natural basat en les propietats mecàniques de les roques. Malgrat que és un mètode estrictament elàstic, és adient per modelitzar el comportament d'estructures geològiques complexes tals com plecs i falles (Maerten & Maerten, 2006). Les unitats estratigràfiques es discretitzen en un conjunt d'elements (tetraedres) als quals se'ls hi assignen les propietats mecàniques. Les falles es representen per superfícies de contacte entre grups de tetraedres. Aquests elements tetraèdrics es deformen elàsticament en resposta a restriccions tals com forces aplicades o/i internes, desplaçaments i regions de contacte entre superfícies (falles). Les equacions de l'algoritme es resolen de forma iterativa i explícita, de forma que les forces es poden transmetre de node a node a través de tot el sistema fins que s'assoleix l'equilibri. La formulació de l'algoritme és doncs adient per modelitzar escenaris geològics complexos que comprenen diverses etapes de deformació,

com és el cas de la restitució estructural. A més, la solució explícita que proporciona l'algoritme és eficient i estable (Maerten & Maerten, 2006).

El model 3D del Pico del Águila es va utilitzar com a estadi deformat per la restitució. La reconstrucció dels estrats de creixement va esdevenir clau per poder establir una cronologia de la deformació a partir de la restitució de les diverses seqüències deposicionals (GS-I a GS-IV). La mida promig dels tetraedres (la resolució) va ser de 310 m per costat, un balanç raonable per representar una estructura d'escala quilomètrica sense excedir el límit de memòria permès per un ordinador personal estàndard. Malgrat això, aquest valor de resolució implica que certs cossos de dimensions inferiors no puguin ser representats o hagin de ser simplificats en cossos de dimensions superiors. És el cas de les unitats del Cretaci superior i el Garumnià, que tenen un gruix estratigràfic molt per sota de la resolució dels tetraedres, i que van haver de ser fusionades en una única unitat mecànica anomenada *Garumnià-Cretaci*, caracteritzada per unes propietats mecàniques promig de les dues unitats inicials. De manera similar, les vuit falles internes de l'anticlinal es caracteritzen per un salt de falla de desenes de metres, valor molt inferior a la resolució dels tetraedres. Aquestes falles, per tant, no van considerades en la restitució de l'estructura.

Com ja s'ha esmentat, l'algoritme que utilitza Dynel3D necessita diverses propietats mecàniques de les roques, que han de ser indicades prèviament a la restitució. Donat que aquestes propietats (densitat, mòdul de Young i coeficient de Poisson) varien amb la litologia al llarg de la seqüència estratigràfica, s'han establert diferents valors en funció de la litologia predominant a cadascuna de les unitats, els quals es resumeixen en la Taula 1.

R.8.2 RESULTATS DE LA RESTITUCIÓ GEOMECÀNICA

S'han considerat cinc estadis de restitució, d'acord amb la reconstrucció dels sostres de les quatre seqüències deposicionals GS-I, GS-II, GS-III i GS-IV, i del sostre de la Formació Guara (Fig. R16). A més de la geometria, es va obtenir també la distribució de la deformació de cisalla (abreviada "deformació" sensu

lato a partir d'ara) per cadascun dels estadis de la restitució, per tal d'entendre la evolució de la deformació a l'estructura (Fig. R17).

La restitució del sostre de la seqüència GS-IV (36.6 Ma) elimina la major part del basculament associat a l'emplaçament de l'encavalcament frontal sudpirinenc (Fig. R16 a i b). A més, s'observa una rotació d'eix vertical d'uns 15º. La deformació es distribueix de forma heterogènia arreu del model (Fig. R17b). La GS-IV mostra una deformació moderadament alta distribuïda al llarg dels sinclinals associats, i que s'incrementa cap a l'anticlinal (els valors més alts coincideixen amb les àrees en les que la GS-IV és més prima; Fig. R17b). La resta de les GS mostren gran deformació a la xarnera dels sinclinals. A la seqüència pre-plegament les unitats del Garumnià-Cretaci i del Triàsic mostren una gran deformació a les zones de xarnera de l'anticlinal i dels sinclinals associats. La Formació Guara mostra una deformació baixa a moderada al llarg d'ambdós flancs, i gran deformació a la xarnera dels sinclinals (Fig. R17b).

La GS-III (37.17 Ma) és la primera seqüència restituïda que no cobreix tot l'anticlinal. La seva restitució dóna com a resultat un modest decreixement de la immersió de l'anticlinal d'uns 4º (Fig. R16c) i una rotació en el sentit de les busques d'uns 2º. S'observa deformació baixa a moderada a la xarnera de l'anticlinal a la GS-III, i baixa deformació en la resta de les GS. La deformació més important es localitza a la Formació Guara, concretament al sinclinal oriental i al llarg del flanc occidental (Fig. R17c). La unitat Garumnià-Cretaci mostra una deformació moderada a alta i un marcat lliscament de capa sobre capa respecte les unitats subjacent i suprajacent. El Triàsic mostra deformació moderada a alta, particularment concentrada a la meitat de la seqüència en les zones de xarnera de l'anticlinal i els sinclinals.

Després de restituir la GS-II (37.74 Ma) la immersió del plec és pràcticament negligible (Fig. R16d) i l'estructura ha rotat 10º addicionals. La deformació (Fig. R17d) és superior respecte l'estadi anterior, particularment a la zona del tancament periclinal de l'anticlinal. La Formació Guara va acomodar una deformació moderada al flanc oest i a la cresta de l'anticlinal, i alta deformació a la xarnera del sinclinal oriental (Fig. R17d). La unitat mecànica Garumnià-Cretaci mostra alta deformació en tota l'estructura a excepció de la

cresta de l'anticlinal. El Triàsic mostra una deformació poc heterogènia i moderada a alta.

La restitució de la GS-I (40.04 Ma) deixa veure ja la geometria de la Formació Guara a la cresta de l'anticlinal (Fig. R16e). S'observa una gran deformació en les unitats pre-plegament, mostrant un anticlinal ben desenvolupat, encara amb molta deformació acumulada. No s'observa una rotació d'eix vertical significativa respecte l'estadi anterior. La deformació a la GS-I es distribueix de forma heterogènia, mostrant una deformació baixa a moderada a la zona de xarnera dels sinclinals i al llarg dels flancs que dibuixen una geometria en *onlap* sobre la Formació Guara (Fig. R17e). La Formació Guara mostra baixa deformació en la cresta de l'anticlinal i una deformació moderada en el tancament periclinal i al llarg dels flancs. La unitat Garumnià-Cretaci mostra una deformació particularment alta a la xarnera de l'anticlinal i al llarg dels flancs. El Triàsic mostra una deformació moderada a alta als sinclinals i al llarg del desenganxament, i una baixa deformació a la cresta de l'anticlinal (Fig. R17e).

Finalment, la restitució de la Formació Guara (41.52 Ma) implica el desplegament de l'estructura així com una rotació addicional d'uns 6º (Fig. R16f). La rotació d'eix vertical varia entre les unitats de la sèrie pre-plegament, mostrant una rotació lleugerament superior de cada unitat respecte a la unitat immediatament subjacent (la rotació és lleugerament superior a mida que es puja a la sèrie; Fig. R16f). La deformació varia de molt baixa a molt alta, amb valors baixos i moderats arreu del model, i pics de deformació molt alta concentrats a la xarnera dels sinclinals i localment a la cresta de l'anticlinal (Fig. R17f). La unitat Garumnià-Cretaci i el Triàsic mostren valors de deformació més alts a la xarnera dels sinclinals(Fig. R17f). El sostre i la base de les unitats mostren valors de deformació lleugerament més baixos al llarg dels contactes amb les altres unitats, i un significatiu lliscament de capa sobre capa entre elles.

Taula 1. Propietats mecàniques emprades per restituir l'anticlinal del Pico del Águila.

Unitat	Litologia Predominant	Mòdul de Young (Pa)	Coeficient de Poisson	Densitat (Kg/m3)
GS-IV*	Gresos	2.2 e+10	0.24	2480
GS-III*	Gresos margosos	2.2 e+10	0.24	2480
GS-II*	Margues	2.8 e+10	0.14	2530
GS-I*	Margues	2.8 e+10	0.14	2530
Guara	Calcàries	4.8 e+10	0.25	2500
Garumnià-Cretaci	Lutites- Calcàries	2.8 e+10	0.14	2530
Triàsic	Calcàries dolomítiques	4.8 e+10	0.25	2500

Aquests són valors promig per cada tipus de roca, i parcialment basats en indicacions de camp.

* GS: Estrats de Creixement de les Formacions Arguis i Belsué-Atarés.

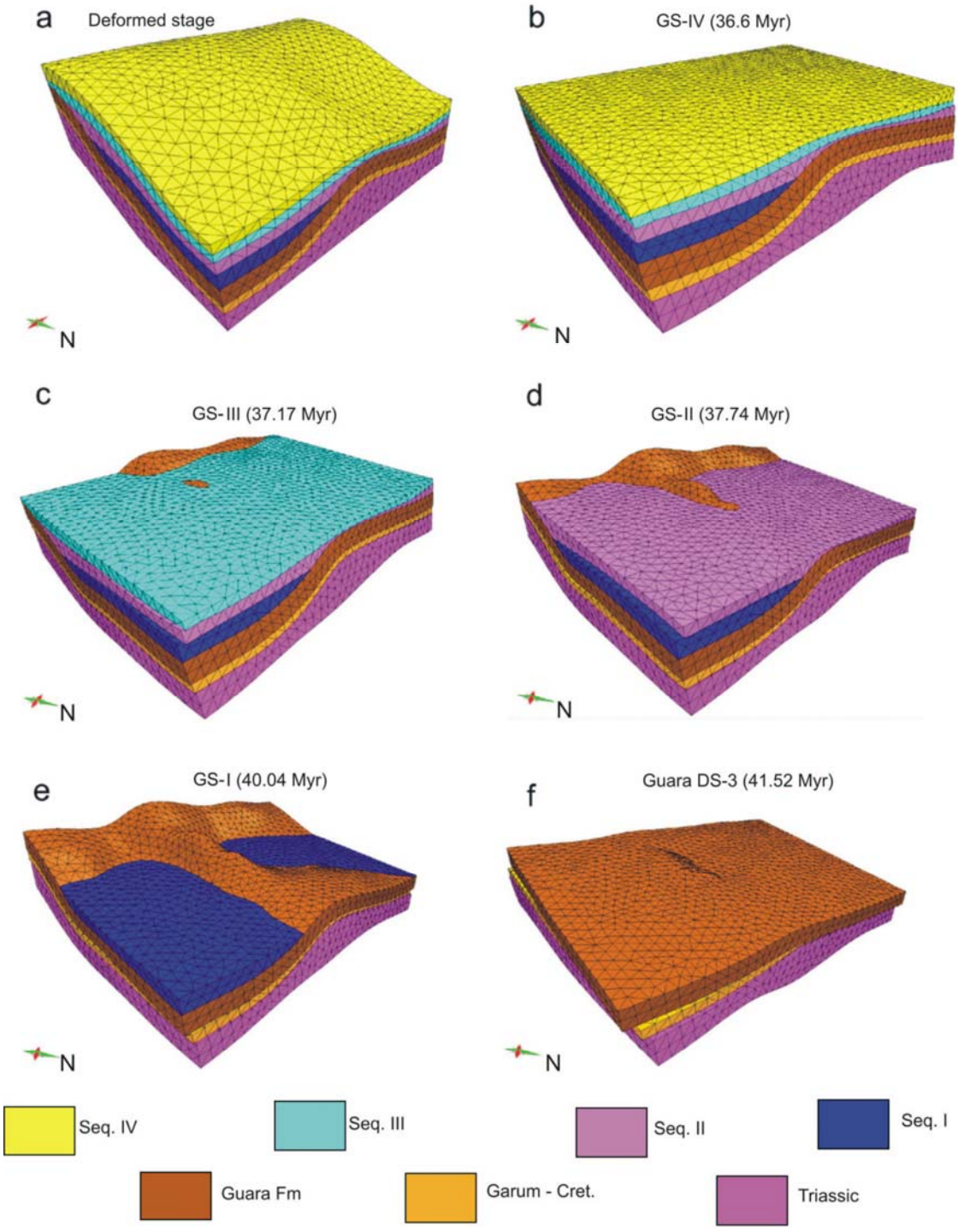

Fig. R16. Diferents estadis de la restitució geomecànica seqüencial de l'anticlinal del Pico del Águila: a) estadi deformat; b) restitució de la GS-IV (36.6 Ma); c) restitució de la GS-III (37.17 Ma); d) restitució de la GS-II (37.74 Ma); e) restitució de la GS-I (40.04 Ma); i f) restitució de la Formació Guara (41.52 Ma).

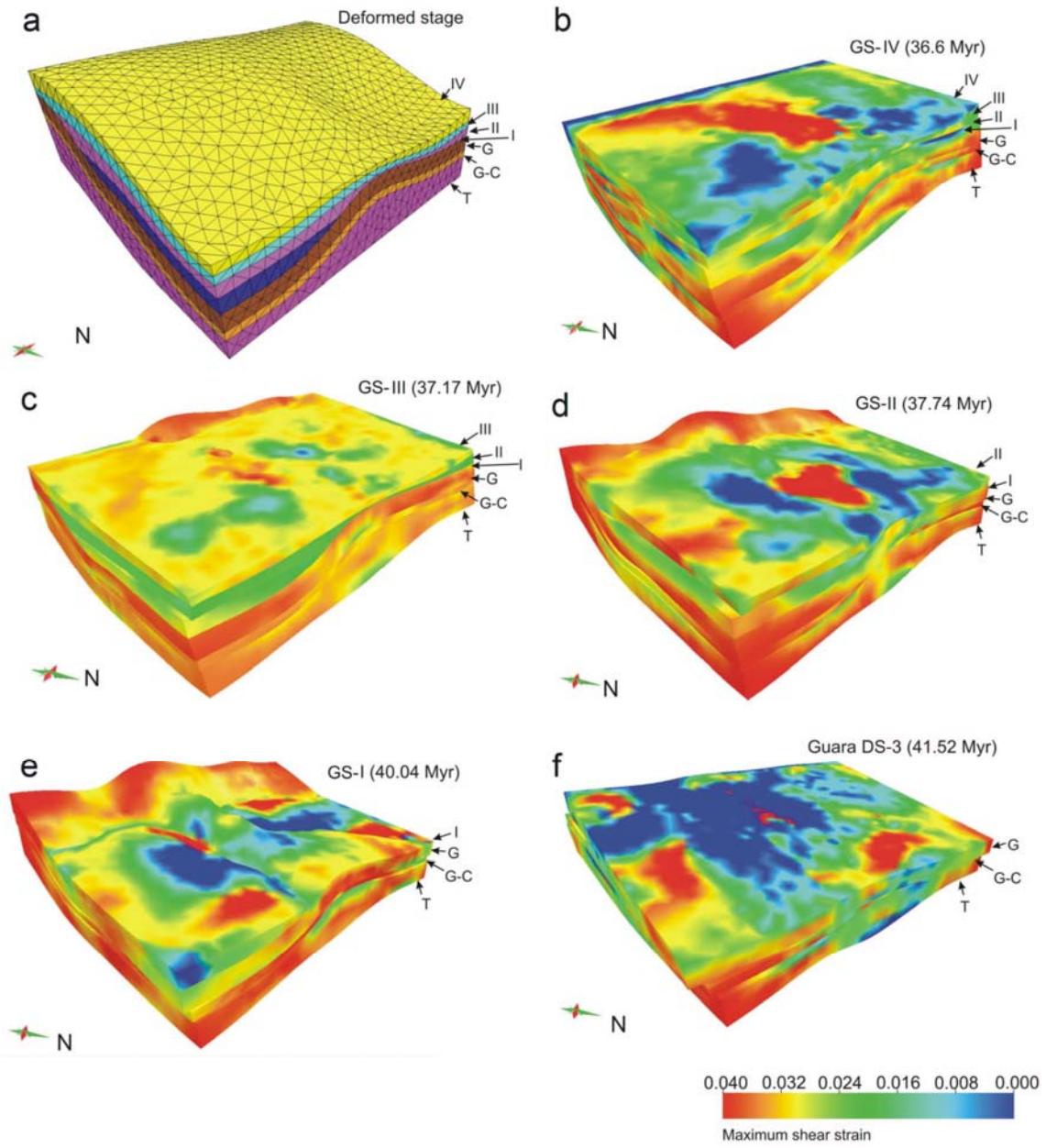

Fig. R17. Distribució de la deformació de cisalla entre els estadis de restitució mostrats a la Fig. R16: a) geometria de l'estadi deformat (com a referència); b) restitució de la GS-IV (36.6 Ma); c) restitució de la GS-III (37.17 Ma); d) restitució de la GS-II (37.74 Ma); e) restitució de la GS-I (40.04 Ma); i f) restitució de la Formació Guara (41.52 Ma). T: Triàsic; G-C: Garumnià-Cretaci; G: Guara; I: GS-I; II: GS-II; III: GS-III; IV: GS-IV.

R.9 RESUM DELS RESULTATS OBTINGUTS I DISCUSSIÓ

A continuació es presenta un resum dels resultats obtinguts mitjançant les diferents tècniques de modelització així com una discussió sobre els avantatges, inconvenients i limitacions de cadascuna d'elles, i la seva aportació al coneixement de l'evolució estructural de l'anticlinal del Pico del Águila.

R.9.1 BENEFICIS I DESAVANTATGES DE LES TÈCNIQUES EMPRADES

Cadascun dels models presentats proporciona nous coneixements sobre l'evolució estructural de l'anticlinal del Pico del Águila, millorant així el coneixement sobre la geologia de les Sierras Exteriores Aragonesas. Cadascun dels models va ser específicament dissenyat per testar certs paràmetres observats a la natura, incorporant les diferents contribucions al model d'evolució estructural. Tanmateix, cal tenir presents les limitacions de cadascuna de les tècniques de modelització per tal d'escollir el mètode més adient per un propòsit concret. D'aquesta manera es pot avaluar el resultat de cada model, extreure'n l'aportació neta i evitar així errors en la interpretació dels resultats.

En aquest sentit, la modelització analògica va ser una tècnica adient per modelitzar les heterogeneïtats del nivell de desenganxament basal a escala regional: va permetre una fàcil visualització en 3D de la resposta del model a la deformació en termes de avenç i aixecament diferencial de la cobertora sedimentària, estil estructural i relleu entre els diferents dominis estructurals. Els models analògics han representat encertadament els importants canvis d'estil estructural observats a escala regional. Els contrastos mecànics entre la sorra seca i la silicona van modelitzar encertadament l'efecte dels canvis laterals entre les fàcies Keuper i Muschelkalk al nivell de desenganxament Triàsic. Van reproduir eficientment un major aixecament d'orientació N-S (paral·lel doncs a la direcció d'escurçament) de les àrees desenganxades sobre un desenganxament friccional (àrees HF) i un major avenç del front de deformació en àrees desenganxades sobre un desenganxament dúctil (àrees LF). Per contra, el fet de treballar amb sorra seca i silicona no proporciona una precisió suficient

en les propietats mecàniques de la cobertora per tal de poder modelitzar la seva complexitat interna: els grans contrastos de comportament mecànic descrits en la columna estratigràfica aflorant, en la que diverses unitats de comportament dúctil hi són presents i controlen el creixement de l'estructura (Fig. R2 i R15), no poden ser modelitzats amb l'ús d'uns pocs materials diferents. Per tal de modelitzar la complexitat interna de la cobertora, doncs, caldria una important quantitat de materials anàlegs diferents i, tot i així, les propietats mecàniques disponibles estarien limitades al nombre de materials diferents emprats en la modelització. Per aquest motiu, es va preferir optar per la Modelització d'Elements Discrets per investigar la importància de l'estratigrafia mecànica i els estrats de creixement en l'evolució del Pico del Águila.

La Modelització d'Elements Discrets (abreviada DEM a partir d'ara), doncs, permet un control precís de la resposta mecànica de cada unitat i, per tant, dóna la possibilitat de configurar una estratigrafia mecànica complexa amb la que modelitzar un gran nombre d'escenaris geològics. Això fa que la DEM sigui un mètode ideal per explorar en detall l'evolució dels anticlinals N-S de les Sierras Exteriores Aragonesas. El mètode permet seguir l'evolució de cadascuna de les partícules que conformen la massa de roca del model mitjançant paràmetres físics tal com els vectors de desplaçament, velocitat i acceleració, posició instantània, etc, a partir dels quals se'n deriva la distribució de la deformació al model. Els models presentats en aquesta Tesi han contribuït amb nous coneixements sobre com la deformació es acomodada de manera diferent en funció del comportament mecànic de cada unitat, portant a importants contrastos en estil estructural entre unitats adjacents de una mateixa cobertora sedimentària. Els models numèrics permeten un control precís dels paràmetres introduïts al model. En els models presentats és de gran importància el control del gruix estratigràfic de les unitats pre-plegament (gruix constant, configurat prèviament a la modelització), i encara més dels estrats de creixement, donat que el mètode és sensible a canvis en l'evolució del sistema depenent del gruix de les unitats i de model en general. Tanmateix, la DEM no contempla la imposició al model de criteris cinemàtics previs. La DEM és una tècnica de modelització d'avenç en la que les propietats físiques de les partícules, les dimensions inicials de la caixa i el gruix estratigràfic són els únics paràmetres

introduïts. En aquest sentit la DEM manté certes similituds amb la modelització analògica, però permet un control més acurat de les propietats mecàniques i una supervisió instantània dels paràmetres cinemàtics i de la distribució de la deformació en qualsevol de les partícules del model. En contrast, els models numèrics presentats són estrictament 2D, donant una representació parcial de la estructura modelitzada (comparable a un tall geològic E-W de l'anticlinal). Malgrat que ja existeixen experiments DEM en 3D (Carmona et al., 2008) aquests són encara molt costosos en termes de consum de temps, especialment per modelitzar escenaris geològics complexos com els anticlinals N-S de les Sierras Exteriores. Per aquest motiu, una aproximació 2D com la presentada en aquesta Tesi ha estat adient per investigar els papers de l'estratigrafia mecànica i els estrats de creixement en una estructura com l'anticlinal del Pico del Águila.

Com ja s'ha dit, el Pico del Águila és certament una estructura 3D, amb un excel·lent grau de preservació dels estrats de creixement. La interferència estructural entre l'anticlinal N-S i l'encavalcament frontal sudpirinenc (E-W) crea doncs una estructura amb una complexa evolució cinemàtica que resulta difícil de representar mitjançant mètodes bidimensionals. Aquests factors motivaren la reconstrucció tridimensional de l'anticlinal i els estrats de creixement, per tal de poder establir un model d'evolució 3D en el que es tingués un control cronològic de la deformació. L'excel·lent grau d'aflorament, preservació i la fàcil accessibilitat van fer del Pico del Águila un cas ideal per portar a terme l'adquisició de dades al camp i una cartografia acurada de traces geològiques. Això va permetre una també acurada reconstrucció en 3D tant de la seqüència pre-plegament com dels estrats de creixement, servint així de punt de partida per realitzar una restitució geomecànica amb la qual conèixer l'evolució estructural de l'anticlinal. Basat en les propietats mecàniques de les roques, doncs, l'algoritme implementat a Dynel3D va suposar una alternativa per portar a terme una restitució en 3D sense necessitat de invocar a criteris cinemàtics complexos dels quals no se'n té un acurat coneixement. Així doncs, el major benefici d'utilitzar la restitució geomecànica és que permet restituir una estructura introduint propietats reals i mesurables de les roques, sense imposar criteris cinemàtics previs, dels quals moltes vegades no se'n té un coneixement quantitatiu. La densitat, el mòdul de Young, el coeficient de Poisson o la

porositat són propietats que es poden mesurar en anàlisis mecànics de materials al laboratori o, altrament, es poden obtenir valors generals publicats en taules de propietats mecàniques per diferents materials comuns a l'escorça terrestre. En qualsevol cas, es poden aconseguir fàcilment valors mesurats o publicats de les propietats mecàniques dels materials i portar a terme una restitució que proporciona un resultat físicament raonable, mecànicament estable, i que està d'acord amb l'evolució cinemàtica derivada a partir d'altres mètodes.

Els principals desavantatges d'aquest mètode estan directament relacionats amb les limitacions tècniques de l'ordinador. L'algoritme implementat a Dynel3D pot requerir una gran quantitat de memòria disponible de l'ordinador, depenent de la resolució desitjada pel model (és a dir, de la mida dels tetraedres que discretitzen la superfície). Això significa que per una estructura d'uns pocs quilòmetres com el Pico del Águila, un ordinador estàndard permet una resolució d'uns pocs centenars de metres. Això fa d'aquest mètode una opció poc recomanable per estudiar en detall i a aquesta escala cossos geològics que es troben per sota del límit de la resolució del model. Per altra banda, l'algoritme es basa en l'ús de les lleis de l'elasticitat per restituir grans quantitats de deformació no recuperable (inelàstica). Aquest fet també implica certes limitacions, particularment quant a magnitud de la deformació es refereix. L'ús d'un mètode elàstic proporciona valors de deformació que són notablement inferiors que els que es puguin predir mitjançant altres tècniques (p.ex. DEM) i que els valors obtinguts en experiments de camp o laboratori. Per tant, aquest mètode és adient per predir patrons o distribucions de deformació, mecanismes de plegament i dominis potencials de fracturació més que no pas per predir magnituds de deformació o/i estructures mesoscòpiques com patrons o orientacions de fractures en el si de l'estructura.

R.9.2 VALIDACIÓ I INTEGRACIÓ DE LES DIFERENTS TÈCNIQUES DE MODELITZACIÓ

Tots els experiments presentats en aquest treball han estat, d'una manera o altra, basats en observacions, descripcions i dades adquirides al camp. Essent

ja conscients dels avantatges i limitacions de cadascun dels mètodes es pot tenir una imatge més clara de la contribució de cadascun dels models, i ser capaç de donar una resposta raonada quan es qüestiona l'ús d'un o un altre determinat mètode. Validar i integrar els resultats de diferents tècniques, mètodes o aproximacions significa, per tant, reunir les contribucions de cadascun dels models per construir un model unificat d'evolució estructural, però també cobrir els forats que cada tècnica deixa al descobert, de manera que els diferents mètodes es complementen els uns als altres.

En aquest sentit els models analògics van proporcionar nous coneixements a escala regional, donant resposta sobre els processos que van ocasionar la generació de les estructures inicialment arquejades i obliqües, i que finalment resultaren en els anticlinals N-S de les Sierras Exteriores. La modelització es va basar en observacions de camp que indicaven una escassa presència de les fàcies Keuper al nucli dels anticlinals N-S, i va replicar molts dels trets de l'anticlinal a la natura: major aixecament N-S associat a l'emplaçament d'un encavalcament d'orientació E-W en àrees amb poca o cap presència de nivell de desenganxament dúctil, un major avenç del front de deformació en àrees entre anticlinals N-S, desenvolupament d'aquests anticlinals en el bloc superior de l'encavalcament frontal i mostrant una immersió cap a l'orogen, rotació d'eix vertical del bloc superior de l'encavalcament a les zones on els plecs N-S es desenvolupen i morfologia ondulada del front d'encavalcament (Figs. R12 i R18).

Tanmateix, la sorra seca no és un material adient per modelitzar plecs estret i de flancs altament inclinats com els anticlinals N-S de les Sierras Exteriores Aragonesas, els quals es caracteritzen per una estratigrafia mecànica complexa en la que les propietats mecàniques varien al llarg de la columna paral·lelament a la litologia (Figs. R12 i R14). En canvi, els models numèrics d'elements discrets van satisfer aquesta limitació i van reproduir l'estil estructural del Pico del Águila després de configurar una estratigrafia mecànica que va simular la seqüència descrita al camp. La manera diferent en la que cada unitat va acomodar la deformació va ser replicada pels models numèrics: falles penetratives i alta deformació interna en les unitats inferiors van cohabitar amb un plegament més suau en les unitats superiors, al mateix temps que els estrats

de creixement van acomodar gran quantitat de deformació i van equilibrar l'anticlinal contra les inestabilitats gravitacionals (Fig. R15). El nivell de desenganxament intern va actuar com una barrera, permetent que les unitats superiors es pleguessin mentre les inferiors concentraven molta més deformació mitjançant falles, deformació interna i plegament més intens. Aquests experiments ens van proporcionar un millor coneixement sobre com es comportà l'estratigrafia de les Sierras Exteriores en resposta a l'escurçament de l'orogènia alpina, i com múltiples mecanismes de plegament poden tenir lloc simultàniament en funció de les propietats mecàniques de cadascuna de les unitats estratigràfiques implicades.

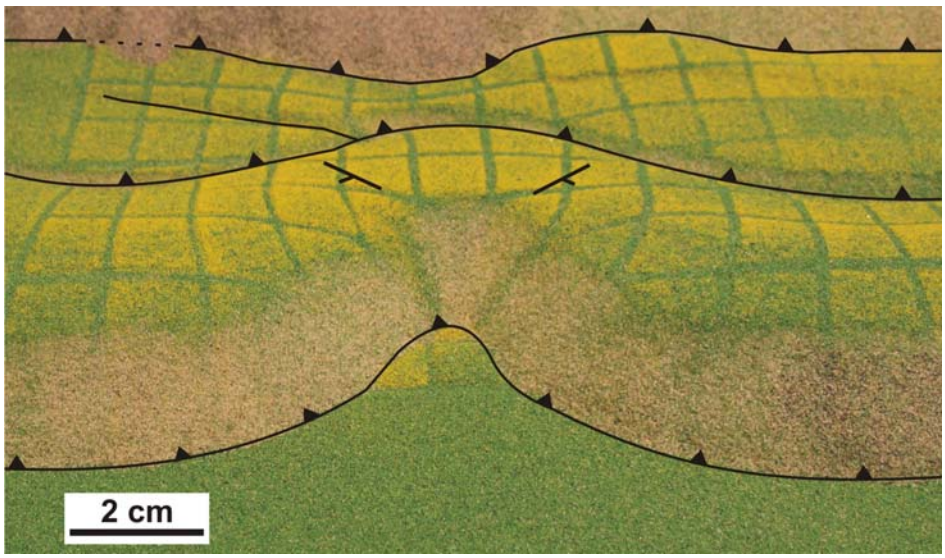

Fig. R18. Fotografia de detall d'una estructura perpendicular a l'orogen formada en el model SExt13 (no presentat en aquesta secció). El front d'encavalcament es caracteritza per una morfologia ondulada en la que la es generen anticlinals perpendiculars a les zones de la cobertora desenganxades sobre nivells friccionals (sorra).

Malgrat això, l'entorn 2D dels models numèrics no va donar resposta sobre altres processos cinemàtics ben documentats al Pico del Águila i que impliquen un estudi tridimensional, com són la rotació d'eix vertical de l'anticlinal, la seva relació amb l'encavalcament frontal sudpirinenc i amb les seves estructures associades. L'efecte del lliscament capa sobre capa (*flexural slip*) tampoc es va investigar en aquests models, essent aquest un mecanisme de

plegament important descrit a l'àrea d'estudi. Aquestes limitacions van ser superades mercès a la reconstrucció i restitució geomecànica tridimensional del Pico del Águila, que va afegir la tercera dimensió, va validar i complementar l'evolució estructural i la resposta mecànica predites pels models analògics i numèrics. La restitució va predir de forma independent i sense cap criteri cinemàtic imposat una rotació d'eix vertical de 33º, validant així la rotació ja descrita per estudis paleomagnètics previs (Pueyo et al., 2002; Rodríguez-Pintó et al., 2008) i pels models analògics (Vidal-Royo et al., 2009). Així mateix, la restitució va evidenciar també una diferent evolució de la sedimentació i l'aixecament entre els flancs, així com la incorporació del mecanisme de lliscament de capa sobre capa tal com s'ha descrit al camp (Fig. R16).

Tal com ja havien suggerit els models numèrics 2D, múltiples mecanismes de plegament es van descriure produint-se simultàniament en diferents unitats, depenent de les propietats mecàniques de cadascuna d'elles. A més, la restitució va posar de manifest que també es produeixen una multitud de mecanismes de plegament simultàniament dins d'una mateixa unitat, depenent del domini estructural del plec en el que es trobi. Aquesta combinació de mecanismes de plegament en diferents unitats i dominis estructurals dóna lloc a una complexa distribució de la deformació a l'estructura, en la que les propietats mecàniques de les unitats causaran que la deformació es concentri en un o altre domini i, per tant, que es deformin donant lloc a un determinat estil estructural (Fig. R17).

Per altra banda, les limitacions associades a la restitució geomecànica realitzada amb Dynel3D ja han estat esmentades prèviament. La falta de informació associada al límit de resolució dels tetraedres queda parcialment coberta pels models numèrics 2D, els quals informen de una resposta mecànica diferent per cadascuna de les unitats modelitzades. Les limitacions associades a l'ús d'un model elàstic per restituir grans quantitats de deformació inelàstica (no recuperable) es solucionen restituint i sumant petits increments de deformació, tot incloent l'efecte de les falles, els nivells de desenganxament i el lliscament de capa sobre capa. D'aquesta manera, es requereix que cada volum es restitueixi elàsticament, però a trets generals el model experimenta deformacions permanents i finites que es manifesten per mitjans de

desplaçaments de falles, desenganxaments i lliscaments de capa sobre capa (Maerten and Maerten, 2006, i Guzofski et al., 2009 que utilitzen una tècnica similar de restitució).

En general, cadascun dels mètodes de modelització presentats en aquesta Tesi afronta un nou interrogant de l'evolució estructural dels anticlinals N-S de les Sierras Exteriores, aportant nous coneixements que estan d'acord amb les observacions fetes al camp i porten un pas més enllà els aspectes que romanien descoberts per altres tècniques. En altres paraules, els models presentats contribueixen amb nous aspectes sobre la geologia de les Sierras Exteriores Aragonesas, validen els resultats obtinguts mitjançant altres mètodes i estudis, i integren part de un model unificat i més robust sobre la historia geològica de les Sierras Exteriores Aragonesas (Fig. R19).

R.9.3 L'ANTICLINAL DEL PICO DEL ÁGUILA: MODEL INTEGRAT D'EVOLUCIÓ ESTRUCTURAL

Els resultats dels diferents models presentats en aquesta Tesi, combinats amb els estudis previs que s'han portat a terme a la regió en diferents disciplines, ens ha permès presentar un model integrat d'evolució estructural per l'anticlinal del Pico del Águila.

L'anticlinal del Pico del Águila és un plec de desenganxament sobre una complexa geometria irregular de fàcies Muschelkalk i Keuper (Triàsic mig i superior, respectivament).

Prèviament a la deposició de la cobertora Cretàcica-Terciària l'àrea ja estava caracteritzada per una complexa estructura i una llarga història geològica. D'acord a les reconstruccions paleogeogràfiques (López-Gómez et al., 2002; Castillo-Herrador, 1974; Jurado, 1990; Salvany, 1990) la regió es localitzava en un alt de la conca extensional Triàsica, en el qual va tenir lloc una molt baixa taxa de sedimentació durant el Triàsic superior. Aquesta posició estructural va influenciar el baix i irregular gruix estratigràfic de les fàcies Keuper (formades per lutites vermelles i capes d'evaporites) observades a l'àrea

i el complex pas lateral amb les fàcies pre- i sin-extensives del Muschelkalk (fàcies M2: lutites, margues i evaporites; M3: dolomies i calcàries dolomítiques) (Fig. R19a). A més, el patró estructural al Triàsic superior es presumeix complex, i la fracturació penetrativa que caracteritza aquestes unitats avui dia es creu parcialment heretada del patró estructural d'edat Triàsica. Aquest marc geològic tan complex va donar com a resultat un substrat Triàsic mecànicament irregular i heterogeni, a sobre del qual la cobertora Cretàcica-Terciària es va dipositar.

Va ser fa uns 42.67 Ma (Lutecià superior) (Poblet & Hardy, 1995) quan l'anticlinal del Pico del Águila va començar a créixer. Donades les heterogeneïtats mecàniques descrites al desenganxament Triàsic, l'anticlinal es va generar formant un alt angle (entre 69º i 57º, depenent de quin valor de rotació total es prengui) respecte la tendència estructural pirinenca E-W (Fig. R19b). La cobertora sedimentària va experimentar un major aixecament d'orientació NNW-SSE a les àrees amb menor gruix de fàcies Keuper (baixa proporció de gruixos entre la cobertora i el desenganxament dúctil), formant un baix angle amb la direcció de transport tectònic dels Pirineus (aproximadament N-S). Aquests grans contrastos mecànics en el desenganxament basal van produir també la rotació d'eix vertical en sentit de les busques, causant que el front de deformació avancés a una velocitat diferent en funció de la naturalesa mecànica del nivell basal de desenganxament Triàsic en diferents àrees. Donada la complexitat mecànica de la cobertora sedimentària, al llarg de la qual s'ha descrit una resposta mecànica heterogènia, l'escurçament N-S va ser acomodat per plegament en comptes de generar rampes d'encavalcament obliqües, formant un petit plec de desenganxament incipient a sobre del qual es dipositaven sediments carbonàtics en un ambient de plataforma marina poc profunda (seqüència deposicional 3 de la Formació Guara).

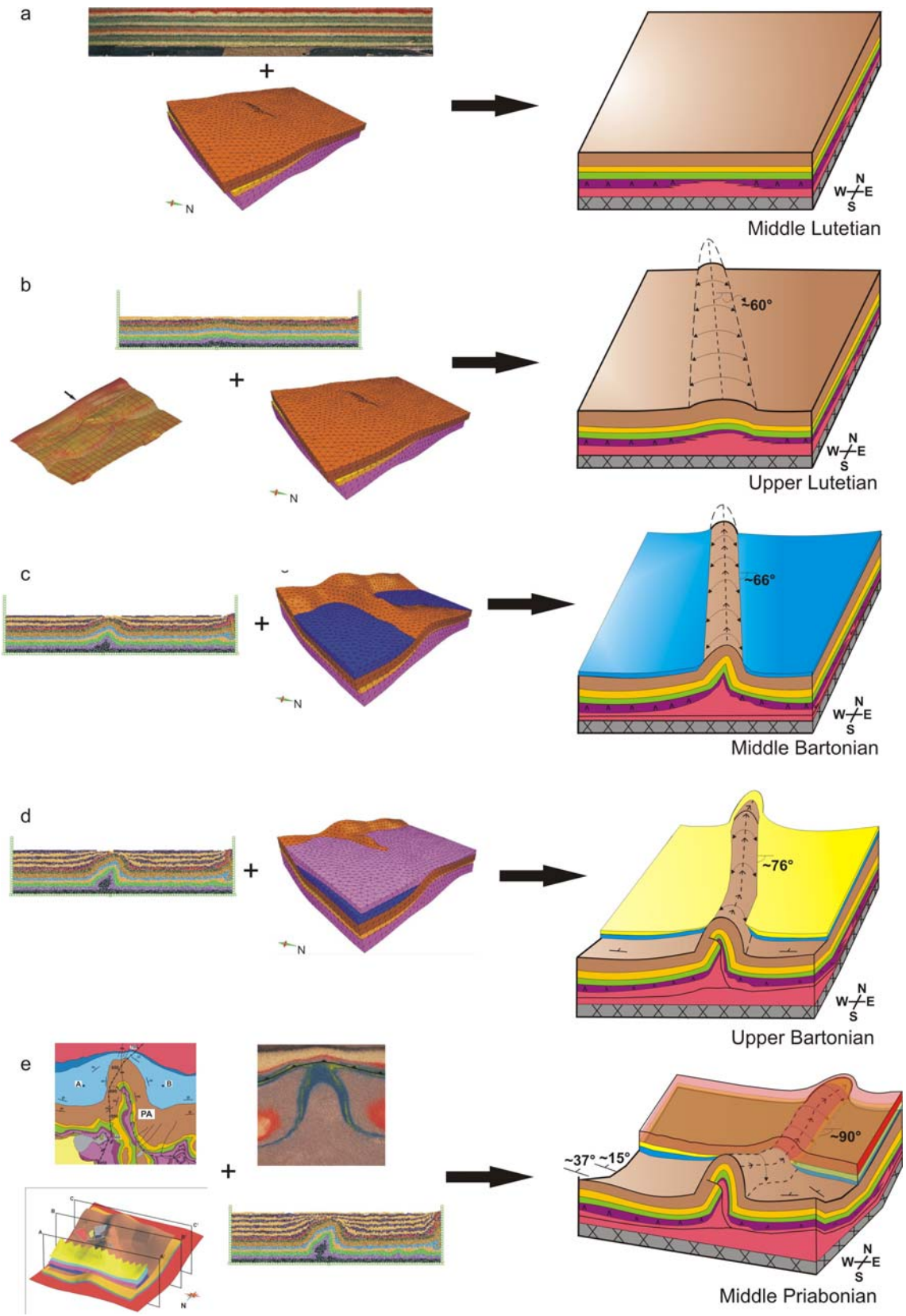

Fig. R19. Blocs - diagrama resumint l'evolució estructural de l'anticlinal del Pico del Águila tal com s'ha deduït a partir dels resultats de la modelització, de la reconstrucció 3D i dels estudis previs sobre la regió: a) estadi no deformat (Lutecià mig); b) Lutecià superior, inici de la deformació; c) Bartonià mig, deposició de la GS-I; d)Bartonià superior, deposició de la GS-II; e) Priabonià mig, deposició de la Formació Campodarbe (post-plegament), cessament de la deformació.

Fa aproximadament 41.52 Ma es va produir una transició brusca d'ambient sedimentari, passant d'una plataforma carbonatada poc profunda a un ambient transicional de talús, començant la deposició de les margues blaves i azoiques, riques en glauconita, de la GS-I de la Formació Arguis. La deposició d'aquests materials va anar acompanyada d'una gran taxa d'aixecament del plec, molt superior a la taxa de sedimentació. Això va resultar en la formació de geometries en *onlap* i en un aprimament dels materials de la GS-I sobre els flancs de l'anticlinal definits per la seqüència 3 de la Formació Guara, que van romandre descoberts sense que els sediments de la GS-I assolissin la cresta de l'anticlinal (Fig. R19c). Aquest gran aixecament, la creació d'espai disponible per a la sedimentació i el cicle transgressiu que va caracteritzar la deposició de les Formacions Guara i Arguis (Millán et al., 1994; Castelltort et al., 2003) van controlar el canvi de fàcies sedimentàries que hi ha entre les calcàries de plataforma soma de la Formació Guara i les margues de talús de la Formació Arguis. En aquest temps i fins fa uns 40.04 Ma la taxa de sedimentació va créixer progressivament. El front d'encavalcament sudpirinenc va començar a generar-se, afegint un lleuger basculament de l'anticlinal cap al nord (Fig. R19c).

Fa uns 40.04 Ma va donar-se un canvi en l'ambient deposicional que va implicar el final de la deposició de la GS-I. Diversos mecanismes de plegament van caracteritzar l'evolució estructural en aquesta etapa: a la GS-I predominà la migració de xarnera en els sinclinals associats a l'anticlinal, mentre que una combinació d'allargament i rotació de flanc es va produir al llarg de la part E-W dels flancs de l'anticlinal. Al mateix temps, a la Formació Guara l'allargament de flanc va predominar en el tancament periclinal i la rotació de flanc ho va fer al llarg de la part N-S dels flancs de l'anticlinal (Fig. R19d). Aquesta complexa interacció de mecanismes de plegament entre diferents unitats i dominis estructurals va caracteritzar tot el creixement del plec, i va portar als contrastos d'estil estructural que es descriuen avui dia al camp: un encavalcament intern paral·lel a la tendència estructural del plec afecta a la seqüència compresa entre les fàcies Muschelkalk i la seqüència 2 de Guara, fallant-la i deformant-la de forma complexa, mentre que la sèrie suprajacent formada per la seqüència 2 de Guara fins a la Formació Campodarbe es troba plegada més suaument. Amb

més escurçament l'emplaçament de la rampa de l'encavalcament frontal sudpirinenc causa un increment en la immersió del plec sincrònicament a la rotació progressiva de l'anticlinal en el sentit de les busques (Fig. R19d).

Fa uns 37.74 Ma l'ambient deposicional va canviar lleugerament, descrivint a partir de llavors la presència de foraminífers bentònics, briozous, bivalves i equínids (Millán et al., 1994). En general, l'anticlinal havia rotat ja un total de 6º respecte el inici de la deformació. Tanmateix, tal com mostra la restitució, el lliscament capa sobre capa accentua aquesta rotació de les capes superiors respecte les inferiors, donat que s'observa una rotació lleugerament superior en les unitats més joves. L'anticlinal, per tant, no va rotar com un bloc rígid: els contrastos mecànics en el desenganxament basal van conduir la rotació general de l'estructura a mida que l'encavalcament frontal sudpirinenc avançava, però el lliscament capa sobre capa entre unitats va causar una rotació incremental lleugerament superior a mida que es puja en la sèrie estratigràfica.

D'acord amb Millán et al (1994), després de la deposició de la GS-III fa uns 37.17 Ma l'ambient deposicional va canviar a una rampa carbonatada de baix angle, amb una sedimentació consistent en fàcies margoses (fàcies de rampa externa) interestratificades amb fàcies carbonàtiques (fàcies de rampa mitja) amb molta presència de comunitats bentòniques de pectínids. Es va produir una rotació addicional d'uns 10º respecte a l'estadi anterior així com un augment de la immersió del plec cap al nord d'uns 4º. Ambdós increments indiquen una activitat creixen en l'emplaçament de l'encavalcament frontal sudpirinenc durant aquest període.

La deposició de la GS-IV (Formació Belsué-Atarés, fa uns 36.6 Ma), en canvi, no va implicar un augment significatiu de la rotació (uns 2º aproximadament) i de la immersió (uns 4º) de l'anticlinal. Aquesta va ser la primera seqüència deposicional que va cobrir tot l'anticlinal (Fig. R19e) , i va implicar un canvi en el sistema deposicional cap a un ambient deltaic en el que lòbuls deltaics progradaven sobre margues de prodelta, i que es va caracteritzar per la sedimentació de gresos granocreixents i fines seqüències margoses (Millán et al., 1994). Degut al lliscament capa sobre capa descrit als estrats de creixement, les GS van acomodar una deformació moderada, amb el màxim de

deformació concentrat a la seqüència pre-plegament, principalment degut a l'emplaçament de la rampa de l'encavalcament frontal sudpirinenc sota l'estructura de l'anticlinal.

Finalment, des de la GS-IV fins al cessament de la deformació (estimat fa uns 34.8 ± 1.72 Ma segons Poblet and Hardy, 1995) el marc deposicional va canviar d'ambients fluviodeltaics a fluvials, caracteritzat per la deposició i sedimentació dels gresos, lutites i conglomerats de la Formació Campodarbe. La rotació registrada en aquest estadi va ser important, d'uns 15º respecte l'estadi anterior, així com també va ser-ho l'increment en la immersió del plec, d'uns 18º (Fig. R19e). Això indica que l'emplaçament de la rampa de l'encavalcament sudpirinenc va mostrar una major activitat durant aquest període. El lliscament capa sobre capa va influenciar un plegament i una rotació diferents entre les diverses unitats que va generar l'asimetria descrita en la geometria actual del plec. També durant aquest últim estadi deformatiu es van produir les falles extensives en la cresta de l'anticlinal que s'observen al llarg de tota la seqüència d'estrats de creixement , principalment degudes a un estirament de l'arc exterior del plec i a inestabilitats gravitacionals de la cresta de l'anticlinal.

R.10 CONCLUSIONS

En aquesta Tesi es presenten diferents tècniques de modelització, les quals s'han integrat posteriorment per tal de conèixer millor l'evolució estructural de l'anticlinal del Pico del Águila i, per tant, dels anticlinals N-S de les Sierras Exteriores Aragonesas.

Els models analògics han proporcionat nous coneixements sobre la formació i evolució d'estructures obliqües i transversals a l'orogen. Basat en una distribució irregular del nivell basal de desenganxament Triàsic, els models simulen les característiques dels plecs N-S de les Sierras Exteriores Aragonesas: generació sincrònica a l'emplaçament de l'encavalcament frontal sudpirinenc, major relleu estructural comparat amb les estructures paral·leles a l'orogen, absència d'un desenganxament dúctil representatiu al nucli de les estructures,

falles penetratives a les unitats inferiors i plegament de les unitats superiors, immersió dels anticlinals cap a l'orogen i tancament periclinal meridional no encavalcat per l'encavalcament frontal sudpirinenc.

Els models d'elements discrets s'han emprat per testar la influència d'una estratigrafia mecànica complexa i la presència d'estrats de creixement en la generació i evolució de l'anticlinal del Pico del Águila. La variabilitat mecànica de la sèrie estratigràfica ha implicat una gran i complexa deformació en les unitats incompetents, mentre que les unitats més competents estan subjectes a una deformació més distribuïda i a plegament simple. Com a resultat de les diferents respostes mecàniques a l'escurçament, és difícil explicar l'evolució d'una estructura com el Pico del Águila en termes de paràmetres cinemàtics. La presència dels estrats de creixement redueix els efectes de l'estirament, de les falles extensives i de les inestabilitats gravitacionals a la cresta de l'anticlinal. La càrrega creada pels sediments sin-cinemàtics implica també que la deformació quedi més confinada al nucli de l'estructura, creant així un plec més estret que en cas d'absència de sedimentació sin-cinemàtica.

La reconstrucció i restitució 3D de l'anticlinal del Pico del Águila també suggereix que el creixement d'un plec de desenganxament en 3D està caracteritzat per la combinació de múltiples mecanismes de plegament produint-se simultàniament en diferents unitats i dominis estructurals durant la formació de l'anticlinal, depenent de les propietats mecàniques dels materials implicats en la deformació. Així doncs, la comprensió de la cinemàtica del plegament no hauria de passar per alt la consideració del comportament mecànic de les roques per tenir un coneixement més encertat de l'evolució d'una estructura.

La correcta integració de les diferents tècniques de modelització està òbviament relacionada amb les aportacions que cada model fa, però també amb les limitacions de cadascun dels mètodes. En aquest sentit, en aquesta Tesi es presenta un model d'evolució estructural per l'anticlinal del Pico del Águila basat en la integració de models estructurals 3D, analògics, numèrics i restitucions geomecàniques de l'estructura, als quals se'ls hi afegeixen les aportacions proporcionades per treballs clau previs sobre la regió. Combinant

múltiples disciplines i mètodes de modelització, per tant, aporta sense dubte una millor comprensió de l'evolució d'una estructura així com dels processos que menaren la generació i evolució dels anticlinals de desenganxament N-S de les Sierras Exteriores Aragonesas dels Pirineus Meridionals.

R.10.1 PERSPECTIVES D'AVENÇ

Després de diversos anys d'estudiar els anticlinals N-S de les Sierras Exteriores Aragonesas han aparegut moltes preguntes, reptes i dificultats, alguns dels quals s'han pogut solucionar satisfactòriament mentre que altres han continuat sense resposta. A més, s'han encetat investigacions paral·leles no recollides en aquest volum i que han hagut de ser apartades en algun moment o altre, bé sigui per falta de temps, per falta de recursos humans, o senzillament perquè no s'ha pogut trobar un enllaç directe amb l'objectiu global d'aquesta Tesi. Una vegada acabada aquesta etapa, però, potser es disposarà de l'ocasió de recuperar-les i dedica'ls-hi el temps i l'esforç necessari. Aquestes qüestions són:

a) La reconstrucció i restitució seqüencial 3D dels anticlinals N-S veïns al Pico del Águila, com són l'anticlinal de Bentué de Rasal i el de Gabardiella. Portant a terme aquest exercici en aquestes estructures veïnes proporcionaria una visió més global de la rotació d'eix vertical dels anticlinals a una escala més regional, donant eines suficients per comparar l'evolució de la deformació al llarg de la traça del front encavalcant sudpirinenc.

b) Un acurat estudi de camp de la fracturació associada a l'anticlinal del Pico del Águila. En Manoel Valcárcel ja va realitzar un primer estudi de les fractures associades a l'anticlinal, en el que va obtenir resultats prometedors per comparar amb el patró de deformació derivat a partir de la restitució geomecànica i els models mecànics 2D. Tanmateix, caldria un estudi més detallat, amb una major inversió de temps i recursos per aconseguir més estacions de mesura i tenir així un millor control de com les fractures es distribueixen arreu de l'anticlinal.

c) Una eina automatitzada per reconstruir la geometria dels estrats de creixement. Les seqüències deposicionals reconstruïdes en els estrats de creixement del Pico del Águila es van realitzar aplicant el mètode dels dominis de cabussament individualment per cada horitzó. Tanmateix, aquest mètode implica un gran consum de temps i pot esdevenir tediós si es disposa d'una gran quantitat de dades (centenars o milers de mesures de cabussament). Mercès a les excel·lents condicions d'aflorament i accessibilitat, les seqüències de creixement reconstruïdes poden esdevenir una excel·lent base de partida a partir de la qual desenvolupar un mètode automatitzat de reconstrucció d'estrats de creixement a partir de paràmetres físics mesurables de les roques.

d) El reprocessat dels perfils sísmics disponibles a la zona d'estudi. Les campanyes d'adquisició sísmica disponibles a la zona van ser realitzades durant els anys 60 del segle XX. Com a resultat, els perfils sísmics són de poca qualitat, i no permeten una interpretació acurada de la geometria de les unitats, particularment en els nivells més soms dels estrats de creixement. Això esdevé una gran limitació per poder entendre correctament la geometria de les Sierras Exteriores Aragonesas en profunditat. Malgrat que això quedi parcialment compensat per unes magnífiques condicions d'aflorament, un reprocessat i filtrat dels perfils sísmics amb les eines actuals de processat sísmic milloraria de forma destacable la interpretació i comprensió dels anticlinals N-S en profunditat.

R.11 REFERÈNCIES

Agterberg, F.P., 1967. Computer techniques in geology. Earth-Science Reviews, 3, 47-77.

Amilibia, A., McClay, K.R., Sàbat, F., Muñoz, J.A., Roca, E., 2005. Analogue Modelling of Inverted Oblique Rift Systems. Geologica Acta, 3 (3), 251-271.

Bonini, M., 2003. Detachment folding, fold amplification, and diapirism in thrust wedge experiments. Tectonics, 22(6), 1065, doi:10.1029/2002TC001458.

Borraccini, F., De Donatis, M., Di Bucci, D., Mazzoli, S., 2002. 3D Model of the active extensional fault system of the high Agri River valley, Southern Apennines, Italy. In: Jessell, M. J. (ed.). General Contributions: 2002. Journal of the Virtual Explorer, 6, 1-6.

Cadell, H.M., 1888. Experimental Researches in mountain building. Royal Society of Edinburgh Transactions, 35, 337-360.

Cagnard, F., Brun, J.P., Gapais, D., 2006. Modes of thickening of analogue weak litospheres. Tectonophysics, 421 (1-2), 145-160.

Camerlo, R.H., Benson, E.F., 2006. Geometric and seismic interpretation of the Perdido fold belt: Northwestern deep-water Gulf of Mexico. American Association of Petroleum Geologists Bulletin, 90 (3), 363-386.

Carmona, A., Clavera, R., Gratacós, O., Hardy, S., 2008. Combining Discrete Element Modelling and process-based models: initial results. Bolletino di Geofisica teorica ed applicata, 49, 358-364.

Carrera, N., Muñoz, J.A., Roca, E., 2009. 3D reconstruction of geological surfaces by the equivalent dip-domain method: An example from field data of the Cerro Bayo Anticline (Cordillera Oriental, NW Argentine Andes). Journal of Structural Geology, 31, 1573-1585.

Castelltort, S., Guillocheau, F., Robin, C., Rouby, D., Nalpas. T., Lafont, F., Echard, R., 2003. Fold control on the stratigraphic record: a quantified sequence stratigraphic study of the Pico del Aguila anticline in the south-western Pyrenees (Spain). Basin Research, 15, 527-551.

Castillo-Herrador, F., 1974. Le Trias évaporitique des basins de la Vallée de l'Ebre et de Cuenca. Bulletin de la Societé Géologique de France, 16, 49-63.

Daudre, A., 1879. Etudes Synthétiques de Géologie Expérimentale, pt. 1. Paris, Dunod, 828 p.

Felleman, J., 1990. There's a GIS in your future. Government Information Quarterly, 7 (3), 261-267.

Fernández, O., Muñoz, J.A., Arbués. P., Falivene, O., Marzo, M., 2004a . Three-dimensional reconstruction of geological surfaces: An example of growth strata and turbidite systems from the Ainsa basin (Pyrenees, Spain). American Association of Petroleum Geologists Bulletin, 88 (8), 1049-1068.

Fernández, O., 2004b. Reconstruction of geological structures in 3D: An Example from the southern Pyrenees. Doctoral Thesis, Departament de Geodinàmica i Geofísica, Universitat de Barcelona, Barcelona, Spain, 376 pp.

Finch, E., Hardy, S., Gawthorpe, R.L., 2003. Discrete element modelling of contractional fault-propagation folding above rigid basement blocks. Journal of Structural Geology, 25, 515-528.

Finch, E., Hardy, S., Gawthorpe, R.L., 2004. Discrete element modelling of extensional fault-propagation folding above rigid basement fault blocks. Basin Research, 16, 489-506.

Ford, M., Le Carlier de Veslud, C., Bourgeois, O., 2007. Kinematic and geometric analysis of fault-related folds in a rift setting: The Dannemarie basin, Upper Rhine Graben, France. Journal of Structural Geology, 29, 1811-1830.

Gente, P., Auzende, J.M., Renard, V., Fouquet, Y., Bideau, D., 1986. Detailed geological mapping by submersible of the East Pacific Rise axial graben near 13º N. Earth and Planetary Science Letters, 78 (2-3), 224-236.

Guzofski, C.A., Mueller, J.P., Shaw, J.H., Muron, P., Medwedeff, D.A., Bilotti, F., Rivero, C., 2009. Insights into the mechanisms of fault-related folding provided by volumetric structural restorations using spatially varying mechanical constraints. American Association of Petroleum Geologists Bulletin, 93 (4), 479-502.

Hall, J. Sir, 1815. On the vertical position and convolutions of certain strata and their relation with granite. Royal Society of Edinburgh Transactions, 7, 79-108.

Harbaugh, J.W., Merriam, D.F., 1968. Computer applications in stratigraphic analysis. John Wiley Sons Inc., New York, USA, 282 p.

Hardy, S., Finch, E., 2005. Discrete-element modelling of detachment folding. Basin Research, 17, 507-520.

Hardy, S., Finch, E., 2007. Mechanical stratigraphy and the transition from trishear to kink-band fault-propagation fold forms above blind basement thrust faults: A discrete-element study. Marine and Petroleum Geology, 24, 75-90.

Hill, K.C., 1991. Structure of the Papuan Fold Belt, Papua New Guinea. American Association of Petroleum Geologists Bulletin, 74 (5), 857-872.

Holl, J.E., Anastasio, D.J., 1993. Paleomagnetically derived folding rates, southern Pyrenees, Spain. Geology, 21 (3), 271-274.

Huyghe, D., Mouthereau, F., Castelltort, S., Filleaudeau. P.Y., Emmanuel, L., 2009. Paleogene propagation of the southern Pyrenean thrust wedge revealed by finite strain analysis in frontal thrust sheets: Implications for mountain building. Earth and Planetary Science Letters, doi:10.1016/j.epsl.2009.10.002.

IGME, 1992. Mapa Geológico de España. Hoja 248, Apiés. Instituto Geológico y Minero de España, Madrid, Unpublished 36 pp report + 1:50000 map.

Jurado, M.J., 1990. El Triásico y el Liásico basal evaporíticos del subsuelo de la cuenca del Ebro. In: Ortí, F., Salvany, J.M. Formaciones evaporíticas de la Cuenca del Ebro y cadenas periféricas, y de la zona de Levante. Enresa, Madrid, 21-28.

Koyi, H.A., 1997. Analogue modelling: from a qualitative to a quantitative technique – a historical perspective. Journal of Petroleum Geology, 20, 223-238.

Krumbein, W.C., Graybill, F.A., 1965. Application of the general linear model to Map Analysis. An Introduction to Statistical Models in Geology, McGraw-Hill, New York, 319-357.

López-Gómez, K., Arche, A., Pérez-López, A., 2002. Permian and Triassic. In: Gibbons, W., Moreno, T. (eds.). The Geology of Spain. The Geological Society of London, 185-212.

Maerten, L., Maerten, F., 2006. Chronologic modeling of faulted and fractured reservoirs using geomechanically based restoration: Technique and industry applications. American Association of Petroleum Geologists Bulletin, 90 (8), 1201-1226.

Millán, H., 1995. Estructura y Cinemática del frente de cabalgamiento surpirenaico en las Sierras Exteriores Aragonesas. Doctoral Thesis, Departamento de Ciencias de la Tierra, Universidad de Zaragoza, Zaragoza, 330 pp + annex.

Millán, H., Aurell, M., Meléndez, A., 1994. Synchronous detachment folds and coeval sedimentation in the Prepyrenean External Sierras (Spain): a case study for a tectonic origin of sequences and system tracts. Sedimentology, 41 (5), 1001-1024.

Mitra, S., 2002. Structural Models of Faulted Detachment Folds. American Association of Petroleum Geologists Bulletin, 86 (9), 1673-1694.

Nalpas, T., Gapais, D., Vergés, J., Barrier, L., Gestain, V., Leroux, G., Rouby, D., Kermarrec, J.J., 2003. Effects of rate and nature of synkinematic sedimentation on the growth of compressive structures constrained by analogue models and field examples. In: McCant, T., Saintot, A. (eds.). Tracing Tectonic Deformation Using the Sedimentary Record. Geological Society, London, Special Publications 208, 307-319.

Nalpas, T., Györfi, I., Guillocheau, F., Lafont, F., Homewood, P., 1999. Influence de la charge sédimentaire sur le développement d'anticlinaux synsédimentaires. Modélisation analogique et exemple du terrain (bordure sud du basin de Jaca). Bulletin de la Societé Géologique de France, 170 (5), 733-740.

Novoa, E., Suppe, J., Shaw, J.H., 2000. Inclined-Shear Restoration of Growth Folds. American Association of Petroleum Geologists Bulletin, 84 (6), 787-804.

Place, D., Mora, P., 2001. A random lattice solid model for simulation of fault zone dynamics and fracture processes. In: Mulhaus, H.B., Dyskin, A.V., Pasternak, E. (eds.). Bifurcation and Localisation Theory for Soils and Rocks '99. A.A. Balkema, Rotterdam/Brookfield.

Poblet, J., Hardy, S., 1995. Reverse modelling of detachment folds, application to the Pico del Aguila anticline in the South Central Pyrenees (Spain). Journal of Structural Geology, 17, 1707-1724.

Poblet, J., McClay, K.R., Storti, F., Muñoz, J.A., 1997. Geometries of syntectonic sediments associated with single-layer detachment folds. Journal of Structural Geology, 19 (3-4), 369-381.

Pueyo, E.L., Millán, H., Pocoví, A., 2002. Rotation velocity of a thrust: a paleomagnetic study in the External Sierras (Southern Pyrenees). Sedimentary Geology, 146 (1), 191-208.

Rodriguez-Pintó, A., Pueyo, E.L., Pocoví, A., Barnolas, A., 2008. Cronología de la actividad rotacional en el sector central del frente de cabalgamiento de Sierras Exteriores (Pirineo Occidental). Geotemas, 10, 1207-1210.

Salvany, J.M., 1990. Introducción a las evaporitas triásicas de las cadenas periféricas de la cuenca del Ebro: Catalánides, Pirineo y Región Cantábrica. In: Ortí, F., Salvany, J.M. (eds.). Formaciones evaporíticas de la Cuenca del Ebro y cadenas periféricas, y de la zona de Levante. Enresa, Madrid, 21-28.

Scheck, M., Bayer, U., 1999. Evolution of the Northeast German Basin - inferences from a 3D structural model and subsidence analysis. Tectonophysics, 313, 145-169.

Soler, M. , Puigdefàbregas, C., 1970. Líneas generales de la geología del Alto Aragón Occidental. Pirineos, 96, 5-20.

Tanner, D.C., Berhmann, J.H., Dresmann, H., 2003. Three-dimensional retro-deformation of the Lechtal Nappe, Northern Calcareous Alps. Journal of Structural Geology, 25, 737-748.

Vidal-Royo, O., Koyi, H.A., Muñoz, J.A., 2009. Formation of orogen-perpendicular thrusts due to mechanical constrasts in the basal décollement in the Central External Sierras (Southern Pyrenees, Spain). Journal of Structural Geology, 31, 523-539.

Vidal-Royo, O., Hardy, S., Muñoz, J.A., 2010. The roles of complex mechanical stratigraphy and syn-kinematic sedimentation in fold development: Insights from discrete-element modelling and application to the Pico del Águila anticline (External Sierras, Southern Pyrenees). In: Poblet, J., Lisle, R.J. (eds.). Kinematic Evolution and Structural Styles of Fold-and-Thrust Belts, Special Publication of the Geological Society, *accepted*.

Vidal-Royo, O., Cardozo, N., Muñoz, J.A., Hardy, S., Maerten, L., 2010. Multiple mechanisms driving detachment folding as deduced from 3D reconstruction and geomechanical restoration: The Pico del Águila anticline (External Sierras, Southern Pyrenees). Basin Research, *submitted*.

Weijermars, R., 1986. Flow behaviour and physical chemistry of bouncing putties and related polymers in view of tectonic laboratory applications. Tectonophysics, 124, 325-358.

Wilsher, W.A., de Wit, M.J., Marrao, E., 1989. A GIS solution for Gondwana geoscientific data. Journal of African Earth Sciences, 9 (2), 371-374.

Zanchi, A., Salvi, F., Zanchetta, S., Sterlacchini, S., Guerra, G., 2009. 3D reconstruction of complex geological bodies: Examples from the Alps. Computers and Geosciences, 35, 49-69.

RESUMEN EXTENSO

Evolución estructural del anticlinal del Pico del Águila mediante modelización estructural 3D, analógica y numérica

En este apartado se presenta un resumen extenso de la Tesis traducido al español, en el que se recogen las razones que motivaron la realización de esta Tesis, los objetivos establecidos, la estructura en la que se organiza la memoria, la metodología aplicada, los principales resultados y una discusión general sobre éstos. Finalmente se presentan una lista de consideraciones globales respecto a los aspectos geológicos y metodológicos más relevantes, así como diversas perspectivas de investigaciones que se han planteado realizar tras la finalización de esta Tesis. Debe aclararse que el resumen de resultados y la discusión general presentados en este apartado se han extraído del **Capítulo V** de esta memoria. Las consideraciones finales y las perspectivas de avance, en cambio, han sido extraídas del **Capítulo VI**.

R.1 SINOPSIS

La presente Tesis tiene como objetivo elaborar un modelo conceptual unificado de la evolución estructural del anticlinal del Pico del Águila (Sierras Exteriores Aragonesas, Pirineos Meridionales) a partir de la integración de diversas técnicas de modelización geológica. El Pico del Águila es un conocido ejemplo de pliegue de despegue, caracterizado por una orientación N-S, paralela a la dirección de transporte tectónico en los Pirineos Meridionales.

Se ha construido a partir de datos de campo e interpretación de perfiles sísmicos un modelo tridimensional de la estructura del Pico del Águila, poniendo especial énfasis en la interferencia entre las estructuras N-S y las E-W, así como en la geometría de los estratos de crecimiento.

En base a observaciones de campo de una distribución irregular del nivel basal de despegue, se realizaron una serie de modelos analógicos que muestran de qué manera pueden generarse estructuras perpendiculares al orógeno que pueden finalmente dar lugar a anticlinales perpendiculares a la tendencia estructural general de la cordillera.

Los modelos numéricos presentados investigan el efecto de una estratigrafía mecánica compleja, caracterizada por el intercalado de unidades con marcadas diferencias de competencia, así como el papel que juega la sedimentación sin-cinemática en el crecimiento de un pliegue de despegue.

A partir del modelo 3D mencionado anteriormente se presenta también una restitución secuencial geomecánica de la estructura que sugiere la coexistencia de múltiples mecanismos de plegamiento produciéndose simultáneamente en diferentes unidades y dominios estructurales del pliegue. Esta superposición de mecanismos produce una distribución compleja de la deformación que difícilmente puede ser evaluada mediante modelos cinemáticos bidimensionales.

Integrando los modelos presentados con datos previos de la región, se discuten los beneficios e inconvenientes de cada una de las técnicas de modelización y se presenta un modelo integrado de evolución estructural del anticlinal del Pico del Águila, el cual nos permite una mayor comprensión de la estructura así como de los procesos que condujeron la evolución de los pliegues de despegue N-S de las Sierras Exteriores Aragonesas.

R.2 MOTIVACIÓN, OBJETIVOS Y ORGANIZACIÓN DE LA TESIS

R.2.1 MOTIVACIÓN

Una de las principales motivaciones para realizar esta Tesis ha sido la de investigar los mecanismos que gobiernan la formación de pliegues de despegue en 3D. Además se disponía de lo que puede ser considerado uno de los mejores laboratorios naturales del planeta para estudiar la geología estructural en contextos compresivos: las Sierras Exteriores Aragonesas de los Pirineos Meridionales. La geología de las Sierras Exteriores se caracteriza por rasgos bastante particulares que tras décadas de estudio siguen siendo objeto se trabajos y discusiones geológicas en cuanto a los procesos que condujeron a su formación y evolución se refiere. En este sentido, los anticlinales N-S de las Sierras Exteriores tienen una gran relevancia geológica y requerían de nuevas metodologías de estudio para abordar los aspectos que permanecían (algunos de ellos permanecen todavía) poco conocidos. Las excelentes condiciones de afloramiento, el alto grado de preservación de las estructuras y la fácil accesibilidad hicieron de esa área el lugar adecuado para testar y aplicar las técnicas de reconstrucción estructural y modelización más recientes desarrolladas en el seno del Institut de Recerca de Geomodels y del Grup de Geodinàmica i Anàlisi de Conques (GGAC-UB) de la Universitat de Barcelona. En este estadio temprano de la memoria de la Tesis se cree necesario reconocer enfáticamente el gran esfuerzo, el trabajo duro y el entusiasmo de todo el personal del GGAC, en concreto de los profesores J.A. Muñoz y Stuart Hardy, que allanaron el camino en las técnicas de Modelización Estructural 4D y Modelización Mecánica de estructuras, de las cuales esta Tesis se ha beneficiado en gran parte. Puede decirse que esta tesitura inicial fue un punto de partida prometedor que constituyó, por sí mismo, una importante motivación adicional.

Como ya se ha mencionado, los procesos que originaron los anticlinales N-S de las Sierras Exteriores son aún objeto de estudio y discusión. La estructura es compleja, y los mecanismos que tuvieron lugar son múltiples y difíciles de abordar por métodos sencillos. Sin embargo, las Sierras Exteriores presentan inmejorables facilidades si nos referimos al grado de exposición y

accesibilidad. Esto significa que los anticlinales N-S de las Sierras Exteriores, y en particular el Pico del Águila, pueden ser considerados ejemplos aflorantes de primer orden mundial de pliegues de despegue. Por tanto, una buena comprensión de los procesos, mecanismos y parámetros que entraron en juego en la evolución de estas estructuras conducirá a una mejor comprensión sobre la formación y evolución de estructuras formadas bajo condiciones similares en otros lugares de la Tierra, en las que la baja calidad de los datos o la difícil accesibilidad pueden comprometer la veracidad de los resultados y conducir a error en la interpretación de los rasgos geológicos que caracterizan la estructura. Además, si estas estructuras son altamente preciadas por contener hidrocarburos u otros recursos naturales explotables comercialmente, una buena comprensión de su geometría, evolución y rasgos característicos puede tener un gran impacto económico en términos de explotación y producción de los posibles reservorios. Este podría ser el caso, por citar algunos ejemplos, de los cinturones de pliegues y cabalgamientos de aguas profundas del Mississipi fan y Perdido (Mitra, 2002; Camerlo & Benson, 2006), o del cinturón de Papua Nueva Guinea (Hill, 1991; Mitra, 2002), entre otros.

R.2.2 OBJETIVOS

La presente Tesis se centra en la generación, evolución estructural y relaciones tecto-sedimentarias de los anticlinales N-S de las Sierras Exteriores Aragonesas, y más concretamente, del anticlinal del Pico del Águila. Aplicando diferentes técnicas de modelización, esta Tesis tiene como finalidad dar respuesta a diversas preguntas nacidas de la observación de los rasgos geológicos de las Sierras Exteriores, y que pueden extenderse a otros ejemplos de pliegues de despegue descritos en otros lugares del mundo. Los objetivos específicos son:

1) Conocer los mecanismos que pueden conducir a la generación de estructuras perpendiculares al orógeno tales como el anticlinal del Pico del Águila en ausencia de otro evento de acortamiento que no sea la compresión de la orogenia alpina, de dirección de transporte tectónico N-S.

2) Mejorar la comprensión de cómo se distribuye la deformación a lo largo de una secuencia estratigráfica heterogénea como la descrita en las Sierras Exteriores y, por tanto, determinar cómo se acomoda la deformación dependiendo de las propiedades mecánicas de cada unidad.
3) Comprender el papel de la sedimentación sin-cinemática (estratos de crecimiento) en la evolución del pliegue y cómo acomoda la deformación.
4) Conocer los mecanismos que gobiernan la formación de pliegues de despegue en 3D y entender cómo se distribuyen a lo largo y ancho de la estructura. Asimismo, comprender cómo la distribución de los mecanismos de plegamiento afecta la geometría del anticlinal y las tasas de sedimentación y levantamiento que, a su vez, también influencian el crecimiento del anticlinal.
5) Presentar un modelo unificado de evolución estructural de acuerdo a las observaciones y estudios previos y a los resultados obtenidos a partir de diferentes herramientas de modelización.
6) Contribuir a un mayor conocimiento sobre la cinemática y la mecánica de los pliegues de despegue para conseguir una mejor interpretación y comprensión de otras estructuras análogas a lo largo del planeta que no exhiban unas condiciones de afloramiento y accesibilidad tan favorables como las del anticlinal del Pico del Águila.

R.2.3 ORGANIZACIÓN DE LA TESIS

Esta Tesis se presenta como una compilación de cuatro publicaciones científicas, y ha sido estructurada en seis capítulos principales organizados de la siguiente manera:

El **Capítulo I** presenta una descripción general de la geología de las Sierras Exteriores Aragonesas de los Pirineos Meridionales. Los artículos científicos disponen de una extensión limitada en la cual únicamente tiene cabida una breve descripción de los rasgos más esenciales de la geología de la región. Sin embargo, el área de estudio se caracteriza por numerosos rasgos geológicos de importancia que no fueron mencionados en las publicaciones o

que se encuentran diseminados en el apartado del marco geológico de cada uno de los artículos. Esta sección presenta una descripción global de estos aspectos a fin de tener un conocimiento más amplio del área de estudio. Se pone especial énfasis en la descripción de la estratigrafía, dada su importancia en la evolución de los anticlinales N-S, y en los rasgos estructurales generales de la región.

El **Capítulo II** contiene el primer artículo científico de la Tesis: **Vidal-Royo, O., Koyi, H.A., Muñoz, J.A., 2009. Formation of orogen-perpendicular thrusts due to mechanical contrasts in the basal décollement in the Central External Sierras (Southern Pyrenees, Spain). Journal of Structural Geology, 31 (5), 523-539.**

Este artículo presenta dos series de modelos analógicos (Series A y B) que se han utilizado para investigar el efecto de las irregularidades mecánicas en el nivel basal de despegue (facies Muschelkalk y Keuper) en la formación de estructuras oblicuas y perpendiculares al orógeno, tales como los anticlinales N-S de las Sierras Exteriores Aragonesas. La serie A de modelos investiga la proporción de grosor estratigráfico entre la cobertera y el nivel de despegue, mientras que la serie B de modelos testa la anchura (perpendicular a la dirección de acortamiento) del despegue friccional.

El **Capítulo III** contiene el segundo artículo científico que constituye esta Tesis: **Vidal-Royo, O., Hardy. S., Muñoz, J.A., 2010. The roles of complex mechanical stratigraphy and syn-kinematic sedimentation in fold development: Insights from discrete-element modelling and application to the Pico del Águila anticline (External Sierras, Southern Pyrenees). En: Poblet, J., Lisle, R.J. (Eds.). Kinematic Evolution and Structural Styles of Fold-and-Thrust Belts, Special Publication of the Geological Society, v.330, doi: 10.1144/SP330.**

En este estudio se presentan dos modelos numéricos en 2D, basados en el método de Modelización de Elementos Discretos, con el fin de investigar el efecto de una estratigrafía mecánica compleja como la descrita en el campo, así como de los estratos de crecimiento en la evolución del anticlinal del Pico del Águila. Se presentan dos modelos: el Modelo 1 explora la respuesta de esta

estratigrafía mecánica compleja al acortamiento bajo condiciones que llevan a la formación de un pliegue de despegue; el Modelo 2 investiga el efecto de la sedimentación sin-cinemática bajo las mismas condiciones de contorno que el Modelo 1.

En el **Capítulo IV** se presenta la tercera publicación científica de esta Tesis: **Vidal-Royo, O., Cardozo, N., Muñoz, J.A., Hardy, S., Maerten, L., (en revisión). Multiple mechanisms driving detachment folding as deduced from 3D reconstruction and geomechanical restoration: The Pico del Águila anticline (External Sierras, Southern Pyrenees).** ***Enviado a Basin Research.***

Este estudio presenta una reconstrucción y restitución geomecánica tridimensionales del anticlinal del Pico del Águila. A partir de datos de campo (medidas de buzamiento y cartografía de trazas geológicas) e interpretación de perfiles sísmicos se presenta una reconstrucción detallada de la geometría de la secuencia pre-pliegue y de los estratos de crecimiento. Gracias a la reconstrucción de cuatro secuencias deposicionales dentro del paquete sedimentario sin-plegamiento, se pudo realizar una restitución secuencial de la estructura en la que se pudo establecer una cronología de la deformación. Basado en un método de Modelización de Elementos Finitos, el algoritmo de restitución considera las propiedades mecánicas de las rocas para llevar a cabo una restitución en la que no se asume ni se impone ningún criterio cinemático previo. A partir de esta restitución se han podio obtener nuevos conocimientos de la evolución del anticlinal en 3D.

El **Capítulo V** contiene el cuarto artículo científico de esta Tesis: **Vidal-Royo, O., Muñoz, J.A., Hardy, S., Koyi, H.A., Cardozo, N., (enviado). Structural evolution of the Pico del Águila anticline (External Sierras, Southern Pyrenees) derived from sandbox, numerical and 3D structural modelling techniques.** ***Enviado a Geologica Acta.***

Este capítulo contiene un resumen de los resultados presentados en los capítulos previos, así como la discusión general de la Tesis. En este capítulo se discuten los beneficios, desventajas, limitaciones e idoneidad de las técnicas de

modelización presentadas, así como los resultados de los modelos y su integración en un modelo unificado de evolución estructural.

En el **Capítulo VI** se presentan las conclusiones finales de esta Tesis, así como una propuesta de tareas futuras a realizar.

R.3 INTRODUCCIÓN

Los modelos geológicos proporcionan explicaciones y ayudan a un mejor conocimiento de los procesos geológicos que acontecen en la Tierra. Sin embargo, en la mayor parte de los casos los modelos geológicos no han de ser entendidos como una réplica de la naturaleza sino como una manera de simular y representar los procesos geológicos a una escala de tiempo observable para el ser humano.

La geología estructural tiene ya una larga tradición en el uso de la modelización como herramienta para mejorar la comprensión de la generación y evolución de estructuras. Desde los primeros experimentos de modelos analógicos de arena (Hall, 1815; Daudre, 1879; Cadell, 1888; entre otros) se han creado y desarrollado numerosas técnicas en respuesta a la necesidad creciente de los geólogos de buscar explicación a nuevos problemas y situaciones. Los modelos analógicos se han sofisticado, incorporando elementos y dispositivos que producen resultados cuantitativos para una mejor comparación con la naturaleza (Koyi, 1997).

Con el auge de la informática y el uso generalizado de los ordenadores aparecieron los modelos numéricos, que contribuyeron a una rápida solución de complejos algoritmos matemáticos, que implicó grandes avances en la comprensión de los procesos geológicos (Krumbein and Graybill, 1965; Agterberg, 1967; Harbaugh & Merriam, 1968). En este sentido, los modelos numéricos añadieron un control cuantitativo de las leyes y parámetros que gobiernan los procesos naturales.

A pesar de todos estos progresos, cada técnica de modelización presenta sus propios puntos fuertes, debilidades y limitaciones, conduciendo a una representación de la naturaleza relativamente simplificada o incompleta. Esto hace que cada técnica sea adecuada para determinadas finalidades, teniendo en cuenta que conocer las limitaciones de cada técnica es esencial para comprender correctamente la aportación de los modelos geológicos. Por este motivo, tras cada modelo ha de haber una serie de parámetros físicos para testar, o un conjunto de procesos perceptibles para esclarecer, en lugar de un mero intento de reproducir detalladamente lo que se ha descrito en la naturaleza.

En esta Tesis se presentan tres técnicas de modelización para mejorar el conocimiento sobre la evolución estructural de los anticlinales N-S de las Sierras Exteriores Aragonesas de los Pirineos Meridionales. Entre ellos, el Pico del Águila ha sido objeto de estudio dado que es una estructura ampliamente conocida como ejemplo de pliegue de despegue, es fácilmente accesible y tiene un grado excelente de preservación y afloramiento. Además, el mapa geológico del Pico del Águila puede ser considerado una sección a lo largo del eje del pliegue, mostrando así la geometría y distribución de las unidades a lo largo de la estructura. Los pliegues N-S de las Sierras Exteriores Aragonesas se caracterizan por una interferencia estructural con las estructuras E-W generales del Pirineo, y muestran un alto grado de preservación de los estratos de crecimiento. Este hecho que permite registrar de forma precisa la evolución de la deformación en el anticlinal. La estructura es bien conocida y ha sido estudiada desde diversas perspectivas. Se han hecho contribuciones sobre la cinemática y la evolución estructural del pliegue a partir de estudios sedimentológicos (Millán et al., 1994; Castelltort et al., 2003), paleomagnetismo (Pueyo et al., 2002; Rodríguez-Pintó et al., 2008), modelos analógicos (Nalpas et al., 1999, 2003), modelos cinemáticos 2D (Poblet and Hardy, 1995; Poblet et al., 1997), restitución de cortes geológicos (Novoa et al., 2000), y otros estudios multidisciplinares (Huyghe, et al., 2009). A pesar de esta cantidad de estudios previos, no existe ningún estudio integrado poniendo en común los resultados derivados de diversas técnicas de modelización y análisis que se complementen y validen mutuamente, construyendo así un modelo de evolución más robusto.

Estos motivos hacen del Pico del Águila una estructura ideal para ser reconstruida en 3D. En este estudio se presenta en primer lugar el modelo 3D del anticlinal, a partir del cual se ha obtenido la geometría del patrón de interferencia entre las estructuras N-S y E-W, así como la geometría de los estratos de crecimiento. Más que proporcionar respuestas sobre la evolución del pliegue, el modelo 3D plantea nuevas preguntas sobre los procesos geológicos que tuvieron lugar. Para obtener respuestas se han empleado tres técnicas de modelización que se presentan a continuación de la reconstrucción 3D del pliegue. En conjunto, este trabajo tiene como objetivo elaborar un modelo conceptual unificado de evolución estructural basado en la integración de los resultados obtenidos a partir de modelos analógicos (Vidal-Royo et al., 2009), modelos mecánicos 2D (Vidal-Royo et al., 2010), y restitución geomecánica 3D del anticlinal del Pico del Águila (Vidal-Royo et al., *enviado*). Los modelos analógicos presentados muestran la formación de estructuras perpendiculares al orógeno en un único evento compresivo, como consecuencia de importantes contrastes mecánicos en el nivel basal de despegue. Los modelos numéricos investigan la importancia de la estratigrafía mecánica y la sedimentación sin-cinemática en el crecimiento de un pliegue de despegue como el Pico del Águila. Finalmente, la restitución geomecánica 3D muestra la complejidad de la interferencia en la estructura del anticlinal, así como su evolución secuencial y la combinación de mecanismos de plegamiento produciéndose simultáneamente durante el crecimiento del pliegue.

R.4 MARCO GEOLÓGICO

La geología de las Sierras Exteriores Aragonesas es bien conocida y ha sido objeto de numerosos estudios a lo largo de los años. Una descripción detallada de los rasgos geológicos de la región se escapa de los objetivos de este resumen, aunque el lector interesado podrá hallar buenas y profundas descripciones en trabajos clave como son Puigdefàbregas (1975), Millán et al. (1994), y Pueyo et al. (2002). A pesar de ello, una descripción general de la región se presenta también en esta sección.

El anticlinal del Pico del Águila se localiza en las denominadas Sierras Exteriores Aragonesas de los Pirineos Meridionales. Las Sierras Exteriores Aragonesas están constituidas por una serie de láminas de cabalgamiento imbricadas, despegadas sobre las facies evaporíticas, calcáreas y dolomíticas del Triásico medio y superior (facies Muschelkalk y Keuper) (Soler & Puigdefàbregas, 1970; IGME, 1992; Millán et al. 1994; Millán, 1995; Pueyo et al., 2002). Las Sierras Exteriores constituyen la parte frontal emergente del cabalgamiento surpirenaico, y se encuentran desplazadas hacia el sur sobre los sedimentos de edad terciaria de la cuenca de antepaís del Ebro.

Una de las peculiaridades de las Sierras exteriores es la presencia de un conjunto de anticlinales con orientación axial N-S a NW-SE. Estas estructuras son, por tanto, perpendiculares a la tendencia estructural de los Pirineos (E-W, con dirección de transporte tectónico hacia el sur) y crean por tanto un patrón de interferencia estructural complejo (Fig. R1). Los anticlinales N-S son más jóvenes y más pequeños hacia el oeste (Millán et al., 1994; Millán, 1995) y su crecimiento fue sincrónico a la deposición de sedimentos del Eoceno medio al Oligoceno y al desarrollo del frente de cabalgamiento surpirenaico (activo hasta el Mioceno inferior; Puigdefàbregas, 1975; Holl & Anastasio, 1993; Millán et al., 1994; Millán, 1995).

El Pico del Águila es uno de los anticlinales N-S más estudiados de todas las Sierras Exteriores Aragonesas. Creció durante el periodo comprendido entre 42.67 ± 0.02 Ma (Luteciense superior) y 34.8 ± 1.72 Ma (Priaboniense medio) (Poblet & Hardy, 1995), y muestra una espectacular secuencia de estratos de crecimiento (Figs. R3 y R4) (Millán et al., 1994; Millán, 1995, Poblet & Hardy, 1995; Pueyo et al., 2002; Castelltort et al., 2003; Vidal-Royo et al., 2010).

La secuencia estratigráfica de las Sierras Exteriores Aragonesas se caracteriza por ser un intercalado de materiales competentes e incompetentes (Millán et al., 1994), cada uno de los cuales muestra una respuesta diferente a la deformación (Vidal-Royo et al., 2010). La estratigrafía de la zona consiste en unos centenares de metros de materiales mesozoicos cubierta por una secuencia más gruesa de materiales terciarios (Fig. R2). La serie mesozoica está compuesta por calcáreas, dolomitas y lutitas con evaporíticas del Triásico medio

y superior, cubiertas por calcáreas de plataforma somera del Cretácico superior. El Terciario está compuesto por areniscas, limolitas y calcáreas lacustres de la transición Cretácico-Terciario (facies del Garumniense), las calcáreas de la plataforma marina somera de la Formación Guara (Luteciense), las margas, calcáreas y areniscas deltaicos de plataforma marina y transicionales de las Formaciones Arguis y Belsué-Atarés (Luteciense superior a Priaboniense medio), y las lutitas, areniscas y conglomerados fluviales de la Formación Campodarbe (Priaboniense medio a Oligoceno medio).

La secuencia pre-plegamiento comprende materiales que van del Triásico al Luteciense, con el límite superior a techo de la secuencia deposicional 2 de la Formación Guara. En el nivel de despegue Triásico, observaciones de campo (IGME, 1992) indican que las calcáreas y dolomitas del Muschelkalk (Triásico medio) son las rocas más antiguas que afloran en el núcleo del anticlinal (Fig. R1), hallándose plegadas, cabalgadas y con una gran deformación interna. Por otro lado, aunque las lutitas y evaporitas del Keuper (Triásico superior) dibujan la geometría del pliegue como el resto de la secuencia mesozoica, se ha observado un notable decrecimiento del grosor estratigráfico hacia las partes internas del anticlinal, donde las facies Keuper son prácticamente inexistentes en el núcleo de la estructura (Fig. R1). De esta manera, las facies Keuper son más gruesas y están mejor expuestas en las áreas entre los anticlinales N-S que en el núcleo de estas estructuras. La secuencia sin-plegamiento comprende desde la secuencia deposicional 3 de la Formación Guara (Fig. R3) y la secuencia de somerización formada por las Formaciones Arguis, Belsué-Atarés y Campodarbe. La base de la Formación Arguis define una discordancia regional, indicando un cambio brusco hacia ambientes deposicionales de talud (Figs. R2 y R4). Millán et al. (1994) definió cuatro secuencias deposicionales principales en las Formaciones Arguis y Belsué-Atarés. La secuencia I (nombrada GS-I de aquí en adelante) está compuesta por margas azules y margas arenosas con importante contenido en glauconita, y tiene una edad comprendida entre el Luteciense superior y el Bartoniense inferior. Esta secuencia se estrecha hacia la cresta del anticlinal y desaparece sin llegar a cubrirla. La secuencia II (nombrada GS-II de aquí en adelante) tiene una edad de Bartoniense medio a superior, y está compuesta por margas azules ligeramente bioturbadas. La

secuencia III (nombrada GS-III de aquí en adelante) corresponde a una plataforma de pectínidos de edad Priarboniense inferior formada por margas azules ricas en contenido fósil marino y con trazas de bioturbación. La secuencia IV (nombrada GS-IV de aquí en adelante) es de edad Priarboniense inferior y está compuesta por margas arenosas deltaicas y niveles siliciclásticos que resultan de una progradación deltaica. El límite inferior de la GS-IV corresponde al contacto entre las Formaciones Arguis y Belsué-Atarés. El límite superior es una discordancia regional, reconocible a lo largo de la cuenca surpirenaica, y que corresponde al contacto entre las Formaciones Belsué-Atarés y Campodarbe (Fig. R2). Esta discordancia representa un tránsito brusco a ambientes deposicionales continentales.

R.5 RECONSTRUCCIÓN 3D DEL ANTICLINAL DEL PICO DEL ÁGUILA

R.5.1 METODOLOGÍA DE RECONSTRUCCIÓN

La reconstrucción del anticlinal del Pico del Águila se basa en un minucioso trabajo de campo con adquisición de datos de superficie y en la interpretación de diversos perfiles sísmicos (ver Fig. R1 para identificación y localización de los perfiles). Todos estos datos fueron posteriormente integrados en un entorno de trabajo GIS (3D). Se obtuvo como resultado un modelo más robusto, que incorpora todos los datos y medidas disponibles. Los datos adquiridos en superficie comprenden medidas de buzamiento, trazas cartográficas de fallas y fracturas y una detallada cartografía de trazas de estratificación de la secuencia de estratos de crecimiento. Estos datos se posicionaron en 3D sobre un Modelo Digital del Terreno (MDT) del área con una resolución de ±2.5 m (Fig. R5). El anticlinal se reconstruyó aplicando el Método de los Dominios de Buzamiento (Fernández et al., 2004 a y b), el cual enuncia que la geometría de una estructura puede simplificarse en volúmenes en los cuales la orientación de la estratificación es constante (Fig. R6). Para aplicar el método ha de establecerse previamente un modelo geométrico a partir de los datos disponibles. Este modelo geométrico debe incluir: 1) una definición de los dominios de buzamiento (orientación promedio de la estratificación del

dominio y polaridad, posición y extensión de los límites del dominio), y 2) una definición de las geometrías estratigráficas en 3D (un modelo de separaciones estratigráficas entre diferentes horizontes). En total se definieron 91 dominios de buzamiento para la reconstrucción del techo de la Formación Guara, asumiendo una variación de ±5º de azimut y ±3º de buzamiento como límites de tolerancia entre dominios de buzamiento. Intersectando los dominios de buzamiento adyacentes se obtuvo un mapa de contornos estructurales en GOCAD (Paradigm™), proporcionando una geometría más suavizada de la superficie de referencia que incorpora y respeta todos los datos de entrada. El resto de las superficies de la secuencia pre-plegamiento fueron reconstruidas empleando una herramienta disponible en 3DMove (Midland Valley Exploration) que permite la creación de nuevas superficies plegadas a partir de una superficie preexistente por pliegues similares y paralelos. Dado que el Pico del Águila está considerado un pliegue paralelo a escala kilométrica (Millán, 1995), la herramienta de creación de superficies se utilizó para reconstruir la geometría de las superficies del techo del Triásico, Cretácico superior y Garumniense. Las superficies de la secuencia sin-plegamiento fueron reconstruidas individualmente, aplicando el Método de los Dominios de Buzamiento. Para controlar la variación de grosor estratigráfico de los estratos de crecimiento se aprovechó el excelente grado de afloramiento de estas unidades en el campo, así como las columnas estratigráficas detalladas publicadas en Millán et al. (1994).

Los datos de profundidad consisten en la interpretación de diversos perfiles sísmicos, la identificación y localización de los cuales puede encontrarse en la Fig. R1. Estos han permitido conocer la geometría del anticlinal en profundidad y validar las interpretaciones a partir de datos de campo. Debido a la baja calidad de los perfiles sísmicos, solamente se han podido interpretar los rasgos geométricos generales de la secuencia pre-plegamiento, así como la geometría del cabalgamiento frontal surpirenaico. Las interpretaciones sísmicas se convirtieron entonces a profundidad utilizando la velocidad de intervalo de cada unidad, deducida a partir de un pozo de exploración situado fuera del área de estudio y de los *Common Depth Points* (CDP's) de los perfiles sísmicos. Esta información se transfirió al entorno de trabajo 3D, con el fin de correlacionar

los horizontes entre los diferentes perfiles interpretados. Se generó entonces un mapa de contornos estructurales en 3D para cada falla u horizonte. En el caso de los horizontes estratigráficos pre-plegamiento, los nuevos datos se incorporaron como puntos de control en profundidad a cada mapa de contornos correspondiente.

R.5.2 RESULTADOS DE LA RECONSTRUCCIÓN

Mediante la metodología expuesta se han reconstruido ocho horizontes estratigráficos y nueve superficies de falla. A partir de la secuencia pre-plegamiento se han reconstruido las superficies correspondientes al techo de las siguientes unidades (Fig. R7): 1) Formación Guara (superficie de referencia del pliegue); 2) las facies del Garumniense; 3) el Cretácico superior; y 4) los materiales Triásicos. Ocho superficies de falla, el cabalgamiento interno N-S del anticlinal así como la geometría del cabalgamiento frontal surpirenaico también han sido reconstruidas. De la secuencia de estratos de crecimiento se ha reconstruido el techo de cuatro superficies, correspondientes a las cuatro secuencias deposicionales principales de las Formaciones Arguis y Belsué-Atarés (GS-I a GS-IV; Figs. R8 y R9).

La geometría del cabalgamiento frontal surpirenaico consiste en una rampa que buza hacia el norte, variando desde 15º en la parte septentrional del anticlinal hasta 37º en la zona frontal emergente, y un rellano subhorizontal que se extiende hacia el norte. El techo de la Formación Guara no se halla demasiado afectado por la presencia de fallas internas, y fosiliza el cabalgamiento interno N-S del anticlinal. Las unidades inferiores, en cambio, muestran un patrón estructural complejo debido a la interferencia entre las fallas (de orientación comprendida entre E-W y NNE-SSW) y el cabalgamiento N-S (Figs. R7 y R10a).

La secuencia sin-plegamiento muestra una geometría más suavizada, caracterizada por un adelgazamiento hacia la cresta del anticlinal y un decrecimiento hacia el techo de la intensidad de la deformación (Figs. R8, R9 y R10b). La secuencia GS-I no alcanza a cubrir la cresta del anticlinal. Las

secuencias superiores cubren progresivamente el techo de la Formación Guara (Figs. R8 y R9)

R.6 MODELIZACIÓN ANALÓGICA: GENERACIÓN DE ESTRUCTURAS PERPENDICULARES AL ORÓGENO

Los modelos analógicos presentados en este trabajo investigan la geometría inicial del nivel basal de despegue como posible factor de control en la generación de estructuras oblicuas y perpendiculares al orógeno, tales como las descritas en las Sierras Exteriores Aragonesas. El diseño del experimento se basa en observaciones de campo que indican una práctica ausencia de las facies Keuper en el núcleo de los anticlinales N-S (p.ej. Anticlinales del Pico del Águila y Gabardiella; Fig. R1), y un grosor más notorio de estos materiales en las zonas intermedias, donde las estructuras generales pirenaicas E-W se forman (p.ej. el frente de cabalgamiento surpirenaico). La finalidad de simular este nivel basal de despegue distribuido heterogéneamente fue la de testar si los cambios laterales de fricción podían ser capaces o no de causar la generación de estructuras arqueadas, oblicuas y perpendiculares, independientemente de la orientación de la dirección de acortamiento.

R.6.1 CONFIGURACIÓN INICIAL

La configuración inicial del experimento se compone de una secuencia de capas de arena interestratificadas y de diferentes colores que cubren un nivel basal irregular formado por tres cuerpos de silicona separados por arena sin cohesión (Fig. R11). La cobertera sedimentaria de materiales del Cretácico superior hasta el Luteciense se simuló mediante arena cuarcítica de densidad 1700 kg m^{-3}, valor de cohesión C de aproximadamente 140 Pa y cribada a una medida de grano promedio de 35 μm. El nivel de despegue irregular Triásico se simuló mediante la silicona SGM36 (con una densidad de 987 kg m^{-3} y viscosidad efectiva η de 5 x 10^4 Pa s a temperatura ambiente, manufacturada por Dow Corning Ltd.) intercalada lateralmente con arena cuarcítica seca y sin cohesión.

El aparato de deformación se situó sobre una placa de aluminio sobre la cual se encolaron granos de arena. Los modelos se caracterizaban por una anchura fija de 45 cm, una longitud inicial de 60 cm y un grosor constante de nivel de despegue de 8 cm (Fig. R11). El motivo de encolar arena sobre la placa basal de aluminio fue la de forzar un comportamiento altamente friccional en el basamento con el fin de acentuar el contraste entre el despegue dúctil (capas de silicona) y el despegue friccional (arena). Se aplicó compresión a una velocidad constante de 2 cm/h (5.56×10^{-6} m/s) desde un único lado, utilizando un pistón movilizado por un motor (Fig. R11). Los modelos fueron comprimidos hasta un 20% durante 6 horas.

R.6.2 RESULTADOS DE LA MODELIZACIÓN ANALÓGICA

El acortamiento aplicado a los modelos causó deformación tanto en las capas de arena como en las de silicona. El patrón de deformación fue diferente entre las zonas despegadas sobre un nivel friccional (arena; áreas HF) y las zonas despegadas sobre un nivel dúctil (silicona; áreas LF). La deformación comenzó con la aparición de tres cabalgamientos, en general rectilíneos, dado que el frente de deformación aún no había alcanzado la posición de la silicona, creando así una diferencia de avance entre las áreas despegadas sobre arena y las despegadas sobre la silicona. Las áreas HF muestran un levantamiento adicional respecto a las áreas LF, que ocasionalmente se manifiesta a través de pequeños cabalgamientos oblicuos que se unen al cabalgamiento frontal principal en la parte posterior del modelo. Tras un 16% de acortamiento (Fig. R12c) las estructuras no pueden acomodar más deformación y el frente migra hacia delante. Como consecuencia, se forma una segunda generación de estructuras paralelas a la dirección de acortamiento. A pesar de esto, en esta segunda generación la posición del frente de deformación coincide con la línea donde finalizan las capas de silicona. Tras un 20% de acortamiento (Fig. R12d) las áreas HF no avanzan tanta distancia como las áreas LF, creando un patrón estructural constituido por cabalgamientos de morfología ondulada que transportan más lejos las áreas despegadas sobre silicona que las áreas despegadas sobre arena.

La deformación de las capas dúctiles por flujo y engrosamiento dúctil y plegamiento se transfiere lateralmente a las áreas HF, de forma que se generan rampas laterales de los cabalgamientos que ascienden en la serie desde la terminación lateral de las capas de silicona. Estas rampas laterales se unen en el núcleo de las áreas HF, produciendo levantamiento y suave deformación en las unidades superiores, mientras que las unidades inferiores sufren gran deformación interna mediante fallas (Fig. R13 a y b). Se produce una migración lateral de las capas dúctiles hacia las áreas HF, así como un engrosamiento a lo largo del límite entre las áreas HF y LF, donde las rampas laterales descritas despegan (Fig. R13 a y b). Las secciones horizontales muestran la geometría interna de las capas en profundidad, pudiéndose observar cabalgamientos dirigidos hacia el antepaís en los que las unidades inferiores se encuentran cabalgadas, mientras que las superiores se encuentran suavemente plegadas. El único cierre periclinal observable se encuentra en el lado más cercano al orógeno de las estructuras transversales (Fig. R13), indicando que estas estructuras tienen una cierta inmersión hacia el orógeno debido al basculamiento creado por el emplazamiento de la lámina cabalgante.

Las áreas despegadas sobre arena, por tanto, acomodan la deformación mediante un levantamiento adicional respecto a las áreas despegadas sobre silicona, desarrollándose suaves anticlinales perpendiculares al orógeno en el bloque superior de los cabalgamientos. La localización de las crestas de estos anticlinales coincide prácticamente con el centro de las áreas HF. Este hecho indica que el contraste de fricción entre la arena y la silicona a lo largo de la dirección de acortamiento ha permitido la nucleación de los cabalgamientos sobre la línea de terminación lateral de las capas de silicona.

R.7 MODELIZACIÓN NUMÉRICA: EFECTO DE LA ESTRATIGRAFÍA MECÁNICA Y SEDIMENTACIÓN SIN-CINEMÁTICA

Este subcapítulo presenta los resultados obtenidos a partir de un modelo numérico, el cual se ha utilizado para mejorar el conocimiento sobre el efecto de

una estratigrafía mecánica compleja (no trivial) y de la sedimentación sin-cinemática en el crecimiento del anticlinal del Pico del Àguila. Con el fin de llevarlo a cabo se ha utilizado una técnica de modelización 2D conocida como Modelización de Elementos Discretos (*Discrete Element Modelling, DEM*).

Este método trata una masa de roca como un conjunto de elementos circulares conectados por parejas mediante enlaces que se rompen superando determinados umbrales de deformación (Hardy & Finch, 2005, 2007). Asignando diferentes valores de umbral de fracturación a cada pareja de elementos es posible modelizar diferentes propiedades mecánicas (p. ej. en una secuencia estratigráfica) en el conjunto de elementos que simulan la masa de roca. Esto nos permite testar el efecto de una determinada estratigrafía mecánica sobre la geometría, la cinemática y los mecanismos que se producen en el pliegue. De esta manera, este método proporciona más información que las técnicas de modelización cinemática previas. Además, permite una fácil supervisión del desplazamiento/localización de los elementos durante la modelización. El trayecto de desplazamiento, la evolución cinemática y la distribución de la deformación dentro del cuerpo de la roca puede ser seguida fácilmente en cualquier estadio de la modelización. Visto el intercalado de materiales competentes e incompetentes que caracteriza la estratigrafía de la zona de estudio (Fig. R2) consideramos adecuado este método para modelizar la evolución del anticlinal del Pico del Águila.

Como ya se ha mencionado, el Pico del Águila ofrece una buena sección a lo largo del eje del pliegue de toda la secuencia estratigráfica, hasta los materiales Triásicos del núcleo, así como una estratigrafía mecánica bien descrita y una excelente preservación y afloramiento de los estratos de crecimiento que registraron el crecimiento del pliegue. Esto proporciona una excelente base para poder comparar cómo la estratigrafía mecánica se comporta tanto en el modelo como en la naturaleza, y cómo la sedimentación sin-cinemática influenció la evolución del pliegue.

R.7.1 CONFIGURACIÓN INICIAL Y PARÁMETROS EXPERIMENTALES

El comportamiento de la masa de roca modelizada es a grandes rasgos elastoplástico y sin fricción (Place and Mora, 2001; Finch et al., 2003, 2004; Hardy and Finch, 2005, 2007), una aproximación que ya se ha empleado previamente en otros estudios para modelizar deformación frágil en rocas sedimentarias en la corteza superior. La deformación de la secuencia sedimentaria se produce en respuesta al acortamiento por subducción de la base del modelo a través de una ranura situada en el centro de la caja, en la cual la mitad derecha del modelo se mueve hacia la izquierda a una velocidad continua de 0,001 m por unidad de tiempo (Fig. R14). Se ha empleado una densidad homogénea de 2500 kg m^{-3} para toda la masa de roca, un valor común en la modelización de rocas sedimentarias en la corteza superior. La constante elástica K es de 5.5 x 10^9 N m^{-2}. El experimento corrió durante 2 x 10^6 unidades de tiempo con entrega de resultados cada 10^5 unidades, es decir, cada 100 m de acortamiento. Esto proporcionó un control preciso sobre la evolución estructural del pliegue y sobre la variación de la deformación, así como una geometría de los estratos de crecimiento bien delimitada. El desplazamiento total del experimento fue de 2km.

En el marco de trabajo de la modelización una *Lattice Unit* (LU) equivale a 250 metros. El conjunto inicial de partículas contiene 10245 elementos, agrupados en cuatro subconjuntos de radios diferentes: 0.125, 0.1, 0.075 y 0.05 LU (es decir, 31.25, 25, 18.75, 12.5 m, respectivamente). Estos elementos están distribuidos aleatoriamente en una caja rectangular cerrada. Consideramos estas dimensiones adecuadas, dado que proporcionan la resolución suficiente para modelizar una estructura de escala kilométrica como el Pico del Águila, evitando la generación de planos preferentes de debilidad y permitiendo, por lo tanto, una localización de la deformación no predefinida. Tras la generación inicial del conjunto de elementos, éstos se dejan reposar hasta que llegan a un equilibrio estable y se les deja compactar bajo el efecto de la gravedad durante 2 x 10^6 unidades de tiempo hasta obtener una configuración inicial de elementos estable, bien empaquetada, que minimiza el espacio entre partículas. La configuración inicial resultante de este proceso de sedimentación y

compactación mide 12.5 km de largo y aproximadamente 1.25 km de espesor estratigráfico, simulando una masa de roca continua que puede deformarse por rompimiento progresivo de los enlaces entre partículas (fracturación/fallas) y movimiento masivo de pares de elementos sin rotura de enlaces (plegamiento). La secuencia sedimentaria sin-cinemática se modelizó añadiendo sedimentos incrementalmente hasta un total de 11708 elementos. La configuración inicial está formada por 32 capas horizontales agrupadas en unidades con diferentes propiedades mecánicas con el fin de crear una compleja estratigrafía mecánica (Fig. R14).

R.7.2 RESULTADOS DE LA MODELIZACIÓN NUMÉRICA

La evolución de la geometría y la deformación de cizalla del modelo se muestran en la Fig. R15.

Tras un 4% de acortamiento (500 m; Fig. R15b) una pequeña estructura incipiente, de poca amplitud, empieza a formarse sobre la discontinuidad de velocidad (ranura en el centro del modelo). Las unidades incompetentes U2 y U4 muestran alta deformación de cizalla (abreviada como “deformación” sensu lato de aquí en adelante) tanto en la estructura como a cierta distancia de ella a lo largo del modelo. La unidad más competente, U1, se encuentra ya muy deformada en el núcleo del anticlinal. Las otras unidades pre-cinemáticas muestran una baja deformación, ligeramente acentuada en la zona del anticlinal (Fig. R15b). Los estratos de crecimiento muestran una gran deformación, aunque variable, a lo largo de la estructura. Sin embargo deben distinguirse dos tipos de deformación dentro de los estratos de crecimiento: en primer lugar, la deformación de cizalla debida a la deposición y continua compactación de las unidades más recientes (deformación restringida esencialmente a las dos capas más superficiales del conjunto; Fig. R15); en segundo lugar, la deformación mostrada por la pila sedimentaria sin-cinemática debida al acortamiento y plegamiento de la estructura. Un efecto de borde se observa en el límite derecho del modelo debido al desplazamiento de la pared de la caja hacia la izquierda. Tras un acortamiento del 8% (1000 m; Fig. R15c) la estructura central ha crecido significativamente, los flancos están más inclinados y muestra una ligera vergencia hacia la derecha. Se observa desarmonía en el plegamiento: bajo U4

se han generado pliegues menores, particularmente entre U2 y U4 hacia la derecha del modelo. U1 muestra una compleja deformación en el núcleo del anticlinal. Por encima de U4 la geometría del anticlinal es más suave, dibujando un pliegue continuo. Los estratos de crecimiento muestran marcadas diferencias de espesor estratigráfico produciendo prismas sedimentarios que se adelgazan hacia la charnela del anticlinal. En los estratos de crecimiento se observa una deformación de moderada a alta, con un contraste distintivo de deformación localizado en la base de los sedimentos sin-cinemáticos. Tras un acortamiento del 12% (1500 m; Fig. R15d) se observa un claro engrosamiento de las capas más incompetentes en las zonas de charnela de los dos sinclinales asociados a la estructura central, así como una deformación muy compleja en el núcleo del anticlinal. En particular, U1 resulta intensamente deformada, mostrando una geometría de cuello de botella. Pliegues menores crecen en U2 entre el anticlinal y el límite derecho del modelo. Se observa plegamiento desarmónico en la charnela del anticlinal, con grandes contrastes en el estilo de plegamiento por encima y por debajo de U4. La mayor parte de la deformación sigue concentrada en las unidades menos competentes. Los estratos de crecimiento rotan y se adelgazan hacia el crecimiento anticlinal, exhibiendo una gran deformación interna. Tras un acortamiento del 16% (2000 m; Fig. R15e) el crecimiento vertical del anticlinal parece estancarse (los estratos de crecimiento cubren la estructura) con el pliegue apretándose mediante la rotación de los flancos. A pesar de esto, el modelo muestra un desplazamiento en la distribución de la deformación hacia la derecha, manifestado por la propagación del plegamiento desde el límite derecho y dando lugar a pequeños pliegues de despegue que se generan sobre U2. En la estructura central, la deformación sigue concentrada en el núcleo, así como en los flancos, especialmente en las unidades U4y U5. En el núcleo U1 muestra una morfología todavía más acentuada de cuello de botella. En este estadio, los estratos de crecimiento muestran un grosor máximo en los sinclinales de 1.2 km, valor similar al descrito en el campo en el anticlinal del Pico del Águila.

R.8 RESTITUCIÓN GEOMECÁNICA 3D DEL ANTICLINAL DEL PICO DEL ÁGUILA

La restitución geomecánica del anticlinal del Pico del Águila se ha realizado utilizando un algoritmo de Modelización de Elementos Finitos (*Finite Element Modelling, FEM*), el cual considera propiedades mecánicas de las rocas para restituir la estructura del anticlinal (lo que se ha venido a nombrar recientemente *restitución geomecánica*), en lugar de considerar cualquier criterio de tipo cinemático. En la mayoría de los casos la cinemática de una estructura es desconocida o, al menos, no se ha cuantificado de forma precisa. De esta manera la restitución geomecánica proporciona un resultado mecánicamente estable basado en la geometría del estadio deformado y en las propiedades mecánicas de las rocas, tales como densidad, módulo de Young y coeficiente de Poisson (Maerten and Maerten, 2006; Guzofski et al., 2009).

R.8.1 METODOLOGÍA Y CONFIGURACIÓN INICIAL

La restitución secuencial del anticlinal del Pico del Águila se llevó a cabo con el programa Dynel3D (igeoss. Maerten & Maerten, 2006). El código implementado a Dynel3D está basado en un algoritmo de tipo FEM, una técnica de medios continuos que permite el estudio de la deformación natural basado en las propiedades mecánicas de las rocas. Aunque es un método estrictamente elástico, es apropiado para modelizar el comportamiento de estructuras geológicas complejas tales como pliegues y fallas (Maerten & Maerten, 2006). Las unidades estratigráficas se discretizan en un conjunto de elementos (tetraedros) a los cuales se le asignan las propiedades mecánicas. Las fallas se representan mediante superficies de contacto entre grupos de tetraedros. Estos elementos tetraédricos se deforman elásticamente en respuesta a restricciones tales como fuerzas aplicadas, desplazamientos y regiones de contacto entre superficies (fallas). Las ecuaciones del algoritmo se resuelven de forma interactiva y explícita, de manera que las fuerzas se pueden transmitir de nodo a nodo a través de todo el sistema, hasta que se alcanza un equilibrio. La formulación del algoritmo es, por lo tanto, adecuada para modelizar escenarios geológicos complejos que abarcan diversas etapas de deformación, como es el

caso de la restitución estructural. Además, la solución explícita que proporciona el algoritmo es eficiente y estable (Maerten & Maerten, 2006).

El modelo 3D del Pico del Águila se utilizó como estadio deformado para la restitución. La reconstrucción de los estratos de crecimiento fue clave para poder establecer una cronología de la deformación a partir de la restitución de las diversas secuencias deposicionales (GS-I a GS-IV). El tamaño promedio de los tetraedros (i.e. la resolución) fue de 310m por lado, un balance razonable para representar una estructura de escala kilométrica sin superar el límite de memoria permitido para un ordenador personal estándar. A pesar de eso, este valor de resolución implica que ciertos cuerpos de dimensiones inferiores no puedan ser representados o hayan de ser simplificados en cuerpos de dimensiones superiores. Éste es el caso de las unidades del Cretácico superior y del Garumniense, que tienen un espesor estratigráfico muy por debajo de la resolución de los tetraedros. Estas unidades fueron fusionadas en una única unidad mecánica llamada Garumniense-Cretácico, caracterizada por unas propiedades mecánicas promedio de las dos unidades iniciales. De manera similar, las ocho fallas internas del anticlinal se caracterizan por un salto de falla de decenas de metros, valor inferior a la resolución de los tetraedros. Estas fallas, por tanto, no fueron consideradas en la restitución de la estructura.

Como ya se ha mencionado, el algoritmo que utiliza Dynel3D requiere la definición de diversas propiedades mecánicas de las rocas, que deben ser indicadas previamente a la restitución. Dado que estas propiedades (densidad, módulo de Young y coeficiente de Poisson) varían con la litología a lo largo de la secuencia estratigráfica, se han fijado diferentes valores en función de la litología predominante en cada una de las unidades. Estos valores se documentan en la Tabla 1.

R.8.2 RESULTADOS DE LA RESTITUCIÓN GEOMECÁNICA

Se han considerado cinco estadios de restitución, de acuerdo con la restitución de los techos de las cuatro secuencias deposicionales GS-I, GS-II, GS-III y GS-IV y del techo de la Formación Guara (Fig. R16). Además de la geometría, se obtuvo también la distribución de la deformación de cizalla

(abreviada “deformación” sensu lato de aquí en adelante) para cada uno de los estadios de la restitución, con el fin de entender la evolución de la deformación de la estructura (Fig. R17).

La restitución del techo de la secuencia GS-IV (36.6 Ma) elimina la mayor parte del basculamiento asociado al emplazamiento del cabalgamiento frontal surpirenaico (Fig. R16 a y b). Además, se observa una rotación de eje vertical de aproximadamente 15º. La deformación se distribuye de forma heterogénea por todo el modelo (Fig. R17b). La GS-IV muestra una deformación moderadamente alta distribuida a lo largo de los sinclinales asociados, y que se incrementa hacia el anticlinal (los valores más altos coinciden con las áreas en las que la GS-IV es más delgada, Fig. R17b). El resto de las GS muestran una intensa deformación en la charnela de los sinclinales. En la secuencia pre-plegamiento las unidades del Garumniense-Cretácico y del Triásico muestran una intensa deformación en las zonas de charnela del anticlinal y de los sinclinales asociados. La Formación Guara muestra una deformación baja a moderada a lo largo de ambos flancos, y gran deformación en la charnela de los sinclinales (Fig. R17b).

La GS-III (37.17 Ma) es la primera secuencia restituida que no cubre todo el anticlinal. Su restitución resulta en un modesto decrecimiento de la inmersión del anticlinal de aproximadamente 4º (Fig. R16c) y una rotación en el sentido de las agujas del reloj de aproximadamente 2º. Se observa deformación baja a moderada en la charnela del anticlinal en la GS-III, y baja deformación en el resto de las GS. La deformación más importante se localiza en la Formación Guara, concretamente en el sinclinal oriental y a lo largo del flanco occidental (Fig. R17c). La unidad Garumniense-Cretácico muestra una deformación moderada a alta y un marcado deslizamiento de capa sobre capa respecto a las unidades subyacentes y suprayacentes. El Triásico muestra deformación moderada a alta, particularmente concentrada hacia la mitad de la secuencia en las zonas de charnela del anticlinal y los sinclinales.

Taula 1. Propiedades mecánicas empleadas para restituir el anticlinal del Pico del Águila

Unidad	Litología Predominante	Módulo de Young (Pa)	Coeficiente de Poisson	Densidad (Kg/m3)
GS-IV*	Areniscas	2.2 e+10	0.24	2480
GS-III*	Areniscas margosas	2.2 e+10	0.24	2480
GS-II*	Margas	2.8 e+10	0.14	2530
GS-I*	Margas	2.8 e+10	0.14	2530
Guara	Calcáreas	4.8 e+10	0.25	2500
Garumniense-Cretácico	Lutitas- Calcáreas	2.8 e+10	0.14	2530
Triásico	Calcáreas dolomíticas	4.8 e+10	0.25	2500

Estos son valores promedio para cada tipo de roca, y parcialmente basados en indicaciones de campo.

* GS: Estratos de Crecimiento de las Formaciones Arguis y Belsué-Atarés.

Tras restituir la GS-II (37.74 Ma) la inmersión del pliegue es prácticamente omitible (Fig. R16d) y la estructura ha rotado 10º adicionales. La deformación (Fig. R17d) es superior respecto al estadio anterior, particularmente en la zona del cierre periclinal del anticlinal. La Formación Guara acomodó una deformación moderada en el flanco oeste y en la cresta del anticlinal, y alta deformación en la charnela del sinclinal oriental (Fig. R17d). La unidad mecánica Garumniense-Cretácico muestra alta deformación en toda la estructura a excepción de la cresta del anticlinal. El Triásico muestra una deformación poco heterogénea y moderada a alta.

La restitución de la GS-I (40.04 Ma) permite observar ya la geometría de la Formación Guara en la cresta del anticlinal (Fig. R16e). Se observa una gran deformación en las unidades pre-plegamiento, mostrando un anticlinal bien desarrollado, todavía con mucha deformación acumulada. No se observa una rotación de eje vertical significativa con respecto al estadio anterior. La deformación en la GS-I se distribuye de forma heterogénea, mostrando una deformación baja a moderada en la zona de charnela de los sinclinales y a lo largo de los flancos que dibujan una geometría *onlap* sobre la formación Guara (Fig. R17e). La Formación Guara muestra baja deformación en la cresta del anticlinal y una deformación moderada en el cierre periclinal y a lo largo de los flancos. La unidad Garumniense-Cretácico muestra una deformación particularmente alta en la charnela y a lo largo de los flancos. El Triásico muestra una deformación moderada a alta en los sinclinales y a lo largo del despegue, y una baja deformación en la cresta del anticlinal (Fig. R17e).

Finalmente, la restitución de la Formación Guara (41.52 Ma) implica el despliegue de la estructura así como una rotación adicional de aproximadamente 6º (Fig. R16f). La rotación de eje vertical varía entre las unidades de la serie pre-plegamiento, mostrando una rotación ligeramente superior de cada unidad respecto a la unidad inmediatamente subyacente (la rotación es ligeramente superior a medida que se asciende en la serie; Fig. R16f). La deformación varía de muy baja a muy alta, con valores bajos y moderados por todo el modelo y picos de deformación muy alta concentrados en la charnela de los sinclinales y localmente en la cresta del anticlinal (Fig. R17f).

La unidad Garumniense-Cretácico y el Triásico muestran valores de deformación más altos en la charnela de los sinclinales (Fig. R17f). El techo y la base de las unidades muestran valores de deformación ligeramente más bajos a lo largo de los contactos con las otras unidades y un significativo deslizamiento de capa sobre capa entre ellas.

R.9 RESUMEN DE LOS RESULTADOS OBTENIDOS Y DISCUSIÓN

A continuación se presenta un resumen de los resultados obtenidos mediante las diferentes técnicas de modelización así como una discusión sobre las ventajas, inconvenientes y limitaciones de cada una de ellas, y su aportación al conocimiento de la evolución estructural del anticlinal del Pico del Águila.

R.9.1 BENEFICIOS Y DESVENTAJAS DE LAS TÉCNICAS EMPLEADAS

Cada uno de los modelos presentados proporciona nuevos conocimientos sobre la evolución estructural del anticlinal del Pico del Águila, mejorando así el conocimiento sobre la geología de las Sierras Exteriores Aragonesas. Cada uno de los modelos fue específicamente diseñado para testar ciertos parámetros observados en la naturaleza, incorporando las diferentes contribuciones al modelo de evolución estructural. Sin embargo, se deben tener presentes las limitaciones de cada una de las técnicas de modelización con el fin de escoger el método adecuado para un propósito concreto. De esta manera puede evaluarse el resultado de cada modelo, extraer la aportación neta y evitar así errores en la interpretación de los resultados.

En este sentido, la modelización analógica ha sido una técnica adecuada para modelizar las heterogeneidades del nivel de despegue basal a escala regional: ha permitido una fácil visualización en 3D de la respuesta del modelo a la deformación en términos de avance y levantamiento diferencial de la cobertera sedimentaria, estilo estructural y relieve entre los diferentes dominios estructurales. Los modelos analógicos han representado acertadamente los

grandes cambios de estilo estructural observados a escala regional. Los contrastes mecánicos entre la arena seca y la silicona modelizaron acertadamente el efecto de los cambios laterales entre las facies Keuper y Muschelkalk en el nivel de despegue Triásico. Reprodujeron eficientemente un mayor levantamiento de orientación N-S (paralela a la dirección de acortamiento) de las áreas despegadas sobre un despegue friccional (áreas HF) y un mayor avance del frente de deformación en áreas despegadas sobre un despegue dúctil (áreas LF). Por contra, el hecho de trabajar con arena seca y silicona no proporciona una precisión suficiente en las propiedades mecánicas de la cobertera como para poder modelizar su complejidad interna: los grandes contrastes de comportamiento mecánico descritos en la columna estratigráfica aflorante en la que diversas unidades de comportamiento dúctil están presentes y controlan el crecimiento de la estructura (Figs. R2 y R5), no pueden ser modelizados usando unos pocos materiales diferentes. Con el fin de modelizar la complejidad interna de la cobertera, por tanto, haría falta una importante cantidad de materiales análogos diferentes y, aún así, las propiedades mecánicas disponibles estarían limitadas al número de materiales diferentes empleados en la modelización. Por este motivo, se prefirió optar por la Modelización de Elementos Discretos para investigar la importancia de la estratigrafía mecánica y los estratos de crecimiento en la evolución del Pico del Águila.

La Modelización de Elementos Discretos (abreviada DEM de ahora en adelante) permite un control preciso de la respuesta mecánica de cada unidad y, por tanto, ofrece la posibilidad de configurar una estratigrafía mecánica compleja con la que modelizar un gran número de escenarios geológicos. Esto hace que la DEM sea un método ideal para explorar en detalle la evolución de los anticlinales N-S de las Sierras Exteriores Aragonesas. El método permite seguir la evolución de cada una de las partículas que conforman la masa de roca del modelo mediante parámetros físicos tales como los vectores de desplazamiento, velocidad y aceleración, posición instantánea, etc., a partir de los cuales se deriva la distribución de la deformación en el modelo. Los modelos presentados en esta Tesis han contribuido a la ampliación de conocimientos sobre cómo la deformación es acomodada de manera diferente en función del

comportamiento mecánico de cada unidad, conduciendo a importantes contrastes en estilos estructural entre unidades adyacentes de una misma cobertera sedimentaria. Los modelos numéricos permiten un control preciso de los parámetros introducidos al modelo. En los modelos presentados, es de gran importancia el control del grosor estratigráfico de las unidades pre-pliegue (grosor constante, configurado previamente a la modelización), y aún más de los estratos de crecimiento, dado que el método es sensible a cambios en la evolución del sistema dependiendo del espesor de las unidades y de modelo en general. Sin embargo, la DEM no contempla la imposición en el modelo de criterios cinemáticos previos. La DEM es una técnica de modelización de avance en la que las propiedades físicas de las partículas, las dimensiones iniciales de la caja y el espesor estratigráfico son los únicos parámetros introducidos. En este sentido la DEM mantiene ciertas similitudes con la modelización analógica, pero permite un control más detallado de las propiedades mecánicas y una supervisión instantánea de los parámetros cinemáticos y de la distribución de la deformación en cada una de las partículas del modelo. En contraste, los modelos numéricos presentados son estrictamente 2D, ofreciendo una representación parcial de la estructura modelizada (comparable a un corte geológico E-W del anticlinal). A pesar de que ya existen experimentos DEM en 3D (Carmona et al., 2008) éstos son todavía muy costosos en términos de consumo de tiempo, especialmente para modelizar escenarios geológicos complejos como los anticlinales N-S de las Sierras Exteriores. Por este motivo, consideramos que una aproximación 2D como la presentada en esta Tesis ha sido adecuada para investigar los papeles de la estratigrafía mecánica y los estratos de crecimiento en una estructura como el anticlinal del Pico del Águila.

Como ya se ha dicho, el Pico del Águila es ciertamente una estructura 3D, con un excelente grado de preservación de los estratos de crecimiento. La interferencia estructural entre el anticlinal N-S y el cabalgamiento frontal surpirenaico (E-W) crea una estructura con una compleja evolución cinemática que resulta difícil de representar mediante métodos bidimensionales. Estos factores motivaron la reconstrucción tridimensional del anticlinal y los estratos de crecimiento, con el fin de poder establecer un modelo de evolución 3D en el que se tuviera un control cronológico de la deformación. El excelente grado de

afloramiento y preservación y la fácil accesibilidad hicieron del Pico del Águila un caso ideal para llevar a cabo la adquisición de datos en el campo y una minuciosa cartografía de trazas geológicas. Esto permitió una también minuciosa reconstrucción en 3D tanto de la secuencia pre-plegamiento como de los estratos de crecimiento, sirviendo así de punto de partida para realizar una restitución geomecánica con la cual conocer la evolución estructural del anticlinal. Basado en las propiedades mecánicas de las rocas, el algoritmo implementado en Dynel3D supuso una alternativa para llevar a cabo una restitución en 3D sin necesidad de imponer criterios cinemáticos complejos de los cuales no se tiene un conocimiento detallado. Así pues, el mayor beneficio de utilizar la restitución geomecánica es que permite restituir una estructura introduciendo propiedades reales y medibles de las rocas, sin imponer criterios cinemáticos previos, de los cuales no se tiene un conocimiento cuantitativo en muchos casos. La densidad, el módulo de Young, el coeficiente de Poisson o la porosidad son propiedades que se pueden medir en análisis mecánicos de materiales en laboratorio o, de otra manera, se pueden obtener valores generales publicados en tablas de propiedades mecánicas para diferentes materiales comunes en la corteza terrestre. En cualquier caso, se puede disponer fácilmente de valores medidos o publicados de las propiedades mecánicas de los materiales y llevar a cabo una restitución que proporciona un resultado físicamente razonable, mecánicamente estable y que está de acuerdo con la evolución cinemática derivada a partir de otros métodos.

Las principales desventajas de este método están directamente relacionadas con las limitaciones técnicas del ordenador. El algoritmo implementado a Dynel3D puede requerir una gran cantidad de memoria disponible del ordenador, dependiendo de la resolución deseada para el modelo (es decir, de la medida de los tetraedros que discretizan la superficie). Esto significa que para una estructura de unos pocos kilómetros como el Pico del Águila, un ordenador estándar permite una resolución de unos pocos centenares de metros. Esto hace de este método una opción poco recomendable para estudiar en detalle y a esta escala cuerpos geológicos que se encuentran bajo el límite de la resolución del modelo. Por otro lado, el algoritmo se basa en el uso de las leyes de la elasticidad para restituir grandes cantidades de deformación

no recuperable (inelástica). Este hecho también implica ciertas limitaciones, particularmente en cuanto a magnitud de la deformación se refiere. El uso de un método elástico proporciona valores de deformación que son notablemente inferiores que los que se puedan predecir mediante otras técnicas (p. ej. DEM) y que los valores obtenidos en experimentos de campo o laboratorio. Por tanto, este método es adecuado para predecir patrones o distribuciones de deformación, mecanismos de plegamiento y dominios potenciales de fracturación más que para predecir magnitudes de deformación y/o estructuras mesoscópicas como patrones u orientaciones de fracturas en el seno de la estructura.

R.9.2 VALIDACIÓN E INTEGRACIÓN DE LAS DIFERENTES TÉCNICAS DE MODELIZACIÓN

Todos los experimentos presentados en este trabajo han estado, de un modo u otro, basados en observaciones, descripciones y datos adquiridos en el campo. Siendo ya conscientes de las ventajas y limitaciones de cada uno de los métodos se puede tener una imagen más clara de la contribución de cada uno de los modelos, y ser capaz de ofrecer una respuesta razonada cuando se cuestiona el uso de uno u otro determinado método. Validar e integrar los resultados de diferentes técnicas, métodos o aproximaciones significa, por tanto, reunir las contribuciones de cada uno de los modelos para construir un modelo unificado de la evolución estructural, pero también cubrir las lagunas que cada técnica manifiesta, de manera que los diferentes métodos se complementen unos con los otros.

En este sentido los modelos analógicos proporcionaron nuevos conocimientos a escala regional, ofreciendo respuesta sobre los procesos que ocasionaron la generación de las estructuras inicialmente arqueadas y oblicuas, y que finalmente derivaron en los anticlinales N-S de las Sierras Exteriores. La modelización se basó en observaciones de campo que indicaban una escasa presencia de las facies Keuper en el núcleo de los anticlinales N-S, y replicó muchos de los rasgos del anticlinal en la naturaleza: mayor elevación N-S asociada al emplazamiento de un cabalgamiento de orientación E-W en las áreas con poca o ninguna presencia de nivel de despegue dúctil, un mayor

avance del frente de deformación en áreas entre anticlinales N-S, desarrollo de estos anticlinales en el bloque superior de cabalgamiento frontal y mostrando una inmersión hacia el orógeno, rotación del eje vertical del bloque superior del cabalgamiento en las zonas donde los pliegues N-S se desarrollan y morfología ondulada del frente de cabalgamiento (Figs. R12 y R18).

Sin embargo, la arena seca no es un material adecuado para modelizar pliegues estrechos y de flancos altamente inclinados como los anticlinales N-S de las Sierras Exteriores Aragonesas, los cuales se caracterizan por una estratigrafía mecánica compleja en la que las propiedades mecánicas varían a lo largo de la columna paralelamente a la litología (Figs. R12 y R14). En cambio, los modelos numéricos de elementos discretos satisficieron esta limitación y reprodujeron el estilo estructural del Pico del Águila después de configurar una estratigrafía mecánica que simuló la secuencia descrita en el campo. La manera diferente en la que cada unidad acomodó la deformación fue replicada por los modelos numéricos: fallas penetrativas y alta deformación interna en las unidades inferiores cohabitaron con un plegamiento más suave en las unidades superiores, al mismo tiempo que los estratos de crecimiento acomodaron gran cantidad de deformación y equilibraron el anticlinal contra las inestabilidades gravitacionales (Fig. R15). El nivel de despegue interno actuó como una barrera, permitiendo que las unidades superiores se plegaran mientras las inferiores concentraban mucha más deformación mediante fallas, deformación interna y plegamiento más intenso. Estos experimentos nos proporcionaron un mayor conocimiento sobre cómo se comporta la estratigrafía de las Sierras Exteriores en respuesta al acortamiento de la orogenia alpina, y como múltiples mecanismos de plegamiento pueden tener lugar simultáneamente en función de las propiedades mecánicas de cada una de las unidades estratigráficas implicadas.

A pesar de esto, el entorno 2D de los modelos numéricos no dio respuesta acerca de otros procesos cinemáticos bien documentados en el Pico del Águila y que implican un estudio tridimensional, como son la rotación del eje vertical del anticlinal, su relación con el cabalgamiento frontal surpirenaico y con sus estructuras asociadas. El efecto del deslizamiento capa sobre capa *(flexural slip)* tampoco se investigó en estos modelos, siendo éste un mecanismo de

plegamiento importante descrito en el área de estudio. Estas limitaciones fueron superadas gracias a la reconstrucción y restitución geomecánica tridimensional del Pico del Águila, que añadió la tercera dimensión, validó y complementó la evolución estructural y la respuesta mecánica predichas por los modelos analógicos y numéricos. La restitución predijo de forma independiente y sin ningún criterio cinemático impuesto una rotación de eje vertical de 33º validando así la rotación ya descrita por estudios paleomagnéticos previos (Pueyo et al., 2002; Rodríguez-Pintó et al., 2008) y por modelos analógicos (Vidal-Royo et al., 2009). Así mismo, la restitución evidenció también una diferente evolución de la sedimentación y la elevación entre los flancos, así como la incorporación del mecanismo de deslizamiento de capa sobre capa tal como se ha descrito en el campo (Fig. R16).

Tal y como ya habían sugerido los modelos numéricos 2D, múltiples mecanismos de plegamiento se describieron produciéndose simultáneamente en diferentes unidades, dependiendo de las propiedades mecánicas de cada una de ellas. Además, la restitución puso de manifiesto que también se producen una multitud de mecanismos de plegamiento simultáneamente dentro de una misma unidad, dependiendo del dominio estructural del pliegue en el que se encuentre. Esta combinación de mecanismos de pliegue en diferentes unidades y dominios estructurales dio lugar a una compleja distribución de la deformación en la estructura, en la que las propiedades mecánicas de las unidades causarán que la deformación se concentre en uno u otro dominio y, por tanto, que se deformen dando lugar a un determinado estilo estructural (Fig. R17).

Por otro lado, las limitaciones asociadas a la restitución geomecánica realizada con Dynel3D ya han sido mencionadas previamente. La falta de información asociada al límite de resolución de los tetraedros queda parcialmente cubierta por los modelos numéricos 2D, los cuales informan de una respuesta mecánica diferente para cada una de las unidades modelizadas. Las limitaciones asociadas al uso de un modelo elástico para restituir grandes cantidades de deformación inelástica (no recuperable) se solucionan restituyendo y sumando pequeños incrementos de deformación, incluyendo el efecto de las fallas, los niveles de despegue y el deslizamiento de capa sobre

capa. De esta manera, se requiere que cada volumen se restituya elásticamente, pero a rasgos generales el modelo experimenta deformaciones permanentes y finitas que se manifiestan mediante desplazamientos de fallas, despegues y deslizamientos de capa sobre capa (Maerten and Maerten, 2006, y Guzofski et al., 2009 que utilizan una técnica similar de restitución).

En general, cada uno de los métodos de modelización presentados en esta Tesis afronta un nuevo interrogante de la evolución estructural de los anticlinales N-S de las Sierras Exteriores, aportando nuevos conocimientos que están de acuerdo con las observaciones hechas en el campo y llevan un paso más allá los aspectos que permanecían descubiertos por otras técnicas. En otras palabras, los modelos presentados contribuyen con nuevos aspectos sobre la geología de las Sierras Exteriores Aragonesas, validan los resultados obtenidos mediante otros métodos y estudios, e integran parte de un modelo unificado y más robusto sobre la historia geológica de las Sierras Exteriores Aragonesas (Fig. R19).

R.9.3 EL ANTICLINAL DEL PICO DEL ÁGUILA: MODELO INTEGRADO DE EVOLUCIÓN ESTRUCTURAL

Los resultados de los diferentes modelos presentados en esta Tesis, combinados con los estudios previos que se han llevado a cabo en la región en diferentes disciplinas, nos ha permitido presentar un modelo integrado de evolución estructural para el anticlinal del Pico del Águila.

El anticlinal del Pico del Águila es un pliegue de despegue sobre una compleja geometría irregular de facies Muschelkak y Keuper (Triásico medio y superior, respectivamente).

Previamente a la deposición de la cobertera Cretácica-Terciaria el área ya se caracterizaba por una compleja estructura y una larga historia geológica. Según las reconstrucciones paleográficas (López-Gómez et al., 2002; Castillo-Herrador, 1974; Jurado, 1990; Salvany, 1990) la región se localizaba en un alto de la cuenca extensional Triásica, en el cual tuvo lugar una muy baja tasa de sedimentación durante el Triásico superior. Esta posición estructural influenció el bajo e irregular grosor estratigráfico de las facies Keuper (formadas por

lutitas rojas y capas de evaporitas) observadas en el área y el complejo paso lateral con las facies pre- y sin-extensivas del Muschelkalk (facies M2: lutitas, margas y evaporitas; M3: dolomías y calcáreas dolomíticas) (Fig. R19a). Además, el patrón estructural en el Triásico superior se presume complejo, y la fracturación penetrativa que caracteriza estas unidades hoy en día se creen parcialmente heredadas del patrón estructural de edad Triásica. Este marco geológico tan complejo dio como resultado un substrato Triásico mecánicamente irregular y heterogéneo, sobre el cual la cobertera Cretácica-Terciaria se depositó.

Fue hace unos 42.67 Ma (Luteciense superior) (Poblet & Hardy, 1995) cuando el anticlinal del Pico del Águila comenzó a crecer. Dadas las heterogeneidades mecánicas descritas en el despegue Triásico, el anticlinal se generó formando un alto ángulo (entre 69º y 57º, dependiendo de qué valor de rotación total se tome) respecto a la tendencia estructural pirenaica E-W (Fig. R19b). La cobertera sedimentaria experimentó una mayor elevación de orientación NNW-SSE en las áreas con menor grosor de facies Keuper (baja proporción de espesores entre la cobertera y el despegue dúctil), formando un bajo ángulo con la dirección de transporte tectónico de los Pirineos (aproximadamente N-S). Estos grandes contrastes mecánicos en el despegue basal produjeron también la rotación de eje vertical en sentido de las agujas del reloj, causando que el frente de la deformación avanzara a una velocidad diferente en función de la naturaleza mecánica del nivel basal de despegue Triásico en diferentes áreas. Dada la complejidad mecánica de la cobertera sedimentaría, a lo largo de la cual se ha descrito una respuesta mecánica heterogénea, el acortamiento N-S fue acomodado por plegamiento en lugar de generar rampas de cabalgamiento oblicuas, formando un pequeño pliegue de despegue incipiente sobre el cual se depositaban sedimentos carbonáticos en un ambiente de plataforma marina poco profunda (secuencia deposicional 3 de la Formación Guara).

Hace aproximadamente 41.50 Ma se produjo una transición brusca de ambiente sedimentario, pasando de una plataforma carbonatada poco profunda a un ambiente transicional de talud, comenzando la deposición de las margas azules y azoicas, ricas en glauconita, de la GS-I de la Formación Arguis. La

deposición de estos materiales fue acompañada de una gran tasa de elevación del pliegue, muy superior a la tasa de sedimentación. Esto resultó en la formación de geometrías en *onlap* y en un adelgazamiento de los materiales de la GS-I sobre los flancos del anticlinal definidos por la secuencia 3 de la Formación Guara, que permanecieron descubiertos sin que los sedimentos de la GS-I alcanzaran la cresta del anticlinal (Fig. R19c). Esta gran elevación, la creación de espacio disponible para la sedimentación y el ciclo transgresivo que caracterizó la deposición de las Formaciones Guara y Arguis (Millán et al., 1994; Castelltort et al., 2003) controlaron el cambio de facies sedimentarias que hay entre las calcáreas de plataforma somera de la Formación Guara y las margas de talud le la Formación Arguis. En aquel tiempo y hasta hace unos 40.04 Ma la tasa de sedimentación creció progresivamente. El frente de cabalgamiento surpirenaico comenzó a generarse, añadiendo un ligero basculamiento del anticlinal hacia el norte (Fig. R19c).

Hace unos 40.04 Ma se dio un cambio en el ambiente deposicional que implicó el final de la deposición de la GS-I. Diversos mecanismos de plegamiento caracterizaron la evolución estructural en esta etapa: en la GS-I predominó la migración de charnela en los sinclinales asociados al anticlinal, mientras que una combinación de alargamiento y rotación de flanco se produjo a lo largo de la parte E-W de los flancos del anticlinal. Al mismo tiempo, en la formación Guara el alargamiento de flanco predominó en el cierre periclinal y la rotación de flanco lo hizo a lo largo de la parte N-S de los flancos del anticlinal (Fig. R19d). Esta compleja interacción de mecanismos de pliegue entre las diferentes unidades y dominios estructurales caracterizaron todo el crecimiento del pliegue, y llevó a los contrastes de estilo estructural que se describen hoy en día en el campo: un cabalgamiento interno paralelo a la tendencia estructural del pliegue afecta a la secuencia comprendida entre las facies Muschelkalk y la secuencia 2 de Guara, fallándola y deformándola de manera compleja, mientras que la serie suprayacente formada por la secuencia 2 de Guara hasta la Formación Campodarbe se encuentra plegada más suavemente. Con más acortamiento, el emplazamiento de la rampa de cabalgamiento frontal surpirenaico causa un incremento en la inmersión del pliegue sincrónicamente

a la rotación progresiva del anticlinal en el sentido de las agujas del reloj (Fig. R19d).

Hace unos 37.74 Ma el ambiente deposicional cambió ligeramente describiendo a partir de entonces la presencia de foraminíferos bentónicos, briozoos, bivalvos y equinodermos (Millán et al., 1994). En general, el anticlinal había rotado ya un total de 6º respecto al inicio de la deformación. Sin embargo, tal como muestra la restitución, el deslizamiento capa sobre capa acentúa esta rotación de las capas superiores respecto a las inferiores, dado que se observa una rotación ligeramente superior en las unidades más jóvenes. El anticlinal, por tanto, no rotó como un bloque rígido: los contrastes mecánicos en el despegue basal condujeron a la rotación general de la estructura a medida que el cabalgamiento frontal surpirenaico avanzaba, pero el deslizamiento capa sobre capa entre unidades causó una rotación incremental ligeramente superior a medida que se asciende en la serie estratigráfica.

De acuerdo con Millán et al (1994), después de la deposición de la GS-III hace unos 37.17 Ma el ambiente deposicional cambió a una rampa carbonatada de bajo ángulo, con una sedimentación consistente en facies margosas (facies de rampa externa) interestratificadas con facies carbonáticas (facies de rampa media) con mucha presencia de comunidades bentónicas de pectínidos. Se produjo una rotación adicional de unos 10º respecto al estadio anterior así como un aumento de la inmersión del pliegue hacia el norte de unos 4º. Ambos incrementos indican una actividad creciente en el emplazamiento del cabalgamiento frontal surpirenaico durante este periodo.

La deposición de la GS-IV (Formación Belsué-Atarés, hace unos 36.6 Ma), en cambio, no implicó un aumento significativo de la rotación (unos 2º aproximadamente) y de la inmersión (unos 4º) del anticlinal. Esta fue la primera secuencia deposicional que cubrió todo el anticlinal (Fig. R19e), e implicó un cambio en el sistema deposicional hacia un ambiente deltaico, caracterizado por la progradación de lóbulos deltaicos sobre margas de prodelta, y por la sedimentación de areniscas granocrecientes y finas secuencias margosas (Millán et al., 1994). Debido al deslizamiento capa sobre capa descrito en los estratos de crecimiento, las GS acomodaron una deformación modelada, con el

máximo de deformación concentrada en la secuencia pre-plegamiento, principalmente debido al emplazamiento de la rampa de cabalgamiento frontal surpirenaico bajo la estructura del anticlinal.

Finalmente, desde la GS-IV hasta el cese de la deformación (estimado hace unos 34.8 ± 1.72 Ma según Poblet and Hardy, 1995) el marco deposicional cambió de ambientes fluviodeltaicos a fluviales caracterizados por la deposición y sedimentación de areniscas, lutitas y conglomerados de la Formación Campodarbe. La rotación registrada en este estadio fue importante, aproximadamente 15º respecto al estadio anterior, así como también lo fue el incremento en la inmersión del pliegue de unos 18º (Fig. R19e). Esto indica que el emplazamiento de la rampa del cabalgamiento surpirenaico mostró una mayor actividad durante este periodo. El deslizamiento capa sobre capa implicó un plegamiento y una rotación diferentes entre las diversas unidades que generó la asimetría descrita en la geometría actual del pliegue. También durante este último estadio deformativo se produjeron las fallas extensivas en la cresta del anticlinal que se observan a lo largo de toda la secuencia de estratos de crecimiento, principalmente debidas a un estiramiento del arco exterior del pliegue y a inestabilidades gravitacionales de la cresta del anticlinal.

R.10 CONCLUSIONES

En esta Tesis se presentan diferentes técnicas de modelización, las cuales se han integrado posteriormente con el fin de conocer mejor la evolución estructural del anticlinal del Pico del Águila y, por tanto, de los anticlinales N-S de las Sierras Exteriores Aragonesas.

Los modelos analógicos han proporcionado nuevos conocimientos sobre la formación y evolución de estructuras oblicuas y transversales al orógeno. Basado en una distribución irregular del nivel basal de despegue Triásico, los modelos simulan las características de los pliegues N-S de las Sierras Exteriores Aragonesas: generación sincrónica al emplazamiento del cabalgamiento frontal surpirenaico, mayor relieve estructural comparado con las estructuras paralelas

al orógeno, ausencia de un despegue dúctil representativo en el núcleo de las estructuras, fallas penetrativas en las unidades inferiores y plegamiento de las unidades superiores, inmersión de los anticlinales hacia el orógeno y cierre periclinal meridional no cabalgado por el cabalgamiento frontal surpirenaico.

Los modelos de elementos discretos se han utilizado para testar la influencia de una estratigrafía mecánica compleja y la presencia de estratos de crecimiento en la generación y evolución del anticlinal del Pico del Águila. La variabilidad mecánica de la serie estratigráfica ha implicado una gran y compleja deformación en las unidades incompetentes, mientras que las unidades más competentes están sujetas a una deformación más distribuida y a plegamiento simple. Como resultado de las diferentes respuestas mecánicas al acortamiento, es difícil explicar la evolución de una estructura como el Pico del Águila en términos de parámetros cinemáticos. La presencia de los estratos de crecimiento reduce los efectos del estiramiento, de las fallas extensivas y de las inestabilidades gravitacionales en la cresta del anticlinal. La carga creada por los sedimentos sin-cinemáticos implica también que la deformación quede más confinada al núcleo de la estructura, creando así un pliegue más estrecho que en el caso de ausencia de sedimentación sin-cinemática.

La reconstrucción y restitución 3D del anticlinal del Pico del Águila también sugiere que el crecimiento de un pliegue de despegue en 3D está caracterizado por la combinación de múltiples mecanismos de plegamiento produciéndose simultáneamente en diferentes unidades y dominios estructurales durante la formación del anticlinal, dependiendo de las propiedades mecánicas de los materiales implicados en la deformación. Por lo tanto, la comprensión de la cinemática del pliegue no tendría que pasar por alto la consideración del comportamiento mecánico de las rocas para tener un conocimiento más acertado de la evolución de una estructura.

La correcta integración de las diferentes técnicas de modelización está obviamente relacionada con las aportaciones de cada modelo, pero también con las limitaciones de cada uno de los métodos. En este sentido, en esta Tesis se presenta un modelo de evolución estructural para el anticlinal del Pico del Águila basado en la integración de modelos estructurales 3D, analógicos,

numéricos y restituciones geomecánicas de la estructura, a los cuales se le añaden las aportaciones proporcionadas por trabajos clave previos sobre la región. Por lo tanto, combinando múltiples disciplinas y métodos de modelización se aporta sin duda una mayor comprensión de la evolución de una estructura así como de los procesos que condujeron la generación y evolución de los anticlinales de despegue N-S de las Sierras Exteriores Aragonesas de los Pirineos Meridionales.

R.10.1 PERSPECTIVAS DE FUTURO

Tras diversos años de estudiar los anticlinales N-S de las Sierras Exteriores Aragonesas se han planteado muchas preguntas, retos y dificultades, algunos de los cuales se han podido solucionar satisfactoriamente mientras que otros han permanecido sin respuesta. Además, se han iniciado investigaciones paralelas no recogidas en este volumen y que han tenido que ser apartadas en un momento u otro, bien sea por falta de tiempo, de recursos humanos, o simplemente porque no se ha podido encontrar un enlace directo con el objetivo global de esta Tesis. Pero una vez finalizada esta etapa, quizás se dispondrá de la ocasión de recuperarlas y dedicarles el tiempo y el esfuerzo necesario. Estas cuestiones son:

a) La reconstrucción y restitución secuencial 3D de los anticlinales N-S vecinos al Pico del Águila, como son el anticlinal de Belsué de Rasal y el de Gabardiella. Llevando a cabo este ejercicio en estas estructuras vecinas se proporcionaría una visión más global de la rotación de eje vertical de los anticlinales a una escala más regional, dando ideas suficientes para comparar la evolución de la deformación a lo largo del trazado del frente de cabalgamiento surpirenaico.

b) Un minucioso estudio de campo de la fracturación asociada al anticlinal del Pico del Águila. Manoel Valcárcel ya realizó un primer estudio de las fracturas asociadas al anticlinal, en el que obtuvo resultados prometedores para comparar con el patrón de deformación derivado a partir de la restitución geomecánica y los modelos mecánicos 2D. Sin embargo, sería necesario un estudio más detallado, con una mayor inversión de tiempo y recursos para

conseguir más estaciones de medida y tener así un mayor control de cómo las fracturas se distribuyen por el anticlinal.

c) Un desarrollo e implementación de una herramienta automatizada para reconstruir la geometría de los estratos de crecimiento. Las secuencias deposicionales reconstruidas en los estratos de crecimiento del Pico del Águila se realizaron aplicando el método de los dominios de buzamiento individualmente para cada horizonte. Sin embargo, este método implica un gran consumo de tiempo y puede resultar tedioso si se dispone de una gran cantidad de datos (centenares o miles de medidas de buzamiento). Gracias a las excelentes condiciones de afloramiento y accesibilidad, las secuencias de crecimiento reconstruidas pueden convertirse en una excelente base de partida a partir de la cual desarrollar un método automatizado de reconstrucción de estratos de crecimiento a partir de parámetros físicos medibles de las rocas.

d) El reprocesado de los perfiles sísmicos disponibles en la zona de estudio. Las campañas de adquisición sísmica disponibles en la zona fueron realizadas durante los años 60 del siglo XX. Como resultado, los perfiles sísmicos son de poca calidad y no permiten una interpretación detallada de la geometría de las unidades particularmente en los niveles más someros de los estratos de crecimiento. Este hecho se presenta como una gran limitación a la hora de entender correctamente la geometría de las Sierras Exteriores Aragonesas en profundidad. Aunque esto quede parcialmente compensado por unas magníficas condiciones de afloramiento, un reprocesado y filtrado de los perfiles sísmicos con las herramientas actuales de procesado sísmico mejoraría de forma destacable la interpretación y comprensión de los anticlinales N-S en profundidad.

R.11 REFERENCIAS

Agterberg, F.P., 1967. Computer techniques in geology. Earth-Science Reviews, 3, 47-77.

Amilibia, A., McClay, K.R., Sàbat, F., Muñoz, J.A., Roca, E., 2005. Analogue Modelling of Inverted Oblique Rift Systems. Geologica Acta, 3 (3), 251-271.

Bonini, M., 2003. Detachment folding, fold amplification, and diapirism in thrust wedge experiments. Tectonics, 22(6), 1065, doi:10.1029/2002TC001458.

Borraccini, F., De Donatis, M., Di Bucci, D., Mazzoli, S., 2002. 3D Model of the active extensional fault system of the high Agri River valley, Southern Apennines, Italy. In: Jessell, M. J. (ed.). General Contributions: 2002. Journal of the Virtual Explorer, 6, 1-6.

Cadell, H.M., 1888. Experimental Researches in mountain building. Royal Society of Edinburgh Transactions, 35, 337-360.

Cagnard, F., Brun, J.P., Gapais, D., 2006. Modes of thickening of analogue weak litospheres. Tectonophysics, 421 (1-2), 145-160.

Camerlo, R.H., Benson, E.F., 2006. Geometric and seismic interpretation of the Perdido fold belt: Northwestern deep-water Gulf of Mexico. American Association of Petroleum Geologists Bulletin, 90 (3), 363-386.

Carmona, A., Clavera, R., Gratacós, O., Hardy, S., 2008. Combining Discrete Element Modelling and process-based models: initial results. Bolletino di Geofisica teorica ed applicata, 49, 358-364.

Carrera, N., Muñoz, J.A., Roca, E., 2009. 3D reconstruction of geological surfaces by the equivalent dip-domain method: An example from field data of the Cerro Bayo Anticline (Cordillera Oriental, NW Argentine Andes). Journal of Structural Geology, 31, 1573-1585.

Castelltort, S., Guillocheau, F., Robin, C., Rouby, D., Nalpas. T., Lafont, F., Echard, R., 2003. Fold control on the stratigraphic record: a quantified sequence stratigraphic study of the Pico del Aguila anticline in the south-western Pyrenees (Spain). Basin Research, 15, 527-551.

Castillo-Herrador, F., 1974. Le Trias évaporitique des basins de la Vallée de l'Ebre et de Cuenca. Bulletin de la Societé Géologique de France, 16, 49-63.

Daudre, A., 1879. Etudes Synthétiques de Géologie Expérimentale, pt. 1. Paris, Dunod, 828 p.

Felleman, J., 1990. There's a GIS in your future. Government Information Quarterly, 7 (3), 261-267.

Fernández, O., Muñoz, J.A., Arbués. P., Falivene, O., Marzo, M., 2004a . Three-dimensional reconstruction of geological surfaces: An example of growth strata and turbidite systems from the Ainsa basin (Pyrenees, Spain). American Association of Petroleum Geologists Bulletin, 88 (8), 1049-1068.

Fernández, O., 2004b. Reconstruction of geological structures in 3D: An Example from the southern Pyrenees. Doctoral Thesis, Departament de Geodinàmica i Geofísica, Universitat de Barcelona, Barcelona, Spain, 376 pp.

Finch, E., Hardy, S., Gawthorpe, R.L., 2003. Discrete element modelling of contractional fault-propagation folding above rigid basement blocks. Journal of Structural Geology, 25, 515-528.

Finch, E., Hardy, S., Gawthorpe, R.L., 2004. Discrete element modelling of extensional fault-propagation folding above rigid basement fault blocks. Basin Research, 16, 489-506.

Ford, M., Le Carlier de Veslud, C., Bourgeois, O., 2007. Kinematic and geometric analysis of fault-related folds in a rift setting: The Dannemarie basin, Upper Rhine Graben, France. Journal of Structural Geology, 29, 1811-1830.

Gente, P., Auzende, J.M., Renard, V., Fouquet, Y., Bideau, D., 1986. Detailed geological mapping by submersible of the East Pacific Rise axial graben near 13º N. Earth and Planetary Science Letters, 78 (2-3), 224-236.

Guzofski, C.A., Mueller, J.P., Shaw, J.H., Muron, P., Medwedeff, D.A., Bilotti, F., Rivero, C., 2009. Insights into the mechanisms of fault-related folding provided by volumetric structural restorations using spatially varying

mechanical constraints. American Association of Petroleum Geologists Bulletin, 93 (4), 479-502.

Hall, J. Sir, 1815. On the vertical position and convolutions of certain strata and their relation with granite. Royal Society of Edinburgh Transactions, 7, 79-108.

Harbaugh, J.W., Merriam, D.F., 1968. Computer applications in stratigraphic analysis. John Wiley Sons Inc., New York, USA, 282 p.

Hardy, S., Finch, E., 2005. Discrete-element modelling of detachment folding. Basin Research, 17, 507-520.

Hardy, S., Finch, E., 2007. Mechanical stratigraphy and the transition from trishear to kink-band fault-propagation fold forms above blind basement thrust faults: A discrete-element study. Marine and Petroleum Geology, 24, 75-90.

Hill, K.C., 1991. Structure of the Papuan Fold Belt, Papua New Guinea. American Association of Petroleum Geologists Bulletin, 74 (5), 857-872.

Holl, J.E., Anastasio, D.J., 1993. Paleomagnetically derived folding rates, southern Pyrenees, Spain. Geology, 21 (3), 271-274.

Huyghe, D., Mouthereau, F., Castelltort, S., Filleaudeau. P.Y., Emmanuel, L., 2009. Paleogene propagation of the southern Pyrenean thrust wedge revealed by finite strain analysis in frontal thrust sheets: Implications for mountain building. Earth and Planetary Science Letters, doi:10.1016/j.epsl.2009.10.002.

IGME, 1992. Mapa Geológico de España. Hoja 248, Apiés. Instituto Geológico y Minero de España, Madrid, Unpublished 36 pp report + 1:50000 map.

Jurado, M.J., 1990. El Triásico y el Liásico basal evaporíticos del subsuelo de la cuenca del Ebro. In: Ortí, F., Salvany, J.M. Formaciones evaporíticas de la

Cuenca del Ebro y cadenas periféricas, y de la zona de Levante. Enresa, Madrid, 21-28.

Koyi, H.A., 1997. Analogue modelling: from a qualitative to a quantitative technique – a historical perspective. Journal of Petroleum Geology, 20, 223-238.

Krumbein, W.C., Graybill, F.A., 1965. Application of the general linear model to Map Analysis. An Introduction to Statistical Models in Geology, McGraw-Hill, New York, 319-357.

López-Gómez, K., Arche, A., Pérez-López, A., 2002. Permian and Triassic. In: Gibbons, W., Moreno, T. (eds.). The Geology of Spain. The Geological Society of London, 185-212.

Maerten, L., Maerten, F., 2006. Chronologic modeling of faulted and fractured reservoirs using geomechanically based restoration: Technique and industry applications. American Association of Petroleum Geologists Bulletin, 90 (8), 1201-1226.

Millán, H., 1995. Estructura y Cinemática del frente de cabalgamiento surpirenaico en las Sierras Exteriores Aragonesas. Doctoral Thesis, Departamento de Ciencias de la Tierra, Universidad de Zaragoza, Zaragoza, 330 pp + annex.

Millán, H., Aurell, M., Meléndez, A., 1994. Synchronous detachment folds and coeval sedimentation in the Prepyrenean External Sierras (Spain): a case study for a tectonic origin of sequences and system tracts. Sedimentology, 41 (5), 1001-1024.

Mitra, S., 2002. Structural Models of Faulted Detachment Folds. American Association of Petroleum Geologists Bulletin, 86 (9), 1673-1694.

Nalpas, T., Gapais, D., Vergés, J., Barrier, L., Gestain, V., Leroux, G., Rouby, D., Kermarrec, J.J., 2003. Effects of rate and nature of synkinematic sedimentation on the growth of compressive structures constrained by analogue models and field examples. In: McCant, T., Saintot, A. (eds.). Tracing Tectonic

Deformation Using the Sedimentary Record. Geological Society, London, Special Publications 208, 307-319.

Nalpas, T., Györfi, I., Guillocheau, F., Lafont, F., Homewood, P., 1999. Influence de la charge sédimentaire sur le développement d'anticlinaux synsédimentaires. Modélisation analogique et exemple du terrain (bordure sud du basin de Jaca). Bulletin de la Societé Géologique de France, 170 (5), 733-740.

Novoa, E., Suppe, J., Shaw, J.H., 2000. Inclined-Shear Restoration of Growth Folds. American Association of Petroleum Geologists Bulletin, 84 (6), 787-804.

Place, D., Mora, P., 2001. A random lattice solid model for simulation of fault zone dynamics and fracture processes. In: Mulhaus, H.B., Dyskin, A.V., Pasternak, E. (eds.). Bifurcation and Localisation Theory for Soils and Rocks '99. A.A. Balkema, Rotterdam/Brookfield.

Poblet, J., Hardy, S., 1995. Reverse modelling of detachment folds, application to the Pico del Aguila anticline in the South Central Pyrenees (Spain). Journal of Structural Geology, 17, 1707-1724.

Poblet, J., McClay, K.R., Storti, F., Muñoz, J.A., 1997. Geometries of syntectonic sediments associated with single-layer detachment folds. Journal of Structural Geology, 19 (3-4), 369-381.

Pueyo, E.L., Millán, H., Pocoví, A., 2002. Rotation velocity of a thrust: a paleomagnetic study in the External Sierras (Southern Pyrenees). Sedimentary Geology, 146 (1), 191-208.

Rodriguez-Pintó, A., Pueyo, E.L., Pocoví, A., Barnolas, A., 2008. Cronología de la actividad rotacional en el sector central del frente de cabalgamiento de Sierras Exteriores (Pirineo Occidental). Geotemas, 10, 1207-1210.

Salvany, J.M., 1990. Introducción a las evaporitas triásicas de las cadenas periféricas de la cuenca del Ebro: Catalánides, Pirineo y Región Cantábrica. In:

Ortí, F., Salvany, J.M. (eds.). Formaciones evaporíticas de la Cuenca del Ebro y cadenas periféricas, y de la zona de Levante. Enresa, Madrid, 21-28.

Scheck, M., Bayer, U., 1999. Evolution of the Northeast German Basin - inferences from a 3D structural model and subsidence analysis. Tectonophysics, 313, 145-169.

Soler, M. , Puigdefàbregas, C., 1970. Líneas generales de la geología del Alto Aragón Occidental. Pirineos, 96, 5-20.

Tanner, D.C., Berhmann, J.H., Dresmann, H., 2003. Three-dimensional retro-deformation of the Lechtal Nappe, Northern Calcareous Alps. Journal of Structural Geology, 25, 737-748.

Vidal-Royo, O., Koyi, H.A., Muñoz, J.A., 2009. Formation of orogen-perpendicular thrusts due to mechanical constrasts in the basal décollement in the Central External Sierras (Southern Pyrenees, Spain). Journal of Structural Geology, 31, 523-539.

Vidal-Royo, O., Hardy, S., Muñoz, J.A., 2010. The roles of complex mechanical stratigraphy and syn-kinematic sedimentation in fold development: Insights from discrete-element modelling and application to the Pico del Águila anticline (External Sierras, Southern Pyrenees). In: Poblet, J., Lisle, R.J. (eds.). Kinematic Evolution and Structural Styles of Fold-and-Thrust Belts, Special Publication of the Geological Society, *accepted*.

Vidal-Royo, O., Cardozo, N., Muñoz, J.A., Hardy, S., Maerten, L., 2010. Multiple mechanisms driving detachment folding as deduced from 3D reconstruction and geomechanical restoration: The Pico del Águila anticline (External Sierras, Southern Pyrenees). Basin Research, *submitted*.

Weijermars, R., 1986. Flow behaviour and physical chemistry of bouncing putties and related polymers in view of tectonic laboratory applications. Tectonophysics, 124, 325-358.

Wilsher, W.A., de Wit, M.J., Marrao, E., 1989. A GIS solution for Gondwana geoscientific data. Journal of African Earth Sciences, 9 (2), 371-374.

Zanchi, A., Salvi, F., Zanchetta, S., Sterlacchini, S., Guerra, G., 2009. 3D reconstruction of complex geological bodies: Examples from the Alps. Computers and Geosciences, 35, 49-69.

PIES DE FIGURA

Fig. R1 Mapa geológico del sector central de las Sierras Exteriores Aragonesas (modificado de IGME, 1992). BR: anticlinal de Bentué de Rasal; PA: anticlinal del Pico del Águila; G: anticlinal de Gabardiella. Las líneas negras indican los perfiles sísmicos interpretados en la reconstrucción 3D del Pico del Águila. **Pág. 13.**

Fig. R2. Columna estratigráfica de la región, describiendo las litologías y gruesos promedio de los materiales aflorantes, M: facies Muschelkalk; K: facies Keuper. DS: secuencias deposicionales definidas en la Formación Guara. GS: secuencias deposicionales definidas en los estratos de crecimiento. Modificada de Millán et al. (1994). **Pág. 15.**

Fig. R3. Fotografía oblicua del flanco occidental del anticlinal del Pico del Águila mostrando una discordancia interna en la Formación Guara que separa la secuencia pre-pliegue (PFS) de la secuencia sin-pliegue (SFS), la cual se adelgaza claramente sobre la anterior. **Pág. 16.**

Fig. R4 Fotografía oblicua del flanco oriental del Pico del Águila. Se puede observar claramente como las margas de la Formación Arguis (en azul) se adelgazan y dibujan *onlaps* sobre el techo de la Formación Guara (en verde). **Pág. 17.**

Fig. R5. Diferentes etapas de la construcción del Modelo Digital del Terreno (DTM) y de la digitalització de los datos de campo. (A) Mapa topográfico 1:5000 a partir del cual se extrae un modelo de elevación en XYZ. Después se lleva a cabo una triangulación creando una malla hecha de triángulos. A partir de esta se crea una malla regular de 5 x 5 m (B), sobre la cual se entapiza la correspondiente ortofotografía (C). Con el MDT disponible ya se pueden digitalizar todos los datos posicionándolos en sus correspondientes coordenadas XYZ (D). **Pág. 19.**

Fig. R6. Diferentes pasos resumiendo el proceso seguido para generar los dominios de buzamiento: a) posicionamiento de las medidas de buzamiento; b) creación de los dominios de buzamiento, c) definición de la extensión, intersección de los diferentes dominios y creación del mapa de contornos estructurales; y d) generación de la superficie. **Pág. 20.**

Fig. R7. Estructura de la secuencia pre-pliegue del anticlinal del Pico del Águila. Marrón: Fm. Guara; amarillo: Garumniense; verde: Cretácico superior; violeta: Triásico. Colores diversos (rojo en los cortes): fallas internas afectando la estructura. **Pág. 21.**

Fig. R8 Estructura de los estratos de crecimiento del anticlinal del Pico del Águila, mostrando la geometría de las secuencies deposicionales reconstruidas sobre el techo de la Formación Guara (en verde). Obsérvese como les GS se adelgazan hacia la cresta del anticlinal y como la GS-I no alcanza la charnela. **Pág. 21.**

PROLOGUE

Motivation, Objectives and Organization of the Thesis

P.1 MOTIVATION

A major motivation for this thesis was to investigate the mechanisms that govern detachment folding in 3D. In addition, we had available what can be considered one of the best natural laboratories in the planet for structural geology in compressional regimes: the External Sierras of the Southern Pyrenees. The geology of the External Sierras is characterized by remarkable folds that after decades of study still are hot points of discussion when it comes to the processes that drove their generation and evolution. In this sense, the N-S anticlines of the External Sierras have great geological relevance and needed new approaches with which to shed light on some of the many aspects that remained unstudied at that stage. The excellent outcropping conditions, the high degree of preservation of the structures and the easy accessibility made this area an ideal place to test and apply the most up to date techniques of structural reconstruction and modelling developed in the Geomodels Research Institute and the Group of Geodynamics and Basin Analysis (GGAC-UB) at University of Barcelona. At this early stage of the memoir it is believed necessary to deeply acknowledge the great effort and hard work of all the personnel at GGAC-UB, and especially to professors J.A. Muñoz and Stuart Hardy who paved the way for the 4D Structural Reconstruction and Mechanical Modelling techniques

from which this Thesis has benefited so much. These initial conditions were definitely a promising kickoff that constituted a great motivation itself.

Geological models in Earth Sciences provide explanations and improve our understanding of the geological processes that may take place in the planet. In most cases, they should not purport to be a direct replica of nature but a comprehensive way to simulate and represent geological processes in a feasible timescale for human-beings.

Structural geology has a long history in the use of modelling as a tool to better understand the generation and evolution of structures. Since the first attempts in sandbox experiments (Hall, 1815; Daudre, 1879; Cadell, 1888; among others), a wide variety of modelling techniques have arisen and been developed as a result of geoscientists' needs to solve new concerns. Analogue models have become more sophisticated, incorporating elements and devices that led to more quantitative results to compare with nature (Koyi, 1997). With the rise and spread of computers numerical models appeared into the scene contributing with mathematical algorithms that brought great advances in the understanding of geological processes (Krumbein and Graybill, 1965; Agterberg, 1967; Harbaugh and Merriam, 1968). In this sense, numerical models provided geology with a quantitative control of the laws and parameters that govern natural processes. The continual advances in software design, satellite data and telecommunication have led to huge advances in numerical quantification/plotting of the geological processes as well as the incorporation of GIS to control/monitor the data positioning on Earth (Gente et al., 1986; Wilsher et al., 1989; Felleman, 1990). During the last decade, the fast advances in computer sciences as well as the efforts from both the Industry and Academia have brought the third dimension to structural geology, making one step further to a more accurate representation of the geological bodies in nature (Scheck and Bayer, 1999; Tanner et al., 2003; Fernández et al., 2004; Ford et al., 2007; Carrera et al., 2009).

Despite all these advances, every modelling technique usually presents its particular strengths, weaknesses and limitations, which end in a relatively simplified or incomplete representation of nature. This makes each approach

suitable for certain purposes, keeping in mind that knowing the limitations of the technique is essential to correctly understand what a model is delivering. For this reason, behind each model there should be feasible parameters to test and/or observable processes to unveil, rather than an attempt to make a detailed replica of a natural case.

In this memoir we present three different modelling approaches to better understand the structural evolution of the N-S anticlines in the External Sierras of the Southern Pyrenees (Spain). Among them, we focused in the Pico del Águila anticline as a target structure, since it is a world-class example of detachment anticline, easily accessible, and exhibiting good exposure that offers a geological map that can be understood as a down-plunge section of the anticline. The N-S transverse anticlines are characterized by the interference pattern with the E-W Pyrenean-trend structures. The N-S anticlines show high degree of preservation of the entire growth strata record, which allows us to constrain the timing of deformation. The structure is fairly well known and has been reported in a plethora of publications of multiple disciplines. New insights about the kinematics and structural evolution of the Pico del Águila have been derived from sedimentological analysis (Millán et al., 1994; Castelltort et al., 2003), paleomagnetism (Pueyo et al., 2002; Rodríguez-Pintó et al., 2008), analogue modelling (Nalpas et al., 1999, 2003), 2D kinematical models (Poblet and Hardy, 1995; Poblet et al., 1997), restoration of cross sections (Novoa et al., 2000) and other multi-disciplinary approaches (Huyghe, et al., 2009). Despite this plethora of multidisciplinary works, there is a lack of integrated studies gathering the insights provided by different modelling techniques to complement and validate each other.

As mentioned above, the N-S anticlines of the External Sierras still are a hot point of discussion regarding the processes and mechanisms that led to their formation and evolution. Their structure is complex, and the mechanisms that took place are multiple and difficult to assess by simplistic approaches. However, the External Sierras present outstanding facilities as far as field exposure and accessibility go. This means that the N-S anticlines of the External Sierras, and particularly the Pico del Águila, can be also considered a world-class example of analogue outcropping detachment fold with associated

marine to fluvio-deltaic sedimentation. A good understanding of the processes, mechanisms and parameters that took place in the evolution of the Pico del Águila anticline, hence, can provide a better comprehension about similar structures where poor data quality or difficult accessibility can lead to a misinterpretation of their geometry. In addition, if structures such as these are highly valued for their hydrocarbons or other natural resources, a good understanding of their geometry and evolution may have great economic impact in exploration and production terms. This may be the case of several fold belts such as the Mississippi fan and Perdido belts (Mitra, 2002; Camerlo and Benson, 2006) or the Papua New Guinea (Hill, 1991; Mitra, 2002), among others.

P.2 OBJECTIVES

The present Thesis focuses on the generation, structural evolution and tecto-sedimentary relations of the N-S anticlines of the External Sierras, and more precisely, of the Pico del Águila anticline. By applying different modelling techniques we aim to address several questions arising from observation of the geological features of the External Sierras, and that we believe can also be applied to other examples of detachment folding around the world. The specific objectives are:

1) To unveil the mechanisms that may lead to the generation of transverse structures such as the Pico del Águila anticline in the absence of any other shortening event beyond the N-S Pyrenean compression.
2) To understand how strain is distributed within the heterogeneous stratigraphic sequence of the External Sierras and, hence, how deformation is accommodated depending on the mechanical properties of each unit.
3) To investigate the role of syn-kinematic sedimentation (growth strata) in fold evolution and strain accommodation.

4) To understand the mechanisms that drive detachment folding in 3D and their interaction during fold growth within different units and structural domains. At the same time, to improve the understanding of how the distribution of folding mechanisms affects the geometry of the fold and the sedimentation and uplift rates, which also influence the growth of the anticline.
5) To present a unified and better constrained model of structural evolution that integrates and honours all the field observations, previous data and the results obtained from different modelling techniques.
6) To improve understanding of the kinematics and mechanics of detachment folding to help in the interpretation and understanding of other similar structures around the planet that do not exhibit as good outcropping and accessibility conditions as the Pico del Águila anticline.

P.3 ORGANIZATION OF THE THESIS

This Thesis is submitted as a compilation of four scientific publications and has been structured in six main chapters, organized as follows:

Chapter I presents a general description of the geology of the External Sierras of the Southern Pyrenees. The scientific articles presented in this Thesis only include a short overview of the geological setting. However, the area of study presents many geological features that were barely mentioned in the publications and thus we feel it necessary to describe them in more detail within this section. Particular effort is placed on the description of the stratigraphic sequence given its importance in the fold evolution, and on the general structural features at a more regional scale.

Chapter II contains the first scientific article of the Thesis: **Vidal-Royo, O., Koyi, H.A., Muñoz, J.A., 2009. Formation of orogen-**

perpendicular thrusts due to mechanical contrasts in the basal décollement in the Central External Sierras (Southern Pyrenees, Spain). Journal of Structural Geology, 31 (5), 523-539.

This article presents two series of analogue models (series A and B) that were used to investigate the effect of an unevenly distributed basal décollement (Middle and Upper Triassic materials; Muschelkalk and Keuper facies) on the formation of oblique and transverse structures (*i.e.* structural trend perpendicular to the orogen) such as the N-S anticlines of the External Sierras. Model series A tests the thickness ratio between overburden and the ductile layer, whereas model Series B tests the width (perpendicular to the shortening direction) of frictional décollement.

Chapter III contains the second scientific article that constitutes this Thesis: **Vidal-Royo, O., Hardy. S., Muñoz, J.A., 2010. The roles of complex mechanical stratigraphy and syn-kinematic sedimentation in fold development: Insights from discrete-element modelling and application to the Pico del Águila anticline (External Sierras, Southern Pyrenees). In: Poblet, J., Lisle, R.J. (Eds.). Kinematic Evolution and Structural Styles of Fold-and-Thrust Belts, Special Publication of the Geological Society, *accepted*.**

In this work we present two numerical models in 2D, based on a Discrete Element Modelling technique, to investigate the effect of the complex mechanical stratigraphy described in the field as well as the influence of the growth strata in the evolution of the Pico del Águila anticline. Two models are presented: Model 1 tests the response of this complex mechanical stratigraphy to shortening under conditions that lead to the formation of a detachment fold; Model 2 tests the effect of syn-kinematic sedimentation under identical boundary conditions as in Model 1.

In **Chapter IV** we present the third scientific publication of the thesis: **Vidal-Royo, O., Cardozo, N., Muñoz, J.A., Hardy, S., Maerten, L., (in review). Multiple mechanisms driving detachment folding as deduced from 3D reconstruction and geomechanical restoration: The Pico del Águila anticline (External Sierras, Southern Pyrenees).** ***Submitted to Basin Research.***

This study presents a field-based 3D reconstruction and geomechanical restoration of the Pico del Águila anticline. From field data (dip measurements and mapping of geological traces) and seismic interpretations an accurate reconstruction of the pre-folding and growth strata geometries was done. We benefited from the reconstruction of the four depositional sequences within the growth strata to carry out a time-constrained sequential restoration back to the non-deformed stage of the Guara Formation (Upper Lutetian). Based on Finite Element technique (FEM), the algorithm of restoration considers mechanical properties of the rocks to perform a restoration in which no previous kinematical criteria are assumed. From the restoration, new insights are obtained on the evolution of the fold in 3D.

Chapter V contains the fourth scientific publication of the present Thesis: **Vidal-Royo, O., Muñoz, J.A., Hardy, S., Koyi, H.A., Cardozo, N., (submitted). Integration of modelling techniques in the understanding of the structural evolution of the Pico del Águila anticline (External Sierras, Southern Pyrenees).** ***Submitted to Geologica Acta.***

This chapter contains a summary of the results presented in the previous chapters, as well as the general discussion of the Thesis. In this chapter we discuss about the benefits, drawbacks, limitations, suitability and applications of the modelling techniques as well as the results of the models and their whole integration in a unified model of structural evolution.

In **Chapter VI** we present the final considerations of the Thesis, as well as a list of tentative investigations envisaged for the future that would constitute a reasonable continuation of the work presented in this Thesis .

P.4 REFERENCES

Agterberg, F.P., 1967. Computer techniques in geology. Earth-Science Reviews, 3, 47-77.

Cadell, H.M., 1888. Experimental Researches in mountain building. Royal Society of Edinburgh Transactions, 35, 337-360.

Camerlo, R.H., Benson, E.F., 2006. Geometric and seismic interpretation of the Perdido fold belt: Northwestern deep-water Gulf of Mexico. American Association of Petroleum Geologists Bulletin, 90 (3), 363-386.

Carrera, N., Muñoz, J.A., Roca, E., 2009. 3D reconstruction of geological surfaces by the equivalent dip-domain method: An example from field data of the Cerro Bayo Anticline (Cordillera Oriental, NW Argentine Andes). Journal of Structural Geology, 31, 1573-1585.

Castelltort, S., Guillocheau, F., Robin, C., Rouby, D., Nalpas. T., Lafont, F., Echard, R., 2003. Fold control on the stratigraphic record: a quantified sequence stratigraphic study of the Pico del Aguila anticline in the south-western Pyrenees (Spain). Basin Research, 15, 527-551.

Daudre, A., 1879. Etudes Synthétiques de Géologie Expérimentale, pt. 1. Paris, Dunod, 828 p.

Felleman, J., 1990. There's a GIS in your future. Government Information Quarterly, 7 (3), 261-267.

Fernández, O., Muñoz, J.A., Arbués. P., Falivene, O., Marzo, M., 2004 . Three-dimensional reconstruction of geological surfaces: An example of growth

strata and turbidite systems from the Ainsa basin (Pyrenees, Spain). American Association of Petroleum Geologists Bulletin, 88 (8), 1049-1068.

Ford, M., Le Carlier de Veslud, C., Bourgeois, O., 2007. Kinematic and geometric analysis of fault-related folds in a rift setting: The Dannemarie basin, Upper Rhine Graben, France. Journal of Structural Geology, 29, 1811-1830.

Gente, P., Auzende, J.M., Renard, V., Fouquet, Y., Bideau, D., 1986. Detailed geological mapping by submersible of the East Pacific Rise axial graben near 13° N. Earth and Planetary Science Letters, 78 (2-3), 224-236.

Hall, J. Sir, 1815. On the vertical position and convolutions of certain strata and their relation with granite. Royal Society of Edinburgh Transactions, 7, 79-108.

Harbaugh, J.W., Merriam, D.F., 1968. Computer applications in stratigraphic analysis. John Wiley Sons Inc., New York, USA, 282 p.

Hill, K.C., 1991. Structure of the Papuan Fold Belt, Papua New Guinea. American Association of Petroleum Geologists Bulletin, 74 (5), 857-872.

Huyghe, D., Mouthereau, F., Castelltort, S., Filleaudeau. P.Y., Emmanuel, L., 2009. Paleogene propagation of the southern Pyrenean thrust wedge revealed by finite strain analysis in frontal thrust sheets: Implications for mountain building. Earth and Planetary Science Letters, doi:10.1016/j.epsl.2009.10.002.

Koyi, H.A., 1997. Analogue modelling: from a qualitative to a quantitative technique – a historical perspective. Journal of Petroleum Geology, 20, 223-238.

Krumbein, W.C., Graybill, F.A., 1965. Application of the general linear model to Map Analysis. An Introduction to Statistical Models in Geology, McGraw-Hill, New York, 319-357.

Millán, H., Aurell, M., Meléndez, A., 1994. Synchronous detachment folds and coeval sedimentation in the Prepyrenean External Sierras (Spain): a case

study for a tectonic origin of sequences and system tracts. Sedimentology, 41 (5), 1001-1024.

Mitra, S., 2002. Structural Models of Faulted Detachment Folds. American Association of Petroleum Geologists Bulletin, 86 (9), 1673-1694.

Nalpas, T., Györfi, I., Guillocheau, F., Lafont, F., Homewood, P., 1999. Influence de la charge sédimentaire sur le développement d'anticlinaux synsédimentaires. Modélisation analogique et exemple du terrain (bordure sud du basin de Jaca). Bulletin de la Societé Géologique de France, 170 (5), 733-740.

Nalpas, T., Gapais, D., Vergés, J., Barrier, L., Gestain, V., Leroux, G., Rouby, D., Kermarrec, J.J., 2003. Effects of rate and nature of synkinematic sedimentation on the growth of compressive structures constrained by analogue models and field examples. In: McCant, T., Saintot, A. (eds.). Tracing Tectonic Deformation Using the Sedimentary Record. Geological Society, London, Special Publications 208, 307-319.

Novoa, E., Suppe, J., Shaw, J.H., 2000. Inclined-Shear Restoration of Growth Folds. American Association of Petroleum Geologists Bulletin, 84 (6), 787-804.

Poblet, J., Hardy, S., 1995. Reverse modelling of detachment folds, application to the Pico del Aguila anticline in the South Central Pyrenees (Spain). Journal of Structural Geology, 17, 1707-1724.

Poblet, J., McClay, K.R., Storti, F., Muñoz, J.A., 1997. Geometries of syntectonic sediments associated with single-layer detachment folds. Journal of Structural Geology, 19 (3-4), 369-381.

Pueyo, E.L., Millán, H., Pocoví, A., 2002. Rotation velocity of a thrust: a paleomagnetic study in the External Sierras (Southern Pyrenees). Sedimentary Geology, 146 (1), 191-208.

Rodriguez-Pintó, A., Pueyo, E.L., Pocoví, A., Barnolas, A., 2008. Cronología de la actividad rotacional en el sector central del frente de

cabalgamiento de Sierras Exteriores (Pirineo Occidental). Geotemas, 10, 1207-1210.

Scheck, M., Bayer, U., 1999. Evolution of the Northeast German Basin – inferences from a 3D structural model and subsidence analysis. Tectonophysics, 313, 145-169.

Tanner, D.C., Berhmann, J.H., Dresmann, H., 2003. Three-dimensional retro-deformation of the Lechtal Nappe, Northern Calcareous Alps. Journal of Structural Geology, 25, 737-748.

Wilsher, W.A., de Wit, M.J., Marrao, E., 1989. A GIS solution for Gondwana geoscientific data. Journal of African Earth Sciences, 9 (2), 371-374.

CHAPTER I

Geological Setting of the External Sierras

Presenting a Doctoral Thesis as a compendium of publications implies limitations in the extent of each section. Consequently, a thorough presentation of the general geology of the study area has remained beyond the scope of the scientific publications presented in this memoir. As a result, we feel it necessary to include this section, in which a comprehensive description of the geology of the External Sierras is presented, particularly focusing in the general stratigraphic and structural features. This chapter is not intended to be a detailed discussion of the geological aspects of each structural domain of the External Sierras. Rather, it tries to offer a general overview of the area within which to place the observations and interpretations discussed in following chapters of the memoir. The interested reader will find more detailed descriptions of the stratigraphic, structural and sedimentary aspects of the External Sierras in key works such as Puigdefàbregas (1975), IGME (1992), Millán (1995) and Pueyo (2000), among others.

The studied area is located in the Southern border of the Jaca piggyback basin, westwards of the South Central Pyrenean Unit (Southern Pyrenees, Spain). It is emplaced in the "Aragonese External Sierras", which corresponds to the Pyrenean Southern Thrust Front, bordering the Ebro foreland basin to the South.

The Pico del Águila anticline is located between Bentué de Rasal and Gabardiella anticlines (to the West and to the East, respectively). Each one of

them constitutes a N-S kilometric scale mountain, separated from each other by the Arguis Valley to the W, and the Belsué Valley to the E. The Isuela river flows down along the Arguis Valley, while the Flumen river flows down along the Belsué Valley, both of them towards the Pico del Águila. The highest peaks in the area are Gabardiella Peak (1695 m) and Pico del Águila (1629 m). See Figure 1.1 for location.

The External Sierras constitute the frontal emerging part of the Gavarnie thrust sheet, formed by a complex of imbricated thrust nappes detaching on evaporitic Triassic facies (Keuper and partially Muschelkalk facies), and displaced southwards over the Tertiary sediments of the Ebro foreland basin. The structural position is completely equivalent to the Serres Marginals Catalanes, interpreted from the ECORS profile by Muñoz (1992). As he points out, the emplacement and structure of the Serres Marginals Catalanes lasts from Lutetian up to Upper Oligocene, reaching 147 km of shortening across the Pyrenees. A general geological framework of the Pyrenees and the area of study are shown in Figure 1.2.

Figure 1.1. Geographic location and morphological appearance of the studied area. The Pico del Águila (understood as a mountain peak) is located on the hinge zone of the eastern limb of the anticline (satellite images from *Google Earth*).

One of the peculiarities of External Sierras is the presence of a set of N-S anticlines. These are perpendicular to the general structural trend in the Pyrenees, where the direction of tectonic transport is southwards and, therefore, the main structural direction is E-W. Among others, Puigdefàbregas (1975), IGME (1992) and Millán (1995) stated that these N-S anticlines become progressively younger as one moves to the W. Their growth is synchronous to the deposition of the Middle Eocene to Oligocene materials, and they become progressively shorter as one move to the W (Puigdefàbregas, 1975; Millán et al., 1994; Millán, 1995). It is important to highlight that the structural style in External sierras becomes more complex as a consequence of the interference between the N-S and the general (an usually later) E-W structures.

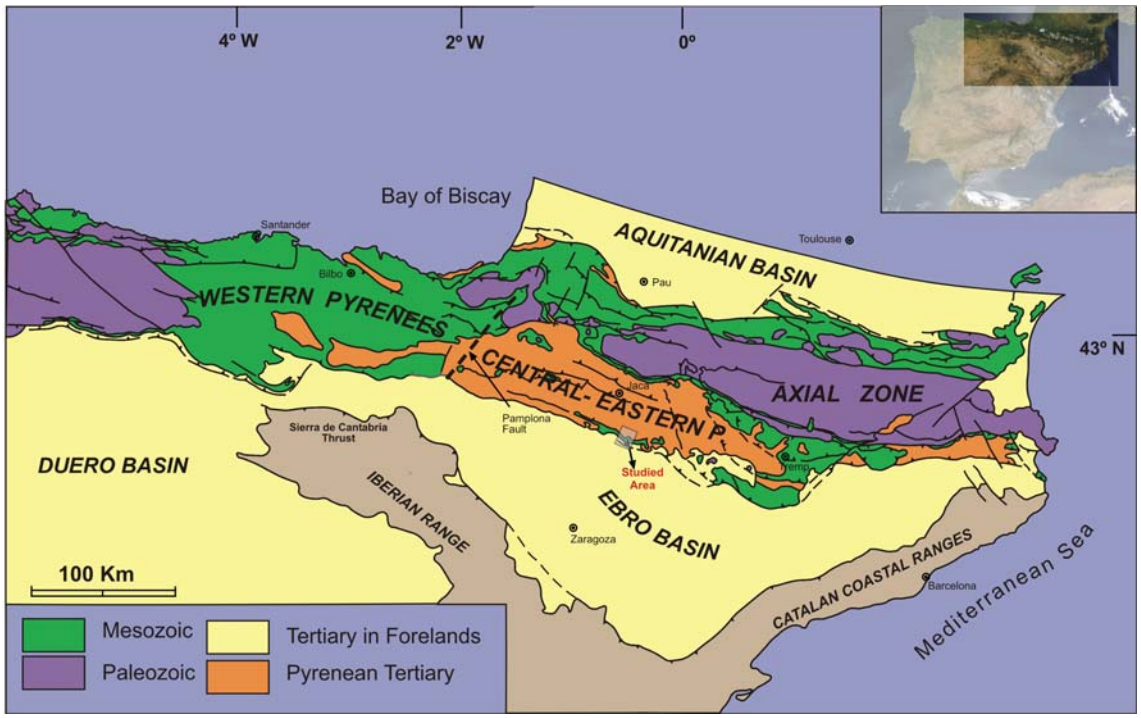

Figure 1.2. General map of the NE Iberian Peninsula, showing the different tectonic units and a general distribution of the materials. The area of study is highlighted with grey square and black arrow.

It was during Middle Eocene to Miocene when the South Pyrenean thrust front was active (Puigdefàbregas, 1975; IGME, 1992; Millán et al., 1994; Millán, 1995) and, therefore, there are interesting E-W, N-S and oblique structures that suffer dramatic lateral changes, creating in such a way an interference structural style characteristic of the External Sierras. Figure 1.3 shows the geological map of the Central External Sierras, where the area of study is located.

Figure 1.3 (NEXT PAGE). Geological map of central External Sierras (modified after IGME, 1992). The red square borders the area studied in the present work. Black lines indicate the trace of the interpreted seismic profiles. A-A', B-B' and C-C' are the trace of the cross-sections showing the general structure of the area (see Figure 1.8).

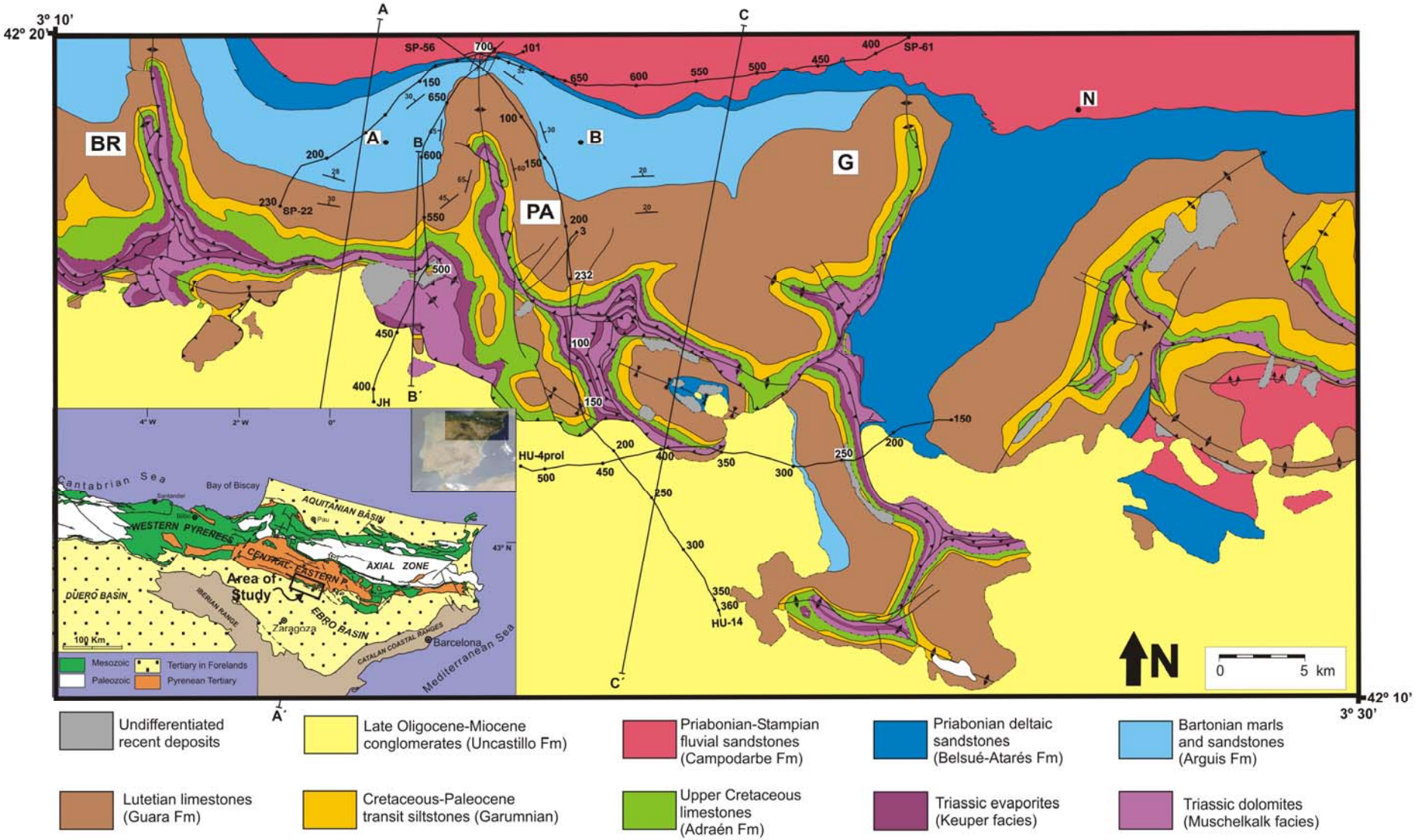
3º 10'
42º 20'
A
C
SP-56
SP-61
BR
PA
G
N
B
SP-22
JH
B´
HU-4prol
HU-14
C´
A´
42º 10'
3º 30'
Cantabrian Sea
Bay of Biscay
Santander
Bilbao
Pau
AQUITANIAN BASIN
WESTERN PYRENEES
CENTRAL - EASTERN P.
AXIAL ZONE
Area of Study
DUERO BASIN
IBERIAN RANGE
EBRO BASIN
Zaragoza
CATALAN COASTAL RANGES
Barcelona
Mediterranean Sea
100 Km
Mesozoic
Paleozoic
Tertiary in Forelands
Pyrenean Tertiary
0
5 km
Undifferentiated recent deposits
Late Oligocene-Miocene conglomerates (Uncastillo Fm)
Priabonian-Stampian fluvial sandstones (Campodarbe Fm)
Priabonian deltaic sandstones (Belsué-Atarés Fm)
Bartonian marls and sandstones (Arguis Fm)
Lutetian limestones (Guara Fm)
Cretaceous-Paleocene transit siltstones (Garumnian)
Upper Cretaceous limestones (Adraén Fm)
Triassic evaporites (Keuper facies)
Triassic dolomites (Muschelkalk facies)

1·1 STRATIGRAPHY

The main stratigraphic units that can be recognized in the area are presented in this chapter. We hereby present a brief description of the diverse units that will help in the comprehension of the growth and development of the structures. A wider and more detailed description of the stratigraphy of the External Sierras can be found in Puigdefàbregas (1975), Millán (1995) and IGME (1992).

All the outcropping materials observed in the area were involved in the Alpine Orogeny, corresponding to ages between the Middle and Upper Triassic to Quaternary. From Upper Cretaceous, the sediments were deposited in the foreland, recording the evolution of the orogen, showing a clear sequence of marine regression, where the series change vertically from a pure marine depositional environment to a pure continental depositional environment, as Puigdefàbregas (1975) stated out.

1·1·1 TRIASSIC

These are the oldest materials that one can find in the area of study. They correspond to the Germanic facies of the Middle and Upper Triassic, Muschelkalk and Keuper facies respectively. The recognized lithologies are mainly gypsum-bearing clays and marls (Keuper facies), with interstratified dolomites and dolomitic limestones (Muschelkalk facies). The Muschelkalk facies are the predominant Triassic material outcropping in the area. It is important to mention that Triassic materials are the main detachment horizon in the External Sierras (even in the Pyrenees), as a consequence of their plastic and ductile behavior. Consequently, in the frontal part of External Sierras (where thrusts emerge), internal deformation within these units is a very important parameter to take into account. This means that to establish a complete stratigraphic sequence is actually a difficult task to carry out. In fact, Triassic materials in frontal parts of the orogen are so refolded, faulted, overthrusted and internally deformed that to evaluate the actual stratigraphic

thickness becomes extremely difficult. Both Keuper and Muschelkalk facies are involved in the detachment level, which is extremely faulted. Furthermore, the thickness of the whole Triassic sequence suffers dramatic lateral changes. From geological cross-sections, one can suggest that from the base of the detachment level, the Triassic sequence reaches a thickness of up to 500 m, although this disagrees with field observations carried out in External Sierras (Millán, 1995).

1·1·2 UPPER CRETACEOUS

This broad term includes materials deposited between Santonian and Maastrichtian ages, in a carbonate platform environment. One can distinguish two different cycles (Millán, 1995, from Lobato & Meléndez, 1988). The first one consists of two 40 m thick units, with a Santonian-Campanian top. The first unit shows an erosive base and starts with siliciclastic conglomerate and sandstone facies, the last one showing planar cross bedding. The sequence passes rapidly to the second unit: a series of bioconstructed limestones, in which the most striking feature are the presence of rudists, with *bafflestone* and *wackstone* textures. It is possible to recognize as well bioclastic and bioturbation facies, with presence of miliolids, rudist fragments and other marine fossil bodies.

The second cycle starts with a third erosive base unit made of reddish calcareous sandstones, showing planar cross bedding and *packstone-grainstone* fabric. It is 25 m thick, and is rich in miliolids and briozoa, among other bioclasts. The next unit, the forth one, is 30 m thick, and is formed by a sequence of black marls and bioclast-rich limestones. Bioturbation is common in the calcareous horizons. The last unit is formed by 50 m of limestones, dolomitic limestones and white dolomites, in which one can find fossil roots, desiccation marks and barely bioclasts. This last unit belongs to the transition Campanian-Maastrichtian and it changes vertically to Garumnian facies.

1·1·3 CRETACEOUS-TERTIARY TRANSITION: GARUMNIAN FACIES

These are the first continental sediments that can be recognized in the studied area. They are formed by up to 100 m of mainly red siltstones and clays, although it is common to find siliciclastic sandstones and conglomerates, frequently showing cross bedding. Often one recognizes extremely white lacustrine limestones with gasteropoda fragments and *Microcodium*. Dolomitic limestone and dolomite banks have been often recognized, usually in the top of the unit. This sequence changes laterally northwards to shallow marine facies, made of rich-in-foraminifera, algal and sandy limestones (sometimes dolomites, too).

As the main lithology corresponds to red silts, this unit has a well-known mechanical role as a secondary detachment level. The Garumnian facies is the horizon where some regional faults and thrusts detach, taking advantage of the wide, continuous and relatively thick silty-clay layers. Furthermore, in highly deformed areas (such as the core of Pico del Águila anticline), the red silts can behave similarly to Keuper facies, and can be easily confused with them.

The Garumnian facies have received various different formation names through history; among others, they have been also defined as the Tremp Fm. For this reason, both terms (Garumnian and Tremp Fm.) will be equally used in this work.

1·1·4 MARINE AND TRANSITIONAL TERTIARY

Marine Eocene is mainly represented by the Guara Fm., which was deposited in a shallow marine platform environment, and by the outer platform and prodelta facies corresponding to the Arguis Fm. The transitional Eocene is represented by the proximal deltaic facies of the Belsué-Atarés Fm.

The deposition of these formations is fully synchronous to the formation and structure of the External Sierras. Millán (1995) (from Canudo et al., 1991)

points out that the deposition of these units ranges from Lower Lutetian (beginning of the Guara Fm. deposition) to Lower Priabonian.

The Guara Fm. is formed by carbonate and terrigenous sediments, all of them deposited in a shallow marine platform environment in the foreland margin of the basin. Its features and facies sequence suggest that it corresponds to a transgressive cycle, lying on an erosive surface that erodes the top of the Garumnian facies. The age ranges from Cuisian-Lutetian boundary at the base to Upper Lutetian-Bartonian boundary at its top. Thickness is highly variable, as the deposition of Guara sediments was synchronous to the beginning of the External Sierras structure and, therefore, geometry and thickness were totally controlled by the growth of syn-sedimentary folds such as the studied anticline.

Three different sequences can be differentiated, which will be briefly described below:

Depositional Sequence 1 (DS1, Lower Lutetian) is formed by 40 m of bioclastic limestones. frequently interbedded with grey marls. At the top of DS1, one can recognize a subsequence of clays, marls and siltstones.

Depositional Sequence 2 (DS2, Middle Lutetian) is 350 m thick and it presents conglomeratic and quartz sandstone levels, interbedded with limestone and sandy limestone levels. Moving up in the sequence one recognizes bioturbed limestones, very rich in foraminifera such as *Nummulites* and *Alveolin*a, alternating with decimetric grey marl horizons.

Depositional Sequence 3 (DS3, Upper Lutetian) is about 110 m thick, showing a base made of a 8-10 m thick sandstone level. It changes vertically to a highly-rich-*Nummulites* limestone, which changes as well to a limestone facies, very rich in shell fragments. The top of DP3 contains a level of macrofossil accumulation (mainly equinids) and an irregular surface.

The Arguis Fm. and Belsué-Atarés Fm (Upper Lutetian-Lower Priabonian) is bounded by important regional unconformities at the bottom and top of the sequence; the first is located at the top of the Guara Fm. and the second is at the bottom of the Campodarbe Fm. From Millán et al. (1994) we

know that there are four different depositional sequences inside the Arguis and Belsué-Atarés formations, based on a sequence stratigraphic study of the area. They will be briefly described in the following:

Sequence I is made up of blue marls and sandy glauconite-bearing marls. This sequence ranges from Late Lutetian to Lower Priabonian, and it reaches a thickness of 400 m in the Arguis valley, being totally non-existent at the hinge area of the Pico del Águila anticline. The main lithology is blue marls, interlayered with more competent levels, with a high component of siliciclastic grains and high concentration of glauconite crystals at the top of the sequence.

Sequence II corresponds to a bryozoan platform. The bottom of the sequence is a low angle unconformity, showing *onlap* geometries in both limbs of the anticline. It ranges from Middle to Upper Bartonian, reaching a maximum thickness of 500 m in the core of the Arguis syncline. In the hinge area of the anticline this value decreases to 200 m. This sequence is formed by blue marls at the bottom, barely bioturbated. Fossil content and bioturbation increase as one moves to the top of the sequence, showing bioclastic decimetric levels rich in briozoa, pectinids, benthonic foraminifera and equinids.

Sequence III is a pectinid platform. It corresponds to the bottom of Lower Priabonian, being 100 m thick in the western limb of the Pico del Águila anticline. The lower part of the sequence is formed by blue marls, barely bioturbated, which become upwards a carbonate series rich in shell, bryozoan equinid, oyster, benthonic foraminifera and coral fragments. In the Arguis syncline, the lithology passes laterally to marly-bioclastic-interbedded levels and more siliciclastic horizons.

Sequence IV is a siliciclastic and coral platform. The lower limit of this sequence is equivalent to the border between the Arguis and Belsué-Atarés formations. The upper limit corresponds to a regional unconformity, recognizable all along the south-Pyrenean basin, and it is also the limit between the Belsué-Atarés and Campodarbe formations. This unconformity represents a rapid transition to continental depositional environments. The unit is age Lower Priabonian in age, and it reaches a thickness of 200 m along the transect of

Arguis village, while it is only 50 m thick in the hinge area of the anticline. It is formed by sandy marls including pure siliciclastic levels, corresponding to deltaic progradation sequences.

1·1·5 CONTINENAL TERTIARY

The outcropping continental tertiary sequence is mainly represented by two different formations inside the studied domain. Both of them have syntectonic features, at least at the beginning or lower part of its deposition. These are the Campodarbe and Uncastillo formations, which will be presented in the following.

The Campodarbe Fm. includes several different depositional environments, being formed by sandstone and siltstone facies and presenting local conglomerate banks. Detritic components came from the inner uplifted zones of the chain, being associated to the deltaic facies of Belsué-Atarés Fm. in the lowest part of the continental sequence. It is the thickest unit of the whole sequence, ranging between 3500 m in the easternmost part of Central External Sierras and 4700 m in Western External Sierras (Millán, 1995). The deposition began at Middle-Upper Priabonian and its end is considered to occur during Lower Stampian.

The Uncastillo Fm. recorded the structure of External Sierras during the period comprised between the Upper Oligocene and the Miocene. It is mainly formed by reddish conglomerates, sandstones, siltstones and clays, although the first one is the most common lithology inside the studied area. The maximum thickness shown in the general cross-sections of the area is about 1400 m (Figure 1.8 - Millán, 1995). The Uncastillo Fm. lies directly on all the units defined above, from Triassic to Oligocene materials, always showing a progressive unconformity.

In order to sum up and clarify the understanding of the whole sequence, Figure 1.4 shows a stratigraphic column of all the outcropping materials described above (excepting Uncastillo Fm. and Quaternary, because it is

considered that did not participate in the construction process of the anticline). It also presents a mean representative thickness of every unit/formation; what sort of contact exists between them; a representative lithology of each one; and an approximate relative strength scale of each material according to the width of the column. Furthermore, every unit is represented by a color according to the color palette used in the geological map (Figure 1.3).

Figure 1.4 (NEXT PAGE). Stratigraphic sequence of all the materials outcropping in the area of study, excepting Uncastillo Fm. and the Undifferentiated recent deposits (modified from Millán, 1994).

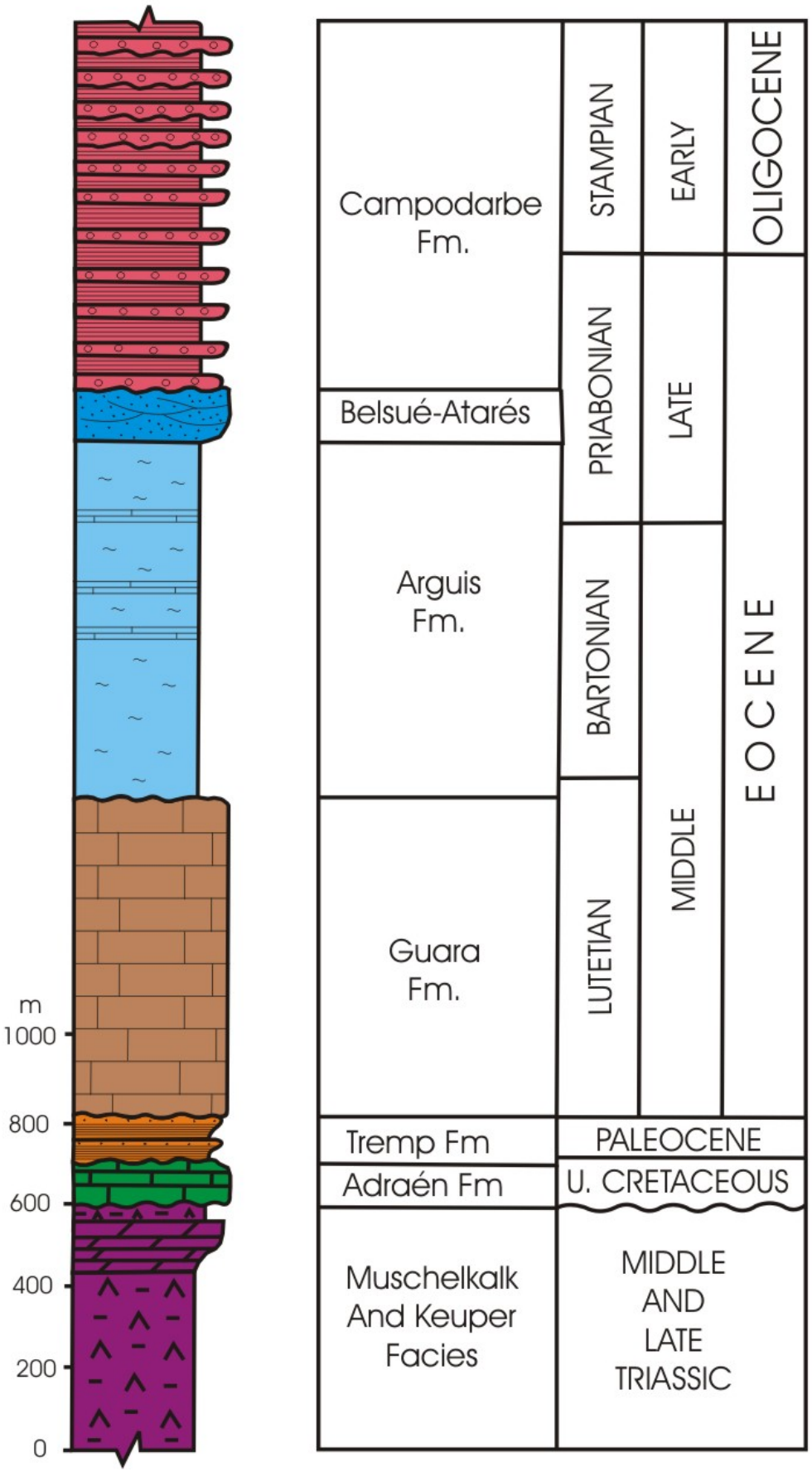
m
1000
800
600
400
200
0
Campodarbe Fm.
Belsué-Atarés
Arguis Fm.
Guara Fm.
Tremp Fm
Adraén Fm
Muschelkalk And Keuper Facies
STAMPIAN
PRIABONIAN
BARTONIAN
LUTETIAN
EARLY
LATE
MIDDLE
OLIGOCENE
EOCENE
PALEOCENE
U. CRETACEOUS
MIDDLE AND LATE TRIASSIC

1·2 STRUCTURE

As discussed previously, the External Sierras are the emergent front of the South-Pyrenean thrust and fold belt, showing a cover which includes Upper Triassic to Lower Miocene rocks and whose development was recorded by the Lower Lutetian–Lower Miocene sedimentary succession. The structural pattern of this part of the belt is characterized by the interference between transverse (N–S to NW–SE) and east-trending folds and thrusts, as pointed out in Pueyo et al. (2002), among others. The transverse folds, such as the Pico del Águila anticline, correspond to detachment folds in which the Triassic plastic-ductile materials are the detachment level. It is important to highlight that although the folded sequence detach over Triassic rocks, these materials present a very high internal deformation, showing small-order fault-bend, fault-propagation and detachment folds. As such, the structure in detail becomes much more complex than just a décollement fold which detaches over a totally ductile detachment level made of gypsum-bearing clays (Keuper facies). In addition, as discussed in the stratigraphic description, the Muschelkalk facies (dolomites and dolomitic limestones) are the dominant materials in the Triassic sequence, showing an important internal thrusting and folding, probably due to the interference between transverse folds development and the N-S general compression.

The Pico del Águila anticline is a symmetric kilometric scale parallel fold, with a 174/64 axial orientation and plunging 29º towards N 353, as it is shown in Figure 1.5. It is, therefore, a westwards verging fold in which the Triassic-Lutetian sequence describes a concentric anticline, showing sub-parallel limbs. The uppermost part of the sequence, from DS3 of the Guara Fm up to the Campodarbe Fm, describes a cartographic scale double sedimentary prism that thins towards the pre-folding sequence in the anticline limbs (outlining an evident onlap over the Guara Fm. Limestones), as it is shown in Figure 1.6.

The geometric relationship of the anticline with the uppermost sedimentary units (See Figures 1.3 and 1.8) shows clear evidence of synchrony between the uplifting of the fold and the deposition of these units. Sequence I and half of Sequence II of Arguis Fm. describe an onlap over both limbs of the anticline, not reaching its crest at either case. This means that the beginning of

the syntectonic deposition occurred when a significant uplift had already taken place. However, the second half of Sequence II, and both Sequences III and IV, show important thinning towards the hinge area, although all of them are continuous across both limbs of the anticline.

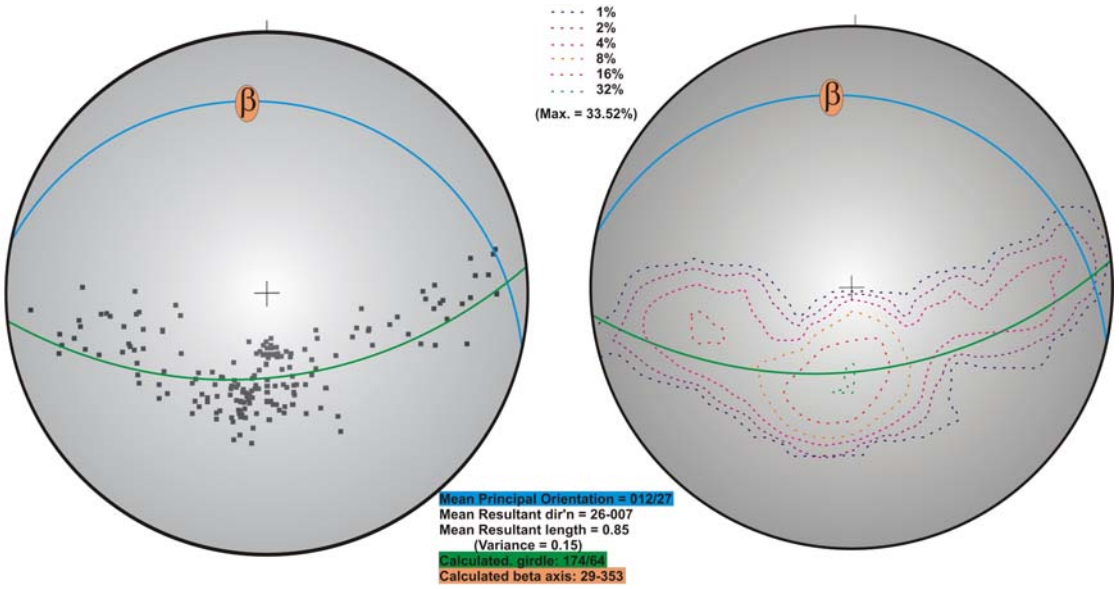

Figure 1.5. Stereonet plotting all the available dip data of the top of Guara Fm, the reference fold surface (see Methodology, chapter 3). Carrying out this structural analysis one can obtain the fold axial plane (green cyclograph) and fold axis orientation (orange ellipse). Statistical distribution and mean values of the data can be also obtained, in order to evaluate the quality of the data.

The first evidence of syntectonic activity in the growth process of the Pico del Águila anticline are previous to the deposition of the Arguis Fm. In fact, it is possible to recognize an internal unconformity and several thinning levels in the uppermost part of the Guara sequence, localized in the western limb of the anticline. These features can be observed in Figure 1.7. Millán (1995) proposes that these stratigraphic features could be related to an older N-S thrust, presently folded, placed in the core of the anticline. It is actually an east-verging

reverse fault that can be followed until the emergent thrust front, where it is probably cut.

This internal, ancient, refolded thrust affects the stratigraphic sequence from the Triassic décollement to the DS2 of the Guara Fm. The tip line outcrops more or less at the top of the DS2, at similar latitude as the Arguis village (see Figure 1.3). Under the termination zone, the thrust places the Upper Cretaceous on the Tremp Fm., in a ramp over ramp relationship. In this zone of the anticline, the footwall sequence (eastern block) describes the hinge area and both limbs of the fold.

The lowest part of the Campodarbe Fm. is the last one in which one can recognize syntectonic features as thinning levels.

The Pico del Águila anticline does not show an important flexural slip displacement, according to IGME (1992) and field observations. In order to accommodate the deformation, this implies an extension regime in the hinge area (upper units; outer arc stretching) and a compressive regime in the core of the fold (lower units). The extension is reflected in a normal fault system affecting the sequence comprised between the top of Guara Fm. and the bottom of Belsué-Atarés Fm. Compression is manifested by means of a set of normal and reverse faults that fault and fold the previous thrust structure, described above. The fold axis is subhorizontal in the southern part of the fold, while in the northern one it plunges up to 45º towards the north (with a mean value of 29 º, as shown in Figure 1.5).

The growth evolution of the fold influenced the great difference in thickness between the associated synclines and the hinge zone (being the first one over three times thicker than the last one). As it is already commented, the maximum progradations and retrogradations (Sequences III and IV of Arguis and Belsué-Atarés Fms.) cross over the fold hinge, as the anticline did not behave as a sedimentation barrier. Paleocurrent measurements from IGME (1992) reveal a supply direction towards the NW, instead of N as it had been if the anticline had totally controlled the sedimentation processes.

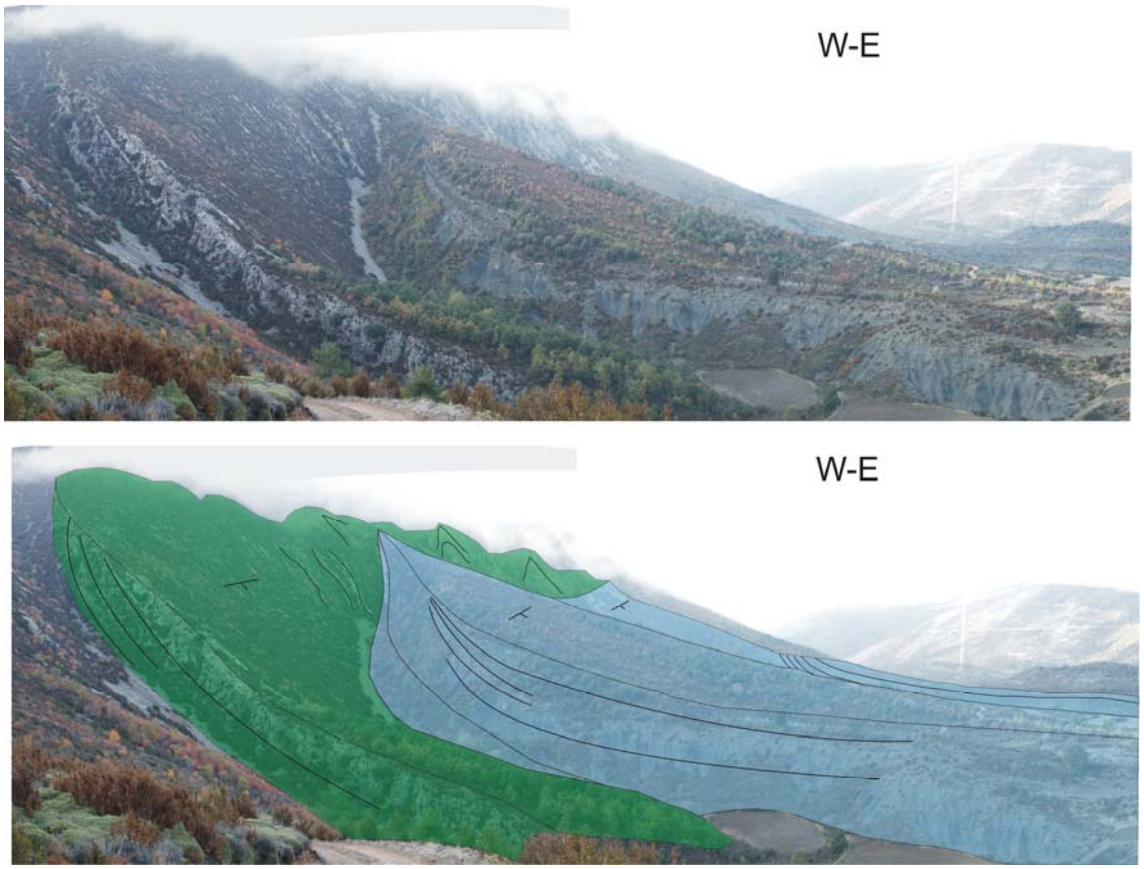

Figure 1.6. Oblique photograph of the eastern limb of Pico del Águila anticline. One can clearly observe the onlap of Arguis marls (in blue) thinning towards the Guara limestones (in green).

IGME (1992) proposes that the Pico del Águila anticline had developed between Bartonian and Lower Priabonian time. According to the age and thickness of materials, they estimate an uplift velocity of approximately 1 mm every 4 years (V=1mm/4y). However, Poblet & Hardy (1995) propose that the anticline started its growth in submarine conditions at approximately 42.67 ± 0.02 Ma (Upper Lutetian), the hinge became emergent at 38.28 ± 0.02 Ma (Priabonian) and deformation continued until 34.8 ± 1.72 Ma (Priabonian), always in subaerial environments. Therefore, the shortening lasted for about 7.87 ± 1.72 Ma, being necessary a total E-W shortening amount of about 2678 m (assuming that the growth-fold shortening was accommodated by limb

rotation). According to these authors, if one assumes a constant limb length detachment fold, the shortening rate was approximately constant at 0.35 ± 0.1 mm/yr, whereas if one assumes a variable limb length detachment fold, the shortening rate decreased with time being as fast as 0.99 ± 0.01 mm/yr during the initial stages of growth.

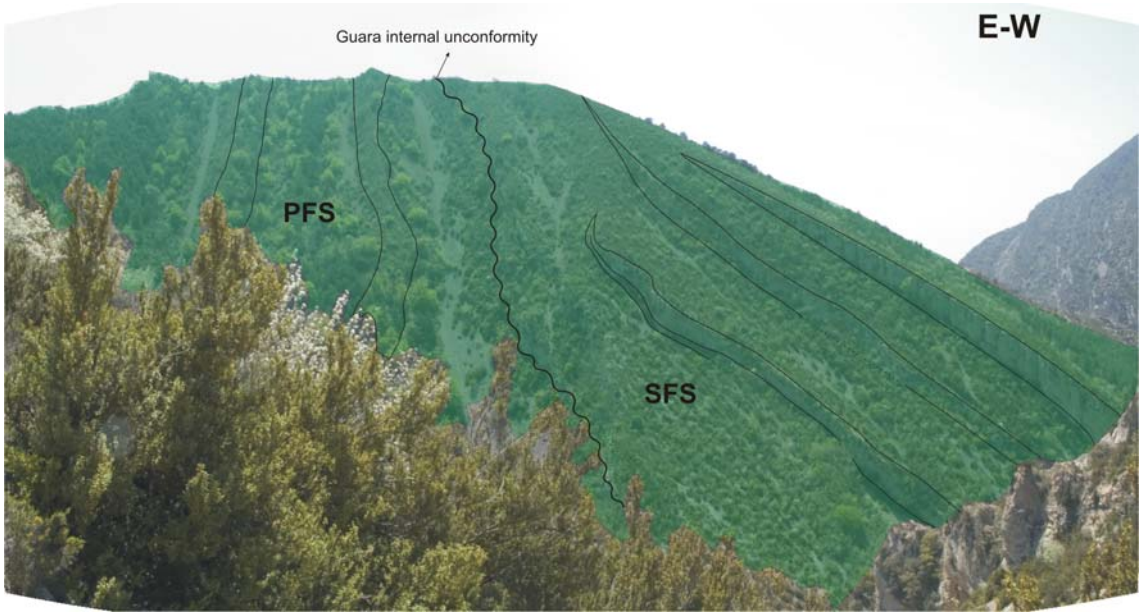

Figure 1.7. Oblique photograph of the uppermost part of the western limb. It shows an internal unconformity of Guara limestone Fm that separates the Pre-Folding Sequence (PFS, DS2 in the photograph) and the Syn-Folding Sequence (SFS, DS3). See how the horizons of the SFS clearly thin towards the E.

Because of the emplacement of the Pico del Águila anticline, two box synclines developed at both sides of the fold: the Arguis syncline to the W and the Belsué syncline to the E. Their box fold morphology is completely determined by the location of the N-S anticline in an E-W structural framework, being forced to partially accommodate the trend interference of both structural families.

In early stages of the evolution, the growth of the N-S anticlines was accompanied by an important regional subsidence, which avoided the emersion

of the fold complex, remaining in a shallow marine platform environment until Lower Bartonian times (IGME, 1992). The sediment supply filled the sea bed from E to W in a structural framework that did not determine the morphology of the sea bed. The sedimentation and re-working rates of the terrigenous materials were much more important than the low uplifting rate. Synclines played the role of sediment traps, while the anticline hinge registered a much lower accumulation rate, not conditioning any barrier or morphological change in the sea bed.

In order to provide an idea of the general structure, distributions and relationship of the materials and sequences described above, Figure 1.8 shows three different general cross-sections of the studied area, taken and modified from Millán (1995). See Figure 1.3 for the location of each cross-section.

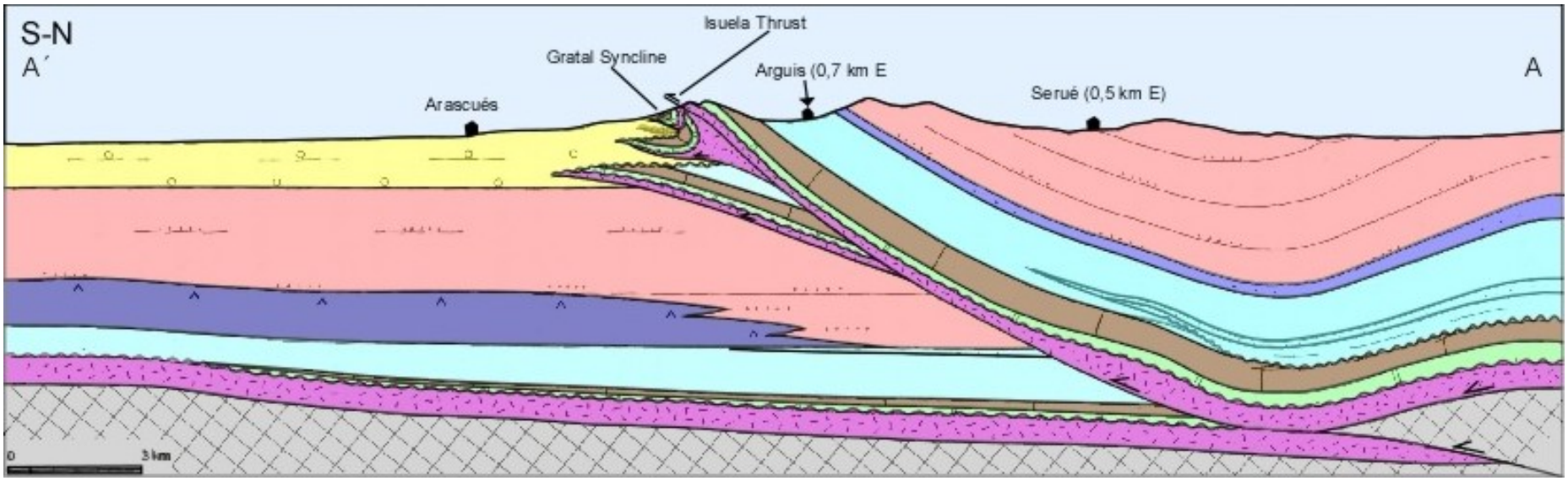
S-N
A´
Isuela Thrust
Gratal Syncline
Arguis (0,7 km E
Seruè (0,5 km E)
A
Arascués
0
3 km

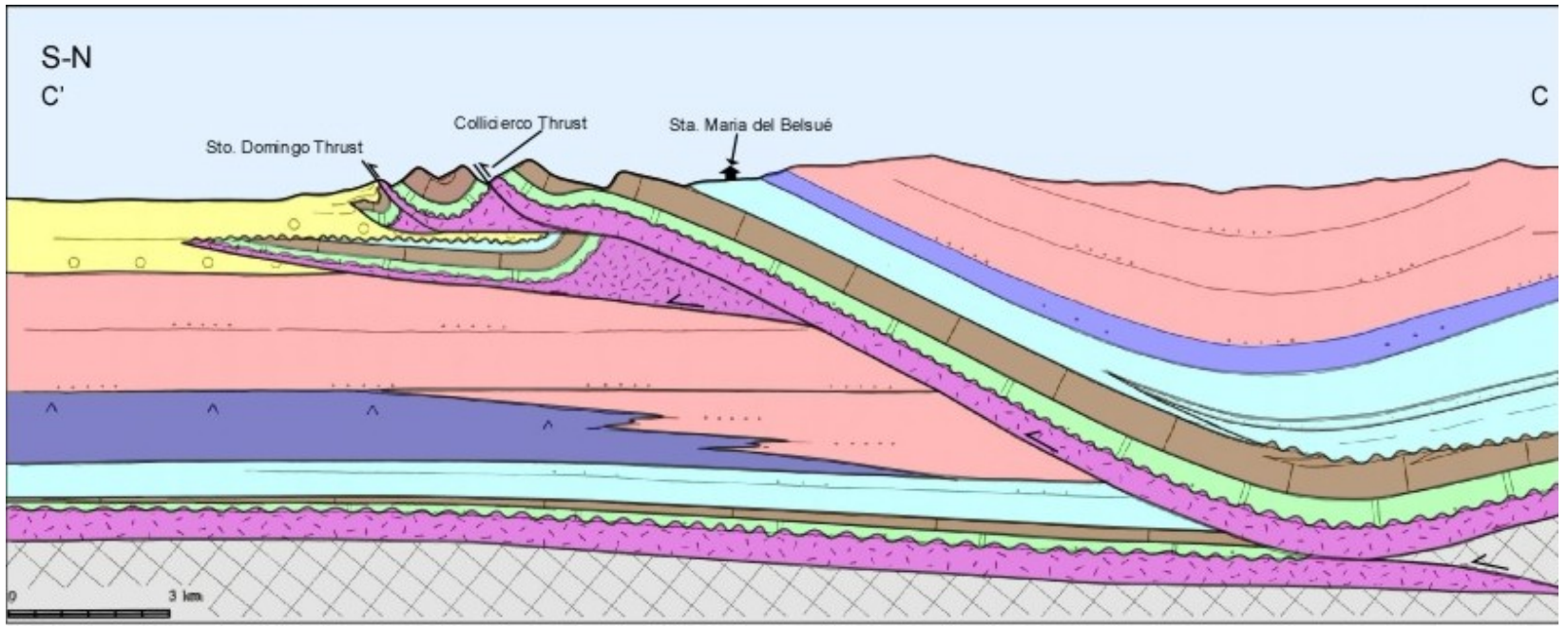
S-N
C'
C
Collidierco Thrust
Sta. Maria del Belsué
Sto. Domingo Thrust
0
3 km

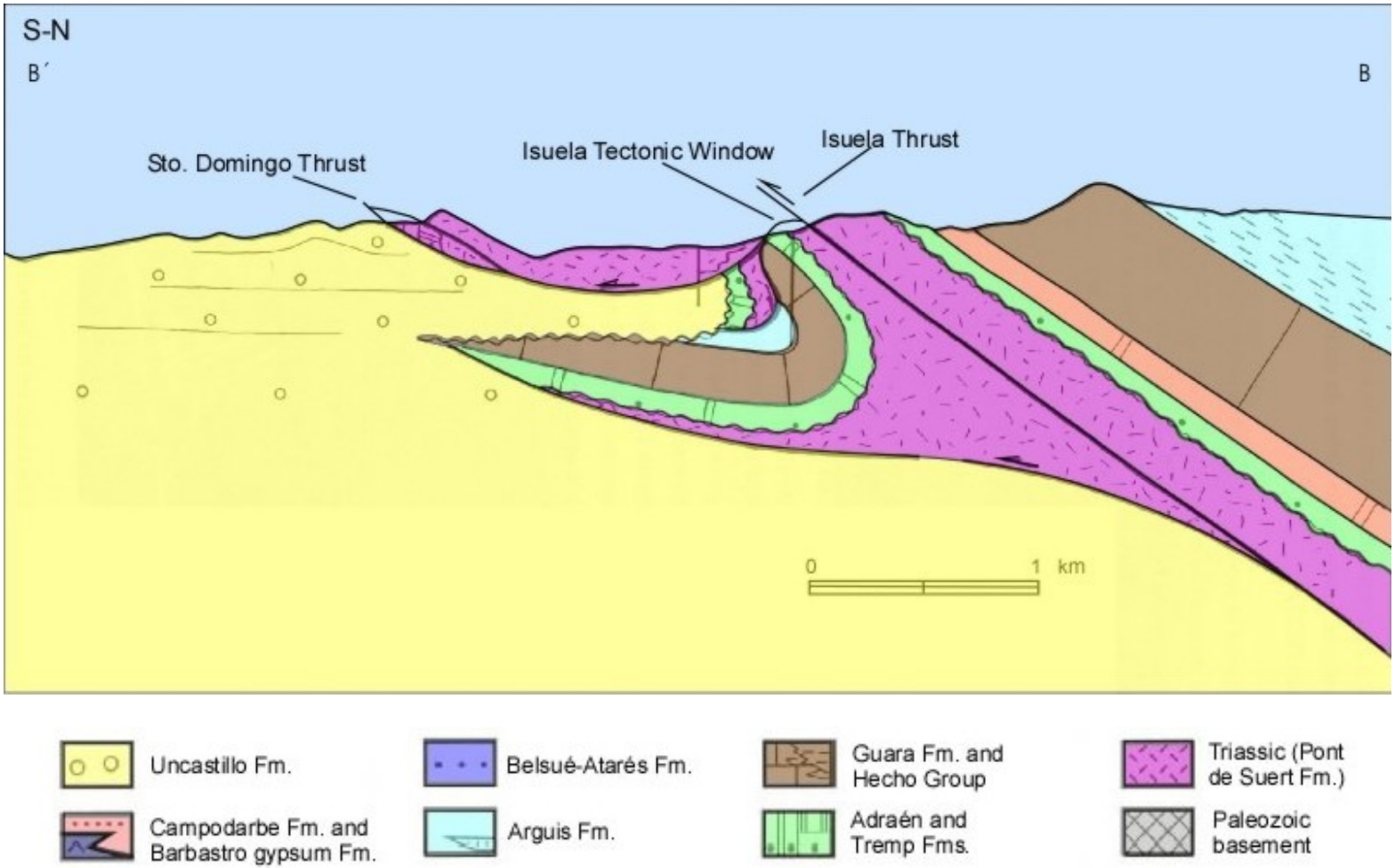

Figure 1.8 (ALSO PREVIOUS PAGE). Three different cross-sections showing the general structure and distribution of materials in the studied area. Notice the important thinning of units towards the South. This is a typical feature of a Thrust-and-fold belt frontal part. See Figure 1.3 for location. Modified after Millán (1995).

CHAPTER II

Formation of orogen-perpendicular thrusts due to mechanical contrasts in the basal décollement

This chapter contains the first scientific article carried out for this Thesis, in which two series of sandbox models are presented to investigate the influence of heterogeneities of the basal detachment level in the formation of transverse (i.e. orogen-perpendicular) structures such as the N-S anticlines of the External Sierras. First, an abridged abstract in Catalan is presented. Secondly, we present an abridged abstract in English and the work published in the *Journal of Structural Geology* and cited as follows:

Vidal-Royo, O., Koyi, H.A., Muñoz, J.A., 2009. Formation of orogen-perpendicular thrusts due to mechanical contrasts in the basal décollement in the Central External Sierras (Southern Pyrenees, Spain). Journal of Structural Geology, 31 (5), 523-539.

2.1 RESUM DEL CAPÍTOL (Summary in Catalan)

Aquest capítol conté el primer article científic realitzat per aquesta Tesi, en el que es presenten dues sèries de models analògics per tal d'investigar l'efecte de les heterogeneïtats en el nivell basal de desenganxament sobre la

formació i evolució d'estructures perpendiculars al sistema orogènic tals com les descrites en les Sierras Exteriores Aragonesas.

Dues sèries de models analògics s'han emprat per explorar l'efecte dels contrastos entre materials dúctils i friccionals en el nivell basal de desenganxament sobre el desenvolupament d'estructures obliqües i perpendiculars durant events d'escurçament a l'escorça superior. Aquests models simulen l'evolució del sector central de les Sierras Exteriores Aragonesas (Pirineus Meridionals, Espanya), que constitueixen la part més frontal i emergent de l'encavalcament frontal Sudpirinenc. Les Sierras Exteriores Aragonesas es caracteritzen per la presència d'estructures anticlinals d'orientació axial N-S a NW-SE, perpendicular a la tendència estructural general dels Pirineus. Es van desenvolupar en el bloc superior de l'encavalcament frontal Sudpirinenc, i estan desenganxades sobre materials Triàsics distribuïts de manera heterogènia i que presenten importants canvis laterals de gruix (es produeixen importants contrastos de comportament mecànic en funció d'una major o menor presència de materials dolomítics del Muschelkalk o evaporítics del Keuper).

Els models simularen el contrast entre materials dúctils (silicona) adjacents a materials friccionals (sorra) durant episodis d'escurçament. La sèrie de models A investiga la relació de gruix estratigràfic entre la cobertora sedimentària i el nivell de desenganxament, mentre que la sèrie de models B investiga la importància de l'amplada (perpendicular a la direcció d'escurçament) dels materials friccionals.

Els resultats de la modelització confirmen que el front de deformació mostra un major avanç en les àrees desenganxades en un nivell dúctil mentre que sobre el nivell de desenganxament friccional l'escurçament s'acomoda mitjançant un major creixement vertical de les estructures i major deformació interna. Aquests trets reprodueixen l'estil estructural de les Sierras Exteriores Aragonesas: major relleu estructural dels anticlinals N-S respecte les estructures paral·leles a l'orogen, absència de un nivell de desenganxament representatiu en el nucli de les estructures, sentit d'immersió dels anticlinals cap a la serralada i

tancament periclinal cap a la conca d'avantpaís no encavalcada per l'encavalcament frontal Sudpirinenc.

2.2 ABRIDGED SUMMARY

Two series of analogue models are used to explore the effect of ductile-frictional contrasts of the basal décollement on the development of oblique and transverse structures during thin-skinned shortening. These models simulate the evolution of the Central External Sierras (CES; Southern Pyrenees, Spain), which constitute the frontal emerging part of the southernmost Pyrenean thrust. The CES are characterised by the presence of N-S to NW-SE anticlines, perpendicular to the Pyrenean structural trend and developed in the hanging-wall of the thrust system. They detach on unevenly distributed Triassic materials (evaporitic-dolomitic interfingering). The models simulated the effect of adjacent ductile versus frictional décollements during shortening. Model Series A tests the thickness ratio between overburden and the ductile layer, whereas model Series B tests the width (perpendicular to the shortening direction) of frictional décollement. Model results confirms that deformation reaches further in areas detached on a ductile layer whereas above frictional décollement areas, shortening is accommodated by additional uplift and penetrative strain. This replicates the structural style of the CES: higher structural relief of N-S anticlines with regard to orogen-parallel structures, absence of a representative ductile décollement in the core, plunging towards the hinterland and foreland-side closure not thrusted by the South Pyrenean thrust.

Journal of Structural Geology 31 (2009) 523–539

Contents lists available at ScienceDirect

Journal of Structural Geology

journal homepage: www.elsevier.com/locate/jsg

Formation of orogen-perpendicular thrusts due to mechanical contrasts in the basal décollement in the Central External Sierras (Southern Pyrenees, Spain)

Oskar Vidal-Royo [a,*], Hemin A. Koyi [b], Josep Anton Muñoz [a]

[a] Geomodels Institute, GGAC, Departament de Geodinàmica i Geofísica, Facultat de Geologia, Universitat de Barcelona, C/ Martí i Franquès s/n, 08028 Barcelona, Spain
[b] Hans Ramberg Tectonic Laboratory, Department of Earth Sciences, Uppsala University, Villavägen 16, SE-752 36 Uppsala, Sweden

ARTICLE INFO

Article history:
Received 24 November 2008
Received in revised form
19 February 2009
Accepted 17 March 2009
Available online 27 March 2009

Keywords:
Analogue modelling
External Sierras
Southern Pyrenees
Pico del Aguila
Detachment
Ductile deformation
Brittle deformation

ABSTRACT

Two series of analogue models are used to explore the effect of ductile-frictional contrasts of the basal décollement on the development of oblique and transverse structures during thin-skinned shortening. These models simulate the evolution of the Central External Sierras (CES; Southern Pyrenees, Spain), which constitute the frontal emerging part of the southernmost Pyrenean thrust. The CES are characterised by the presence of N–S to NW–SE anticlines, perpendicular to the Pyrenean structural trend and developed in the hanging-wall of the thrust system. They detach on unevenly distributed Triassic materials (evaporitic–dolomitic interfingering). The models simulated the effect of adjacent ductile versus frictional décollements during shortening. Model Series A tests the thickness ratio between overburden and the ductile layer, whereas model Series B tests the width (perpendicular to the shortening direction) of frictional décollement. Model results confirms that deformation reaches further in areas detached on a ductile layer whereas above frictional décollement areas, shortening is accommodated by additional uplift and penetrative strain. This replicates the structural style of the CES: higher structural relief of N–S anticlines with regard to orogen-parallel structures, absence of a representative ductile décollement in the core, plunging towards the hinterland and foreland-side closure not thrusted by the South Pyrenean thrust.

1. Introduction

The evolution and final geometry of a fold-and-thrust belt is strongly dependant on the mechanical properties of the basal detachment level (Davis and Engelder, 1985; Cotton and Koyi, 2000; Costa and Vendeville, 2002; Bahroudi and Koyi, 2003; Koyi and Cotton, 2004; Massoli et al., 2006). Scaled analogue models have been widely used to simulate the kinematics of thrust-and-fold belts detached on brittle substrates (Mulugeta and Koyi, 1987; Mulugeta, 1988; Mulugeta and Koyi, 1992; Liu et al., 1992; Koyi, 1995, 1997; Storti et al., 2001; Koyi and Vendeville, 2003; Lohrmann et al., 2003; McClay et al., 2004; McClay and Whitehouse, 2004) and less often on viscous ductile substrates (Letouzey et al., 1995; Cotton and Koyi, 2000; Costa and Vendeville, 2002; Grelaud et al., 2002; Schreurs et al., 2002; Smit et al., 2003; Dooley et al., 2007; Crespo-Blanc, 2008). The dynamic evolution and the final geometry of fold and thrust belts depend on the mechanical behaviour of the basal décollement and its interaction with the overlying overburden (Davis and Engelder, 1985; Koyi, 1988; Cobbold et al., 1989; Talbot, 1992; Harrison, 1995; Cotton and Koyi, 2000; Costa and Vendeville, 2002; Grelaud et al., 2002; Schreurs et al., 2002; Bahroudi and Koyi, 2003; Luján et al., 2003; Bonini, 2007; Storti et al., 2007).

The geometry and structural style of the Pyrenees depend on the interaction between the intracrustal inhomogeneities inherited from the pre-collisional Early Cretaceous extensional event and the weak horizons in the cover sequence, mostly Triassic and Eocene salts, shales and evaporites (Beaumont et al., 2000). The external domains of the southern Pyrenees commonly show a highly irregular and hard to predict distribution of the detachment level (widely believed to be Triassic evaporitic facies; e.g. Keuper or middle Muschelkalk), often with scarce and variable thickness of allochtonous transported detachment materials at the frontal emerging thrust areas (Pocoví, 1979; Muñoz, 1992; Millán, 1995; Teixell and García-Sansegundo, 1995; Oliva et al., 1996; Teixell and Koyi, 2003; Oliva-Urcía and Pueyo, 2007). These external domains (e.g. Serres Marginals and External Sierras) correspond to pieces of the South-Pyrenean foreland basin that were incorporated into the orogen as deformation progressed southwards. Paleogeographic reconstructions indicate that in late Triassic, the region was located

* Corresponding author. Geomodels Institute, GGAC, Departament de Geodinàmica i Geofísica, Facultat de Geologia, Universitat de Barcelona, C/ Martí i Franquès s/n, 2nd floor, office 227, 08028 Barcelona, Spain. Tel.: +34 934 035 957; fax: +34 934 021 340.
E-mail addresses: oskarvidal@ub.edu, vidal.oskar@gmail.com (O. Vidal-Royo).

0191-8141/$ – see front matter © 2009 Elsevier Ltd. All rights reserved.
doi:10.1016/j.jsg.2009.03.011

in a structural high of the Triassic extensional basin (see Fig. 10.12 of López-Gómez et al., 2002; Castillo-Herrador, 1974; Jurado, 1990; Salvany, 1990). Consequently, in the External Sierras just a thin sequence of Upper Triassic sediments was deposited.

Many modelling studies have focused on the structure of the Pyrenean external domains and provided new insights on their evolution (Nalpas et al., 1999; Soto et al., 2002, 2006; Teixell and Koyi, 2003; Koyi and Sans, 2006; Storti et al., 2007). Our study focuses on the central sector of the External Sierras (CES; Southern Pyrenees, Spain), where the main structural pattern is characterised by the interference between E–W orogen-parallel structures and a set of N–S kilometric-scale, thrust-related anticlines.

Different hypothesis have been suggested to explain the geodynamic evolution of the Central External Sierras. Based on the irregular fold geometries, the ubiquitous evaporitic strata along the décollement and in the core of the fold cores, the timing of folding and palinspastic restorations of the folds and Jaca basin, it has been suggested that the N–S anticlines could be a consequence of the halotectonic deformation related to the extensional faults affecting the older part of the stratigraphic sequence (Anastasio, 1992; Anastasio and Holl, 2001) or rotation of the thrust sheets (Pueyo et al., 2002). Pueyo et al. (2002), used paleomagnetic data to report a 40° clockwise rotation of the South-Pyrenean thrust sheets.

Based on field evidence of inhomogeneous distribution of Upper Triassic gypsum-bearing clays, this paper explores the mechanical contrasts in the basal décollement and the consequent differential propagation of the deformation in the overburden to explain the generation of oblique and transverse N–S anticlines during a single N–S shortening phase in the CES. Marques and Cobbold (2002, 2006) have also tackled the differential propagation of deformation in compressional regimes, in which the thickness variation resulted in differential topographic formation and differential propagation. However, the aim of this work is to give new insights on the geodynamic evolution of the central sector of the External Sierras by carrying out series of analogue models that explore the differential propagation of deformation as a direct response of mechanical changes in the basal detachment.

2. Geological setting

The External Sierras constitute the frontal emerging part of the southernmost Pyrenean thrust sheets (Soler and Puigdefàbregas, 1970; IGME, 1992; Millán et al., 1994; Millán, 1995; Pueyo et al., 2002). The External Sierras consist of a system of thin-skinned imbricated thrust sheets detached on clayish, dolomitic and evaporitic Middle and Late Triassic facies (Keuper and Muschelkalk facies). The hanging-wall of the frontal Pyrenean thrust involves an Upper Triassic to Lower Miocene sedimentary sequence (Puigdefàbregas, 1975; Millán et al., 1994; Millán, 1995) which was displaced southwards over the Tertiary sediments of the Ebro foreland basin. The External Sierras also constitute the southern limit of the Jaca piggy-back basin, which was incorporated into the Pyrenean orogen during the last stages of deformation, since Middle Eocene times (Millán, 1995).

One of the peculiarities of External Sierras is the presence of a set of irregularly spaced transverse NW–SE to N–S anticlines. These structures are at high angle or perpendicular to the general structural trend of the Pyrenees (E–W; tectonic transport towards the south) and create a complex interference structural pattern (Fig. 1). These N–S anticlines become younger and smaller westwards (Millán et al., 1994; Millán, 1995) and their growth was synchronous with the deposition of the Middle Eocene to Oligocene sediments and the development of the South-Pyrenean thrust front (which was active until Early Miocene; Puigdefàbregas, 1975; Holl and Anastasio, 1993; Millán et al., 1994; Millán, 1995). From an accurate observation of the growth strata pattern, Poblet et al. (1997) considered N–S folds to form by partially limb lengthening, limb rotation and flexural slip mechanisms, under high

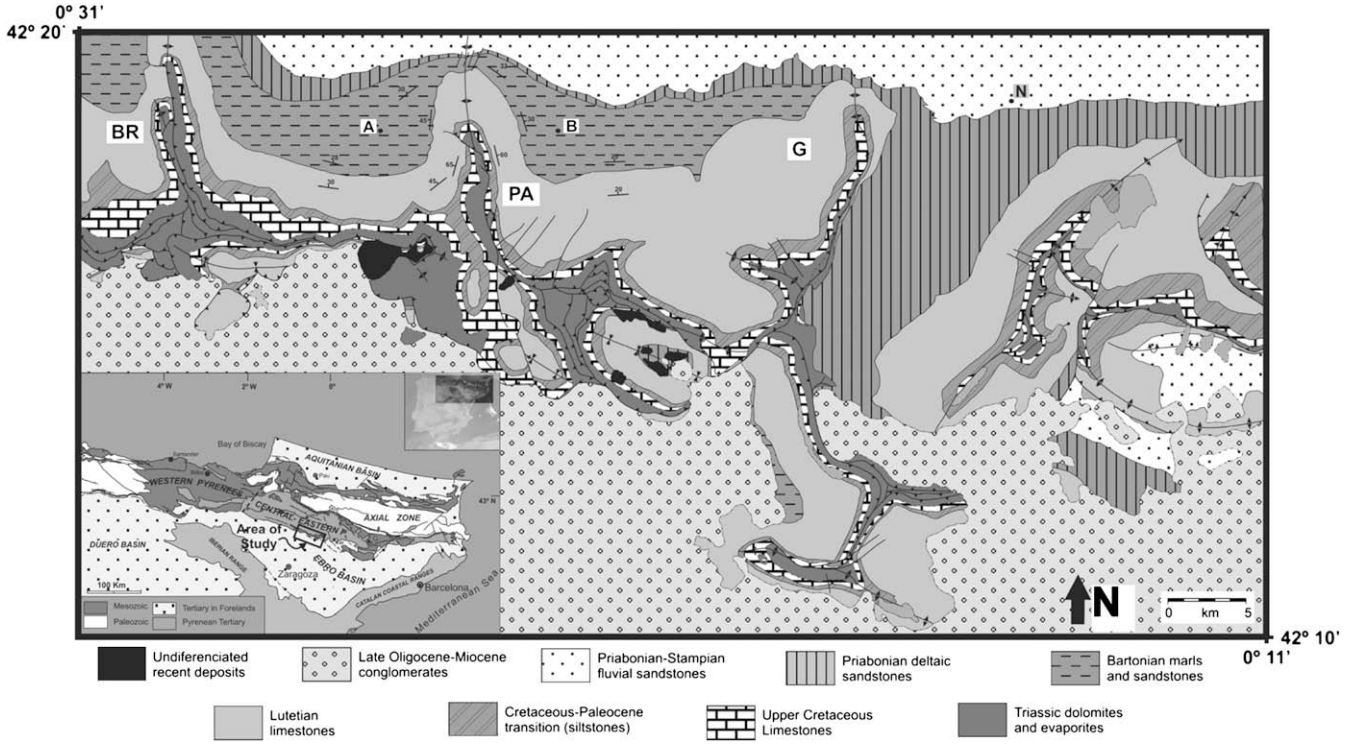

Fig. 1. Geological map of Central External Sierras (modified after IGME, 1992). BR: Bentué de Rasal anticline; PA: Pico del Águila anticline; G: Gabardiella anticline complex; A: Arguis Village; B: Belsué Village; N: Nozito Village.

sedimentation rates. Given that the size of the N–S anticlines decreases westwards, it can be assumed that the deformation also diminished in the same direction (i.e. the amount of shortening decreased westwards). Since the present study especially focuses on the processes that took place in the N–S anticlines of the central sector of the Sierras (Fig. 1), the general descriptions will mainly refer to this area, and not necessarily to the rest of the External Sierras.

The stratigraphy in the study area consists of a relatively thin (few hundred metres thick) Mesozoic succession, covered by a thicker Paleogene sequence (Fig. 2). The Mesozoic is made of Triassic limestones, dolomites and gypsum-bearing clays, and Upper Cretaceous shallow marine limestones. The Paleogene comprises continental sandstones, siltstones and lacustrine limestones of the Cretaceous–Paleocene transition (Garumnian facies), shallow marine platform limestones of the Guara Formation (Lutetian), shallow marine and transitional marls, limestones and sandstones of the Arguis and Belsué–Atarés Formations (Upper Lutetian to Middle Priabonian), and the fluvial clays, sandstones and conglomerates of the Campodarbe Formation (Middle Priabonian to Middle Oligocene).

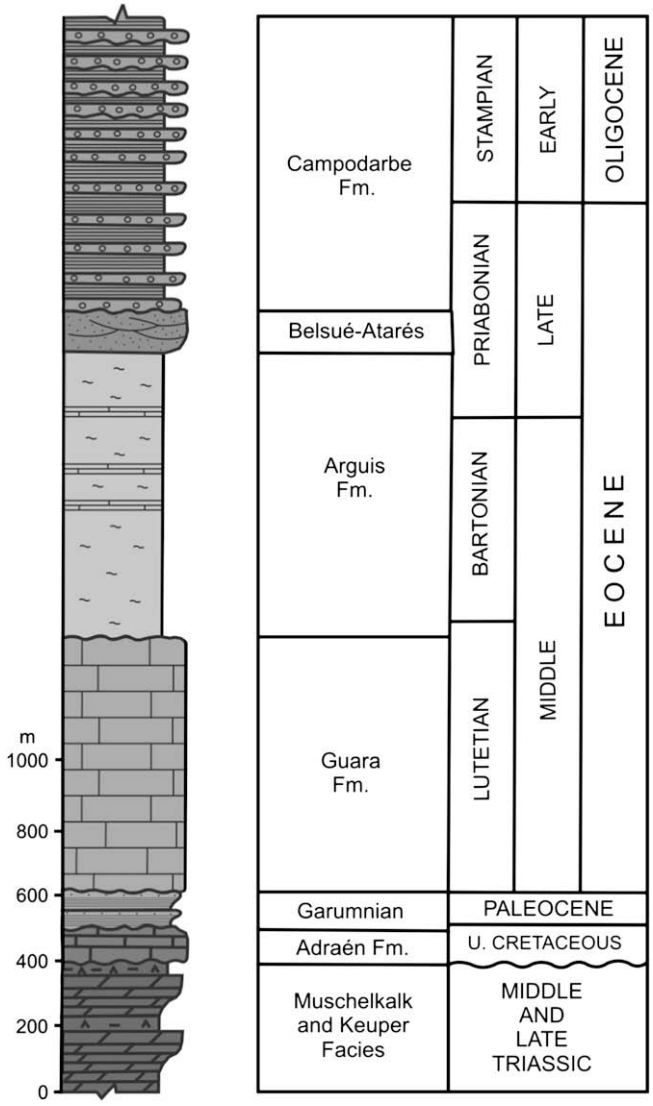

Fig. 2. Stratigraphic sequence described in Central External Sierras (modified after Millán et al., 1994). Note that the stratigraphic thickness of Guara Fm. may vary across the region.

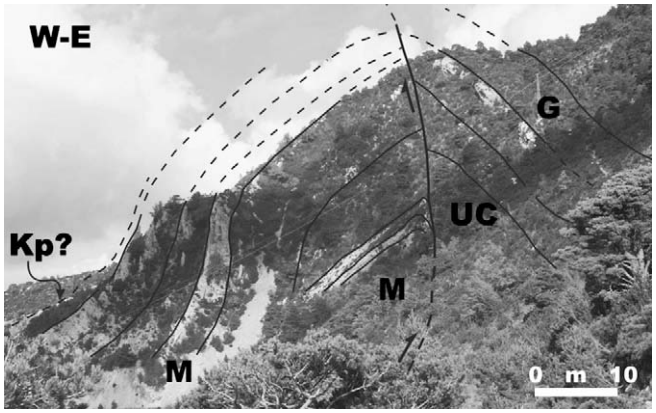

Fig. 3. Sketch of the core of Pico del Águila anticline. The internal folded thrust affects the core of the structure placing Muschelkalk Middle Triassic rocks (M) on Upper Cretaceous (UC) and Garumnian (G) rocks. Keuper evaporitic facies (Kp) can not be recognised and just a thin sequence may outcrop at the left of the picture.

The first attempts to determine the geodynamic evolution of the External Sierras were given by Mallada (1878), Selzer (1948) and Almela and Ríos (1951), who proposed a progressive westward migration of the deformation. Anastasio (1992) and Anastasio and Holl (2001) proposed a halokinetic origin of the N–S trending folds of the External Sierras. According to those studies, the N–S structures developed as a result of the differential loading caused by the progradation of Paleogene clastic distributary systems. This differential loading resulted in the flow of the Triassic mobile décollement towards the west, where the overburden units are thinner. Flow of Triassic evaporites in front of the wedge resulted in the formation of a trough that accommodated additional loading. However, this argument does not seem to hold for the study area because according to Poblet and Hardy (1995), the thickness of the overburden is 4.3–1.6 times the thickness of the ductile unit. Moreover, the overburden/substrate thickness ratio was possibly higher if we take into account the fact that Triassic sediments

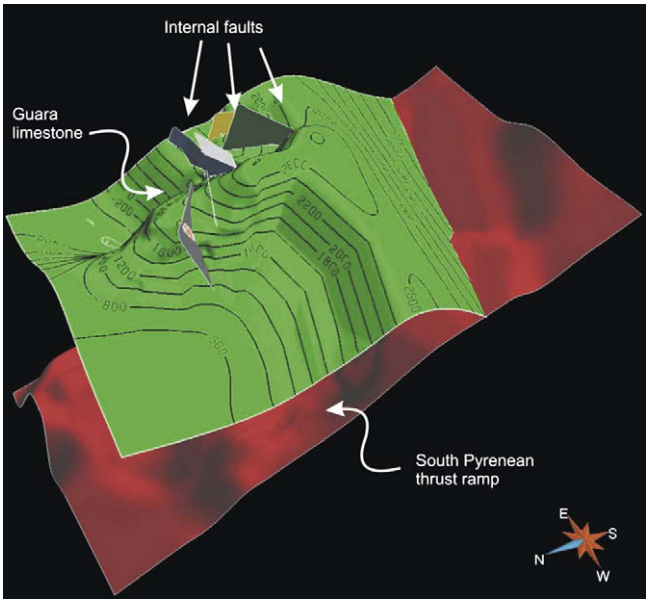

Fig. 4. 3D reconstruction of the Pico del Águila anticline (top of Guara Fm. in green) and the ramp of the frontal South-Pyrenean emergent thrust (in red). Notice both northern and southern closures of the anticline. Guara Fm. describes an orogen-parallel E–W structural trend in the accommodation area of the thrust.

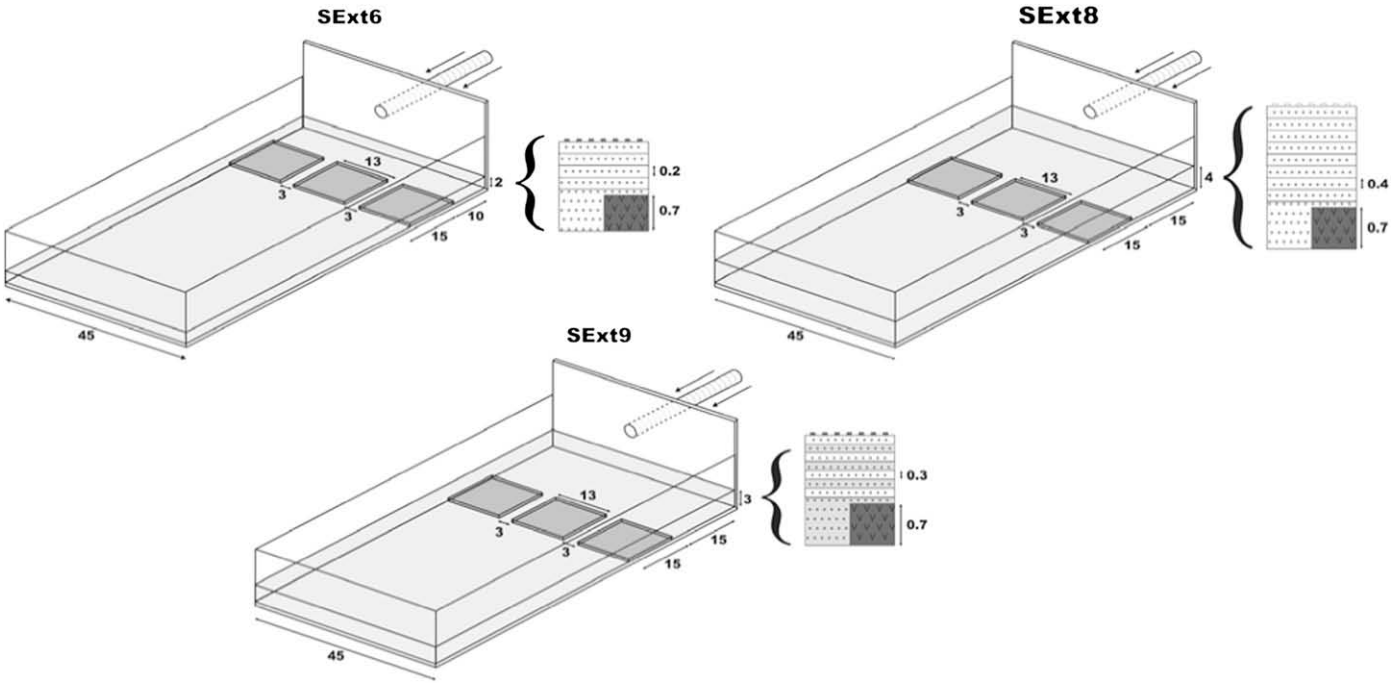

Fig. 5. Initial setup of model series A showing the distribution of ductile (SGM-36) and brittle (sand) décollements and direction of shortening. The stratigraphic sequence of each model is also presented. All the values are in cm.

predominantly consist of competent lithologies such as Muschelkalk limestones and dolomites, and Keuper evaporites and gypsum-bearing clays are nearly absent. These facts led us to decline the halokinetic origin of N–S anticlines proposed by Anastasio (1992) and Anastasio and Holl (2001).

Later, based on a meticulous mapping and stratigraphic analysis of the synfolding sequence (Millán et al., 1994) as well as several paleomagnetic studies (Pueyo, 2000; Pueyo et al., 2002, 2003a), a new evolutionary model was proposed, which we outline below. During the early stages of the evolution of the External Sierras (Early Lutetian to Chattian), the thrust system was characterised by a south-verging main thrust and a set of arcuate north–eastward concave, oblique thrusts. The N–S trending folds are interpreted as a more evolved stage of the initially oblique thrusts, which were generated as detachment folds on a hanging-wall flat over footwall flat thrust configuration. In addition to a general translation towards the south, a regional clockwise rotation process characterised the kinematics of the thrust system (up to 40° measured at the base of Arguis Fm, western limb of Pico del Águila anticline; Pueyo et al., 2002). Clockwise rotation has played an important role on the kinematics of the Sierras, as it is reported in many studies (e.g., Dinarés et al., 1992; Bentham and Burbank, 1996; Hogan and Burbank, 1996; Pueyo et al., 1997, 2000, 2002, 2003a,b; Pueyo, 2000; Larrasoaña et al., 2001; Oliva et al., 1996; Oliva-Urcía and Pueyo, 2007). However, during Chattian to Early Miocene, the structural evolution changed abruptly. The rotating thrust system was folded and truncated by the formation of the Santo Domingo detachment anticline and its associated south-directed thrust system, located in the western sector of the External Sierras (beyond the western limits of Fig. 1). Consequently, the remaining N–S trending folds occurred at the hanging-wall of the new Santo Domingo thrust system, representing the northernmost portion of those oblique structures (the rest of the structures are supposed to be either buried under the continental deposits of the Ebro foreland basin or

Table 1
Scaling parameters between models and nature.

Parameter	Nature	Models	Scaling ratio
Acceleration due to gravity	9.81	9.81	$a_m/a_n = 1$
Thickness (m)			
Overburden	~750–1000	0.013–0.033	$l_m/l_n = 10^{-5}$
Substrate	~300	0.007	$l_m/l_n = 10^{-5}$
Mean density ρ (kg/m^3)			
Overburden	2550	1700	$\rho_m/\rho_n = 0.67$
Substrate	2200[a]–2550[b]	987[a]–1700[b]	$\rho_m/\rho_n = 0.45$–0.67
Density contrast $\Delta\rho$ (ρo–ρs)	350[a]–0[b]	713[a]–0[b]	$\Delta\rho_m/\Delta\rho_n = 2.04$–?
Friction coefficient of overburden	0.85	0.73	0.86
Viscosity of ductile layer (Pa · s)	$10^{-18\ (\text{to}\ -19)}$[c]	5×10^4	$10^{-14\ (\text{to}\ -15)}$
(ρl g/τ_0) ratio	0.75	0.16	0.21
Shortening rate	0.35–0.99 mm/year[d]	16.2×10^4 mm/year	46.3×10^4–16.2×10^4

Subscripts m, n, o, s denote, respectively, model, nature, overburden and substrate.
[a] Ductile substrate.
[b] Frictional substrate.
[c] Estimated value.
[d] Extracted from Poblet and Hardy (1995).

isolated by erosion under the southern limb of the Santo Domingo anticline, according to (Pueyo et al., 2002). The emplacement of these N–S trending folds in a hanging-wall flat over footwall ramp position of the Santo Domingo thrust system is the cause to their 30° plunge towards the North (Millán, 1995; Pueyo et al., 2002).

Although this is the best reported and data-based hypothesis about the evolution of the Central External Sierras, it presents some weak points that have led us to look for other complementary processes. Previous studies have stated that the N–S trending Pico del Águila fold detach on Upper Triassic rocks (Pueyo et al., 2002). Nonetheless, both field observations and geological mapping (IGME, 1992) indicate that Muschelkalk limestones and dolomites (Middle Triassic rocks) are the oldest materials outcropping in the core of the anticline (Fig. 3) and are internally thrusted, showing high internal deformation. On the other hand, although Keuper clays and evaporites (Upper Triassic rocks) outline the geometry of the fold as the rest of the upper Mesozoic sequence do, important decrease of thickness is observed towards the inner part, where it is nearly absent in the core of the anticline (Fig. 3). In such a way, Keuper facies are thicker and better exposed in the areas between, rather than in the core of the N–S anticlines, where the frontal South-Pyrenean thrust emerges.

From the reported 40° clockwise rotation it can be inferred that the initial oblique structures had to form at least at 50° relative to the shortening direction. This is a decisive fact in the present orientation of these transverse structures. However, there is no explanation for the mechanism of generation of those arcuate, oblique structures formed in Early Lutetian to Chattian times. In addition, the 3D geometrical reconstruction of the N–S trending

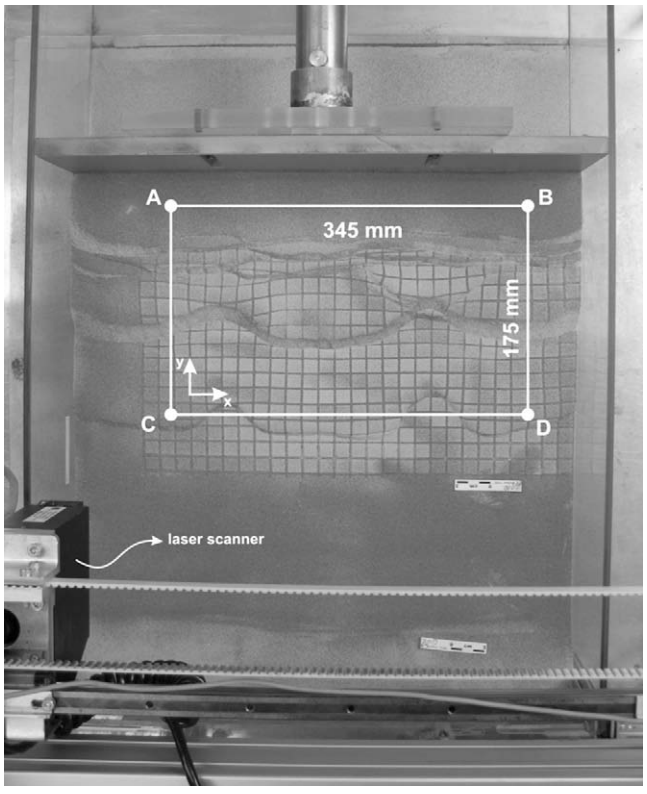

Fig. 6. Top view of model SExt10 after 20% shortening. Laser scanner is visible at the left bottom of the picture. ABCD indicate the dimensions of the scanned area in the last stage of deformation. The area covers only the central portion of the model, avoiding wall perturbations of the laser beam. AB distance was kept constant for all the scans, whereas AC distance was decreased as shortening increased. C and D positions were constant. A and B positions were progressively closer to the fix wall.

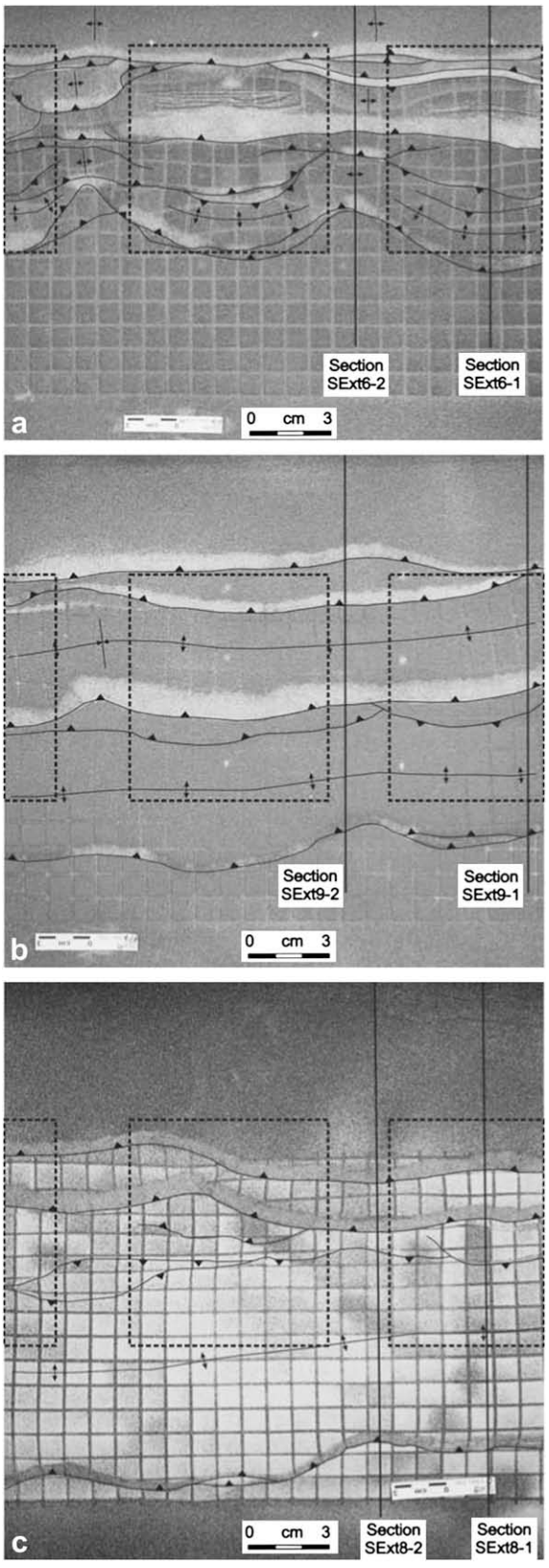

Fig. 7. Top view of models SExt6 (a), SExt9 (b) and SExt8 (c) after 20% of shortening. Representative sections of the models are indicated on the top view and showed in Fig. 8 for SExt6, Fig. 9 for SExt9 and Fig. 10 for SExt8. Dashed rectangles indicate the initial position of the ductile layers in the basal décollement. Notice the clear differential propagation of deformation and the generation of transverse structures in model SExt6 (a) and the general orogen-parallel style of models SExt8 (b) and SExt9 (c).

Pico del Águila anticline (Fig. 4) indicates that this structure was not truncated by the Santo Domingo thrust system. As shown, both northern and southern closures of Pico del Águila are observable northwards of the South-Pyrenean thrust. The southern closure of Pico del Águila shows a slight plunge towards the south (around 10°), and the bedding of Guara Formation shows an orogen-parallel E–W attitude along the thrust front. Therefore, there are no evidences of structural interference in the South-Pyrenean frontal emergent thrust supporting the truncation of the initially arcuate oblique structures by the emplacement of the Santo Domingo thrust system.

3. Model series

3.1. Modelling procedure and materials

Two series of experiments were executed for this study. The experimental design is based on field observations indicating a nearly absence of Keuper facies in the core of the transverse anticlines (e.g. Pico del Águila and Gabardiella anticlines, Fig. 1), and a thicker presence of these materials where the orogen-parallel structures develop (e.g. South-Pyrenean thrust front). All the models consisted of a colour interlayered sequence of sand covering an uneven basal level where three ductile silicone patches were present (Fig. 5). Dry quartz sand with a density of 1700 kg m^{-3}, cohesive strength C of 140 Pa and sieved to an average grain size of 35 μm was used to simulate the brittle sedimentary cover of Upper Cretaceous to Lutetian rocks. The Triassic irregular detachment level was simulated by means of the Newtonian viscous silicone putty SGM36 (density of 987 kg m^{-3} and effective viscosity η of 5×10^4 Pa s at room temperature, manufactured by Dow Corning Ltd.) neighbouring dry quartz sand (Fig. 5). A summary of the scaling parameters used in this study is shown in Table 1. For detailed analysis of these materials and their suitability as model analogues, see Weijermars (1986) and Weijermars and Schmeling (1986). All the experiments were built at the Hans Ramberg Tectonic Laboratory, in a deformation rig with a basal aluminium plate on which sand was glued to give a high friction. All models had a fixed width of 45 cm, an initial length parallel to the compression piston of 60 cm, a constant detachment thickness of 7 mm (for both silicone and sand), and were shortened at a constant rate of 1.85 cm h^{-1} ($5.14\ 10^{-6}$ m s^{-1}) up to 20% during 6 h. A passive grid of square markers (12×12 mm) was printed on the top surface of the models, which was photographed during shortening at regular intervals in order to record the evolution of the model at surface. After 20% of shortening, the deformed models were covered by loose sand and impregnated by water, which increased the cohesive strength of sand and allowed sectioning of the model.

In one of the Series B models (model SExt10) we used a high-accuracy laser scanner (±0.1 mm; Nilforoushan et al., 2008) to monitor the topographic evolution of the model. Technical descriptions of this device and discussions about its use and benefits can be found in Williams et al. (2000), Swantesson (2005),

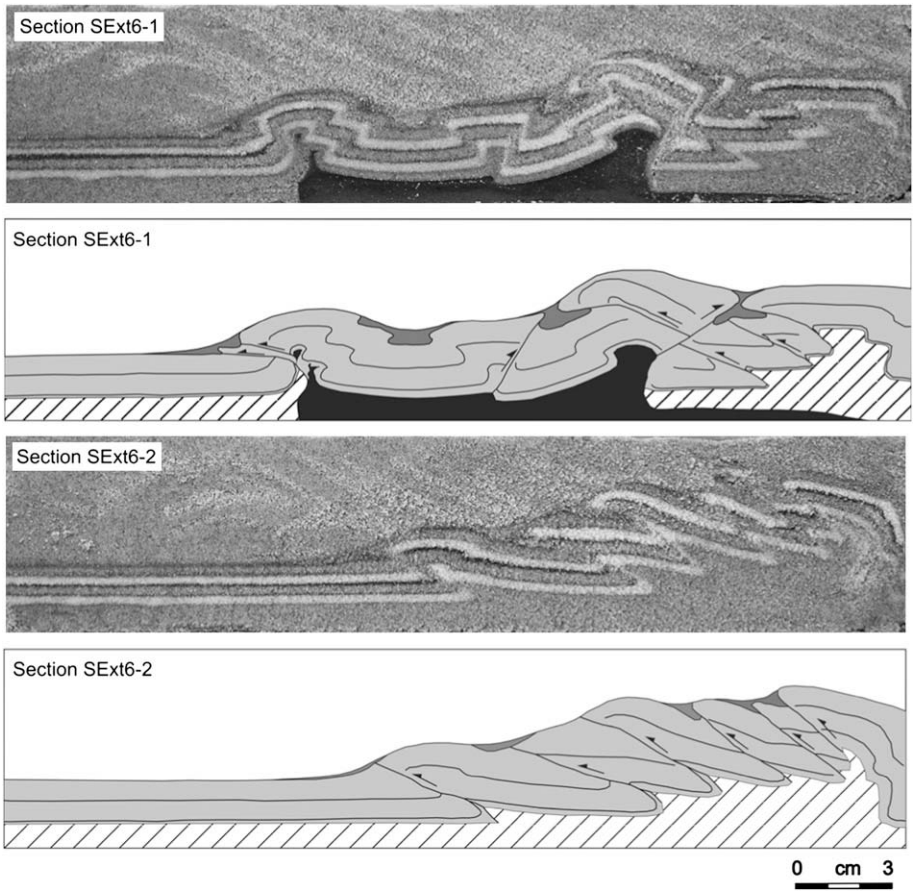

Fig. 8. Pictures and line-drawings of two representative cross-sections of model SExt6 (see Fig. 7a for location) showing the low friction domain (Section SExt6-1) and the high friction domain (Section SExt6-2). Black area represents the ductile layer (SGM-36) and dashed line areas represent the frictional décollement (pure loose sand). Notice how deformation front reaches further in SExt6-1 than in SExt6-2. In contrast, SExt6-2 shows a slightly additional uplift compared to SExt6-1. The structural pattern is also different: interference of fore-thrusts and back-thrusts in SExt6-1, and an imbricate foreland verging stack in SExt6-2.

Swantesson et al. (2006) and Nilforoushan et al. (2008). By using a laser scanner, lateral and vertical movements of the model surface were monitored during shortening. In such a way, model SExt10 was scanned at every 3–4% of bulk shortening, monitoring the differential advance of the deformation front and the surface topography. To avoid edge effects on the laser beam only the central portion of the model was scanned (Fig. 6).

3.2. Modelling strategy

Our intention by gluing sand onto the basal plate was to force high friction behaviour in the basement in order to accentuate the contrast between the ductile décollement (silicon layers) and the frictional décollement (sand). The aim of this irregularly distributed detachment level was to test how lateral contrasts in friction were able to cause the generation of arcuate, oblique and even transverse structures regardless of the orientation of the shortening.

The series of experiments aimed to test different parameters that have demonstrated to be decisive in the formation of shortening-parallel structures. In Series A, we explored the ratio between cover and detachment thicknesses as a parameter to control the generation of wavy structures. In Series B, the width of the high friction detachment areas was changed.

3.3. Limitations of the models

We have not investigated the effect of mechanical properties of the cover units; increasing competence of cover units is expected to have a similar effect as increasing the thickness of the cover units. In addition, the role of strain rate and its influence on the brittle-ductile coupling have not been investigated in our modelling, although this could be an important factor able to influence model deformation. Folds developed above very weak décollements (i.e., with low viscosity and deformed at low strain rates) are expected to become comparatively more amplified (and localise more deformation) than in case of stronger décollements (Bonini, 2003). From this point of view, one may thus speculate that, by producing more amplified folds, weak décollements may reduce the variations in topographic altitudes between HF and LF compartments, whereas strong décollements would tend to amplify such differences. In this work, the effect of syntectonic sedimentation was not studied either.

Finally, these models have been designed with a regular distribution of the detachment materials: three rectangular ductile layers separated by two rectangular sand layers. Although this regularity is necessary to understand the role of each parameter investigated, the distribution of the detachment materials in nature must be more complicated and irregular, creating a wide variety of particular structures and styles.

4. Model kinematics and results

Shortening of the models caused deformation in both the sand and the silicone layers. The deformation pattern was different between areas detached on the high frictional level and those detached on the ductile level. The results presented hereby are

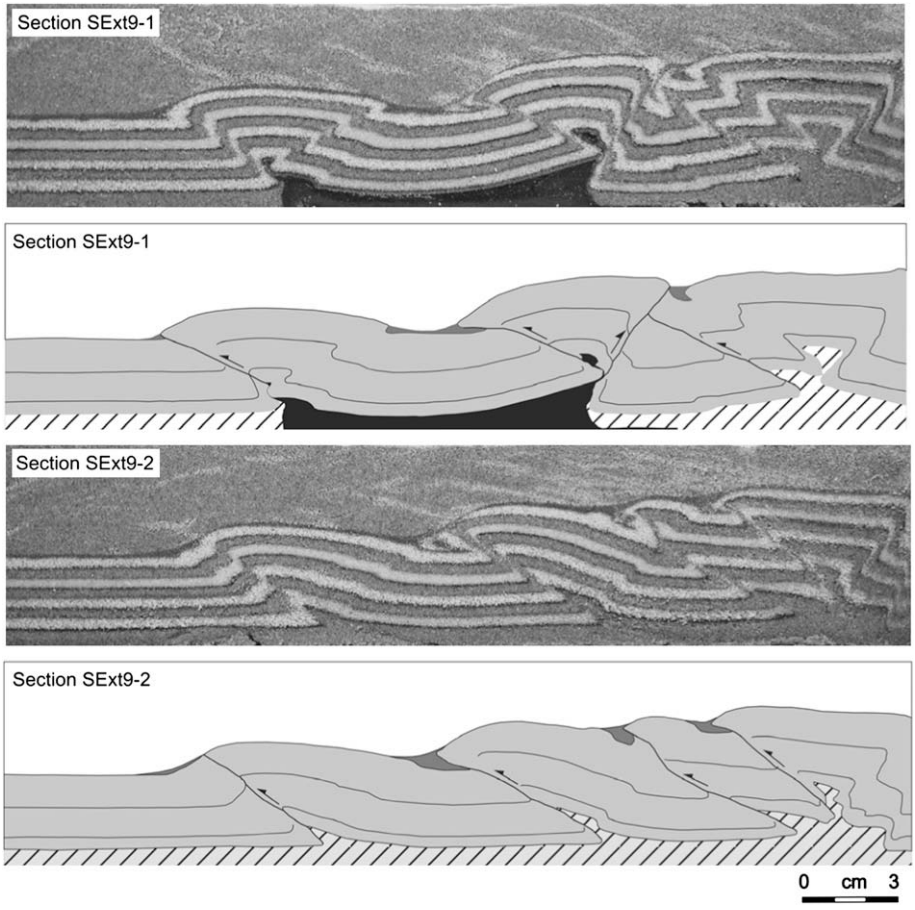

Fig. 9. Pictures and line-drawings of two representative cross-sections of model SExt9 (see Fig. 7b for location) showing the low friction domain (Section SExt9-1) and the high friction domain (Section SExt9-2). Symbols and abbreviations are as those in Fig. 8. Although no steep changes were found in top view between the frictional and the ductile domain, the structural pattern is noticeably different in both sections: interference of forward and backward thrusts in SExt9-1, and an imbricate foreland verging stack in SExt9-2.

shown by following an order according to the explored parameter. In such a way, the resulting experiments are classified in Series A and Series B since they are evaluating cover/detachment thickness ratio and distance between ductile layers (i.e. width of high friction areas), respectively.

4.1. Model Series A

Three experiments have been conducted to evaluate the role of the thickness ratio between the cover and the detachment. To do so, a constant detachment thickness of 0.7 cm was kept in different models, whereas cover thickness was changed (Fig. 5): 2 cm in model SExt6, 3 cm in model SExt9, and 4 cm in model SExt8. Transverse structures have been obtained only in model SExt6, while the other two models showed only slightly wavy structures (SExt9) or even a general straight structural style (SExt8) (Fig. 7). Despite this, both models SExt6 and SExt9 show a steep contrast in structural style between areas detached on ductile layers and areas detached on sand (Cotton and Koyi, 2000). The areas detached on frictional décollement (high friction areas = HF areas) are characterised by a forward directed imbricate stack developed by a piggyback thrusting sequence (Cotton and Koyi, 2000; Costa and Vendeville, 2002; Luján et al., 2003) (Figs. 8 and 9). On the other hand, areas detached on ductile décollement (low friction areas = LF areas) are characterised by the development of both forward and backward thrusts. Nevertheless, model SExt8 shows a homogeneous straight structural pattern that does not change across the model, regardless of the basal detachment changes. In this model, the structural style is characterised by a set of foreland verging, widely-spaced thrusts (Fig. 10). In this particular case, the forward edge of the silicon patches (pinch-out) has acted as a buttress to nucleate the development of the frontal thrust all across the model.

The transverse anticlines generate above the high friction areas where the hanging-wall shows the least advance, accommodating the deformation by uplift in comparison to the neighbouring LF areas, where deformation front advances further forwards. Topographic evolution above the LF and HF areas differs significantly (Fig. 11). Reference points located above the high friction décollement reach a higher altitude than the points located above the ductile décollements. In model SExt6, this differential topographic uplift occurs after 15% shortening, whereas in model SExt9 it occurs after 13% shortening. Despite this, the contrast in uplift between high friction and ductile areas is clearly less in model SExt9. In model SExt6, the altitude increases by 9% above the frictional décollement relative to the ductile décollement. In models SExt8 and SExt9, the difference in elevation is around 6%. In models SExt6 and SExt9, deformation front above LF areas reached further than above HF areas. However, thickness of the cover units influences this differential propagation, which is larger in model SExt6, where cover units are thinner, than in SExt9, where cover units are thicker (Figs. 7a,b). However, in model SExt8, propagation of the deformation front above the frictional and ductile décollements is entirely different compared to the other two models (models SExt6 and SExt9). At early stages of shortening, the advance of the deformation front and the increase of the altitude follow a progressive, continuous, sub-parallel path in HF and LF areas, with

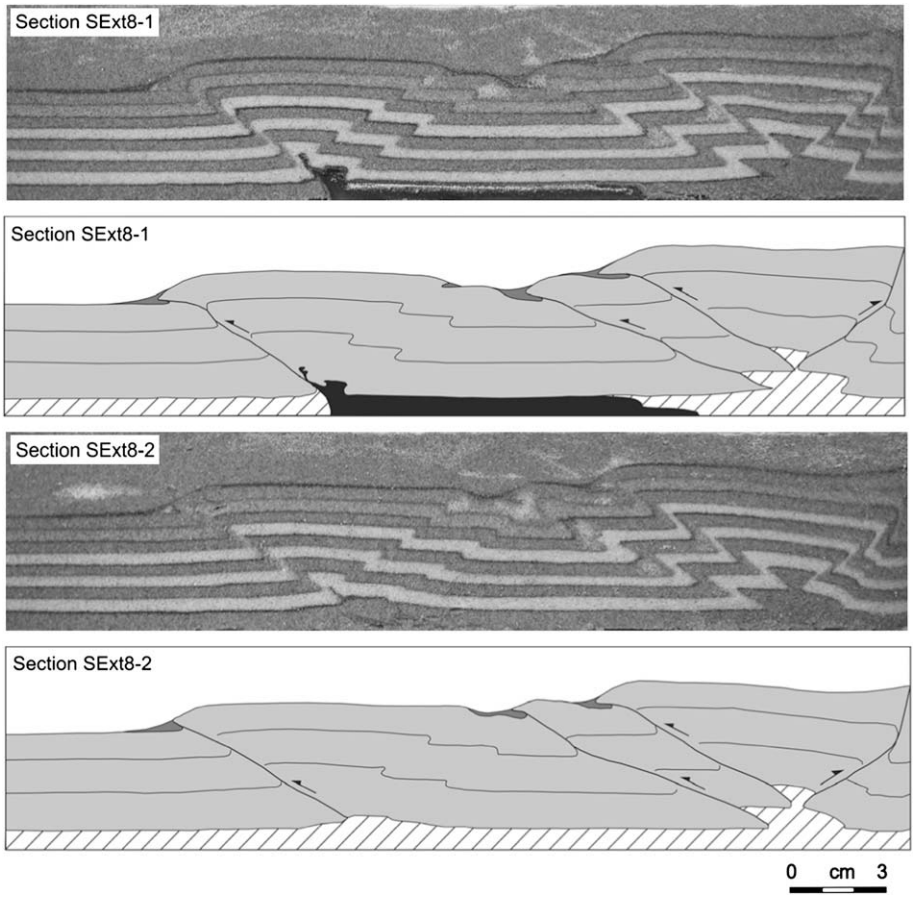

Fig. 10. Pictures and line-drawings of two representative cross-sections of model SExt8 (see Fig. 7c for location) showing the low friction (Section SExt8-1) and the high friction domains (Section SExt8-2). Symbols and abbreviations are as those in Fig. 8. Since the overburden unit is thicker than in other models (3.3 cm), the structural style does not change across the model, which is characterised by predominant foreland verging thrusts with associated smaller backward structures developed in the back limbs.

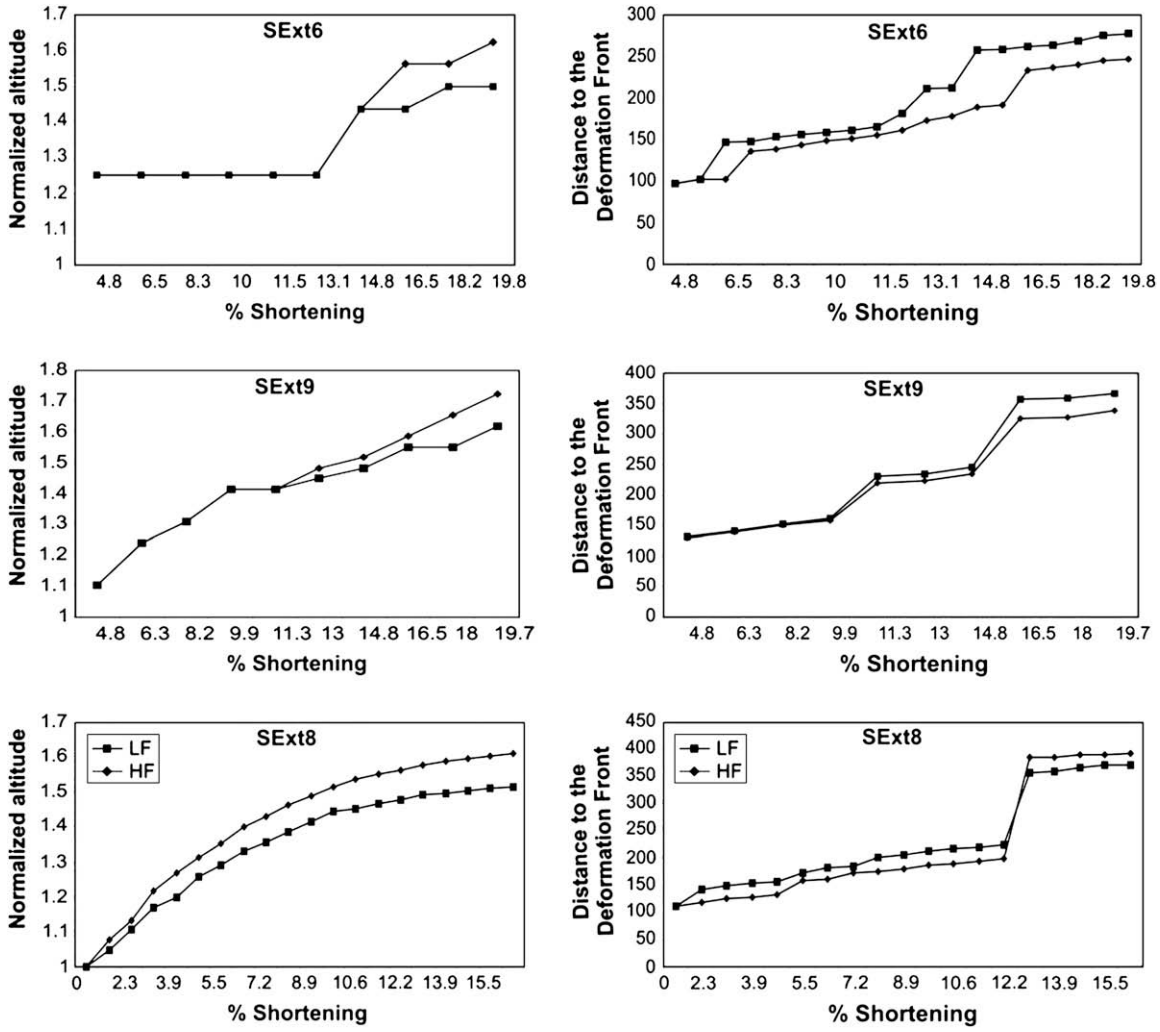

Fig. 11. For each experiment, left plots show the variation of the normalised altitude of the model at two control points plotted against percentage of shortening, whereas right plots show distance to deformation front plotted against percentage of shortening. Control points were placed on the surface of the model; one on HF areas and one on LF areas, before shortening to track the displacement/altitude variation. These plots show the evolution of the different domains of each model. SExt6 and SExt9 show the expected response of the overburden to an irregularly distributed décollement: higher advance of LF areas and higher uplift of HF areas. However, SExt8 shows a larger uplift and a larger advance of HF areas. Consequently, SExt8 behaviour is considered to be independent of the detachment distribution due to the larger thickness of the overburden.

LF areas reaching slightly further than HF ones. Nevertheless, after 12.2% of shortening, the last frontal thrust is created, and causes a slight extra advance of HF areas with respect to LF areas. However, this shift is considered to be negligible and the frontal thrust is interpreted as a nearly straight structure, formed regardless the mechanical contrasts in the basal décollement.

4.2. Model Series B

The width of HF areas has been explored in this series of experiments to test its effect on the generation of oblique/transverse structures. For a given stratigraphic thickness, two different HF widths have been considered. Model SExt9, described previously, had a HF area width of 3 cm and a LF area width of 13 cm, whereas model SExt10 had a HF area width of 6 cm (twice as that in model SExt9) and a LF area width of 11 cm (Fig. 12). During shortening, transverse structures formed only in model SExt10, while model SExt9 showed just slightly wavy structures at the deformation front. As model SExt9 has been described earlier, descriptions will mainly refer to model SExt10, whose top-view was monitored with a high-resolution scanner.

Using the data from the laser-scanner, topographic evolution of the model in 3D was monitored (Fig. 13) and topographic profiles were generated which were compared between different areas of the model (Fig. 14).

Deformation in model SExt10 started with formation of three straight forward directed thrusts, formed in the rear part of the model in a piggy-back style after 6% bulk shortening (Fig. 13b). After 9% bulk shortening, deformation reached the ductile layers, when a clear differential advance of the deformation front was noticed between areas detached on the ductile layers and areas detached on sand; deformation front propagated further above the DD (Figs. 13c and 14). With further shortening, model top view shows that deformation front above HF areas does not advance as far as it does above LF areas (Fig. 15). This creates a structural pattern constituted by wavy thrusts (along strike) that transport further the areas detached on a ductile layer than the areas detached on sand (Cotton and Koyi, 2000; Bahroudi and Koyi, 2003). As a consequence, areas detached on sand accommodate the deformation by an additional uplift with regard to areas detached on a ductile layer, developing gentle transverse anticlines in the hanging-wall of the thrusts (Figs. 14C–C′). After 16% of bulk shortening, existing structures are not

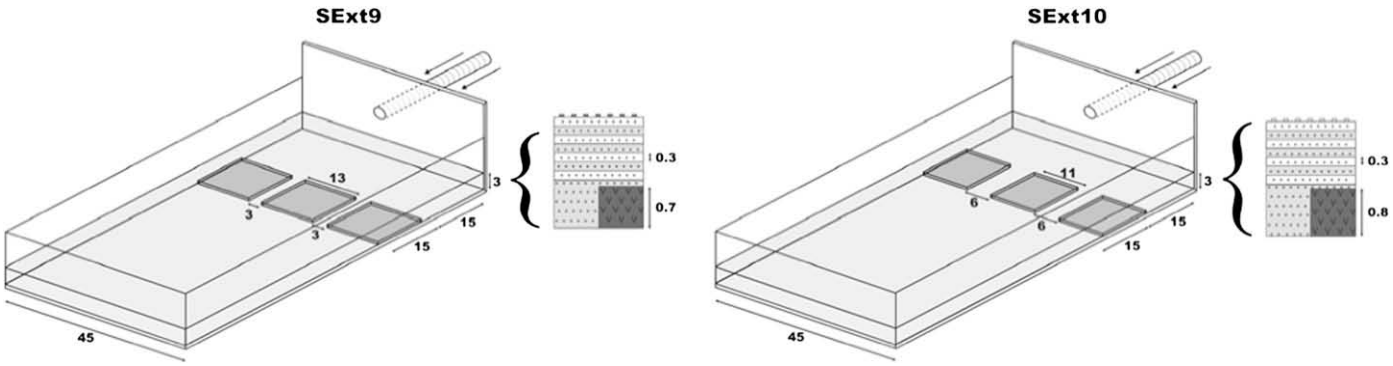

Fig. 12. Initial setup of model Series B showing the distribution of ductile (SGM-36) and brittle (sand) décollements and the shortening orientation. The stratigraphic sequence of each model is presented aside. All the values are in cm.

able to accommodate more deformation and new structures form causing the deformation front to migrate towards the foreland (Fig. 13e). At this stage, a second generation of transverse structures is formed in continuation with the previous ones. After 20% bulk shortening (Figs. 13f and 15), the geometry of the deformation front is similar to that observed in the previous generation of transverse structures (formed after 9% bulk shortening). Nevertheless, the location of the thrust front in the LF areas coincides with the frontal pinch-out of the basal ductile layers (Fig. 16). This indicates that the last generation of structures has been forced to form above the pinch-out of the ductile layers, as a consequence of the mechanical contrast between silicone and sand.

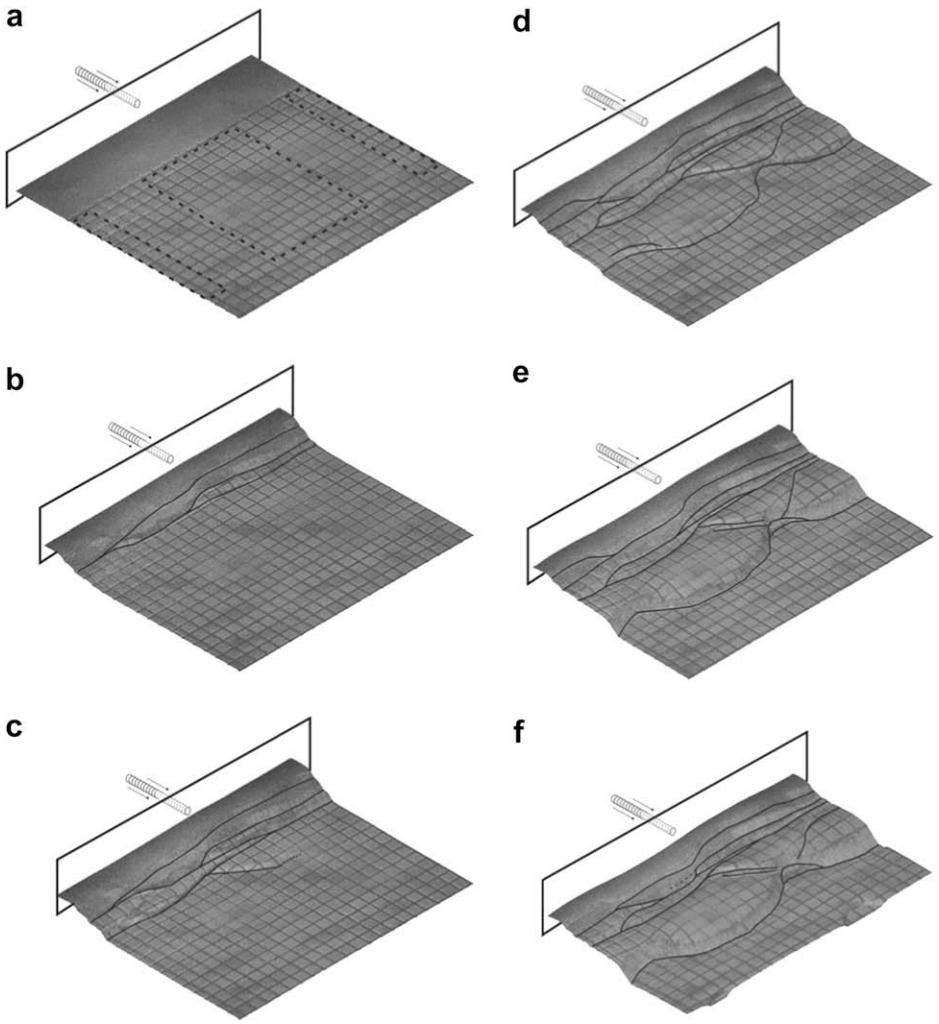

Fig. 13. 3D views of the model topography generated from laser scan data with the main thrusts mapped onto it, at different stages of deformation: (a) initial setup (dashed rectangles indicate the initial position of the ductile layers in the basal décollement); (b) 3% of shortening; (c) 6% of shortening; (d) 10% of shortening; (e) 16% of shortening; and (f) and 20% of shortening. This allows controlling the three-dimensional variation of topography depending on which type of décollement is located beneath.

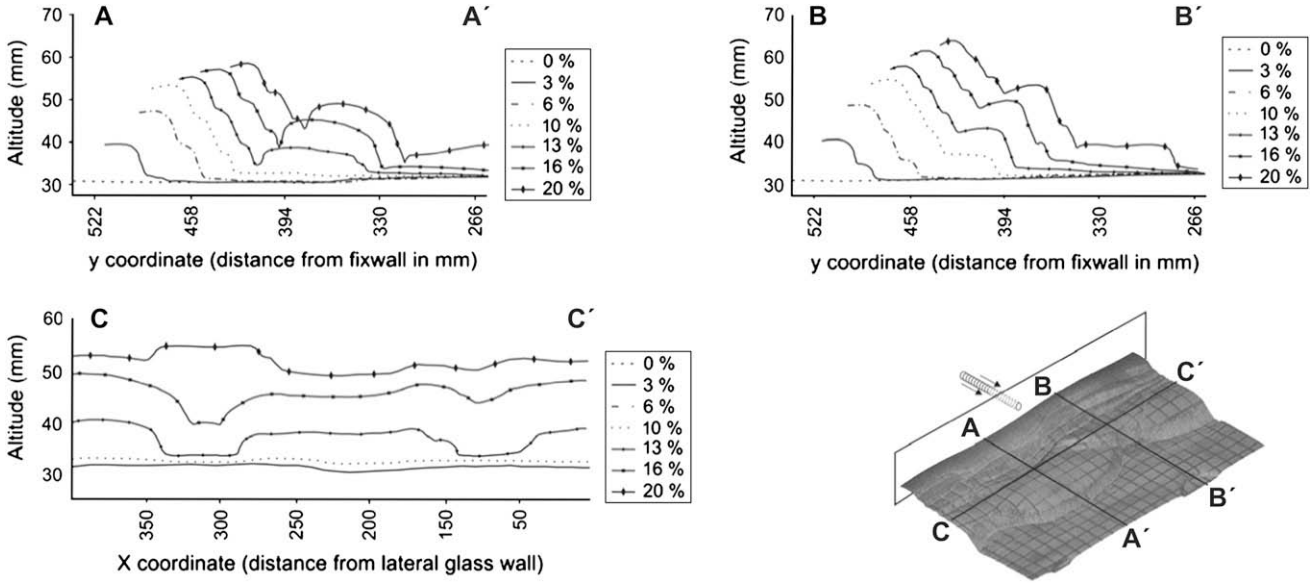

Fig. 14. Topographic variation of the models along three profiles. Vertical scale exaggerated. A–A′: profile located along LF décollement. B–B′: profile located along HF décollement. C–C′: profile located across the model, involving both LF and HF décollements. Comparison of A–A′ and B–B′ points out the different evolution of the cover along the different décollements. C–C′ profile shows how HF areas were initially depressed since deformation front arrives later than in LF areas (curves at 0%, 3% and 6% are overlapped since deformation front reaches C–C′ after 6% bulk shortening). In other words, LF areas were firstly but less uplifted. However, when deformation front reaches the profile location at the HF domain, it becomes uplifted since higher friction causes a different accommodation of shortening.

For model SExt10, three different types of sections have been taken: (1) vertical sections parallel to the shortening direction; (2) vertical sections perpendicular to the shortening direction; and (3) horizontal sections (Figs. 16 and 17). The structural style along shortening direction is similar to the one reported for model SExt6 (Fig. 16). A set of foreland verging thrusts and some associated minor back-thrusts are the common features. In sections perpendicular to shortening direction, higher uplift of HF with regard to LF areas (Figs. 17a,b) is observed. The horizontal section shows depth variation in the structural style and the change in the differential propagation of the thrusts with depth (Fig. 17c). In general, horizontal sections show the internal geometry of the layers with depth as well as the relation between orogen-parallel structures and the oblique/transverse ones.

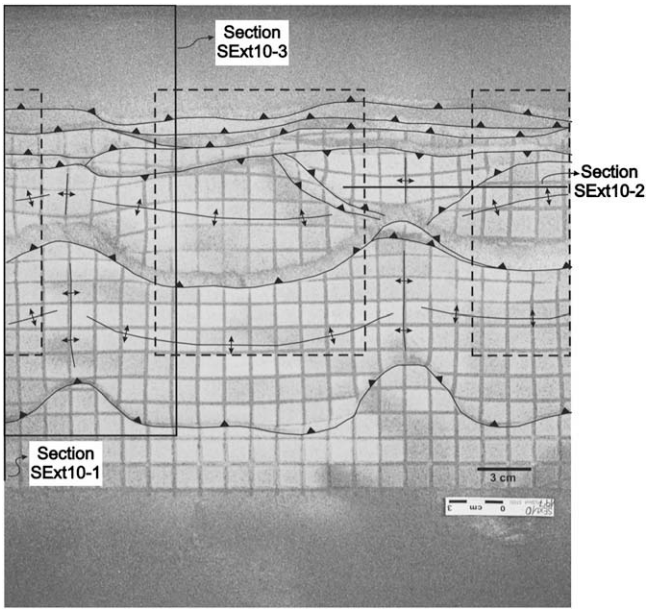

Fig. 15. Top view of the model SExt10 after 20% of shortening. Three types of sections have been taken for this model: parallel-to-shortening (Section SExt10-1, Fig. 16), perpendicular-to shortening (Section SExt10-2, Figs. 17a,b) and horizontal sections (Section SExt10-3; Fig. 17c). Dashed rectangles indicate the initial position of the ductile layers in the basal décollement. As in model SExt6, both orogen-parallel structures (LF areas) and transverse structures (HF areas) have been obtained in the hanging-wall of the thrusts.

Development of oblique and transverse structures shown in model SExt10 is a consequence of the mechanical contrast between HF and LF areas. In such a way, the deformation of ductile layers by flow, ductile thickening and folding is laterally transferred to HF areas, where lateral thrust ramps climb up section from the ductile layers at their lateral pinch-outs. These lateral ramps merge in the core of the HF areas, uplifting and gently deforming the units above, and highly faulting the units below (Figs. 17a,b). This results in a lateral migration of ductile layers towards HF areas and the thickening along the HF/LF boundary where the lateral ramps detach (Figs. 17a,b). In horizontal sections, where the internal geometry of the layers is shown at depth, the layers show general foreland verging thrusts in which lower units are thrusted and upper units are gently folded. Only a periclinal closure is observed in the orogen-side of the transverse structures (Fig. 17c). This indicates that these structures slightly plunge towards the orogen ought to the tilting created by the emplacement of the frontal foreland verging thrust.

5. Discussion

The main aim of this work is to understand the oblique and transverse structures in the Central External Sierras. Here, a new idea is proposed based on the influence of the irregularity of the detachment level without invoking either longitudinal E–W contraction or significant rotations along a vertical axis (which would only accommodate only maximum 40° of clockwise rotation of the structure; Pueyo et al., 2002).

The intention of this paper is naturally not to "replace" the hypothesis of the vertical axis rotation in External Sierras, which is documented in the field. The aim of this study is to give a viable

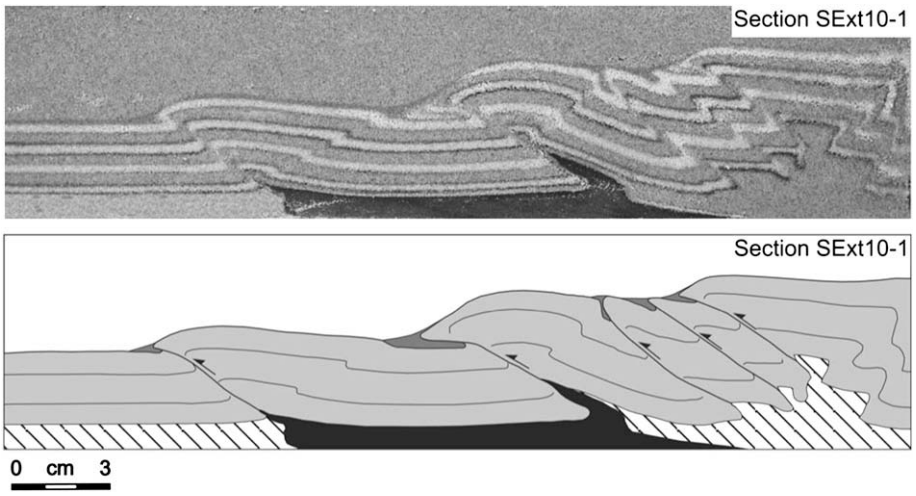

Fig. 16. Pictures and line-drawings of a parallel-to-shortening section of model SExt10 (see Fig. 15 for location) showing the low friction domain. Black area represents the ductile layer (SGM-36). In this case, the structural style is characterised by predominant foreland-verging thrusts with associated small backward structures developed in the back limbs.

explanation for this rotation and complement the knowledge of the structural evolution of CES with new insights about how to generate oblique and perpendicular structures. According to the paleomagnetic data, a clockwise rotation of up to 40° took place in the Pico del Águila anticline. In fact, the rotation documented in the field is also visible in the models presented in this study (Fig. 18) and we argue that no additional mechanism is needed to accommodate the rotation. In the models, at the boundary zones between the ductile and frictional décollements, the passive grid markers (placed at the surface of he models before shortening) locally show a rotation of up to *ca.* 30° from their initial position during the differential propagation of the deformation front. In other words, the rotation in the overburden units is a direct response to the differential propagation; further propagation of the deformation front above the ductile décollement and its retard above the high friction décollement lead to rotation of the markers/layers locally. Model results show that the rotation is bimodal (clockwise on one limb of the anticline and anti-clockwise on the other).

Until now, no viable explanation satisfying the relatively well-known geology of the area and the field observations has been proposed to explain the formation of these structures at such a high angle. In this contribution, we are demonstrating that it is possible to generate structures at high angle and even perpendicular to shortening direction with a single event of shortening. It is argued here that generation of the N–S trending structures of CES is likely to be the result of differential propagation of the deformation front above mechanical contrasts in the basal décollement (generation of structures at very high angle). With progressive shortening, this differential propagation also must have lead to rotation of the high-angle-trending structures at the boundary areas between the low and high friction décollements.

Based on field evidences about the distribution of the Triassic detachment, models were prepared to study the effect of changes in the mechanical behaviour of basal detachment on the generation of these oblique and transverse structures. In addition, the main outcropping rocks in the core of N–S trending structures are competent Upper Muschelkalk limestones and dolomites (M3 facies; Middle Triassic). Consequently, it is interpreted here that transverse anticlines are less likely to have been detached on less competent Upper Triassic rocks. The combination of these factors led us to think about a different distribution of deformation due to

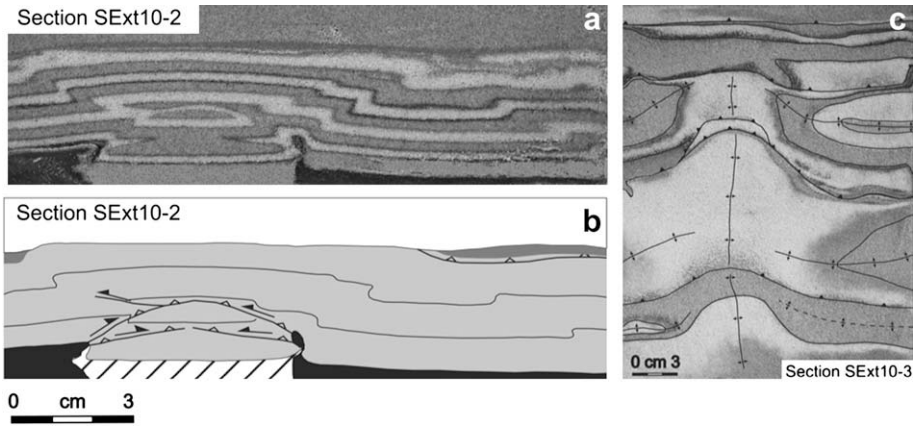

Fig. 17. Pictures and line-drawings of perpendicular-to-shortening and horizontal sections of model SExt10 (see Fig. 15 for location). Section SExt10-2 clearly shows the additional uplift of HF areas with regard to LF areas. In addition, deformation is assimilated by high faulting in the lower units and by gentle folding and small oblique reverse faults in the upper units (the small faults caused for the pure brittle behaviour of loose dry sand). Notice the thickening of ductile layers towards HF areas, and how lateral ramps detach on LF/HF limits and merge in the core of the structure, uplifting the upper units. Section SExt10-3 shows the interference structural pattern between orogen-parallel and transverse structures. This provides valuable information since allows to observe how units modify their geometry when changing the behaviour of the basal décollement.

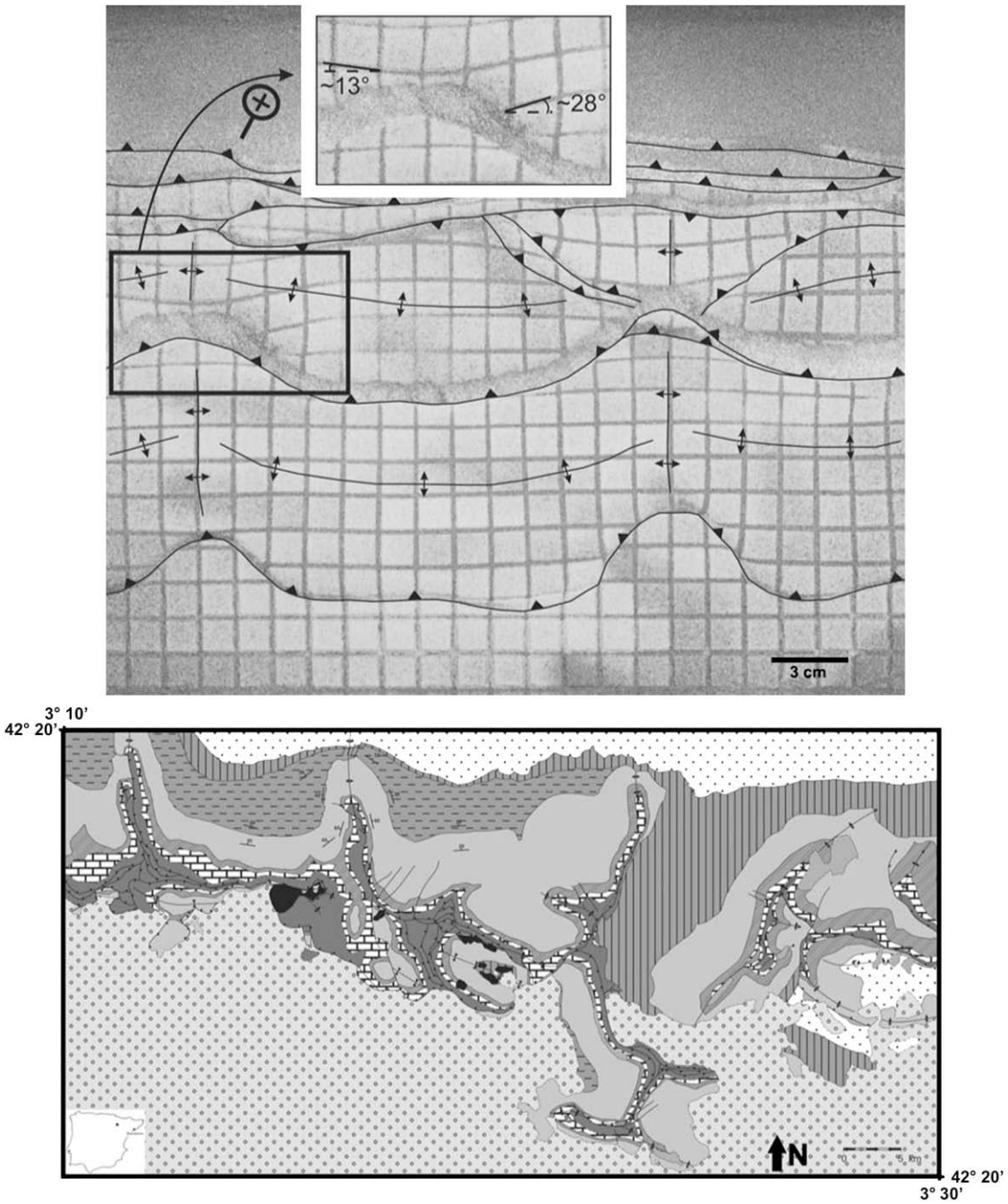

Fig. 18. Comparison between the last stage of model SExt10 in top view and the geological map of Central External Sierras (modified from IGME, 1992). Notice the geometrical similarities between both pictures: larger advance of areas performing orogen-parallel structures (LF areas in the model), and generation of transverse N–S anticlines, internally thrusted (HF areas in the model). The enlarged view shows the vertical axis rotation of the grid markers in the HF areas.

an uneven distribution of the basal detachment level in this part of the External Sierras.

After exploring two different parameters systematically, models have reproduced the general structural style of the area. Geometrical similarities between the mapped structures and models can be observed at regional scale in Fig. 18 and at single-structure scale in Fig. 19. Model results show that formation of oblique and orogen-perpendicular structures depends on the cover/detachment thickness ratio and the width of high friction detachment areas between the ductile décollements. Since the sedimentary cover is partially detached on a frictional material and partially detached on a ductile material, forming arcuate, oblique and transverse structures is only a matter of differential advance of the deformation front, which depends on the initial geometry and distribution of the ductile detachment.

In model Series A, we tested the thickness ratio between cover and detachment as a possible factor controlling the generation of orogen-perpendicular structures. For a given constant width of the HF areas (i.e. the distance between the ductile layers; 3 cm in Series A models), the different behaviour of the experiments depends on the sand cover thickness. This led us to consider the thickness ratio between cover and décollement layers as a parameter controlling the generation of oblique/transverse structures. In other words, there is a minimum value of cover thickness from which HF areas

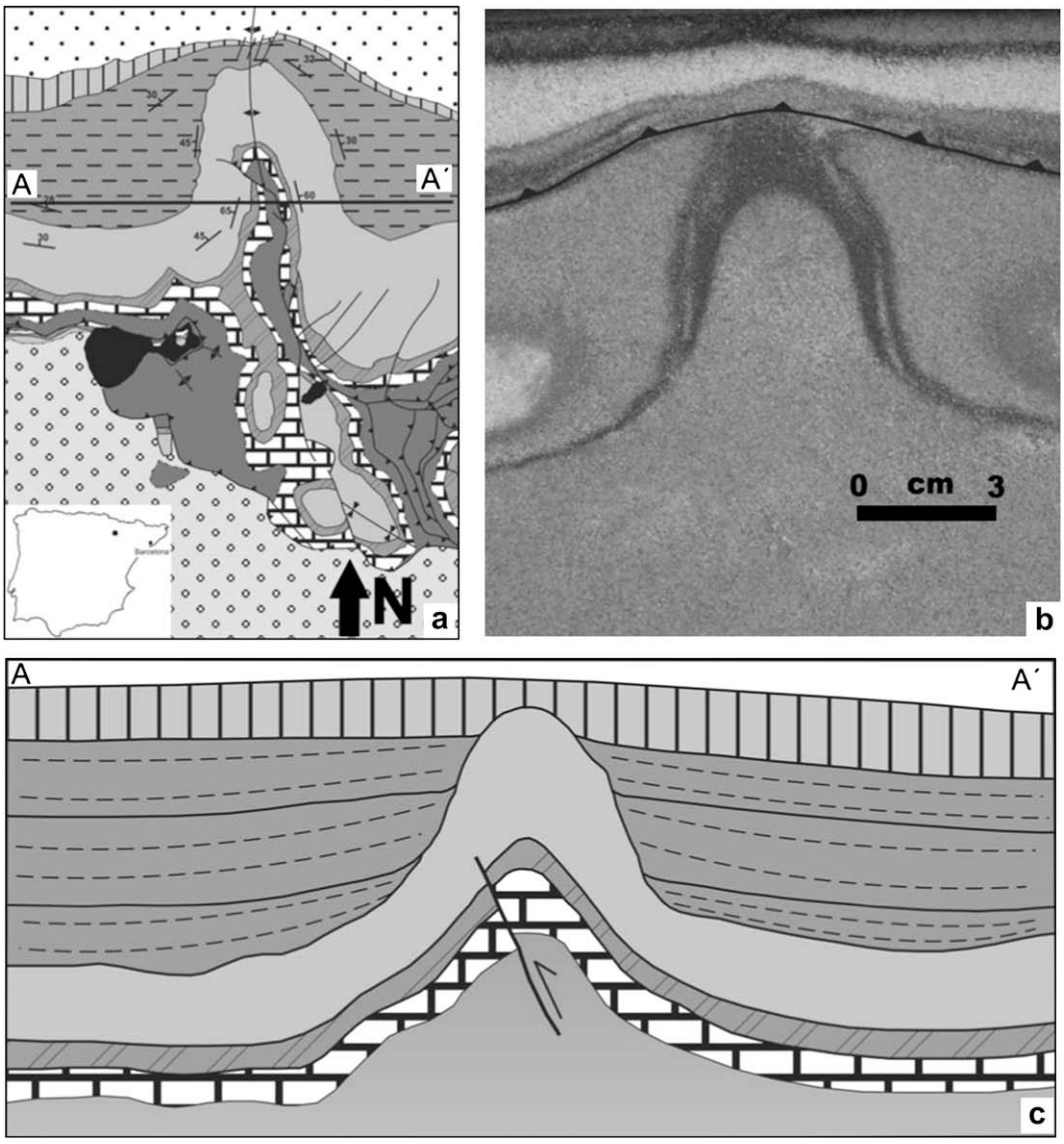

Fig. 19. Comparison between Pico del Águila geological map (modified from IGME, 1992) (a), a detailed horizontal section taken from the model (b), and a schematic cross-section generated from the 3D reconstruction of the Pico del Águila anticline (c; see Fig. 4). In (a) and (b) shortening comes from the top of the picture (~transport direction towards the south). Despite the geometrical similarities, notice that in (a) the thickness decrease of the units adjacent to the anticline is due to a thinning of the syntectonic growth strata towards the crest, whereas in (b) there is no thickness decrease but the emplacement of a thrust affecting the entire sequence (in this work no syntectonic sedimentation was added at any model during shortening).

become too narrow to affect the geometry of the structures while they advance. Decreasing the ratio of cover/décollement layer thicknesses results in formation of oblique structures, which may become transverse as cover thickness decreases further.

Since we are focusing on the most external unit of the orogen (South-Pyrenean thrust front at the southern limit of the Jaca Eocene piggy-back basin), the pre-kinematic stratigraphic sequence of the area is one of the thinnest (around 1100 m in Pico del Águila area) with regard to other Pyrenean structural units. In this area, only a thin sequence of Triassic units is preserved (outcropping around 300 m thick), and neither Jurassic nor Lower Cretaceous units are present. A thin sequence of Santonian–Maastrichtian rocks (around 150 m thick) is found in the area. Above this, units of the Cretaceous/Tertiary transition (Garumnian facies) are *ca.* 100 m thick, covered by 475–1000 m of Lutetian limestones (Guara Fm) that thin westward (Millán, 1995). In total, the pre-kinematic cover sequence ranges between 750 and 1250 m, whereas the Triassic detachment is considered to be approximately 300 m thick. Consequently, the thickness ratio between cover and detachment ranges from 2.5 (Eastern Central External Sierras) to 4.1 (Western Central External Sierras). In the models, the ratios considered have been 1.86 for SExt6, 3.83 for SExt9, 4.71 for SExt8 and 2.75 for SExt10. As mentioned earlier, oblique and transverse structures have formed only in models SExt6 and SExt10 where the thickness ratio is below the range observed in the field. For ratio values above 4.1 (SExt8) a homogeneous orogen-parallel structural pattern is observed and no clear oblique-transverse structures have been obtained. For ratios close to the upper limit (SExt9), the structural style changes between HF and LF areas but only slight wavy structures have been obtained (Figs. 7b and 9).

Width of the HF area between two ductile layers has also a significant influence on the formation of oblique and orogen-perpendicular structures. This is clearly shown when comparing top views of models SExt6 and SExt10 after 20% of shortening (Figs. 7a and 15). Due to the larger cover thickness in model SExt10, structures are bigger than in model SExt6. In nature, transverse anticlines of Central

External Sierras become shorter towards the West (Puigdefàbregas, 1975; Millán et al., 1994; Millán, 1995), and thickness of Guara Fm. ranges from 1000 m in Nasarre and Balces anticlines (Eastern Central External Sierras) down to 475 m in Bentué de Rasal and Pico del Águila anticlines (Western Central External Sierras). The combination of these facts led us to consider that the decrease in size of these anticlines towards the west is a consequence of the thickness decrease of Guara Fm. In such a way, cover thickness influences not only the formation but also the size of the oblique and transverse structures. In addition, the decrease of thickness of the cover influences in the relative strength between the brittle and the ductile layer, conditioning the geometry and size of the structures (Smit et al., 2003).

Model results show that there is a minimum HF width for a given cover thickness beyond which oblique and transverse structures do not form. Below this value, HF areas become too narrow and orogen-parallel thrusts advance forward regardless of the mechanical contrast in the basal level. For wider HF areas, the geometry of the structures becomes gentler and more open and their wavelength increases. In such a way, narrow HF areas produce tighter folds. This observation from the models is important to understand the different geometry between the orogen-perpendicular anticlines of Central External Sierras. Pico del Águila anticline in the west is a tight, nearly isoclinal fold (Millán, 1995) whereas Gabardiella anticline complex shows a gentler, more open geometry, with a larger wavelength (Fig. 1). In such a way, the superficial geometry of the folds can provide an idea about the approximate distribution of the detachment level in depth and/or the thickness ratio between the cover and ductile units.

Both studied parameters (i.e. cover/detachment thickness ratio and width of HF areas) can be considered together by plotting them in a unique graph (Fig. 20). If we divide the thickness ratio (parameter A) by the width of HF areas (parameter B), we obtain the ratio *k*. This new parameter gives an idea of the suitable proportions within which oblique and transverse structures may develop. According to model results, orogen-oblique and orogen-transverse structures may form for $k < 1$ (models SExt6 and SExt10), whereas for $k > 1$ only orogen-parallel structures are obtained (models SExt8 and SExt9) (Table 2). Therefore, oblique and transverse structures may develop if the width of the HF areas is larger than a well-suited ratio between cover and décollement thicknesses.

Transverse and oblique anticlines of Central External Sierras display the highest structural relief of the area, reaching the highest topographic altitudes and creating the main mountain chains in the region. Model results reproduced this behaviour above the HF areas where a significant amount of uplift takes place relative to the LF areas (Figs. 14 and 17a,b).

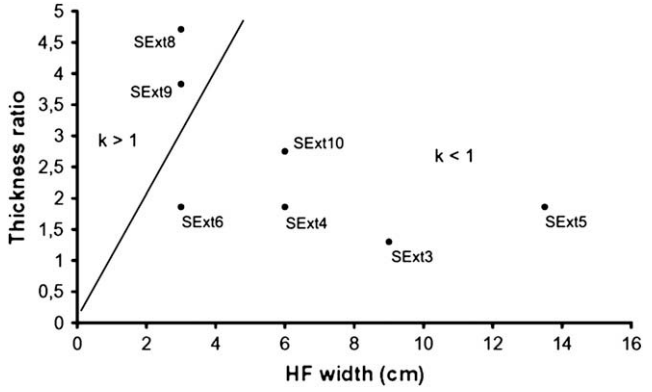

Fig. 20. Plot of the cover/detachment thickness ratio against width of HF areas. The parameter k indicates the ratio between thickness ratio and HF width. Oblique and transverse structures may form if HF width is larger than the thickness ratio ($k < 1$).

Table 2
Cover/décollement thickness ratio, width of HF areas and *k* value of each model.

Model	Thickness ratio	HF width	*k* value[a]	Transverse structures obtained?
SExt6	1.86	3	0.62	Yes
SExt8	4.71	3	1.57	No
SExt9	3.83	3	1.1	No
SExt10	2.75	6	0.46	Yes
SExt3[b]	1.3	9	0.14	Yes
SExt4[b]	1.86	6	0.31	Yes
SExt5[b]	1.86	13.5	0.14	Yes

[a] *k* is equal to the thickness ratio divided by the width of the HF areas.
[b] Models SExt3, SExt4 and SExt5 were also performed in the same series of experiments, although not discussed in this study.

The use of loose sand and silicone in analogue modelling presents some limitations when reproducing certain case-studies (for a detailed description of materials, properties and their suitability as analogues see Weijermars, 1986; and Weijermars and Schmeling, 1986). As stated, models have reproduced the differential uplift of HF areas by means of gentle anticlines in the upper units, usually showing open limbs uplifted by two lateral ramps that merge in the core of the structure. In other cases, this extra uplift of the upper units is solved via some local oblique small-throw reverse faults. However, transverse anticlines of Central External Sierras perform steep dipping, in some cases overturned limbs, and a higher plunge value towards the hinterland. Due to the mechanical behaviour of loose cohesionless sand, it becomes easily faulted when a minimum amount of deformation is applied. Consequently, it is not possible to reproduce such geometry observed in nature by using loose sand to model the entire sedimentary cover. The stratigraphy of the area is more complex in terms of mechanical behaviour, exhibiting an interlayering of brittle-plastic materials that allow the generation of steep dipping folds. Despite this, if a sand–silicone multilayering was used to model the sedimentary cover, and syn-kinematic sedimentation was added, higher dip values of a gravitationally stable pre-kinematic sequence could be achieved (Nalpas et al., 1999, 2003). In this sense, improving the mechanical stratigraphy by using multiple décollements as secondary detachment levels (Nalpas et al., 1999; Massoli et al., 2006) would help in the construction of higher steeper structures.

6. Conclusions

Model results provide new insights on the evolution of the oblique and transverse structures of the Central External Sierras. Based on the uneven distribution of the Triassic detachment level, models simulate the characteristics of the N–S trending anticlines of Central External Sierras: generation synchronous with the emplacement of the South-Pyrenean frontal thrust, higher structural relief compared to orogen-parallel structures, absence of a representative ductile décollement in the core, faulting of lower units and folding of upper ones, plunge towards the hinterland, and foreland-side closure not thrusted by the frontal emerging South-Pyrenean thrust. The generation of the N–S structures of CES (at high angle to the shortening direction) and the rotation documented in the field are illustrated to be due to differential propagation of the deformation front above mechanical contrasts in the basal décollement.

Acknowledgements

We would like to thank Alejandro Amilibia and Ruth Soto for their brilliant ideas and suggestions. Paradigm™ is acknowledged

for providing a GoCad® Academic license. Authors also wish to thank the Group of Geodynamics and Basin Analysis (GGAC) at Universitat de Barcelona. This research has been supported by StatoilHydro, the Geomod 3D project (CGL2004-05816-C02-01/BTE), the MODES-4D project (CGL2007-66431-C02-01/BTE) and the Geomodels Institute Consortium. O. Vidal-Royo wish to thank Agència de Gestió d'Ajuts Universitaris i a la Recerca (AGAUR) for providing a PhD grant (2005 FI 00200) and additional funds (2006 BE-2 00095) for a 3-month stay at Hans Ramberg Tectonic Laboratory of Uppsala University. H.A. Koyi is funded by the Swedish Research Council (VR). Authors are grateful to Dr. M. Bonini for a thorough and constructive review, which improved both the content and presentation of the manuscript. An anonymous reviewer is also acknowledged for comments and suggestions.

References

Almela, A., Ríos, J.M., 1951. Mapa geológico de España 1:50000 serie Antigua, 248 (Apiés). IGME Ed.Madrid, 50 pp + map.

Anastasio, D.J., 1992. Structural evolution of the External Sierras, Southern Pyrenees, Spain. In: Mitra, S., Fisher, G.W. (Eds.), Structural Geology of Fold and Thrust Belts. Johns Hopkins University Press, Baltimore, pp. 239–251.

Anastasio, D.J., Holl, J.E., 2001. Transverse fold evolution in the External Sierras, Southern Pyrenees, Spain. Journal of Structural Geology 23 (2–3), 379–392.

Bahroudi, A., Koyi, H.A., 2003. Effect of spatial distribution of Hormuz salt on deformation style in the Zagros fold and thrust belt: an analogue modeling approach. Journal of the Geological Society 160, 719–733.

Beaumont, C., Muñoz, J.A., Hamilton, J., Fullsack, P., 2000. Factors controlling the Alpine evolution of the central Pyrenees inferred from a comparison of observations and geodynamical models. Journal of Geophysical Research 105, 8121–8145.

Bentham, P., Burbank, D.W., 1996. Chronology of Eocene foreland basin evolution along the western oblique margin of the South-Central Pyrenees. In: Friend, P.F., Dabrio, C.J. (Eds.), Tertiary Basins of Spain. Cambridge University Press, Cambridge, pp. 144–152.

Bonini, M., 2003. Detachment folding, fold amplification, and diapirism in thrust wedge experiments, Tectonics, 22(6), 1065, doi:10.1029/2002TC001458.

Bonini, M., 2007. Deformation patterns and structural vergence in brittle-ductile thrust wedges: an additional analogue modelling perspective. Journal of Structural Geology 29, 141–158.

Castillo-Herrador, F., 1974. Le Trias évaporitique des basins de la Vallée de l'Ebre et de Cuenca. Bulletin de la Societé Géologique de France 16, 49–63.

Cobbold, P.R., Rossello, E.A., Vendeville, B.C., 1989. Some experiments on interacting sedimentation and deformation above salt horizons. Bulletin de la Societé Géologique de France 8, 453–460.

Costa, E., Vendeville, B.C., 2002. Experimental insights on the geometry and kinematics of fold-and-thrust belt above weak, viscous evaporitic décollement. Journal of Structural Geology 24, 1729–1739.

Cotton, J.T., Koyi, H.A., 2000. Modelling of thrust fronts above ductile and frictional detachments: application to structures in the Salt Range and Potwar Plateau, Pakistan. Geological Society of America Bulletin 112, 351–363.

Crespo-Blanc, A., 2008. Recess drawn by the internal zone outer boundary and oblique structures in the paleomargin-derived units (Subbetic Domain, central Betics): an analogue modeling approach. Journal of Structural Geology 30, 65–80.

Davis, D.M., Engelder, T., 1985. The role of salt in fold-and-thrust belts. Tectonophysics 119, 67–88.

Dinarés, J., McClelland, E., Santanach, P., 1992. Contrasting rotations within thrust sheets and kinematics of thrust tectonics as derived from paleomagnetic data: an example from the Southern Pyrenees. In: McClay, K.R. (Ed.), Thrust Tectonics. Chapman & Hall, London, pp. 265–276.

Dooley, T.P., Jackson, M.P.A., Hudec, M.R., 2007. Initiation and growth of salt-based thrust belts on passive margins: results from physical models. Basin Research 19, 165–177.

Grelaud, S., Nalpas, T., Vergés, J., Karpuz, R., 2002. Role of décollement levels in thrust systems: field examples and analogue modelling. Bolletino di Geofisica teorica ed applicata, 42 N(½ Suppl.), 178–180.

Harrison, J.C., 1995. Tectonics and Kinematics of a foreland folded belt influenced by salt, Arctic Canada. In: Jackson, M.P.A., Roberts, D.G., Snelson, S. (Eds.), Salt Tectonics: A Global Perspective, vol. 65. AAPG Memoirs, pp. 379–412.

Hogan, P.J., Burbank, D.W., 1996. Evolution of the Jaca Piggyback basin and emergence of External Sierras, Southern Pyrenees. In: Friend, P.F., Dabrio, C.J. (Eds.), Tertiary Basins of Spain. Cambridge University Press, pp. 153–160.

Holl, J.E., Anastasio, D.J., 1993. Paleomagnetically derived folding rates, southern Pyrenees, Spain. Geology 21 (3), 271–274.

IGME, 1992. Mapa Geológico de España; Hoja 248, Apiés; Instituto Geológico y Minero de España, Madrid, Unpublished 36 pp report +1:50000 map.

Jurado, M.J., 1990. El Triásico y el Liásico basal evaporíticos del subsuelo de la cuenca del Ebro. In: Ortí, F., Salvany, J.M. (Eds.), Formaciones evaporíticas de la Cuenca del Ebro y cadenas periféricas, y de la zona de Levante. Enresa, Madrid, pp. 21–28.

Koyi, H.A., 1988. Experimental modeling of role of gravity and lateral shortening in Zagros mountain belt. AAPG Bulletin 72, 1381–1394.

Koyi, H.A., 1995. Mode of internal deformation in sand wedges. Journal of Structural Geology 17, 293–300.

Koyi, H.A., 1997. Analogue modelling: from a qualitative to a quantitative technique – a historical perspective. Journal of Petroleum Geology 20, 223–238.

Koyi, H.A., Vendeville, C.B., 2003. The effect of décollement dip on geometry and kinematics of model accretionary wedges. Journal of Structural Geology 25, 1445–1450.

Koyi, H.A., Cotton, J., 2004. Experimental insights on the geometry and kinematics of fold-and-thrust belts above weak, viscous evaporitic décollement; a discussion. Journal of Structural Geology 26, 2139–2141.

Koyi, H.A., Sans, M., 2006. Deformation transfer in viscous detachments: comparison of sandbox models to the South Pyrenean Triangle Zone. Geological Society, London, Special Publications, January 1, 2006; vol. 253(1), pp. 117-134.

Larrasoaña, J.C., Parés, J.M., Pueyo, E.L., 2001. Stable eocene magnetization carried by magnetite and iron sulphides in marine marls (Pamplona-Arguis Formation, Southern Pyrenees, Northern Spain). Studia Geophysica et Geodaetica 47 (2), 237–254.

Letouzey, J., Colletta, B., Vially, R., Chermette, J.C., 1995. Evolution of salt-related structures in compressional settings. In: Jackson, M.P.A., Roberts, D.G., Snelson, S. (Eds.), Salt Tectonics: A Global Perspective, vol. 65. American Association of Petroleum Geologists Memoir, pp. 41–60.

Liu, H., McClay, K.R., Powell, D., 1992. Physical models of thrust wedges. In: McClay, K.R. (Ed.), Thrust Tectonics. Chapman & Hall, pp. 71–81.

Lohrmann, J., Kukowski, N., Adam, J., Oncken, O., 2003. The impact of analogue material properties on the geometry, kinematics and dynamics of convergent sand wedges. Journal of Structural Geology 25, 1691–1711.

López-Gómez, K., Arche, A., Pérez-López, A., 2002. Permian and Triassic. In: Gibbons, W., Moreno, T. (Eds.), The Geology of Spain. The Geological Society of London, pp. 185–212.

Luján, M., Storti, F., Balanyá, J.C., Crespo-Blanc, A., Rosetti, F., 2003. Role of décollement material with different rheological properties in the structure of the Aljibe thrust imbricate (Flysch Trough, Gibraltar Arc): an analogue modelling approach. Journal of Structural Geology 25, 867–881.

Mallada, L., 1878. Geología de la provincial de Huesca. Mem. Com. Mapa geológico de España, Madrid, 559 pp.

Marques, F.O., Cobbold, P.R., 2002. Topography as a major factor in the development of arcuate thrust belts: insights from sandbox experiments. Tectonophysics 348, 247–268.

Marques, F.O., Cobbold, P.R., 2006. Effects of topography on the curvature of fold-and-thrust belts during shortening of a 2-layer model of continental lithosphere. Tectonophysics 415, 65–80.

Massoli, D., Koyi, H.A., Barchi, M.R., 2006. Structural evolution of a fold and thrust belt generated by multiple décollements: analogue models and natural examples from Northern Apennines (Italy). Journal of Structural Geology 28, 185–199.

McClay, K.R., Whitehouse, P., 2004. Analogue modelling of doubly vergent thrust wedges. In: McClay, K.R. (Ed.), Thrust Tectonics and Hydrocarbon Systems, vol. 82. American Association of Petroleum Geologists, Memoir, pp. 372–399.

McClay, K.R., Whitehouse, P.S., Dooley, T., Richards, M., 2004. 3D evolution of fold and thrust belts formed by oblique convergence. Marine and Petroleum Geology 21, 857–877.

Millán, H., 1995. Estructura y Cinemática del frente de cabalgamiento surpirenaico en las Sierras Exteriores Aragonesas; PhD Thesis, Departamento de Ciencias de la Tierra, Universidad de Zaragoza, Zaragoza, 330 pp + annex.

Millán, H., Aurell, M., Meléndez, A., 1994. Synchronous detachment folds and coeval sedimentation in the Prepyrenean External Sierras (Spain): a case study for a tectonic origin of sequences and system tracts. Sedimentology 41 (5), 1001–1024.

Mulugeta, G., 1988. Modelling the geometry of Coulomb thrust wedges. Journal of Structural Geology 10, 847–859.

Mulugeta, G., Koyi, H.A., 1987. Three-dimensional geometry and kinematics of experimental piggy-back thrusting. Geology 15, 1052–1056.

Mulugeta, G., Koyi, H., 1992. Episodic accretion and strain partitioning in a model sand wedge. Tectonophysics 202, 319–333.

Muñoz, J.A., 1992. Evolution of a continental collision belt: ECORS-Pyrenees crustal balanced cross-section. In: McClay, K.R. (Ed.), Thrust Tectonics. Chapman & Hall, pp. 235–246.

Nalpas, T., Györfi, I., Guillocheau, F., Lafont, F., Homewood, P., 1999. Influence de la charge sédimentaire sur le développement d'anticlinaux synsédimentaires. Modélisation analogique et exemple du terrain (bordure sud du basin de Jaca). Bulletin de la Societé Géologique de France 170 (5), 733–740.

Nalpas, T., Gapais, D., Vergés, J., Barrier, L., Gestain, V., Leroux, G., Rouby, D., Kermarrec, J.J., 2003. Effects of rate and nature of synkinematic sedimentation on the growth of compressive structures constrained by analogue models and field examples. In: McCant, T., Saintot, A. (Eds.), Tracing Tectonic Deformation Using the Sedimentary Record, vol. 208. Geological Society, London, Special Publications, pp. 307–319.

Nilforoushan, F., Koyi, H.A., Swantesson, J.O.H., Talbot, C.J., 2008. Effect of basal friction on surface and volumetric strain in models of convergent settings measured by laser scanner. Journal of Structural Geology 30, 366–379.

Oliva, B., Millán, H., Pocoví, A., Casas, A.M., 1996. Estructura de la Cuenca de Jaca en el sector occidental de las Sierras Exteriores Aragonesas. Geogaceta 20 (4), 800–802.

Oliva-Urcía, B., Pueyo, E.L., 2007. Gradient of shortening and vertical-axis rotations in the Southern Pyrenees (Spain), insights from a synthesis of paleomagnetic data. Revista de la Sociedad Geológica de España 20 (1–2), 105–118.
Poblet, J., Hardy, S., 1995. Reverse modeling of detachment folds; application to the Pico de Aguila anticline in the south central Pyrenees (Spain). Journal of Structural Geology 17 (12), 1707–1724.
Poblet, J., McClay, K.R., Storti, F., Muñoz, J.A., 1997. Geometries of syntectonic sediments associated with single-layer detachment folds. Journal of Structural Geology 19 (3–4), 369–381.
Pocoví, A.J., 1979. Estudio geológico de las Sierras Marginales Catalanas (Prepirineo de Lérida). Acta Geológica Hispánica 13, 73–79.
Pueyo, E.L., 2000. Rotaciones Paleomagnéticas en Sistemas de Pliegues y Cabalgamientos. Tipos, Causas, Significado y Aplicaciones (Ejemplos de las Sierras Exteriores y Cuenca de Jaca, Pirineo Aragonés); PhD Thesis, Departamento de Ciencias de la Tierra, Universidad de Zaragoza, Zaragoza, 300 pp + annex.
Pueyo, E.L., Millán, H., Pocoví, A., Parés, J.M., 1997. Determination of the folding mechanism by AMS data: study of the relation between shortening and magnetic anisotropy in the Pico del Águila anticline (Southern Pyrenees). Physics and Chemistry of the Earth 22 (1–2), 195–201.
Pueyo, E.L., Millán, H., Pocoví, A., Parés, J.M., 2000. Cinemática rotacional del cabalgamiento basal surpirenaico en as Sierras Exteriores Aragonesas: datos magnetotectónicos. Acta Geológica Hispánica 32 (3–4), 119–137.
Pueyo, E.L., Millán, H., Pocoví, A., 2002. Rotation velocity of a thrust: a paleomagnetic study in the External Sierras (Southern Pyrenees). Sedimentary Geology 146 (1), 191–208.
Pueyo, E.L., Pocoví, A., Parés, J.M., Millán, H., Larrasoaña, J.C., 2003a. Thrust ramp geometry and spurious rotations of paleomagnetic vectors. Studia Geophysica Geodetica 47, 331–357.
Pueyo, E.L., Parés, J.M., Millán, H., Pocoví, A., 2003b. Conical folds and apparent rotations in paleomagnetism (a case study in the Southern Pyrenees). Tectonophysics 362, 345–366.
Puigdefàbregas, C., 1975. La Sedimentación Molásica en la Cuenca de Jaca; Monografias del Instituto de Estudios Pirenaicos. Número Extraordinario de Revista Pirineos, 104, Instituto de Estudios Pirrenaicos, Jaca, 153 pp + annexes.
Salvany, J.M., 1990. Introducción a las evaporitas triásicas de las cadenas periféricas de la cuenca del Ebro: Catalánides, Pirineo y Región Cantábrica. In: Ortí, F., Salvany, J.M. (Eds.), Formaciones evaporíticas de la Cuenca del Ebro y cadenas periféricas, y de la zona de Levante. Enresa, Madrid, pp. 21–28.
Schreurs, G., Hänni, R., Vock, P., 2002. Analogue modeling of transfer zones in fold and thrust belts: a 4-D analysis. Journal of the Virtual Explorer 6, 43–49.
Selzer, G., 1948. Geología de las sierras surpirenaicas del Alto Aragón. (Translated from the original version, "Geologie der sudpyrenäische Sierren inOberaragonien", Berlin, 1934). Publicación Extraordinaria Geol. España. C.S.I.C.; Madrid, IV, pp. 185–231.
Smit, J.H.W., Brun, J.P., Sokoutis, D., 2003. Deformation of brittle-ductile thrust wedges in experiments and nature. Journal of Geophysical Research 108 (B10), 2480, doi:10.1029/2002JB002190.
Soler, M., Puigdefàbregas, C., 1970. Líneas generales de la geología del Alto Aragón Occidental. Pirineos 96, 5–20.
Soto, R., Casas, A.M., Storti, F., Faccena, C., 2002. Role of lateral thickness variations on the development of oblique structures at the Western end of the South Pyrenean Central Unit. Tectonophysics 350, 215–235.
Soto, R., Casas-Sainz, A.M., Pueyo, E.L., 2006. Along-strike variation of orogenic wedges associated with vertical axis rotations. Journal of Geophysical Research 111, B10402, doi:10.1029/2005JB004201.
Storti, F., Soto-Marin, R., Faccena, C., Casas-Sainz, A., 2001. Role of the backstop-to-cover thickness ratio on vergence partitioning in experimental thrust wedges. Terra Nova 13 (6), 413–417.
Storti, F., Soto-Marin, R., Rossetti, F., Casas-Sainz, A., 2007. Evolution of experimental thrust wedges accreted from along-strike tapered, silicone-floored multilayers. Journal of the Geological Society of London 164, 73–85.
Swantesson, J.O.H., 2005. Weathering and erosion of rock carvings in Sweden during the period 1994–2003. Micro Mapping with Laser Scanner for Assessment of Breakdown Rates, 29. Karlstad University Studies, pp. 99.
Swantesson, J.O.H., Moses, C.A., Berg, G.E., Jansson, M.J., 2006. Methods for measuring shore platform micro erosion: a comparison of the micro-erosion meter and laser scanner. Zeitschrift für Geomorphologie N.F 144 (Suppl), 1–17.
Talbot, C.J., 1992. Centrifuge models of Gulf of Mexico profiles. Marine and Petroleum Geology 9, 412–432.
Teixell, A., García-Sansegundo, J., 1995. Estructura del sector central de la Cuenca de Jaca (Pirineos Meridionales). Revista de la Sociedad Geológica de España 8 (3), 215–228.
Teixell, A., Koyi, H.A., 2003. Experimental and field study of the effects of lithological contrasts on thrust-related deformation. Tectonics 22, 1054, doi:10.1029/2002TC001407.
Weijermars, R., 1986. Flow behaviour and physical chemistry of bouncing putties and related polymers in view of tectonic laboratory applications. Tectonophysics 124, 325–358.
Weijermars, R., Schmeling, H., 1986. Scaling of Newtonian and non-Newtonian fluid dynamics without inertia for quantitative modelling of rock flow due to gravity (including the concept of rheological similarity). Physics of the Earth and Planetary Interiors 43, 316–330.
Williams, R.B.G., Swantesson, J.O.H., Robinson, D.A., 2000. Measuring rates of surface downwearing and mapping microtopography: the use of micro-erosion meters and laser scanners in rock weathering studies. Zeitschrift für Geomorphologie N.F 120 (Suppl), 51–66.

CHAPTER III

Mechanical stratigraphy and syn-kinematic sedimentation in fold development

This third chapter presents the second scientific article of this Thesis. In this work we used a 2D Discrete Element Modelling technique to investigate the effect of the complex mechanical stratigraphy described in the field as well as the influence of the growth strata in the evolution of the Pico del Águila anticline. Firstly, an abridged abstract in Catalan is presented. Secondly, the abridged summary in English and the work published in a Special Volume of the Geological Society of London entitled *Kinematic Evolution and Structural Styles of Fold-and-Thrust Belts* are presented. This Special Volume will be released in mid-2010. In the meantime, our study is cited as follows:

Vidal-Royo, O., Hardy. S., Muñoz, J.A., 2010. The roles of complex mechanical stratigraphy and syn-kinematic sedimentation in fold development: Insights from discrete-element modelling and application to the Pico del Águila anticline (External Sierras, Southern Pyrenees). In: Poblet, J., Lisle, R.J. (Eds.). Kinematic Evolution and Structural Styles of Fold-and-Thrust Belts, Special Publication of the Geological Society, v.330, doi: 10.1144/SP330.

3.1 RESUM DEL CAPÍTOL (Summary in Catalan)

Aquest tercer capítol presenta el segon article científic d'aquesta Tesi. En aquest treball es va utilitzar la Modelització per Elements Discrets en 2D per tal d'investigar l'efecte d'una estratigrafia mecànica complexa com la descrita a la zona de camp, així com la influència de la sedimentació sin-cinemàtica sobre l'evolució de l'anticlinal del Pico del Águila.

La sèrie estratigràfica descrita al camp té una edat compresa entre el Triàsic mig i l'Oligocè i es caracteritza per una intercalació de materials competents i incompetents, la qual porta a una gran variació d'estil estructural i de deformació a escala d'afloramententre les unitats observades al camp. Els models numèrics presentats pretenen reproduir aquesta variabilitat estratigràfica mitjançant l'ús d'una estratigrafia mecànica que conté una complexa intercalació de unitats competents i incompetents. Per fer-ho es presenten dos experiments. El Model 1 explora la resposta d'aquesta estratigrafia mecànica a l'escurçament en unes condiciones que resultaren en la formació d'un plec de desenganxament. Aquest primer model mostra com els mecanismes de plegament varien d'una forma abrupta depenent de les propietats mecàniques de cadascuna de les unitats: les unitats més incompetents presenten gran deformació interna, acomodant gran quantitat de cisalla paral·lela a les capes, mentre que les unitats més competents es deformen per rotació/translació rígida, fracturació localitzada i una menor deformació interna. El Model 2 explora la influència de la sedimentació sin-cinemàtica sota les mateixes condicions de contorn: els sediments estabilitzen el plec contra inestabilitats gravitacionals i causen una major concentració de la deformació en el nucli de l'anticlinal, donant com a resposta una estructura més vertical, de flancs més estrets i menor longitud d'ona.

3.2 ABRIDGED SUMMARY

A 2D discrete-element modelling technique is used to explore the effects of complex mechanical stratigraphy and syn-kinematic sedimentation in the

development of the Pico-del-Águila anticline (External Sierras, Southern Pyrenees). The stratigraphy (Middle Triassic to Oligocene in age) involved in this structure is characterised by a gross interlayering of competent and incompetent units, which leads to a striking variation in outcrop-scale deformation of the units observed in the field. The numerical model attempts to reproduce the stratigraphic variation seen in the field by using a mechanical stratigraphy that contains a complex interlayering of competent/incompetent units. Two experiments are presented. Model 1 tests the response of this complex mechanical stratigraphy to shortening under conditions that lead to the formation of a detachment fold. This experiment shows that folding mechanisms vary abruptly depending on the mechanical properties of the materials involved: the incompetent units are strongly internally deformed, accommodating much layer-parallel shearing; the competent units deform by rigid-body translation/rotation, localised faulting and minor internal shearing. Model 2 tests the effect of syn-kinematic sedimentation under identical boundary conditions: these sediments stabilise the fold against gravitational instabilities and cause a concentration of deformation in the core of the structure, leading to a tighter, narrower fold.

The roles of complex mechanical stratigraphy and syn-kinematic sedimentation in fold development: Insights from discrete-element modelling and application to the Pico del Águila anticline (External Sierras, Southern Pyrenees)

OSKAR VIDAL-ROYO [1], STUART HARDY [1,2],
JOSEP ANTON MUÑOZ [1]

[1] *Geomodels Research Centre. GGAC, Departament de Geodinàmica i Geofísica, Facultat de Geologia, Universitat de Barcelona. C/ Martí i Franquès s/n, 08028, Barcelona, Spain.*
[2] *ICREA (Institució Catalana de Recerca i Estudis Avançats), Catalonia, Spain.*

Abstract: A 2D discrete-element modelling technique is used to explore the effects of complex mechanical stratigraphy and syn-kinematic sedimentation in the development of the Pico-del-Águila anticline (External Sierras, Southern Pyrenees). The stratigraphy (Middle Triassic to Oligocene in age) involved in this structure is characterised by a gross interlayering of competent and incompetent units, which leads to a striking variation in outcrop-scale deformation of the units observed in the field. The numerical model attempts to reproduce the stratigraphic variation seen in the field by using a mechanical stratigraphy that contains a complex interlayering of competent/incompetent units. Two experiments are presented. Model 1 tests the response of this complex mechanical stratigraphy to shortening under conditions that lead to the formation of a detachment fold. This experiment shows that folding mechanisms vary abruptly depending on the mechanical properties of the materials involved: the incompetent units are strongly internally deformed, accommodating much layer-parallel shearing; the competent units deform by rigid-body translation/rotation, localised faulting and minor internal shearing. Model 2 tests the effect of syn-kinematic sedimentation under identical boundary conditions: these sediments stabilise the fold against gravitational instabilities and cause a concentration of deformation in the core of the structure, leading to a tighter, narrower fold.

From: POBLET, J. & LISLE, R.J. (eds) 2010. *Kinematic Evolution and Structural Styles of Fold-and-Thrust Belts*. Geological Society, London, Special Publications, **330**, xxx-xxx.
doi: 10.1144/SP330

Many studies have considered mechanical stratigraphy as an important control on the present-day geometry of fault-related folds, influencing their evolution (e.g. Homza & Wallace, 1995, 1997; Nalpas et al., 1999; Atkinson & Wallace, 2003; Mitra, 2003; Hardy & Finch, 2005; Hardy & Finch, 2007). However, most of these works treat mechanical stratigraphy in a qualitative manner, either considering it as a possible theoretical factor, or modelling a very simplified mechanical stratigraphy. In addition, growth strata, a common component of fault-related folds, have been mainly used as an indicator of folding mechanisms/kinematics, to estimate chronology and sedimentation/uplift rates, to reveal fold types and geometries or to recognize internal deformation features in the syn-kinematic package (e.g. Poblet & Hardy, 1995; Poblet et al., 1997; Storti & Poblet, 1997; Nigro & Renda, 2004; Strayer et al., 2004; Casas-Sainz et al., 2005; Grando & McClay, 2007; Tavani et al., 2007). However, most of these works neglect the effect of the syn-kinematic sedimentary load on the evolution of the fold itself.

The Pico del Águila is one of the best known N-S anticlines in the Central External Sierras (CES; Southern Pyrenees), which are interpreted to be in the hangingwall of the large-displacement South-Pyrenean thrust that places the Triassic décollement over a ramp that cuts far up-section through Tertiary syn-tectonic deposits. These anticlines are interpreted to have rotated clockwise ca. 40º (Pueyo et al., 2002), towards the direction of tectonic transport. Previous numerical modelling techniques applied to the Pico del Águila anticline have used kinematic modelling (Poblet & Hardy, 1995; Poblet et al., 1997) and inclined-shear restoration (Novoa et al., 2000). Based on accurate observations/mapping of the growth strata pattern, these studies focused on folding mechanisms/kinematics, and assumed a homogeneous pre-folding sequence. The main drawback of these works is that they consider the evolution of the structure only from geometrical and kinematical viewpoints, overlooking the importance of mechanical heterogeneities in the pre-folding sequence. As a result, even though the obtained geometries broadly agree with field data, the proposed folding mechanisms may not fully represent the structural evolution of the Pico del Águila anticline and its expression in the field, which is far from being fully unravelled by those techniques alone.

In contrast to these studies, this work uses a discrete element model to explore the effects of a complex (non-trivial) mechanical stratigraphy and the syn-folding sedimentary load on the structural evolution of a detachment fold.

The Pico del Águila provides a well-exposed down-plunge view of a fold down to the Triassic core, with a well described mechanical stratigraphy and spectacular growth strata that record the fold development. This provides an excellent basis to compare how the mechanical stratigraphy behaved in the natural fold vs. the model, and how the syn-kinematic sedimentation influenced the fold evolution. Although the numerical model does not purport to be a direct replica of the natural fold (i.e., it is constrained to deform by plane strain, does not contain vertical axis rotations, etc), we compare the results to the Pico del Águila anticline, gaining insight on the folding mechanisms and structural evolution of this area.

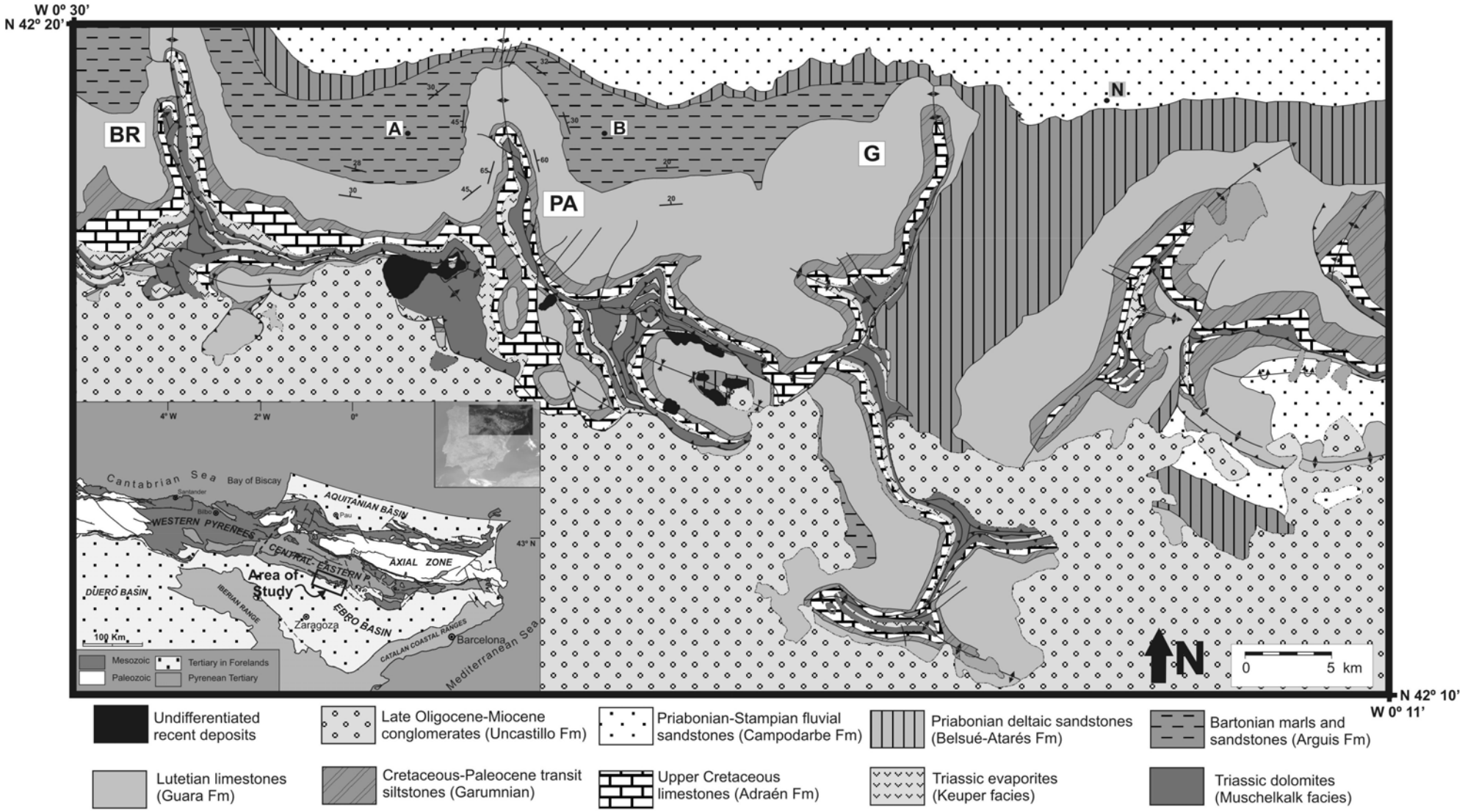

Fig. 1. Geological map of the Central External Sierras (modified from IGME, 1992). BR: Bentué de Rasal anticline; PA: Pico del Águila anticline; G: Gabardiella anticline complex; A: Arguis village; B: Belsué village; N: Nozito village.

Geological setting of the Pico del Águila anticline

The Pico del Águila is a widely studied anticline in the External Sierras of the Spanish Southern Pyrenees (Fig. 1). It grew from 42.67 ± 0.02 Ma (Upper Lutetian) until 34.8 ± 1.72 Ma (Lower Priabonian) (Poblet & Hardy, 1995) and displays a spectacular growth strata record (Millán et al., 1994; Millán, 1995, Poblet & Hardy, 1995; Pueyo et al., 2002; Castelltort et al., 2003). A complete discussion on the regional geology is beyond the scope of this paper. The interested reader is referred to key works such as Puigdefàbregas (1975), IGME (1992), Millán et al. (1994) and Pueyo et al. (2002). Nevertheless, since this study models the effect of the mechanical stratigraphy in the fold development, a brief description of the geological setting and the stratigraphy of the Central External Sierras is provided (CES; Figs. 2 & 3a).

The External Sierras constitute the frontal emergent part of the southernmost Pyrenean thrust sheets (Soler & Puigdefàbregas, 1970; IGME, 1992; Millán et al. 1994; Millán, 1995; Pueyo et al., 2002) and consist of a system of imbricated thrust sheets detached on clayish, dolomitic and evaporitic Middle and Late Triassic facies (Keuper and Muschelkalk facies). The hanging-wall of the frontal Pyrenean thrust involves an Upper Triassic to Lower Miocene sedimentary sequence (Puigdefàbregas, 1975; Millán et al. 1994; Millán, 1995) which was displaced southwards over the Tertiary sediments of the Ebro foreland basin. During the early stages of the evolution of the External Sierras (Early Lutetian to Chattian), the thrust system was characterized by a south-directed main thrust and a set of arcuate north-eastward concave, oblique thrusts. Generated as detachment folds on a hangingwall flat over footwall flat thrust configuration, the N-S trending folds are interpreted as a more evolved stage of the initially arcuate oblique thrusts. In addition to a general translation towards the South, a regional clockwise rotation characterized the kinematics of the thrust system (up to 40° measured at the base of Arguis Fm, western limb of Pico del Águila anticline; Pueyo et al., 2002). However, during the Chattian to the Early Miocene, the structural evolution changed abruptly. The rotating thrust system was folded and truncated by the formation of the Santo Domingo detachment anticline and its associated south-directed thrust system, located in the western sector of the External Sierras (beyond the limits of Fig. 1, to the west). Consequently, the remaining N-S trending folds occurred at the hanging-wall of the new Santo Domingo thrust system, representing the northernmost portion of those oblique structures (the rest of the structures are supposed to be either buried under the continental deposits of the Ebro foreland basin or isolated by erosion under the southern limb of the Santo Domingo anticline, according to Pueyo et al., (2002)). The emplacement of these N-S trending folds in a hanging-wall flat over footwall ramp position of the Santo Domingo thrust system caused their 30º plunge towards the hinterland (Millán, 1995; Pueyo et al., 2002).

In common with other similar structures in Central External Sierras, the Pico del Águila has been commonly assessed to be either a detachment fold (Millán et al., 1994; Poblet & Hardy, 1995; Pueyo et al., 2002; Castelltort et al., 2003) or a fault-propagation fold (McElroy, 1990; Millán et al., 1994). Based on field and mapping observations as well as on ideas already suggested by previous authors (cf. Millán, 1995; Pueyo et al., 2002), it is our hypothesis that the Pico del Águila anticline generated as a detachment fold (on

OLIGOCENE	EARLY	STAMPIAN	Campodarbe Fm.	- Thickness variation across structure due to sedimentation during fold growth (wedge shape thinning towards the crest of the anticline) - Deformation characterized by decimetric non-strata bounded fractures, at a high angle to bedding
EOCENE	LATE	PRIABONIAN	Belsué-Atarés	- Thickness variation across structure due to sedimentation during fold growth. Deformation characterized by metric spaced non-strata bounded fractures, at a high angle to bedding
	MIDDLE	BARTONIAN	Arguis Fm.	- Thickness variation across structure due to sedimentation during fold growth - Deformation characterized by pervasive flexural slip and minor decimetric to metric spaced non-strata bounded fractures, nearly perpendicular to bedding
		LUTETIAN	Guara Fm.	- Top of the pre-folding sequence - Constant layer thickness - Stylolitic bedding planes - Macroscopically outlines the fold geometry, not affected by mesoscale faulting - At outcrop scale, penetrative strain characterized by multiple centimetric-spaced fracture sets, at a high angle to bedding
PALEOCENE			Garumnian	- Non-localized deformation in mudstone layers and pervasive cleavage in sandstone layers
U. CRETACEOUS			Adraén Fm.	- Localized metric spaced fracture pattern, non-strata bounded, at *ca.* 60º to bedding
MIDDLE AND LATE TRIASSIC			Muschelkalk and Keuper Facies	- Keuper facies: non-localized deformation exhibiting large variation of thickness and high internal deformation expressed by milimetric to decimetric folds. - Muschelkalk facies: pervasive strain expressed by centimetric spaced fractures at a high angle to bedding, and internal metric to decametric box and detachment folds

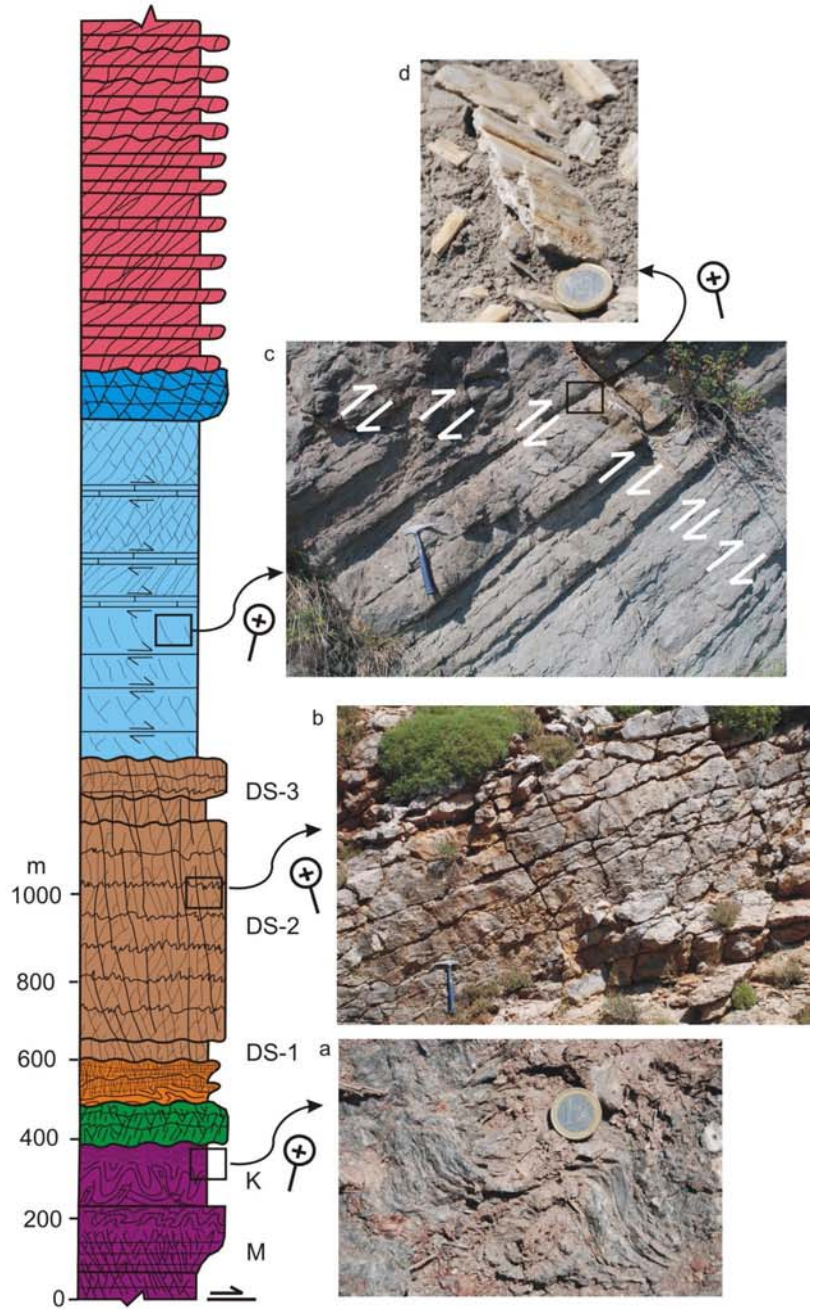

Fig. 2. *(Previous page)* Stratigraphic sequence cropping out in Central External Sierras (modified after Millán et al., 1994) showing the deformation style that characterises each unit: a) folded Keuper gypsiferous clays (photograph oriented E-W); b) fracture pattern within the Guara limestones (photograph oriented NW-SE); c) flexural slip and minor fractures within the Arguis marls (photograph oriented SW-NE); d) detail of a remnant slickenslide parallel to bedding in the Arguis marls (dipping 29º to the N), indicating layer parallel displacement (c and d belong to different outcrops). Right side of the stratigraphic column: M is Muschelkalk, K is Keuper; DS-1, DS-2 and DS-3 are, respectively, Depositional Sequences 1, 2 and 3 within Guara Fm.

a hangingwall flat over footwall flat thrust configuration according to Pueyo et al., 2002) and, with increasing shortening, the core of the anticline broke through, propagating upwards while folding the upper units of Guara Fm and overlying growth strata, finally evolving into a hybrid detachment/fault-propagation fold.

The stratigraphic record of the Pico del Águila anticline is composed by a pile of sedimentary rocks from Triassic to Oligocene in age (Fig. 2). The pre-folding stratigraphic sequence is made up of a relatively thin Mesozoic pile, consisting of Triassic limestone, dolomite and gypsum-bearing clay (the oldest outcropping material), and Upper Cretaceous shallow marine limestone. This is followed by a thicker Paleogene sequence comprising the continental sandstone, siltstone and lacustrine limestone of the Cretaceous-Paleocene transition (Garumnian facies), and the heterogeneous Lutetian shallow marine platform limestone of the Guara Formation. The syn-folding stratigraphic sequence comprises the uppermost part of the Guara Fm, the shallow marine and transitional marl, limestone and sandstone of the Arguis and Belsué-Atarés Fms (Upper Lutetian to Middle Priabonian), and the basal part of the fluvial mudstone, sandstone and conglomerate of the Campodarbe Fm (Middle Priabonian to Middle Oligocene).

It is important to highlight that the Muschelkalk dolomites and limestones are the oldest outcropping material exposed in the core of the anticline. However, data from the well Surpirenaica-1 located in the Ebro basin (to the South, beyond the limits of the studied area; IGME, 1987) indicate the existence of an underlying thin Middle Muschelkalk material made up of clayish and evaporitic rocks, which might have behaved as a basal décollement in the CES. While we have no evidence of this material beneath the Muschelkalk limestones and dolomites, it is likely that the N-S anticlines of the CES are detached on a very thin sequence of Middle Muschelkalk claystone and evaporites. This unit is expected to be relatively thin (around dozens of metres) since it does not crop out in any of the N-S anticlines of the CES.

Summarizing, the whole stratigraphic sequence is an interlayering of competent and incompetent units (see Fig. 3; Millán et al., 1994). We use "competent" and "incompetent" in this paper sensu lato, that is we make the distinction between rocks that preferentially show discrete localised deformation and those that deform by more general distributed deformation. The stratigraphic sequence is characterised by the presence of at least two "incompetent" levels that can accommodate the deformation by means of flexural slip/flow: the Upper Triassic evaporitic clay (Keuper facies) and the mudstone-siltstone of the Cretaceous-Paleocene transition (Garumnian facies). Although less important, the Guara Fm also presents mechanical heterogeneities with

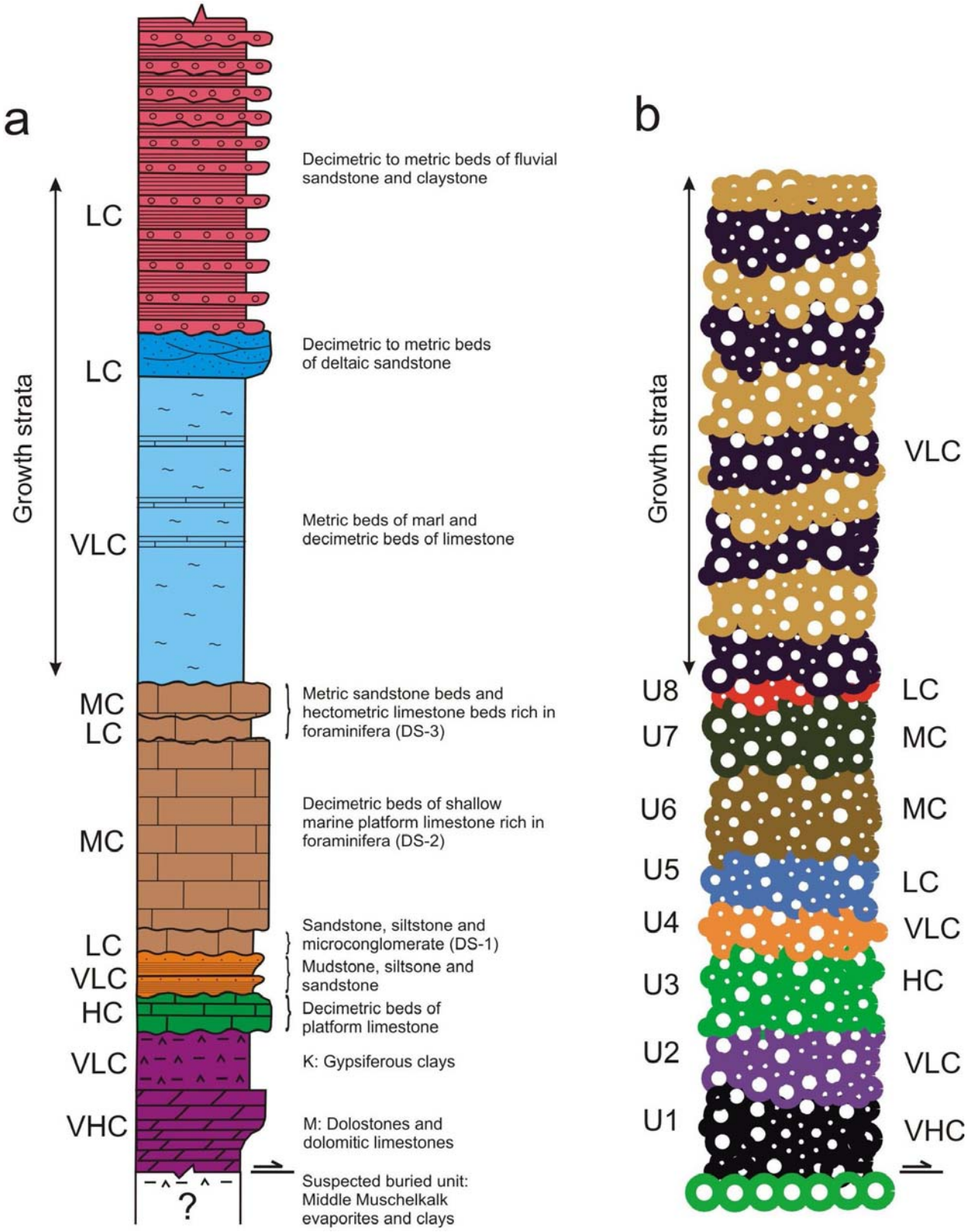

Fig. 3. Comparison between stratigraphic sequences: (a) sequence seen in the field (modified after Millán et al., 1994) with a brief description of the predominant lithologies observed in each unit (M: Muschelkalk, K: Keuper); and (b) sequence used to model the mechanical behaviour of the natural sequence. Next to each field/model unit there is an indication of its average mechanical behaviour: VHC is Very High Competence; HC is High Competence; MC is Medium Competence; LC is Low Competence; and VLC is Very Low Competence.

three differentiated depositional sequences (DS's; Millán, 1995): a decametric sequence of sandstone, marl, siltstone and microconglomerate (DS-1), interpreted as a material of low competence; a hectometric sequence of shallow marine platform limestone rich in foraminifera (DS-2; middle competence); and one hundred metres composed of a thin sequence of sandstone overlain by limestone rich in Nummulites and bivalves (DS-3; middle competence). As such, the stratigraphic record of Pico del Águila anticline shows large heterogeneities in terms of mechanical behaviour which may have influenced the growth and evolution of the structure.

Modelling Methodology

Discrete-element modelling

In this work, a two dimensional discrete-element modelling technique (DEM) has been used to test the effect of mechanical stratigraphy and syn-kinematic sedimentation on an idealised stratigraphic sequence. Discrete-element models have become commonly used in the description of the non-linear interaction of a large number of particles (e.g. Donzé et al., 1996; Kuhn, 1999; Camborde et al., 2000; Finch et al., 2003; Hardy et al., 2009). Unlike continuum techniques, these discontinuum methods use simple particle interactions and, therefore, permit the dynamic evolution of a system to be modelled and observed. It is a technique well-suited to studying problems in which mechanical discontinuities (shear zones, faults, joints, or fractures) are important as it allows deformation involving large (unlimited) relative motion of individual elements, and by definition does not require the complex re-meshing at moderate to high strains that other techniques such as finite-element typically require.

This method treats a rock mass as an assemblage of circular elements (Fig. 4a) connected in pairs by breakable springs or bonds (Fig. 4b). Thus, it is possible to model different mechanical properties (e.g. a stratigraphic sequence) by assigning different values of breaking strains to each pair of elements (cf. Hardy & Finch, 2005), allowing us to test the effect of a given mechanical stratigraphy on geometry, fold kinematics and folding mechanisms. As such, the method provides more information than previous kinematic modelling approaches. Furthermore, it allows for easy monitoring of displacement/location of the elements through time. In this way, the displacement path, the kinematic evolution and the strain distribution within the body can be easily tracked at any stage of the modelling. Given the competent/incompetent interlayering that characterizes the stratigraphic record (Fig. 3; Millán et al., 1994), we believe it to be an ideal method with which to model the Pico del Águila anticline. Finally, while sandbox models can be applied to similar complex boundary conditions, they are not ideally suited to modelling complex stratigraphic sequences and only rarely are model results analysed in a quantitative way to extract, for example, incremental shear strain.

Since this work aims to apply a DEM technique to understand the evolution of the Pico del Águila anticline, only a general overview of the method will be given. For a detailed description of the method as well as its mathematical background, we refer the reader to previous works such as Finch et al. (2003) or Hardy & Finch (2005, 2007). This modelling approach treats a rock mass as an assemblage of circular elements that interact

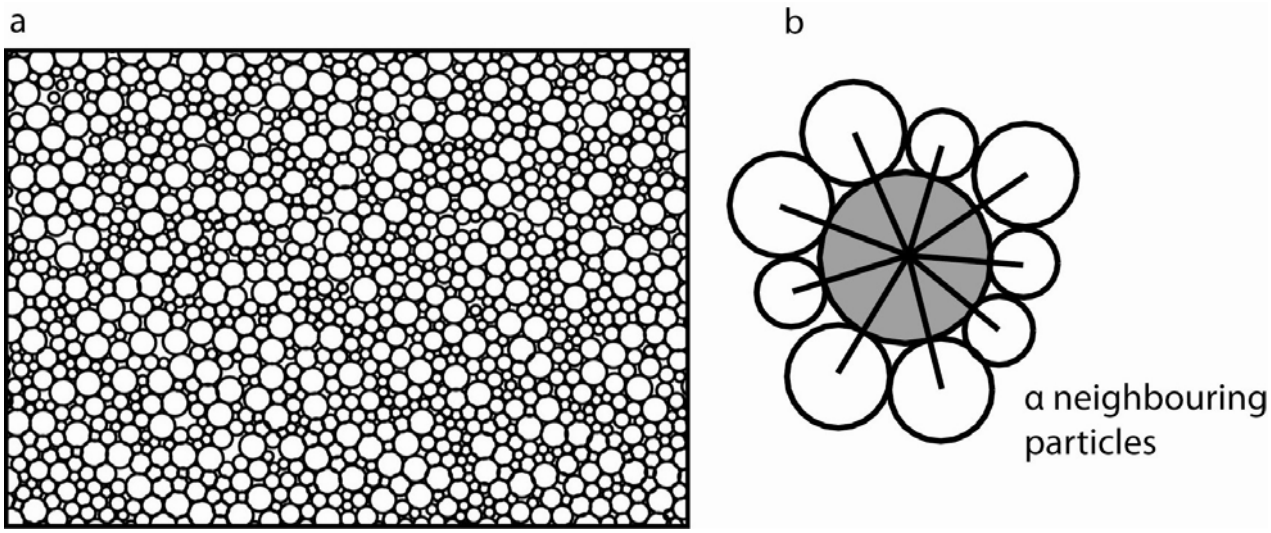

Fig. 4. Illustration of the discrete-element technique used in this work: (a) packing of particles with four different radii; (b) relationship between a given particle (grey shaded) and its neighbours (particles are connected by breakable elastic springs).

in pairs, as if connected by breakable elastic springs. The behaviour of the elements assumes that the particles interact through a repulsive-attractive force (Mora & Place, 1993; Hardy & Finch, 2005), in which the resultant elastic-interaction force (Fs) between two elements is given by:

$$Fs = \begin{cases} K\,(r - R), & r < r0, \text{ intact bond} \\ K\,(r - R), & r < R, \text{ broken bond} \\ 0, & r \geq R, \text{ broken bond} \end{cases} \quad \text{(Eq.1)}$$

where K is the elastic constant (spring stiffness) of the bond, R is the equilibrium separation between the particles (that is, the initial distance), r0 is a breaking separation that is a breaking threshold and r is the current separation between particles.

Particles within the model remain bonded until the separation r exceeds the breaking threshold r0. From that time onwards, the bond becomes irreversibly broken and the particle pair will not experience an attractive force anymore. However, if the pair of elements return into a compressive contact (r < R), a repulsive force acts between them. The force acting on a bond at the breaking threshold is equivalent to the force necessary for a bond to fail (i.e., the stress acting on a particle at failure). Large values of the threshold (e.g. 0.05R) produce "competent" materials that fail by localised faulting. In contrast, low threshold values (e.g. 0.002R) produce "incompetent" materials that deform in a macroscopically ductile manner as a result of non-localized deformation (flow) caused by the relative motion of many hundreds of elements.

The total elastic force applied on a particle is the sum of the forces on each bond that links an element to its neighbours. A viscous damping term (proportional to the velocity of the particle) is also included, in order to dampen reflected waves from the edges of the model. This avoids a build-up of kinetic energy within the system. In addition, gravitational forces are also considered, acting on each element only in the y vertical direction. Particles are displaced to their new positions within the model at each discrete

time step, by integrating their equations of motion obeying Newtonian physics and using a velocity Verlat-based solution scheme.

Finally, to avoid any isotropy in the orientation of the strain/displacement fields of the particles (i.e., preferential predefined breaking planes between the particles) the assemblage is composed of particles of different sizes distributed at random. This reduces the likelihood for preferred planes of weakness and allows a non-predefined localisation of deformation.

Model Setup and Experimental Parameters

In this work, the method described above is used to test the role of both complex mechanical stratigraphy (Model 1) and syn-kinematic sedimentation (Model 2) in the evolution of the Pico del Águila anticline. The behaviour of the simulated rock mass is broadly elasto-plastic and frictionless (Place & Mora, 2001; Finch et al., 2003, 2004; Hardy & Finch, 2005, 2007), an approach used in previous studies to model the brittle deformation in sedimentary rocks in the upper crust. Deformation of the modelled sedimentary sequence occurs in response to shortening at a subduction slot at the base of the model (a common configuration in sandbox experiments). A velocity discontinuity is created at the subduction slot in the central basal part of the box, in which the right half of the model moves leftwards at a continuous rate of 0.001 m per time step (Fig. 5). A homogeneous rock density of 2500 kg m-3 has been used, a typical value of upper-crustal sedimentary rocks. A value of 5.5 x 109 N m-2 is used for the elastic constant (K) in the experiments. Experiments were run for 2,000,000 time steps with output of the assembly every 25,000 time steps (i.e. every 25 m shortening) for Model 1 and every 100,000 steps (i.e. every 100 m shortening) for Model 2. The total displacement in both experiments was 2 km. This provided a precise control on the structural evolution and variation of the strain distribution (Models 1 and 2) and a well constrained geometry of the syn-kinematic sedimentation (Model 2).

Within the modelling framework, one lattice unit (LU) corresponds to 250 metres. The initial particle assembly contains 10245 elements with four different radii of 0.125, 0.1, 0.075 and 0.05 LU (i.e. 31.25, 25, 18.75 and 12.5 m, respectively) distributed at random in an enclosed rectangular box. We believe these dimensions are suitable, since they provide enough resolution to model a kilometric-scale structure like the Pico del Águila anticline, avoiding the generation of preferred planes of weakness and allowing a non-predefined localisation of deformation that a homogeneous particle size would imply. After initial generation, the elements are allowed to relax to a stable equilibrium and are left to settle under gravity for ~2,000,000 time steps to obtain a stable, well-packed initial assemblage and to further minimise void space. The resulting initial assembly is 12.5 km long and ca. 1.25 km thick, simulating a continuous rock mass that can deform by progressive bond breakage (fracturing/faulting) and bulk motion of unbroken pairs of elements (folding). In addition, in Model 2 the syn-kinematic sedimentary sequence was modelled by adding incrementally a total of 11708 elements.

The initial particle assembly was composed of 32 flat layers grouped into units with different mechanical properties to create a complex mechanical stratigraphy (Figs. 3 & 5). We have constructed a mechanical stratigraphy that we believe is suitable to model the behaviour of that observed in the

field (see Fig. 3 and Table 1 for a comparison between the sequence in the field and the model), reproducing a complex interlayering of competent/incompetent units as described below (from bottom to top; Fig. 5):

- Unit U1 - Highly competent unit. Five layers. Breaking separation (bst) = 0.05R
- Unit U2 - Highly incompetent unit. Four layers. bst = 0.00R
- Unit U3 - Competent unit. Five layers. bst = 0.04R
- Unit U4 - Incompetent unit. Three layers. bst = 0.002R
- Unit U5 - Low competence unit. Three layers. bst= 0.01R
- Unit U6 - Medium competence unit. Six layers. bst= 0.025R
- Unit U7 - Medium competence unit. Four layers. bst= 0.02R
- Unit U8 - Low competence unit. Two layers. bst= 0.01R

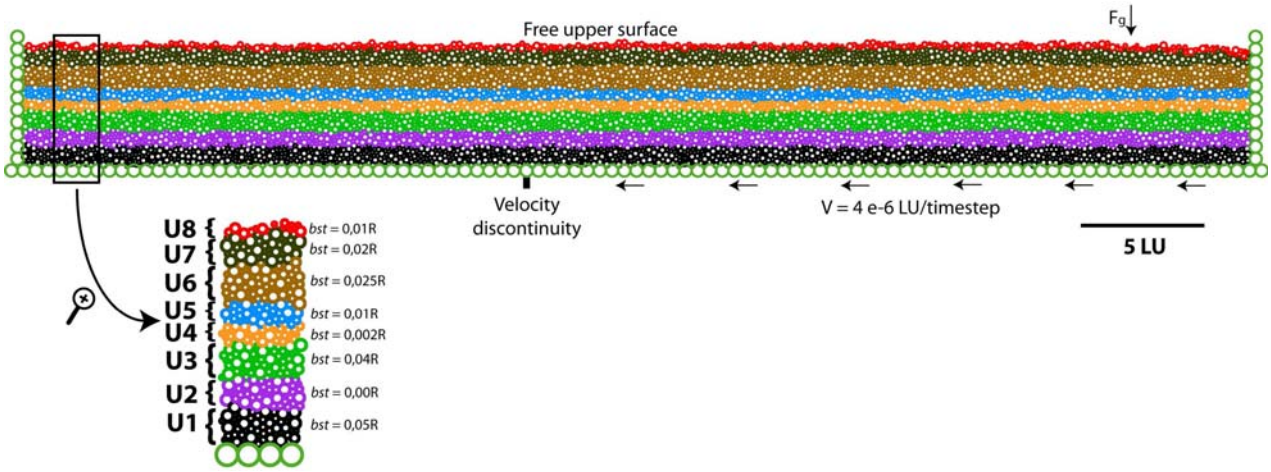

Fig. 5. Initial setup and boundary conditions applied in both Models 1 & 2. The initial assembly contains 10245 elements with radii of 31.25, 25, 18.75, and 12.5 m, positioned at random in a box that measures 12.5 x 1.25 km. The assemblage is composed of 32 flat-lying layers that are later grouped in eight units with different mechanical properties. Displacement is increased at 0.001 m/time-step. Fg corresponds to the force of gravity.

The mechanical behaviour of the stratigraphy observed in the field is used to guide that of the modelled units. In this sense, U1 simulates the behaviour of the M3 Muschelkalk facies, U2 models Keuper facies, U3 models Upper Cretaceous rocks, U4 models Garumnian facies, U5 models DS-1 of Guara Fm., U6 models DS-2 of Guara Fm., U7 models DS-3 of Guara Fm and U8 models the top of the Guara Fm. The syn-kinematic materials deposited during shortening of Model 2 are regarded as being highly incompetent (i.e. bst = 0.00R).

The breaking strain values have been chosen based on the expected mechanical behaviour of each unit guided by field observations (cf. Fig. 2). Our previous work has discussed in detail the effect of larger and smaller values of the breaking separation (see Finch et al., 2003; 2004). Large values of the threshold (e.g. 0.05R), equivalent to high elastic moduli, produce “competent” materials

Table 1. *Correlation between field and model stratigraphic units*

Field units	Model units
Campodarbe	Growth Strata
Belsué Atarés	Growth Strata
Arguis	Growth Strata
Guara DS-3	U7 & U8
Guara DS-2	U6
Guara DS-1	U5
Garumnian	U4
Upper Cretaceous	U3
Keuper	U2
Muschelkalk	U1

which fail by localised faulting, whereas low values (e.g. 0.002R) produce "incompetent" materials which deform in a macroscopically ductile manner as a result of non-localised deformation. It is important to note that we have set up the elements of U1 to be unlinked to the base of the box, in an attempt to reproduce the geological setting of the Muschelkalk dolomites and limestones, which are bounded by two ductile materials: the Keuper evaporitic claystone above and tentatively the unreported thin Middle Muschelkalk claystone and evaporites below: - as such the basal décollement is the boundary between U1 and the base of the model. Maps of the shear strain distribution at every stage of the model have also been generated, in order to identify the locii of deformation during shortening. To do so, we have used a free academic version of SSPX® developed by N. Cardozo (Cardozo & Allmendinger, 2009). SSPX calculates best-fitting strain tensors given displacement or velocity vectors at a minimum of three points in 2D. The shear strain plots presented here were generated by SSPX using a Delaunay algorithm to construct a mesh of triangles (at the start and end of the considered period) using the centre of each discrete element as a vertex.

Experimental Results

Two experiments have been carried out: Model 1 tests the effect of a complex mechanical stratigraphy on fold development; Model 2 explores the additional influence of growth strata. Both experiments have the same initial configuration with the aforementioned mechanical properties.

Model 1: Complex interlayering of competent/incompetent units

In this experiment, we only consider a pre-kinematic sequence with the mechanical properties described above (Fig. 5). The geometry and the shear strain distribution of the model at five stages are shown in Fig. 6 and are discussed below.

As expected, the structure starts to grow above the velocity discontinuity. After 4% bulk shortening (500 m; Fig. 6b) an open, gentle fold has developed: in the lower parts of the stratigraphic sequence it can be seen that a right-dipping fault has developed within U1 in the core of the fold, and that U2 has thickened in both flanks of the structure. In contrast, the upper units U3-U8 display a parallel, open anticline with no thickness variations or faulting. At the right border of the model, a small perturbation/fold has also formed due to the boundary effect of the nearby moving wall and this continues growing throughout the model run. However, it does not propagate from the right edge at any time and remains far from the central detachment fold of interest. The shear strain distribution map shows that shear strain (i.e. faulting) is concentrated in the incompetent units U2 and U4, and in the basal competent

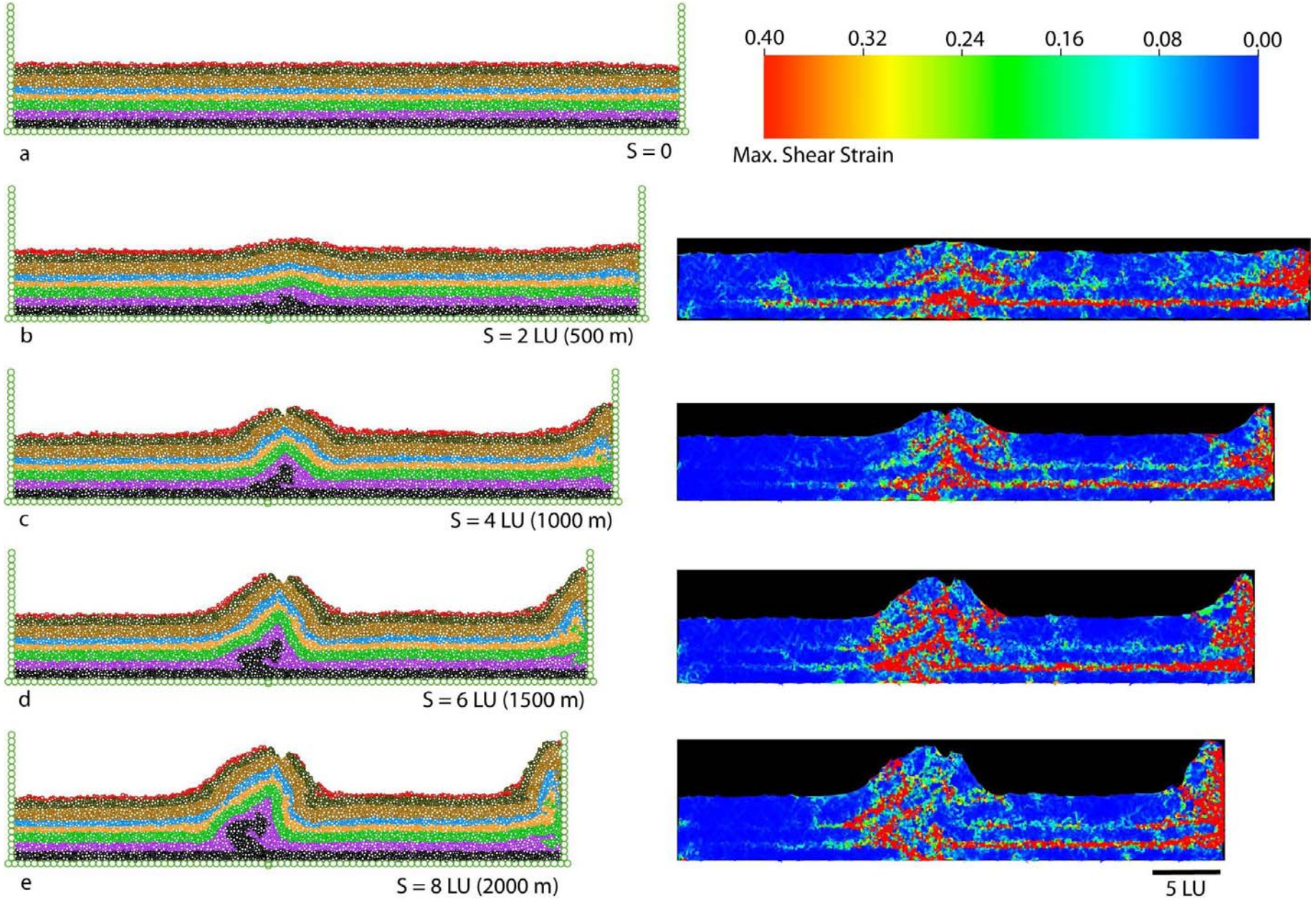
0.40
0.32
0.24
0.16
0.08
0.00
Max. Shear Strain
a
S = 0
b
S = 2 LU (500 m)
c
S = 4 LU (1000 m)
d
S = 6 LU (1500 m)
e
S = 8 LU (2000 m)
5 LU

Fig. 6. *(Previous page)* Evolution of Model 1 shown at: a) 0 m; b) 500 m; c) 1000 m; d) 1500 m; and e) 2000 m. The left column illustrates the geometrical evolution of the model as shortening continues. The right column shows the distribution of the incremental shear strain at the reported stages. Scale at the top-right of the figure illustrates the range of shear strain considered.

unit U1 (Fig. 6b). In U2 and U4 shear strain is continuous and high across much of the model from the right wall to the growing structure and towards the left wall. In the other units (U3 and U5-U8), shear strain is more diffuse and discontinuous. After 8% bulk shortening (1000 m; Fig. 6c) the disharmonic nature of the fold has been accentuated. Units U1 and U2 are now highly deformed, with marked hinge thickening and rightward thrusting of U1 on top of U2. However, above U2 an almost symmetric anticline continues to grow. Normal faulting is now seen in the crest of the structure, particularly in units U7 and U8. As before, U2 and U4 display high shear strain, particularly in the right-hand limb of the structure. In the other units (U3 and U5-U8), shear strain is more diffuse and discontinuous (Fig. 6c). After 12% bulk shortening (1500 m; Fig. 6d) the lower units, U1 and U2, are now complexly deformed. The wavelength of the anticline has increased, and the fold is now asymmetric with slight vergence towards the right. Deformation in U4 (as illustrated by incremental shear strain) is mainly concentrated in the left-hand limb, in contrast to the previous stage. During this stage fold growth is complex: the left-hand limb grows by a combination of limb-rotation and lengthening (this last one due to transport of material into the limb through the bounding synclinal hinge), with evident hinge migration of the left-hand syncline towards the left. Large hinge thickening of the anticline is observed, particularly in U2. On the other hand, the right-hand limb appears to grow mainly by rotation. Stretching in the outer arc persists, as indicated by continued normal faulting in the crestal region (Fig. 6d). Finally, after 16% bulk shortening (2000 m; Fig. 6e), the anticline appears to lock and the right-hand limb shows evidence of rightward thrusting cutting this limb. The right-hand limb is now vertical in U3 and almost overturned in U5. Crestal normal faulting has not developed further, suggesting a cessation of outer arc stretching. However, the hinge and the crestal normal faults have rotated clockwise (around 10º) with respect to the previous stage. Shear strain is particularly concentrated in the core of the structure (U1 and U2), but also along the limbs in units such as U3 and U5 (Fig. 6e).

The final structure is shown after 2000 m of total (boundary) shortening. At that stage, the central structure had reached the maximum amount of shortening that it could accommodate by folding. However, of this total, only ca. 1080 m of shortening were needed to form the central structure. The rest of the boundary displacement is consumed in layer-parallel shortening and in the formation of the right-border structure which in a regional/field sense can be thought of as an earlier or contemporaneous structure.

Model 2: Inclusion of syn-kinematic sedimentation

This experiment explores the effect of the syn-kinematic sedimentation on the structural evolution of a growing fold. The initial setup (Figs. 5 & 7a) comprises the same mechanically-interlayered (pre-kinematic) sequence as before. The geometrical and shear strain evolution of this model are shown in Fig. 7.

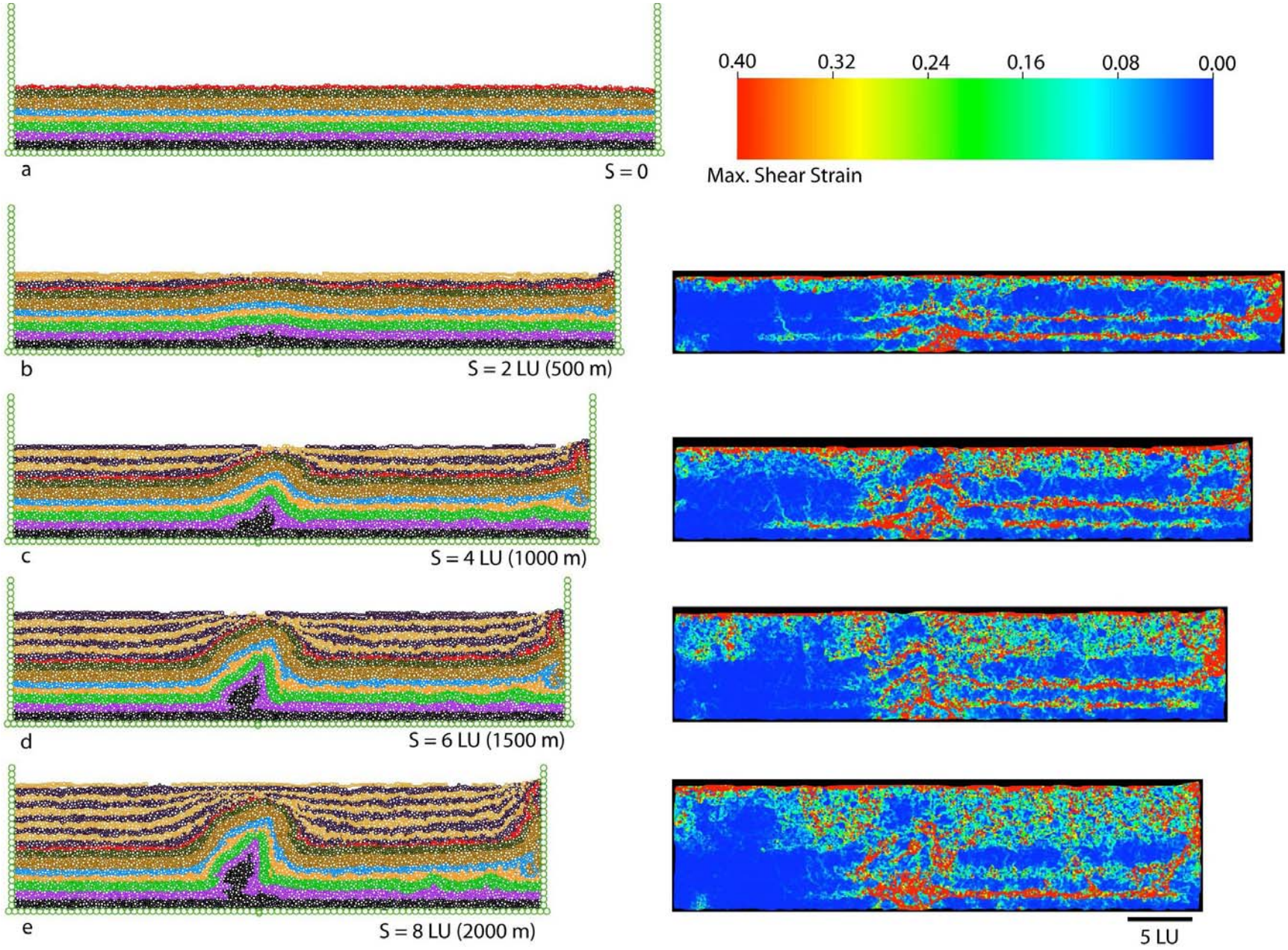
0.40
0.32
0.24
0.16
0.08
0.00
Max. Shear Strain
a
S = 0
b
S = 2 LU (500 m)
c
S = 4 LU (1000 m)
d
S = 6 LU (1500 m)
e
S = 8 LU (2000 m)
5 LU

Fig. 7. *(Previous page)* Evolution of Model 2 shown at: a) 0 m; b) 500 m; c) 1000 m; d) 1500 m; and e) 2000 m. The left column illustrates the geometrical evolution of the model as shortening continues. The right column shows the distribution of the incremental shear strain at the reported stages. Scale at the top-right of the figure illustrates the range of shear strain considered.

After 4% bulk shortening (500 m; Fig. 7b) a small, low amplitude, structure has started to grow above the velocity discontinuity, as a perturbation with layer-parallel geometry. The incompetent units U2 and U4 exhibit high shear strain in both the structure itself and some distance across the model. Competent unit U1 shows high shear strain and is complexly deformed in the core of the anticline. The other pre-kinematic units only exhibit low shear strain which is slightly accentuated in the fold (Fig. 7b). On the other hand, the growth strata show high but variable amounts of shear strain. However, two types of strain within the growth strata package must be distinguished. Firstly, the shear strain due to the recent deposition and ongoing compaction of the recently deposited units, essentially restricted to the uppermost two layers of the assembly (i.e. the thin horizontal red area at the top of the strain distribution maps; Fig. 7). Secondly, the shear strain exhibited by the growth pile due to shortening and consequent fold development. As in Model 1, a border-effect is generated at the right-hand edge of the model due to the displacement of this wall towards the left. After 8% bulk shortening (1000 m; Fig. 7c), the central structure has grown significantly, its limbs have steepened and now it verges slightly towards the right. Disharmonic folding is now observed in the stratigraphic sequence. Below U4 minor folds have developed, particularly in U2-U4 towards the right-hand edge of the model, and the core of the structure is now becoming complexly deformed in U1. Above U4, the pre-kinematic units define a gentler fold geometry, with no thickness changes or minor folds observed. The syn-kinematic sequence now shows marked thickness variations producing flanking sedimentary wedges which thin towards the crest of the anticline. In contrast to Model 1, no normal faulting is observed in the crest of the structure. Within the growth strata package, moderate to high shear strain is observed and a distinct contrast in shear strain is observed at the base of the growth strata package. After 12% bulk shortening (1500 m; Fig. 7d), thickening of the incompetent units is seen in the hinge of both flanking synclines and the core of the fold becomes highly deformed. In particular, U1 starts to become dramatically deformed, displaying a bottle-neck geometry. Small folds continue to grow in U2 between the anticline and the right-hand model border. Disharmonic folding is observed in the hinge of the anticline, with folding style above and below U4 differing markedly. Shear strain continues to be concentrated within the incompetent units involved in the fold and their continuation towards the right-hand wall. Growth strata continue to rotate and thin against the growing structure displaying much internal shear strain. At 16% bulk shortening (2000 m; Fig. 7e) the anticline appears to cease to grow upwards (note that growth strata now overlap the structure) with the fold tightening by limb rotation. However, the model shows a shift in the distribution of shortening from the central fold to the right edge, manifested by propagation of folding from the right edge, and giving rise to small décollement folds detached on U2. In the main fold, shear strain continues to be concentrated in the core of the structure,

together with shear of the fold limbs particularly in U4 and U5. In the core of the fold U1 is further "pinched" into a bottle-neck structure. At this stage, the growth strata package is about 1.2 km thick, similar to the one observed in nature at Pico del Águila.

Discussion

The aim of this work has been to test the effect of a complex mechanical stratigraphy and growth strata on the development of detachment folds and compare the results to the Pico del Águila anticline (Central External Sierras, Southern Pyrenees). This was the primary motivation for this work: in the core of this anticline, field observations and geological mapping suggest a potentially complex structure and only scarce, poor-quality seismic data are available. In addition, outcrop data do not help to reveal much of the structure at depth (Fig. 8). Our objective was therefore to use the discrete element approach to provide new insights into the geometry and evolution of this structure.

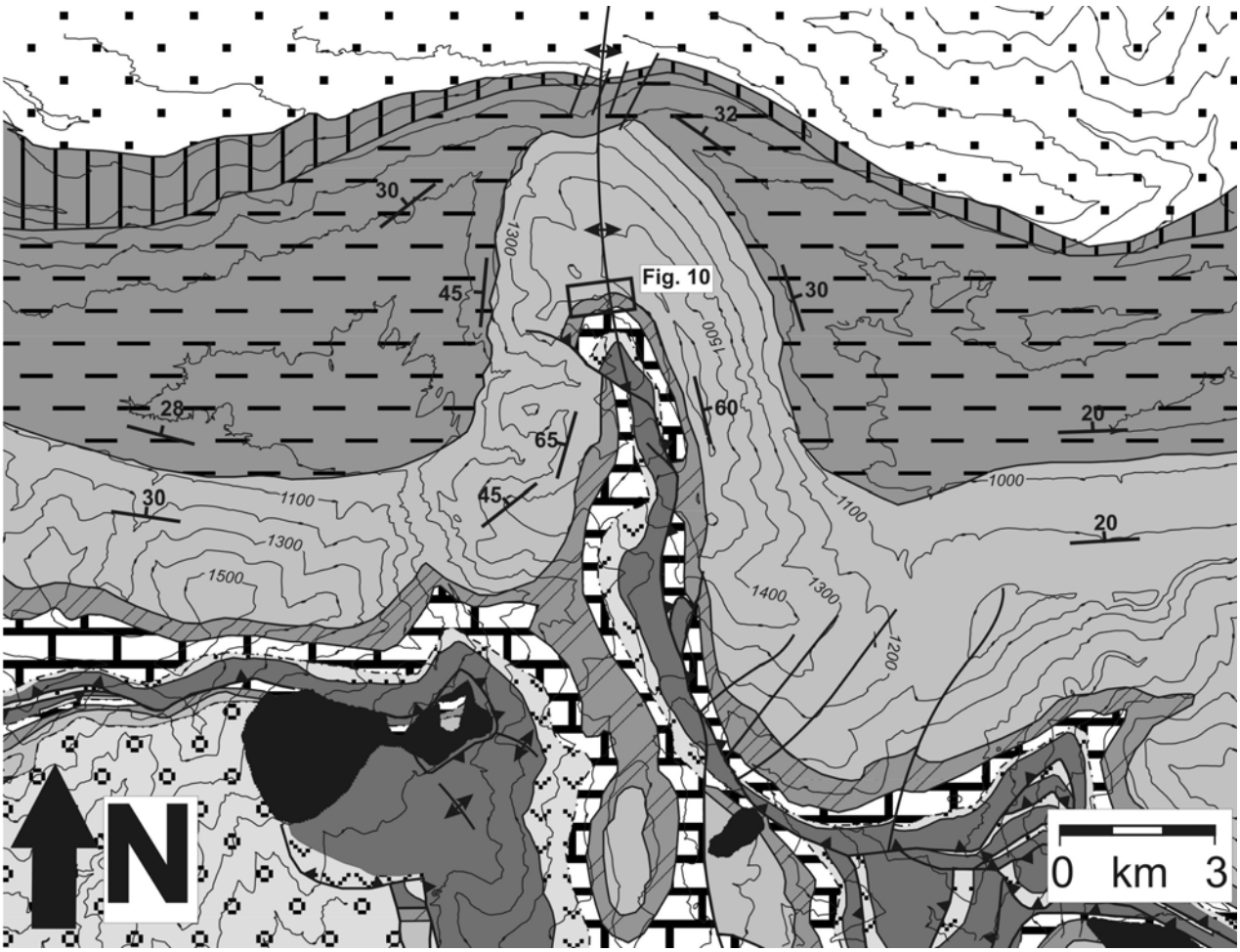

Fig. 8. Geological map of the Pico del Águila anticline (modified from IGME, 1992). Notice the geometrical similarities between the model results and the structure in nature: growth strata sedimentary prism, folding in the upper units, and faulting in the lower units. See Fig.1 for legend.

In general, the modelling results have proven informative and the approach successful. In particular, model results have highlighted the dramatic change in structural style between units U1-U2 and the overlying stratigraphic sequence. The model results re-emphasise that the structural evolution of a growing fold strongly depends on the mechanical behaviour of the stratigraphic sequence involved. The presence of multiple incompetent levels (U2 and U4 in Models 1 and 2; and, less importantly, the syn-kinematic package in Model 2), leads to a complex partitioning of shear strain within the stratigraphic sequence. As a consequence, disharmonic folding is seen in both Models 1 and 2.

In both models fold growth started at an early stage above the velocity discontinuity as a nearly symmetric, constant-thickness, open fold with gently-dipping limbs. Further shortening resulted in fold growth by a combination of limb lengthening and limb rotation. This development, however, is not homogeneous throughout the stratigraphic sequence. The upper units above U4 grew mainly by limb lengthening whereas the units below grew mainly by limb rotation. This led to disharmonic folding, as the upper, outer layers dip more gently than the inner ones, which reach vertical and overturned dip values. It appears that folding mechanisms do not solely depend on the mechanical behaviour of a given unit, but they are also driven by its relationship with the immediately adjacent units (i.e., the mechanical contrast between a unit and its neighbours, or brittle-ductile coupling in the sense of Smit et al., 2003).

It is notable that small-scale extensional faulting took place at the crest of the anticline in Model 1 (Fig. 9a). This was mainly due to the stretching produced in the outer layers and to the gravitational instability of the structure produced as its amplitude increased. This effect was diminished in Model 2 as flanking sedimentation took place during shortening and fold growth (Fig. 9b). Since the pre-kinematic outer arc was buried under the growth strata, the syn-kinematic sedimentary load minimised the stretching and supported the fold, reducing any potential gravitational instabilities.

Syn-kinematic materials have been modelled as a mass of cohesionless elements and, thus, have acted as an incompetent level on top of the pre-kinematic sequence. Syn-kinematic materials are thus deformed pervasively, as observed in the shear strain distributions shown in Fig. 7. This deformation has been mainly by small-scale folding and distributed faulting. However, due to the additional load, the syn-kinematic pile also influences the deformation within the pre-growth sequence. In other words, this additional load confines the deformation to the core of the structure, which is tighter in Model 2 compared to in Model 1 (Fig. 9), by means of multiple faults and disharmonic folding (see the bottle-neck structure in Fig. 9b). As observed in Model 1 (Figs. 6 & 9a), the lack of a syn-kinematic load leads to a fold which is more open, and which widens with increasing shortening. Summarizing, the effect of syn-kinematic sedimentation in the development of a growing fold is double: firstly, it minimises stretching in the upper, outer units of the structure; and secondly, it influences growth of the anticline generating a tighter, more complex and upright structure in the inner, lower units.

In both models, it is also noticeable that shortening produces a detachment fold in a stratigraphic sequence in which the basal unit is not a simple, homogeneous ductile unit. Both competent and incompetent units

(U1 and U2) are involved and highly deformed in the core of the anticline. The lack of any bonding between U1 and the base of the box (modelling the suspected interaction between Muschelkalk dolomites and the underlying evaporitic clays) as well as the presence of the incompetent U2 above it means that the basal highly competent unit is bordered by two ductile materials and thus it can fold freely.

Most of the features described above have parallels in the Pico del Águila anticline. Given that the anticline plunges towards the North up to 40º, the down-plunge view offered by the geological map can be considered as an equivalent to a cross-section of the structure (Fig. 8), comparable to the results obtained in Models 1 and 2. The stratigraphic record of the area is characterised by an interlayering of competent/incompetent units (Figs. 2 & 3), which appear to have exerted a strong influence on the generation and development of the fold. As observed in Fig. 8, a dramatic change in structural style exists between the lower and the upper units: the Muschelkalk-middle Guara sequence is faulted and complexly deformed whereas the overlying upper Guara-Campodarbe sequence is more simply folded. Model 2 (Fig. 9b) has reproduced this behaviour since the U1-U4 sequence is complexly faulted and folded whereas the overlying strata are more simply folded. Such disharmonic folding is observed in the hinge area of Pico del Águila (Fig. 10).

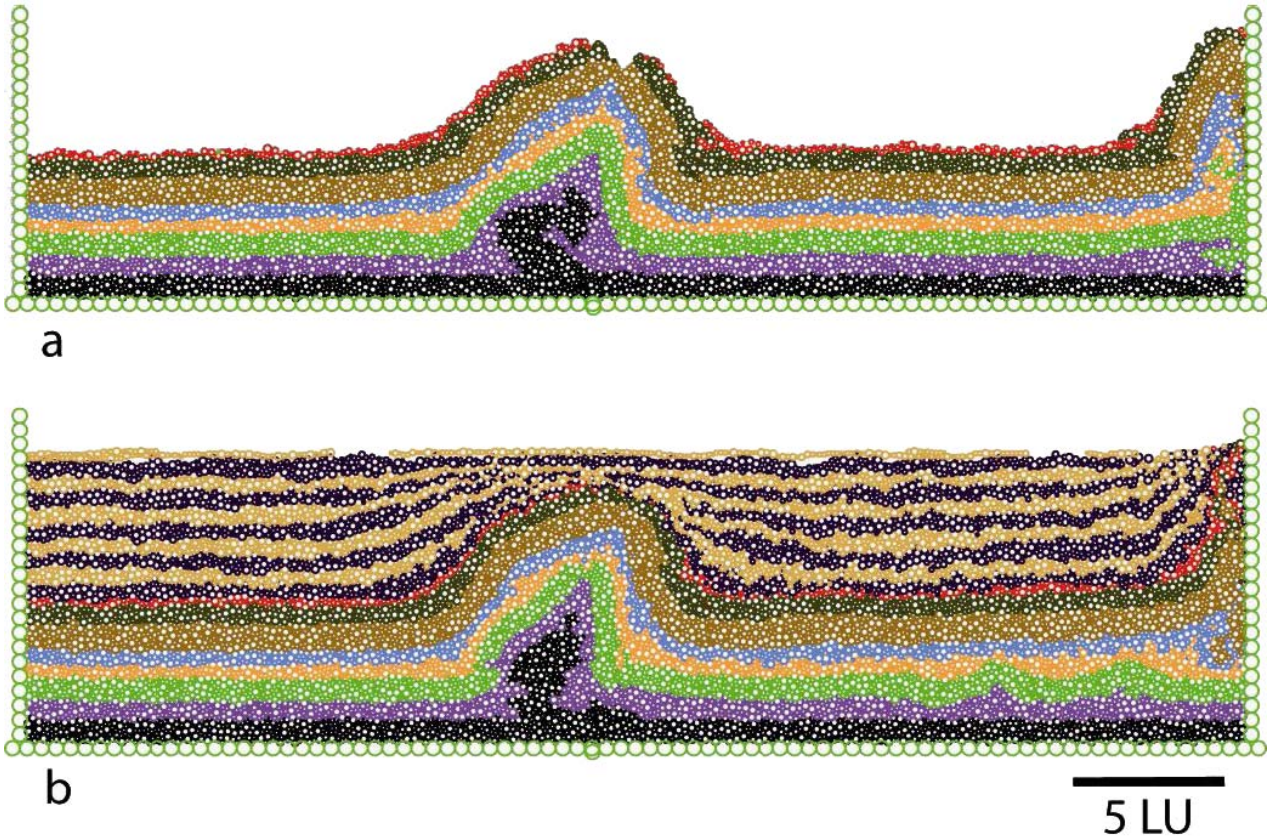

Fig. 9. Final geometries of Model 1 (a) and Model 2 (b) after 2000 m of shortening. Both experiments had identical initial configurations (see Fig. 5) and mechanical properties. However, Model 2 included sedimentation during shortening, producing the observed growth strata pattern.

Model results suggest a non-concentric geometry for the Pico del Águila, in which some pre-kinematic units (U6, U5 and U3) show minor disharmonic folds in the crest of the anticline whereas U2 does not display such behaviour. An almost identical phenomenon is observed in Fig. 10, where Guara Fm shows minor metric folds in the crest of the Pico del Águila, above the Garumnian, which does not exhibit such disharmonic folding. In addition, the geometry of the growth strata bears a striking resemblance to that seen in Model 2, including small scale reverse faulting along the limbs (observed in the field) and very local normal faulting in the crest of the anticline (see Fig. 8). This crestal normal faulting, however, is not well represented in Model 2 since the scale of these faults in the field (ca. 50 m) is within the order of magnitude of the element sizes used in the models (ca. 12-31 m).

Fig. 10. Photograph illustrating the disharmonic folding observed in the hinge of the Pico del Águila anticline (see Fig. 8 for location): upper layers showing minor associated folds correspond to the base of Guara Fm., whereas lower highly-vegetated layers correspond to the top of the Garumnian facies.

Summarising, the modelling indicates that it is unlikely that the complex interplay of parameters occurring in nature can be easily explained in terms of simple, single folding mechanisms/kinematics. Limb rotation, limb lengthening, faulting, hinge migration, hinge thickening, among others, usually act coevally depending on the mechanical properties of individual units and their stratigraphic position. In addition, this contribution indicates that growth strata, when present during the evolution of a structure, are not just simple passive markers - rather they are

mechanically important in the evolution of a structure.

Conclusions

A 2D discrete-element modelling technique has been used to test the influence of complex competent/incompetent interlayering and the presence of growth strata in the generation and development of the Pico del Águila anticline. The model simulates the sedimentary sequence as an assemblage of circular elements that interact in pairs with elastic forces influenced by gravity and obey Newton's equations of motion. The mechanical interlayering leads to high shear strain and complex deformation within the incompetent units, whereas the competent units are subject to more distributed shear strain and simple folding. As a result of the differing mechanical responses to shortening, it is difficult to explain the evolution of such a structure in terms of simple kinematic models. Furthermore, the addition of growth strata reduces the effects of stretching, extensional faulting and gravitational instabilities on the crest of the anticline. Finally, the load of the syn-kinematic package also led the deformation to be more confined to the core of the structure, which is thus tighter than in the case where growth strata are lacking.

Acknowledgements: We would like to thank Néstor Cardozo for the free academic use of SSPX to generate the shear strain distribution maps presented in this work. In addition, discussions with Stefano Tavani are gratefully acknowledged. The Group of Geodynamics and Basin Analysis (GGAC) at Universitat de Barcelona is also acknowledged for their support (2005SGR 00397 and 2009 SGR 1198). This research has also been supported by ICREA, StatoilHydro, the Geomod 3D project (CGL2004-05816-C02-01/BTE), the MODES-4D project (CGL2007-66431-C02-01/BTE) and the Geomodels Institute Consortium. O. Vidal-Royo is grateful to Agència de Gestió d'Ajuts Universitaris i a la Recerca (AGAUR) for providing a PhD grant (2005 FI 00200). Dr W. Wallace, Dr S. Castelltort, Dr. J. Poblet and Dr R. J. Lisle are gratefully acknowledged for thorough reviews that have definitely improved the quality of this work.

References

ATKINSON, P.A. & WALLACE, W.K. 2003. Competent unit thicknesses in detachment folds in the Northeastern Brooks Range, Alaska: geometric analysis and a conceptual model. *Journal of Structural Geology*, **25**, 1751-1771.

CAMBORDE, F., MARIOTTI, C. & DONZÉ, F.V. 2000. Numerical study of rock and concrete behaviour by discrete element modelling. *Computers and Geotechnics*, **27 (4)**, 225-247.

CARDOZO, N. & ALLMENDINGER, R.W. 2009. SSPX: A program to compute strain from displacement/velocity data. *Computers and Geosciences*, **35 (6)**, 1343-1357.

CASAS-SAINZ, A.M., SOTO-MARÍN, R., GONZÁLEZ, A. & VILLALAÍN, J.J. 2005. Folded onlap geometries: implications for recognition of syn-sedimentary folds. *Journal of Structural Geology*, **27**, 1644-1657.

CASTELLTORT, S., GUILLOCHEAU, F., ROBIN, C., ROUBY, D., NALPAS. T., LAFONT, F. & ECHARD, R. 2003. Fold control on the stratigraphic record: a quantified sequence stratigraphic study of the Pico del Aguila anticline in the south-

western Pyrenees (Spain). *Basin Research*, **15**, 527-551.

DONZÉ, F., MAGNIER, S.A. & BOUCHEZ, J. 1996. Numerical modelling of a highly explosive source in an elastic-brittle rock mass. *Journal of Geophysical Research*, **101 (2)**, 3103-3112.

FINCH, E., HARDY, S. & GAWTHORPE, R.L. 2003. Discrete element modelling of contractional fault-propagation folding above rigid basement blocks. *Journal of Structural Geology*, **25**, 515-528.

FINCH, E., HARDY, S. & GAWTHORPE, R.L. 2004. Discrete element modelling of extensional fault-propagation folding above rigid basement fault blocks. *Basin Research*, **16**, 489-506.

GRANDO, G. & MCCLAY, K.R. 2007. Morphotectonics domains and structural styles in the Makran accretionary prism, offshore Iran. *Sedimentary Geology*, **196**, 157-179.

HARDY, S & FINCH, E. 2005. Discrete-element modelling of detachment folding. *Basin Research*, **17**, 507-520.

HARDY, S & FINCH, E. 2007. Mechanical stratigraphy and the transition from trishear to kink-band fault-propagation fold forms above blind basement thrust faults: A discrete-element study. *Marine and Petroleum Geology*, **24**, 75-90.

HARDY, S., MCCLAY, K.R. & MUÑOZ, J.A. 2009. Deformation and fault activity in space and time in high resolution numerical models of doubly vergent thrust wedges. *Marine and Petroleum Geology*, **26**, 232-248.

HOMZA, T.X. & WALLACE, W.K. 1995. Geometric and kinematic models for detachment folds with fixed and variable detachment depths. *Journal of Structural Geology*, **17**, 475-488.

HOMZA, T.X. & WALLACE, W.K. 1997. Detachment folds with fixed hinges and variable detachment depth, Northeastern Brooks Range. *Journal of Structural Geology*, **19**, 337-354.

IGME. 1987. *Contribución de la exploración petrolífera al conocimiento de la geología de España*. Instituto Geológico y Minero de España. Published report plus maps.

IGME. 1992. *Mapa Geológico de España*, Map **248** (Apiés), Instituto Geológico y Minero de España, Madrid, Unpublished 36 pp report + 1:50000 map.

KUHN, M.R. 1999. Structured deformation in granular materials. *Mechanics of Materials*, **31**, 407-429.

MCELROY. R. 1990. *Thrust kinematics and syntectonic sedimentation: the Pyrenean frontal ramp, Huesca, Spain*. PhD Thesis, University of Cambridge.

MILLÁN, H. 1995. *Estructura y Cinemática del frente de cabalgamiento surpirenaico en las Sierras Exteriores Aragonesas*, PhD Thesis, Universidad de Zaragoza.

MILLÁN, H., AURELL, M. & MELÉNDEZ, A. 1994. Synchronous detachment folds and coeval sedimentation in the Prepyrenean External Sierras (Spain): a case study for a tectonic origin of sequences and system tracts. *Sedimentology*, **41 (5)**, 1001-1024.

MITRA, S. 2003. A unified kinematic model for the evolution of detachment folds. *Journal of Structural Geology*, **25**, 1659-1673.

MORA, P. & PLACE, D. 1993. A lattice solid model for the non-linear dynamics of earthquakes. *International Journal of Modern Physics C*, **4 (6)**, 1059-1074.

NALPAS, T., GYÖRFI, I., GUILLOCHEAU, F., LAFONT, F. & HOMEWOOD, P. 1999. Influence de la charge sédimentaire sur le développement d'anticlinaux synsédimentaires. Modélisation analogique et exemple du terrain (bordure sud du basin de Jaca). *Bulletin de la Societé Géologique de France*, **170 (5)**, 733-740.

NIGRO, F. & RENDA, P. 2004. Growth patterns of underlithified strata during thrust-related folding. *Journal of Structural Geology*, **26,** 1913–1930.

NOVOA, E., SUPPE, J. & SHAW, J.H. 2000. Inclined-Shear Restoration of Growth Folds. *AAPG Bulletin*, **84 (6)**, 787-804.

PLACE, D. & MORA, P. 2001. A random lattice solid model for simulation of fault zone dynamics and fracture processes. *In:* Mulhaus, H.B., Dyskin, A.V. & Pasternak, E. (eds), *Bifurcation and Localisation Theory for Soils and Rocks '99*. A.A. Balkema, Rotterdam/Brookfield.

POBLET, J. & HARDY, S. 1995. Reverse modelling of detachment folds, application to the Pico del Aguila anticline in the South Central Pyrenees (Spain). *Journal of Structural Geology*, **17**, 1707-1724.

POBLET, J., MCCLAY, K.R., STORTI, F. & MUÑOZ, J.A. 1997. Geometries of syntectonic sediments associated with single-layer detachment folds, *Journal of Structural Geology*, **19**, 369-381.

PUEYO, E.L., MILLÁN, H. & POCOVÍ, A. 2002. Rotation velocity of a thrust: a paleomagnetic study in the External Sierras (Southern Pyrenees*). Sedimentary Geology*, **146 (1)**, 191-208.

PUIGDEFÀBREGAS, C. 1975. La Sedimentación Molásica en la Cuenca de Jaca. *Monografias del Instituto de Estudios Pirenaicos. Número Extraordinario de Revista Pirineos*, **104**, Instituto de Estudios Pirenaicos, Jaca, 153 pp + appendix.

SMIT, J.H.W., BRUN, J.P. & SOKOUTIS, D. 2003. Deformation of brittle-ductile thrust wedges in experiments and nature. *Journal of Geophysical Research*, **108 (B10)**, 2480, doi: 10.1029/2002JB002190.

STORTI, F. & POBLET, J. 1997. Growth stratal architectures associated to décollement folds and fault-propagation folds. Inferences on fold kinematics. *Tectonophysics*, **282**, 353-373.

STRAYER, L.M., ERICKSON, S. G. & SUPPE, J. 2004. Influence of growth strata on the evolution of fault-related folds: Distinct-element models. *In:* McClay, K. (ed), *Thrust Tectonics and Hydrocarbon Systems*. American Association of Petroleum Geologists Memoir, **82**, 413-437.

TAVANI, S., STORTI, F. & SALVINI, F. 2007. Modelling growth stratal architectures associated with double edge fault-propagation folding. *Sedimentary Geology*, **196**, 119-132.

CHAPTER IV

Multiple mechanisms driving detachment folding as deduced from 3D reconstruction and geomechanical restoration

The third scientific article is presented herein. This chapter presents a field-based 3D reconstruction and geomechanical restoration of the Pico del Águila anticline, from which multiple folding mechanisms acting in different units and structural domains have been derived. An abridged summary in Catalan is presented firstly, followed by the abridged abstract in English and the publication itself. The work has been submitted to the journal *Basin Research* and is cited as follows:

Vidal-Royo, O., Cardozo, N., Muñoz, J.A., Hardy, S., Maerten, L., (in review). Multiple mechanisms driving detachment folding as deduced from 3D reconstruction and geomechanical restoration: The Pico del Águila anticline (External Sierras, Southern Pyrenees). Submitted to Basin Research.

4.1 RESUM DEL CAPÍTOL (Summary in Catalan)

En aquest capítol es presenta el tercer article científic de la Tesi. Es tracta en aquest cas de una reconstrucció 3D a partir de dades de camp de l'anticlinal del Pico del Águila, seguida d'una restitució geomecànica de l'estructura. Aquest exercici ha permès posar de manifest la complexitat associada als plecs de desenganxament quant a mecanismes de plegament es refereix. Múltiples mecanismes s'han deduït a partir de la reconstrucció i restitució 3D de l'anticlinal, els quals actuen simultàniament en diferents unitats i dominis estructurals del plec.

La modelització 3D permet la representació i observació d'aspectes geològics que poden romandre desapercebuts en entorns bidimensionals. Aquest fet és d'especial rellevància en el cas de l'anticlinal del Pico del Águila, donada la gran variabilitat de geometria que presenta l'estructura en les tres dimensions de l'espai. El Pico del Águila és un plec d'orientació N-S, perpendicular a la tendència estructural general dels Pirineus (E-W). L'anticlinal exhibeix també un registre complet dels estrats de creixement associats a la seva evolució, amb unes excel·lents condicions d'afloració i accessibilitat. Aquest fet permet doncs una acurada reconstrucció de la geometria dels estrats de creixement en 3D, i una conseqüent restitució seqüencial de l'estructura amb control temporal de cadascuna de les seqüències deposicionals descrites al Capítol I.

Malgrat tractar-se d'una estructura ben estudiada, la cinemàtica del plec és complexa i no ha estat precisada d'una manera quantitativa. Es caracteritza per una rotació d'eix vertical, amb múltiples mecanismes de plegament actuant simultàniament en una estratigrafia mecànicament heterogènia. Per tal de millorar el coneixement sobre l'evolució estructural del Pico del Águila, s'han portat a terme una reconstrucció i restitució geomecànica 3D de l'estructura.

L'algoritme de restitució emprat es basa en les propietats mecàniques de les roques (mòdul de Young, coeficient de Poisson, densitat, entre d'altres) sense assumir cap criteri cinemàtic previ. Per contra, la restitució de l'anticlinal dedueix una rotació d'eix vertical en sentit destre de 33°, així com una notable

variabilitat de les taxes de sedimentació i aixecament entre flancs i durant l'evolució de l'estructura. La restitució revela una combinació de mecanismes de plegament produint-se simultàniament en diferents unitats i dominis estructurals durant el creixement de l'anticlinal. En aquest sentit, hom dedueix que les variacions espacials de les propietats mecàniques de les roques són de gran rellevància en el control de l'evolució estructural d'un plec de desenganxament, i per tant no poden ser eludides a l'hora d'establir un model conceptual de creixement.

4.2 ABRIDGED SUMMARY

3D modelling allows the observation of geological features that may not be evident by classical 2D approaches. This is particularly important in the Pico del Águila anticline (Central External Sierras, Southern Pyrenees, Spain), a structure characterized by important geometrical variability in 3D. The Pico del Águila is a N-S trending fold, transverse to the E-W trending South-Pyrenean thrust front, and with well-exposed growth strata that record the evolution of the structure and the interference effect of the South-Pyrenean thrust front. The kinematics of the fold is complex and not precisely quantified. It is characterized by vertical axis rotation, with multiple folding mechanisms acting simultaneously in a heterogeneous stratigraphic sequence. To better understand its structural evolution, 3D reconstruction and geomechanical restoration of the structure were performed. The restoration takes into account rock mechanical properties without assuming a kinematic model. A clockwise rotation of the structure of 33º is deduced from the restoration, as well as variable uplift/sedimentation rates through time and between fold limbs. The restoration reveals a combination of multiple folding mechanisms occurring simultaneously in different units and structural domains during anticlinal growth. Spatial variations in rock mechanical properties are very important to understand the evolution of the structure.

*Submitted to **Basin Research** (in review)*

Multiple mechanisms driving detachment folding as deduced from 3D reconstruction and geomechanical restoration: The Pico del Águila anticline (External Sierras, Southern Pyrenees)

O. Vidal-Royo*, N. Cardozo†, J.A. Muñoz [*], S. Hardy * ‡ and L. Maerten §

* *Geomodels Research Centre. GGAC, Departament de Geodinàmica i Geofísica, Facultat de Geologia, Universitat de Barcelona. C/ Martí i Franquès s/n, 08028, Barcelona, Spain*

† *Department of Petroleum Engineering, University of Stavanger. 4036 Stavanger, Norway*

‡ *ICREA (Institució Catalana de Recerca i Estudis Avançats), Catalonia, Spain*

§ *IGEOSS sarl, Parc Euromédecine, 340 rue Louis Pasteur, 34790, Grabels, France*

ABSTRACT

3D modelling allows the observation of geological features that may not be evident by classical 2D approaches. This is particularly important in the Pico del Águila anticline (Central External Sierras, Southern Pyrenees, Spain), a structure characterized by important geometrical variability in 3D. The Pico del Águila is a N-S trending fold, transverse to the E-W trending South-Pyrenean thrust front, and with well-exposed growth strata that record the evolution of the structure and the interference effect of the South-Pyrenean thrust front. The kinematics of the fold is complex and not precisely quantified. It is characterized by vertical axis rotation, with multiple folding mechanisms acting simultaneously in a heterogeneous stratigraphic sequence. To better understand its structural evolution, 3D reconstruction and geomechanical restoration of the structure were performed. The restoration takes into account rock mechanical properties without assuming a kinematic model. A clockwise rotation of the structure of 33º is deduced from the restoration, as well as variable uplift/sedimentation rates through time and between fold limbs. The restoration reveals a combination of multiple folding mechanisms occurring simultaneously in different units and structural domains during the anticline growth. Spatial variations in rock mechanical properties are very important to understand the evolution of the structure.

INTRODUCTION

Fault-related folds are principal elements of fold-and-thrust belts. They result from the combination of local deformation associated to folding and regional deformation due to faulting. Detachment folds are common features in a large number of fold-and-thrust belts occurring above a basal detachment within a ductile unit (Mitra, 2003). In these structures, folding mechanisms are strongly dependent on mechanical stratigraphy and the coupling between incompetent/competent units (Davis and Engelder, 1985; Mitra, 2003; Vidal-Royo *et al.*, 2009). This has influence on how strain, fractures, and petrophysical properties are distributed throughout the structure, which has major implications for the exploration and production of natural reservoirs.

In this study, we explore the folding mechanisms and the structural evolution of the Pico del Águila, a world-class example of a detachment anticline in the External Sierras of the Southern Pyrenees (Spain). The good exposure of the structure allows the creation of a geological map that can be understood as a down-plunge projection of the anticline (Fig. 1). The high degree of preservation of the growth strata record allows us to constrain the fold kinematics as well as the timing of deformation. The Pico del Águila is a N-S anticline, transverse to the E-W Pyrenean-trend structures, and characterized by an interference pattern with the Pyrenean structures. The anticline is thus a truly 3D structure. The Pico del Águila is well known and has been reported in a plethora of publications. The kinematics and structural evolution of the anticline have been derived from sedimentological analysis (Millán *et al.*, 1994; Castelltort et al., 2003), paleomagnetism (Pueyo *et al.*, 2002; Rodríguez-Pintó *et al.*, 2008), 2D kinematical models (Poblet and Hardy, 1995; Poblet *et al.*, 1997), restoration of cross sections (Novoa *et al.*, 2000), and multi-disciplinary approaches (Huyghe, *et al.*, 2009). However, no studies have tackled the structural evolution of the anticline in 3D, in spite of its good 3D exposure. This makes the Pico del Águila an ideal structure to carry out a field-based 3D reconstruction and sequential restoration in order to understand the mechanisms that created the structure and lead its evolution.

One of the advantages of 3D reconstruction of geological bodies is the capability of integrating all available data (field mapping, dip measurements, 2D and 3D seismic, wells, gravimetry, resistivity, etc.) in the same framework, such that the data sets validate each other and give rise to a reliable model. 3D reconstructions have proven useful to better visualize and understand the geometry and property distribution of geological bodies (Borraccini et al., 2002; Tanner et al., 2003; Fernández et al., 2004; Ford et al., 2007; Zanchi et al., 2009), which is very important in hydrocarbons exploration and production, well planning, and civil engineering among others (Bistacchi et al., 2007; Guzofski et al., 2009; Moretti, 2008). Many investigations can be carried out based on 3D geomodels. Strain distribution analysis (Moretti, 2008; Guzofski et al., 2009), discrete fracture network modelling (Sanders et al., 2004; Maerten et al., 2006), characterization of sedimentary facies (Falivene, 2007; Braathen et al., 2009), kinematical (Sanders et al., 2004; Moretti, 2008) or mechanical-based restorations (Maerten and Maerten, 2006; Guzofski et al., 2009), to mention a few, are one step further in the understanding of 3D sedimentary and tectonic processes.

Geologists have used structural restoration of 3D geomodels as a tool to better understand the chronology and building mechanisms of geological structures. 3D structural restoration has proven useful to reproduce the stress and strain fields associated with the development of structures, and to predict from these fields mesoscopic structures such as fractures (Sanders et al., 2004; Maerten

and Maerten, 2006; Maerten, 2007; Grando et al., 2009). A variety of approaches considering different assumptions and parameters are used to restore the geometry of the structure back to its initial non-deformed state. Most of the restoration algorithms consist of geometric/kinematic methods. These methods aim to check the robustness of the structural interpretation and to emulate natural deformation by means of geometric (conservation of line/area, limb/fault dip, curvature, aperture, angle between flanks, etc) or kinematic (rate of deformation, displacement path, etc) criteria (Poblet and Hardy, 1995; Rouby and Cobbold, 1996; Poblet et al., 1997; Novoa et al., 2000; Tanner et al., 2003; Moretti, 2008). However, the kinematics of the geological structures is often unknown or, at least, not precisely quantified. Therefore, these methods present a major limitation which is that an ad-hoc kinematics must be assumed to perform the restoration, with the geometry of

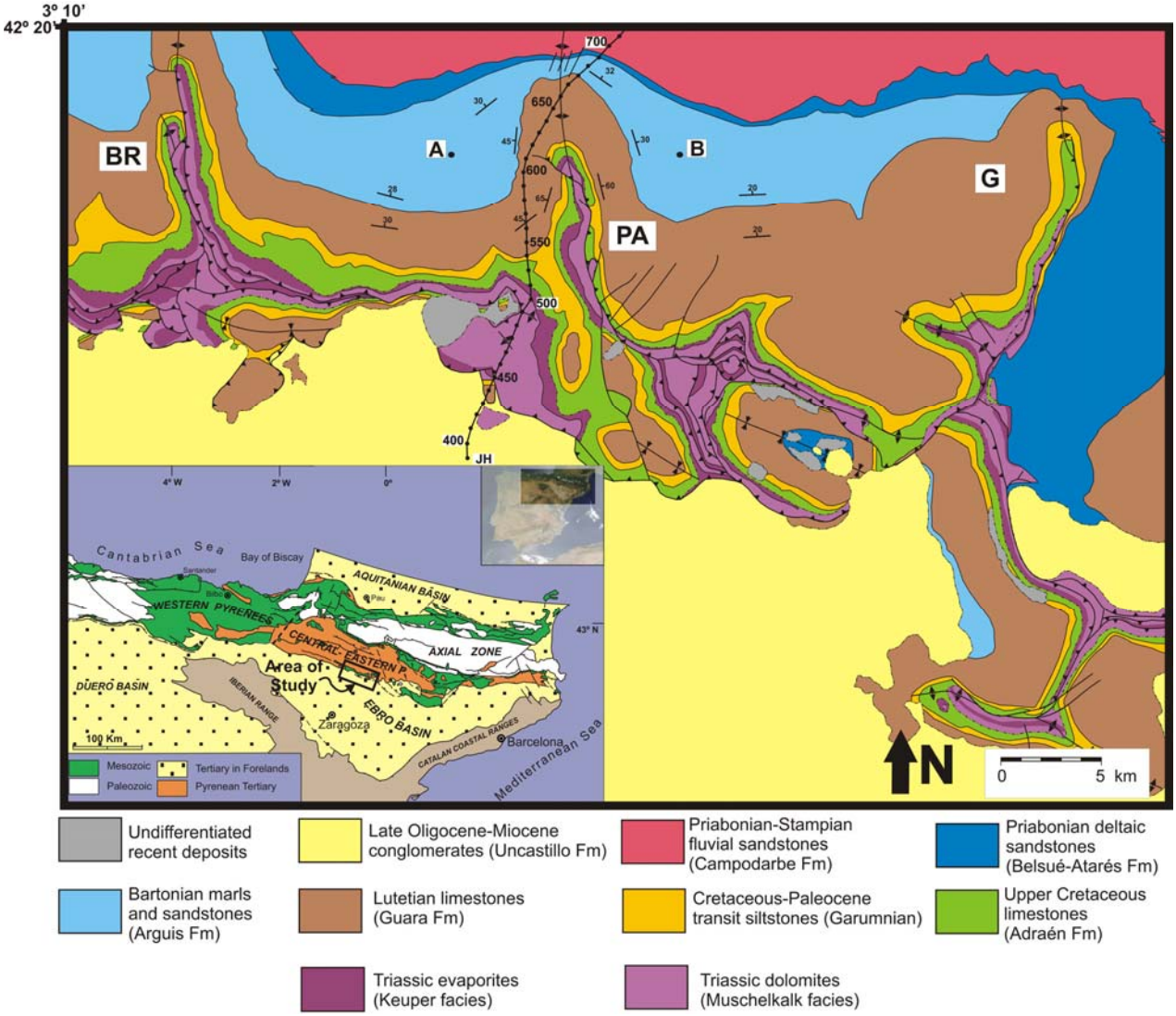

Fig. 1. Geological map of the Central External Sierras (modified from IGME, 1992). BR: Bentué de Rasal anticline; PA: Pico del Águila anticline; G: Gabardiella anticline complex; A: Arguis Village; B: Belsué Village. Line JH is the seismic profile shown in Fig. 6 (numbers along JH indicate shotpoints). Inset shows the location and the regional tectonic setting of the study area.

the deformed stage as the only criterion to rely on. Alternatively, during the last years there has been an increase in what has been called *geomechanical* or *physical-based* restoration, which assume no kinematics and carry out a mechanically stable restoration by taking into account measurable rock parameters such as density, Young modulus, Poisson's ratio, among others (Maerten and Maerten, 2006; Guzofski et al., 2009). This last group of methods is particularly suitable for modelling complex structural scenarios, in which the kinematics is unknown, difficult to quantify, or implement in the model.

In this work, we first present a 3D reconstruction of The Pico del Águila anticline based on field data (geological mapping and dip measurements) and seismic interpretation. Second, thanks to the preservation of the growth strata, we present a time-constrained restoration of the 3D model based on geomechanical criteria using the software Dynel3D (igeoss. Maerten and Maerten, 2006). Finally, we compare our results with previous kinematic and mechanical models of the anticline (Poblet and Hardy, 1995; Poblet et al., 1997; Vidal-Royo et al., 2010). Using these techniques, we investigate the complexity of detachment folding in 3D of the anticline, and point up the errors that may arrive by assuming single/simplistic, 2D folding mechanisms and unknown/qualitative kinematics.

GEOLOGICAL SETTING

The Pico del Águila anticline is located in the External Sierras ("Sierras Exteriores Aragonesas") of the Southern Pyrenees (Fig. 1). The External Sierras consists of several imbricated thrust sheets detached on evaporitic, calcareous and dolomitic facies of the Middle and Upper Triassic (Muschelkalk and Keuper facies. Soler and Puigdefàbregas, 1970; IGME, 1992; Millán et al. 1994; Millán, 1995; Pueyo et al., 2002). They constitute the emerging part of the frontal South-Pyrenean thrust sheets and are displaced southwards over the Tertiary sediments of the Ebro foreland basin.

One of the peculiarities of the Central External Sierras (CES from now on) is the presence of a set of transverse N-S to NW-SE anticlines. These structures are perpendicular to the general E-W structural trend of the Pyrenees and create a complex interference pattern (Fig. 1). The N-S anticlines become younger and smaller westwards (Millán et al., 1994; Millán, 1995), and their growth was synchronous with the deposition of Middle Eocene to Oligocene sediments and the development of the South-Pyrenean thrust front (active until Early Miocene times; Puigdefàbregas, 1975; Holl and Anastasio, 1993; Millán et al., 1994; Millán, 1995).

The Pico del Águila is one of the most studied N-S anticlines of the CES. This structure displays a spectacular growth strata record (Millán et al., 1994; Millán, 1995, Poblet and Hardy, 1995; Pueyo et al., 2002; Castelltort et al., 2003; Vidal-Royo et al., 2010), which indicates that the anticline grew from 42.67 ± 0.02 Ma (Upper Lutetian) to 34.8 ± 1.72 Ma (Lower Priabonian) (Poblet and Hardy, 1995).

In general, the stratigraphic record of the CES is an interlayered sequence of competent and incompetent units (Millán et al., 1994), each of them showing a different mechanical response to deformation (Fig. 2; Vidal-Royo et al., 2010). The stratigraphy of the

Fig. 2. *(Next page)* Stratigraphic sequence in the Central External Sierras (modified after Millán et al., 1994) showing the deformation that characterizes each unit: a) folded Keuper gypsiferous clays; b) fracture pattern within the Guara limestones; c) flexural slip and minor fractures within the Arguis marls; d) detail of a remnant slickenslide parallel to bedding in the Arguis marls, indicating layer parallel displacement (d does not belong to the same outcrop as c). M: Muschelkalk facies; K: Keuper facies.

OLIGOCENE	EARLY	STAMPIAN	Campodarbe Fm.	- Thickness variation across structure due to sedimentation during fold growth (wedge shape thinning towards the crest of the anticline) - Deformation characterized by decimetric non-strata bounded fractures, at a high angle to bedding
EOCENE	LATE	PRIABONIAN	Belsué-Atarés	- Thickness variation across structure due to sedimentation during fold growth. Deformation characterized by metric spaced non-strata bounded fractures, at a high angle to bedding
	MIDDLE	BARTONIAN	Arguis Fm.	- Thickness variation across structure due to sedimentation during fold growth - Deformation characterized by pervasive flexural slip and minor decimetric to metric spaced non-strata bounded fractures, nearly perpendicular to bedding
		LUTETIAN	Guara Fm.	- Bottom of the syn-folding sequence - Constant layer thickness - Stylolitic bedding planes - Macroscopically outlines the fold geometry, not affected by mesoscale faulting - At outcrop scale, penetrative strain characterized by multiple centimetric-spaced fracture sets, at a high angle to bedding
PALEOCENE			Garumnian	- Non-localized deformation in mudstone layers and pervasive cleavage in sandstone layers
U. CRETACEOUS			Adraén Fm.	- Localized metric spaced fracture pattern, non-strata bounded, at *ca.* 60º to bedding
MIDDLE AND LATE TRIASSIC			Muschelkalk and Keuper Facies	- Keuper facies: non-localized deformation exhibiting large variation of thickness and high internal deformation expressed by milimetric to decimetric folds. - Muschelkalk facies: pervasive strain expressed by centimetric spaced fractures at a high angle to bedding, and internal metric to decametric box and detachment folds

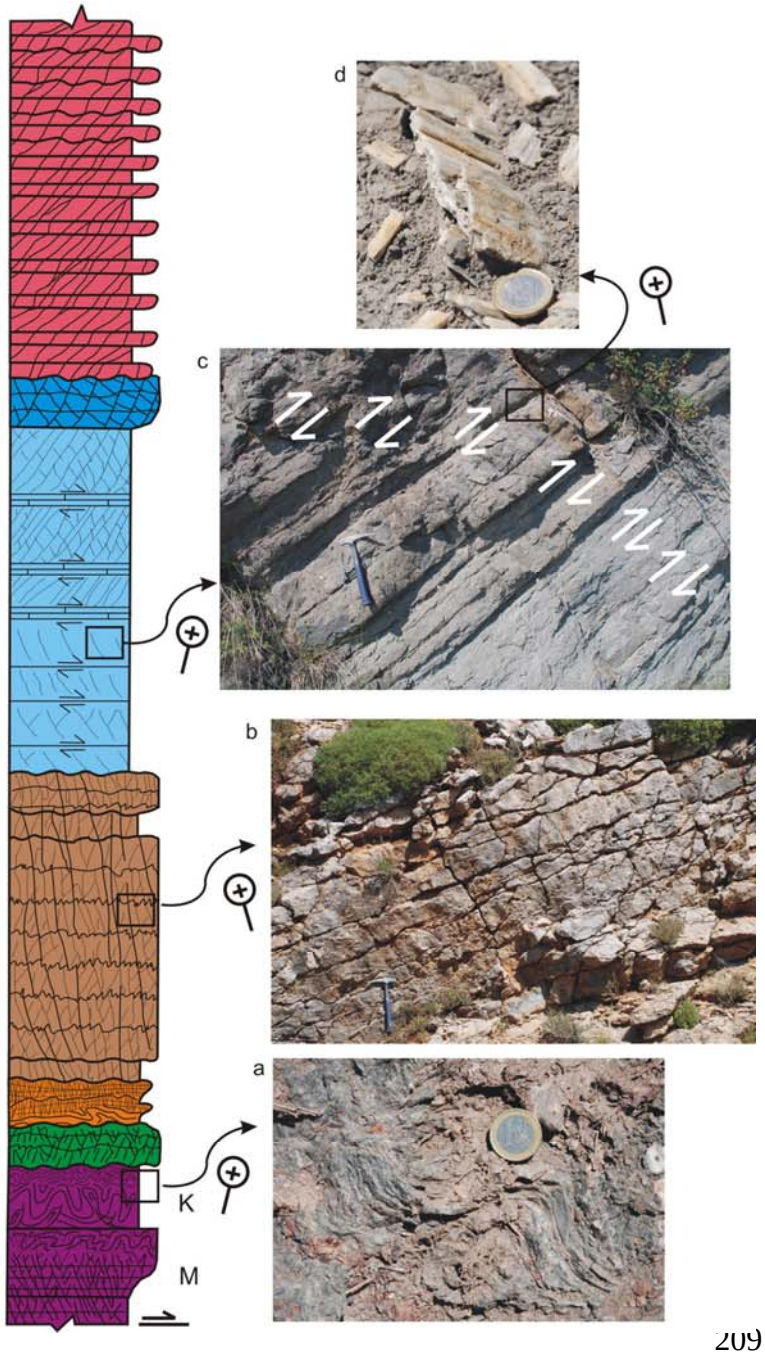

area consists of a few hundred metres thick Mesozoic succession covered by a thicker Paleogene sequence (Fig. 3). The Mesozoic consists of Triassic limestones, dolomites and gypsum-bearing clays, and Upper Cretaceous shallow marine limestones. The Paleogene comprises continental sandstones, siltstones and lacustrine limestones of the Cretaceous-Paleocene transition (Garumnian facies), shallow marine platform limestones of the Guara Formation (Lutetian), shallow marine and transitional marls, limestones and deltaic sandstones of the Arguis and Belsué-Atarés Formations (Upper Lutetian to Middle Priabonian), and fluvial clays, sandstone and conglomerates of the Campodarbe Formation (Middle Priabonian to Middle Oligocene).

The pre-folding sequence comprises Triassic to Lutetian rocks with the upper limit atop of the depositional sequence 2 of the Guara Formation. The syn-folding sequence comprises the depositional sequence 3 of the Guara Formation and the shallowing upwards sequence formed by the Arguis, the Belsué-Atarés and the base of the Campodarbe Formations. The base of the Arguis Formation defines a regional unconformity, indicating a steep change from shallow platform to slope depositional environments (Figs. 2 and 3). Millán et al. (1994) defined four major depositional sequences within the Arguis and Belsué-Atarés Formations. Sequence I (GS-I in figures and tables) is made of Late Lutetian to Early Bartonian blue marls and sandy glauconite-bearing marls. This sequence thins towards the crest of the anticline and is not existent at the hinge area. Sequence II (GS-II in figures and tables) is Middle to Late Bartonian in age, and comprises barely bioturbated blue marls. Sequence III (GS-III in figures and tables) is a pectinid platform of Early Priabonian age formed by barely bioturbated blue marls rich in marine fossil content. Sequence IV (GS-IV in figures and tables) is formed by Early Priabonian deltaic sandy marls and pure siliciclastic levels formed by deltaic progradation. The lower limit of this sequence is equivalent to the contact between the Arguis and Belsué-Atarés Formations. The upper limit is a regional unconformity, recognizable all along the South-Pyrenean basin, corresponding to the contact between the Belsué-Atarés and Campodarbe Formations (Figs. 2 and 3). This unconformity represents a sharp transition to continental depositional environments.

The first attempts to determine the geodynamic evolution of the External Sierras were made by Mallada (1878), Selzer (1948) and Almela and Ríos (1951), who proposed a progressive westward migration of the deformation. Anastasio (1992) and Anastasio and Holl (2001) proposed a halokinetic origin of the N-S trending folds of the External Sierras. However, field evidences in the CES reveal an uneven distribution of the Triassic décollement, which in many areas is formed by Muschelkalk limestones and dolomites and almost no evaporites or gypsum-bearing clays. In addition, recent analogue models show that in a single event of shortening, large mechanical contrasts in the basal décollement as those observed in the CES, can give rise to orogen-perpendicular structures (Vidal-Royo et al., 2009).

Previous works (Millán et al., 1994; Pueyo 2000; Pueyo et al., 2002; Pueyo et al., 2003) suggest that in an early stage of the evolution of the CES (Early Lutetian to Chattian), the thrust system was characterized by a south verging main thrust and a set of arcuate northeastward concave oblique thrusts. Generated as detachment folds on a flat over flat thrust configuration, the N-S trending folds are interpreted as a more evolved stage of those initially oblique thrusts. From careful observations of the growth strata, Poblet et al. (1997) considered the N-S trending folds to form by partially limb lengthening, limb rotation and flexural slip mechanisms, under high sedimentation rates. Given that the size of

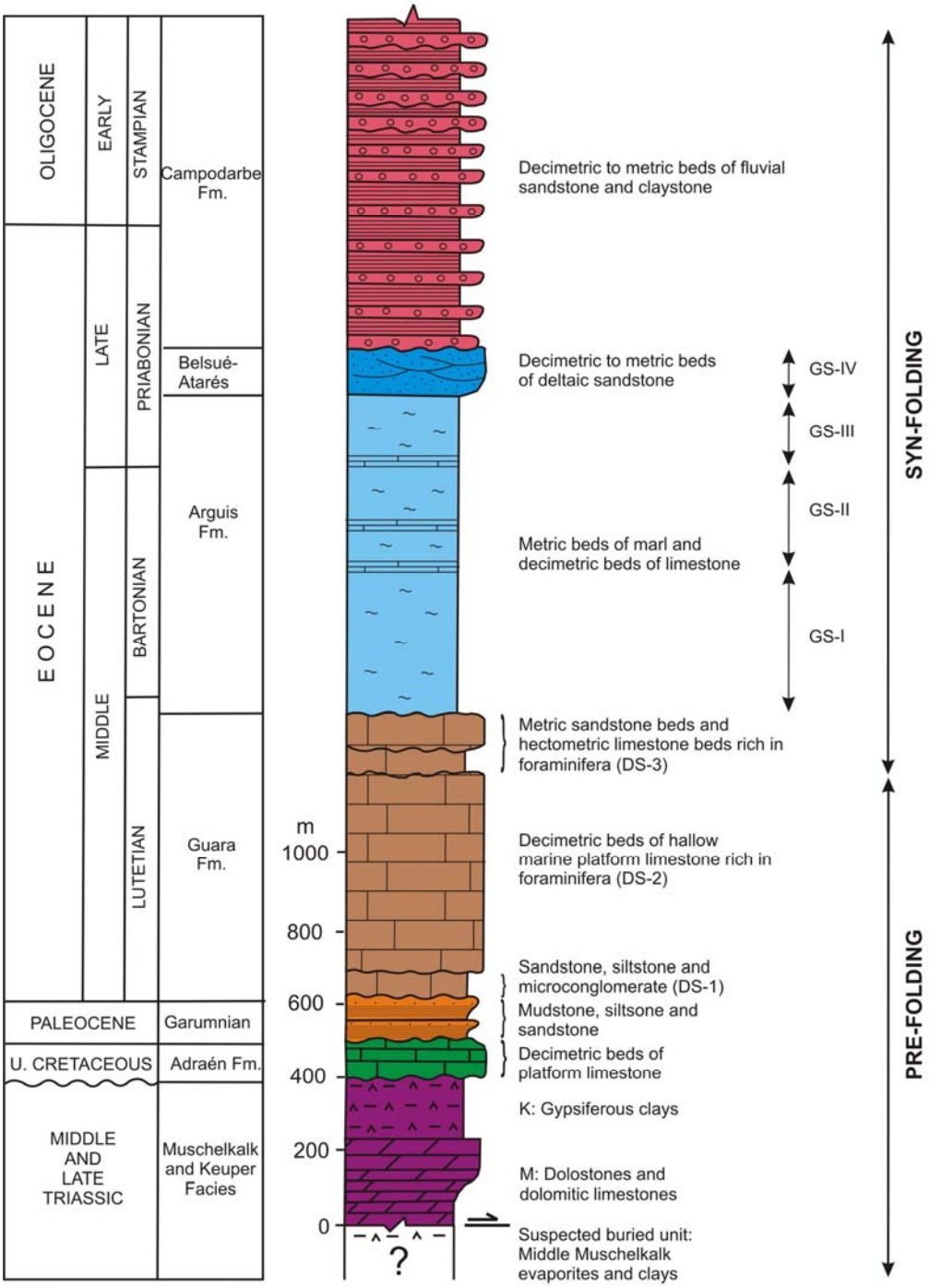

Fig. 3. Stratigraphic column describing the lithologies and average thicknesses of the materials involved in the Central External Sierras. M: Muschelkalk facies; K: Keuper facies. DS: Depositional sequences within Guara Fm. GS: Depositional sequences within the growth strata (Arguis and Belsué-Atarés Fms.). Modified after Millán et al., 1994.

the N-S anticlines decreases westwards, it can also be assumed that the deformation and shortening diminished in that direction. In addition to general translation towards the south, a vertical axis clockwise rotation characterized the kinematics of the thrust system from Upper Lutetian to Early Priabonian. Paleomagnetism measurements

suggest at least 40º of clockwise rotation at the base of the Arguis Formation, in the western limb of the Pico del Águila (Pueyo et al., 2002). Given that the southern periclinal closures of the N-S anticlines are not easily observable in the field, different authors have suggested that the rotating thrust system was finally folded and truncated in Chattian to Early Miocene times by the Santo Domingo thrust system (located beyond the western limits of Fig. 1). Consequently, the remaining N-S trending folds occurred at the hanging-wall of the new Santo Domingo thrust system, representing the northernmost portion of those oblique structures (the rest of the structures are supposed to be either buried under the continental deposits of the Ebro foreland basin or isolated by erosion under the southern limb of the Santo Domingo anticline. Millán et al., 1994; Pueyo et al.; 2002). The rotation, differential advance and extra uplifting of the N-S anticlines with respect to the neighbour orogen-parallel structures was facilitated by major mechanical contrasts in the Triassic basal décollement (Vidal-Royo et al., 2009). Areas of the thrust front detached on a ductile décollement reached further south than areas detached on a high friction décollement. However, to accommodate the same amount of bulk shortening, areas detached on a high friction décollement experienced larger uplift.

3D RECONSTRUCTION OF THE PICO DEL ÁGUILA ANTICLINE

Methodology

The reconstruction of the Pico del Águila anticline benefited from surface and subsurface data which were integrated in a common 3D framework. This results in a reliable and constrained model that honours all the available data (Fig. 4). The acquired data at surface comprise bedding dip measurements, fault traces and fracture measurements, and a detailed field map of bedding traces within the growth strata record. The subsurface data consist of several seismic profiles which have been interpreted to better understand the structure in depth and validate the field interpretations.

Surface data: DTM construction, data managing and Dip Domain Method

The acquired 3D topographic maps (in vectorial format; public data from the Aragonese Government) are scaled at 1:5000 with a contour interval of 5 m. Contours and elevation spots were extracted from the maps in a 3D environment, to generate a XYZ dataset of the topography. The interpolation of these XYZ nodes allowed the generation of a regularly spaced XY net or lattice composed of square 5 x 5 m cells with nodes preserving their corresponding Z values. This regular lattice is smoother than the maps and has a maximum precision of ± 2.5 m; a suitable precision for a kilometre-scale structure such as The Pico del Águila anticline. Aerial ortophotographs (1 x 1 m pixel resolution) were draped onto the lattice, obtaining a digital elevation model with a clear image of the area.

The Pico del Águila anticline was reconstructed by applying the *Dip Domain Method* (Fernández et al., 2004 a and b), which states that geometries can be simplified into volumes in which bedding attitude is constant. These volumes, or dip domains, are bounded by surfaces that can have different geological significance: axial surfaces, faults, and stratigraphic discontinuities.

Dip data and mapped traces were used to reconstruct the geometry of the structure, whereas other types of data such as fold axes or paleocurrents were used to constrain the validity of the reconstruction. Mapped traces and geological boundaries control the stratigraphic position of each dip measurement, and also were used to obtain dip

measurements, calculated from the XYZ position of digitized nodes (Fig. 5; Fernández, 2005).

Simplifying the geometry of a structure into a group of dip domains implies a certain error and lack of precision, since the real geological surfaces are not planar but irregular. Consequently, a significant amount of good quality data is essential to reach a good precision. For the present work, 663 mapped traces have been used to calculate new dip measurements, bringing up a total of 1410 dips to control the geometry of the structure. To apply the dip-domain method, a comprehensive geometrical model must be established from the available data (Fernández et al., 2004; Fernández, 2004). This geometrical model must include: 1) a definition of dip domains (average bedding attitude of the domain and polarity, position, and extent of boundaries); and 2) a definition of 3D stratigraphic geometries (a model of stratigraphic separations between different horizons).

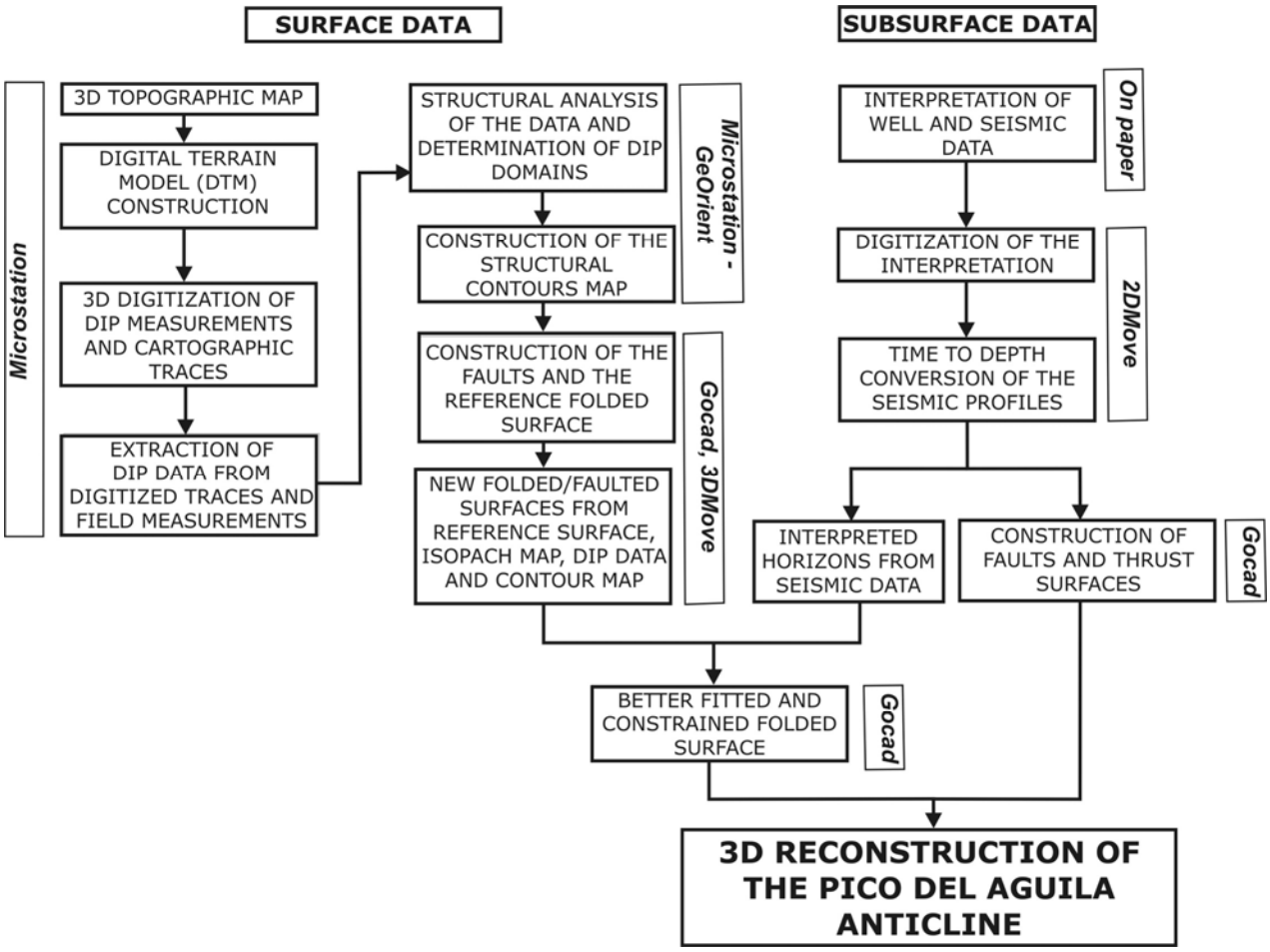

Fig. 4. Workflow for 3D structural reconstruction of The Pico del Águila anticline.

The top of the Guara Formation, which was selected as a reference surface, is the best outcropping, most easily accessible pre-folding level controlling the structural relief of the anticline. A totality of 91 dip domains have been defined at this stratigraphic level, assuming ± 5º in strike direction and ± 3º in dip value as a tolerance limit between domains. By intersecting the adjacent dip domains (Fig. 5), the map of structural contours is obtained. This is the first approach to the 3D reconstruction of the structure. From this, the interpolation of the structural contours was easily performed in GOCAD (Paradigm™), obtaining a smoother geometry of the reference surface that honours all the input data. The rest of the pre-folding

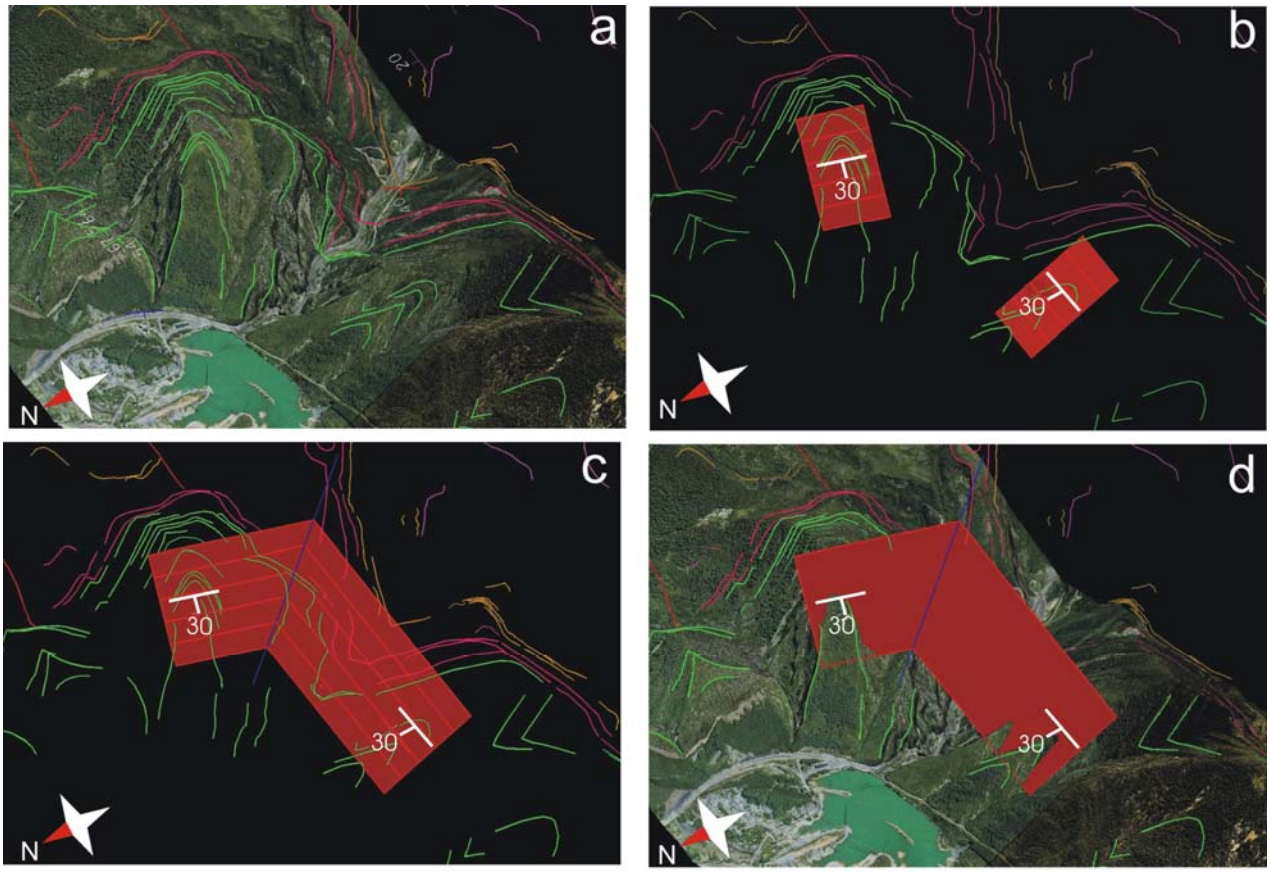

Fig. 5. Sketches summarizing the procedure followed in the creation of the 3D reconstruction: (a) positioning of the dip data, (b) creation of dip domains, (c) definition of the extension and intersection of dip domains, and generation of structural contours, (d) generation of the surface. For simplicity not all dip data is shown in the figure.

surfaces were reconstructed using a tool in 3DMove (Midland Valley Exploration) that allows creating folded surfaces from a previous reference surface, for parallel and similar folds. Since the Pico del Águila is considered a kilometric-scale parallel fold (no large thickness changes are observed in the pre-folding units; Millán, 1995), the parallel fold tool was used to reconstruct the geometry of the pre-folding Triassic, Upper Cretaceous and Garumnian top surfaces. The nodes of the reference surface (top of the Guara Formation) were projected by

vectors perpendicular to bedding, a distance equivalent to the stratigraphic thickness between the reference surface and the new surface. Unlike the pre-folding surfaces, the syn-folding surfaces show significant changes on the geometry and thickness between adjacent beds (Fernández et al., 2004). Therefore, the syn-folding surfaces were reconstructed individually using the dip-domain method. To control the variation in thickness in the syn-folding units we took advantage of the excellent exposure of the growth strata and the stratigraphic logs from Millán et al. (1994).

Subsurface data: thrust reconstruction and horizon constraints

The subsurface data consist of six seismic profiles and an exploratory well located outside the studied area. Seismic data has been used to reconstruct the geometry of the South-Pyrenean frontal thrust and to constrain the geometries reconstructed from surface data (Fig. 4).

Due to the poor quality of the seismic data, only the general features of the pre-folding sequence were interpreted, as well as the geometry of the South-Pyrenean thrust (Fig. 6). The quality of the profiles does not allow interpretation of the growth strata.

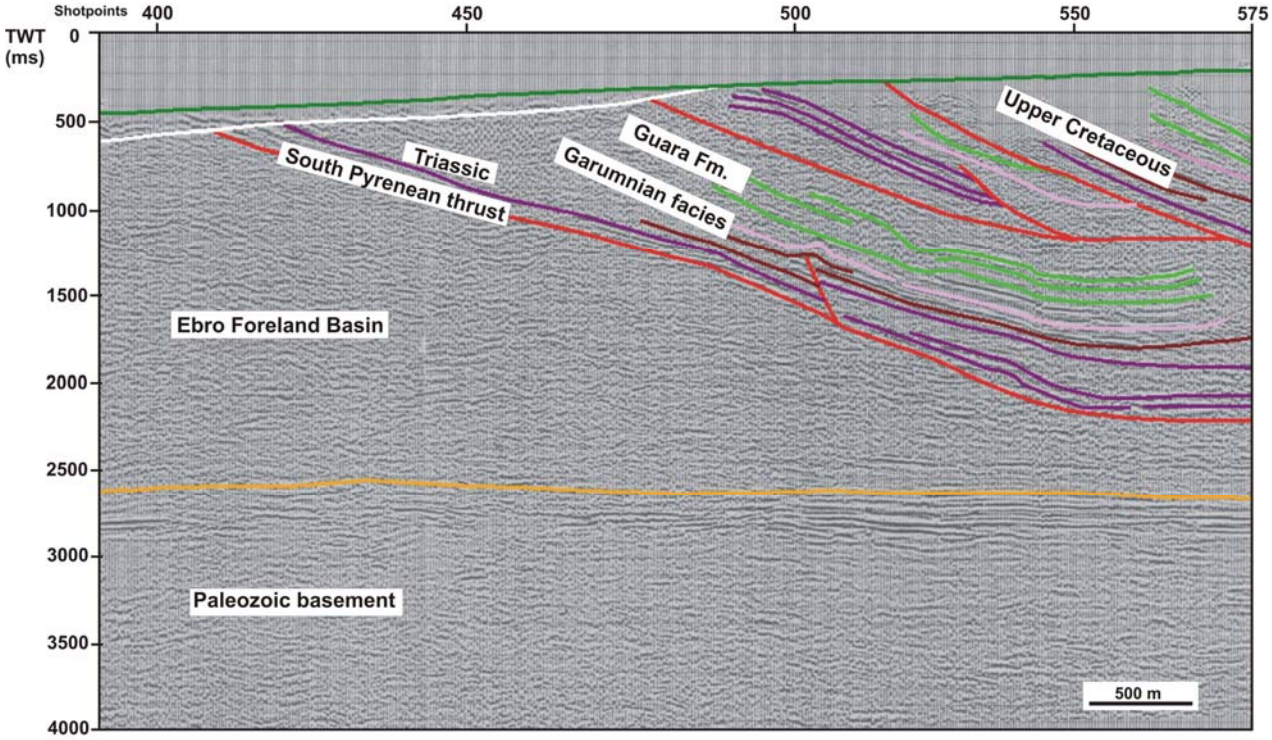

Fig. 6. Interpretation of the Jaca-Huesca survey seismic profile. Vertical scale is two way travel time in milliseconds. Horizontal scale is in meters. See Fig. 1 for location of the seismic profile.

The seismic interpretation was then converted to depth using the interval velocity of each unit as deduced from the exploratory well and the Common Depth Points (CDP's) of the seismic profiles. This information was brought to the reference 3D framework in order to correlate between the different seismic profiles. After that, a map of structural contours in 3D

was created for each fault/horizon. In case of the pre-folding stratigraphic horizons, the subsurface data were attached as control points in depth to the corresponding surface contour map. Each fault surface was constructed as described above in the surface data subsection.

Results: 3D model of the Pico del Águila anticline

A total of eight stratigraphic surfaces and nine faults were reconstructed. For the pre-folding sequence, the reconstructed horizons are (Figs. 7 and 8): 1) the top of the Guara Formation (reference surface of the fold); 2) the top of the Garumnian facies (Cretaceous-Tertiary transition); 3) the top of the Upper Cretaceous; and 4) the top of the Triassic rocks. Associated to these units, eight fault surfaces that affect the core of the structure (Fig. 7), as well as the geometry of the South-Pyrenean frontal thrust (Fig. 7) were reconstructed. Regarding the syn-folding sequence, the top of the four main depositional sequences within the Arguis and Belsué-Atarés Formations were reconstructed (Figs. 7 and 8).

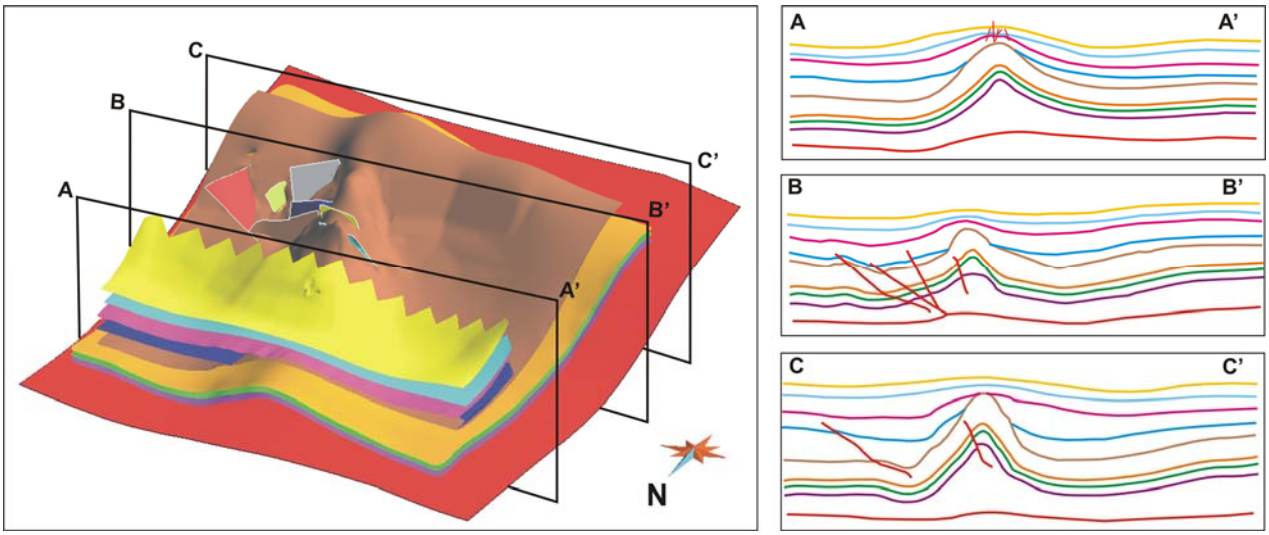

Fig. 7. Sections across the 3D reconstruction of the Pico del Águila anticline showing its internal structure. From bottom to top: South-Pyrenean thrust (red); Top of Triassic (violet); Top of Upper Cretaceous (green); Top of Garumnian facies (orange); Top of Guara Formation (brown); Top of Growth Sequence 1 (blue); Top of Growth Sequence 2 (pink); Top of Growth Sequence 3 (cyan); Top of Growth Sequence 4 (yellow). Inner faults of the anticline are in red. Notice how the growth strata thin towards the crest of the anticline and how the first depositional sequence does not reach the crest of the anticline.

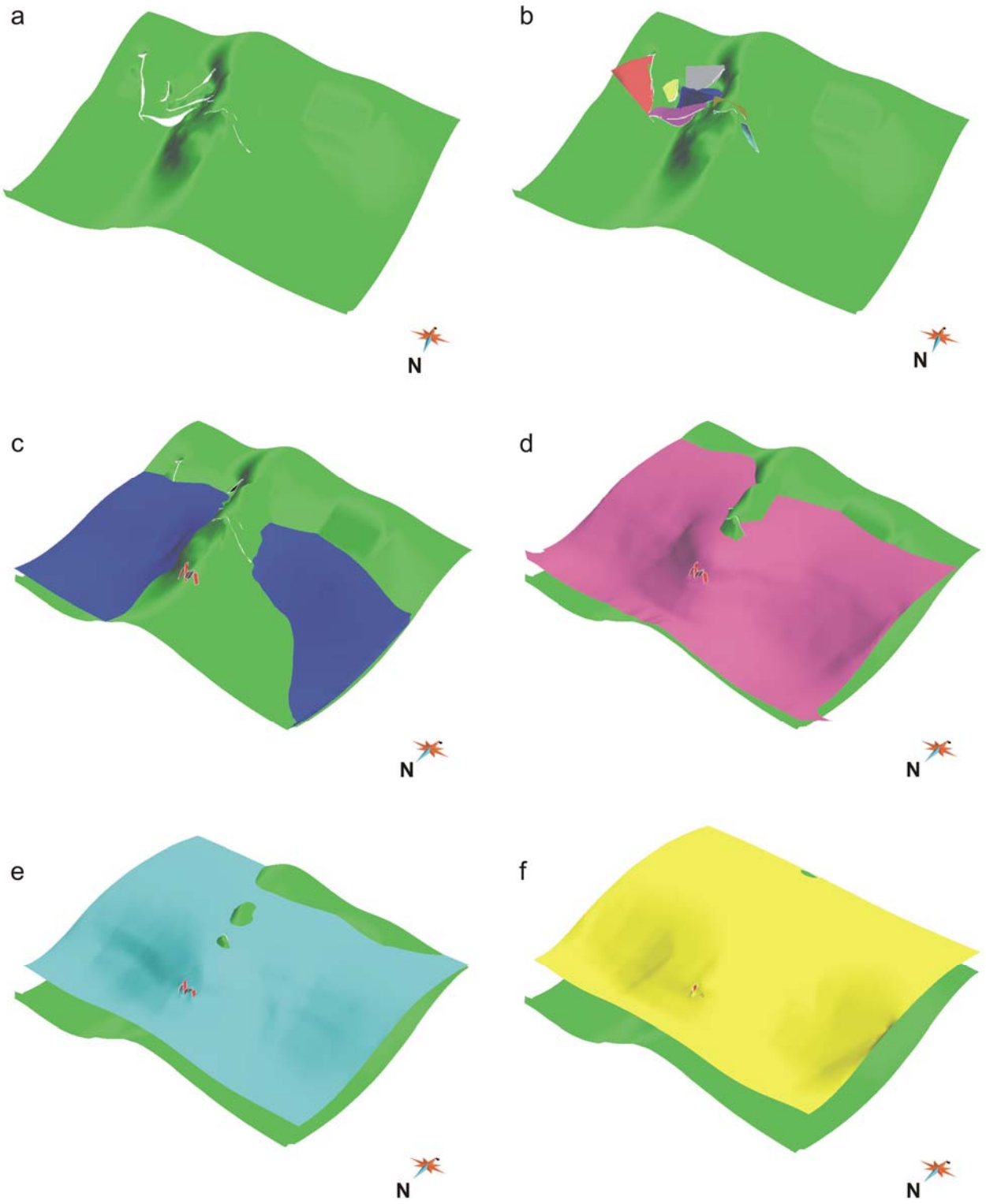

Fig. 8. Spatial extent of the reconstructed syn-folding depositional sequences. (a) Top of pre-folding Guara Formation (surface in brown in Fig. 7) for reference; (b) Top of Guara Formation plus inner faults; (c) Top of Guara Formation covered by depositional sequence 1; (d) Top of Guara Formation covered by depositional sequence 2; (e) Top of Guara Formation covered by depositional sequence 3; and f) Top of Guara Formation covered by depositional sequence 4.

The geometry of the South-Pyrenean frontal thrust surface consists of a ramp that dips towards the N, ranging in dip from 15º in the northern rear part to 37º in the southern frontal emerging zone, and a sub-horizontal flat extending to the north (Fig. 7). In the core of the anticline, the pre-folding sequence is deformed by a set of reverse and normal faults (Fig. 7) as well as by a N-S minor thrust. The top of the Guara Fm is barely affected by this set of faults and clearly unconformably overlies the minor thrust (Figs. 7 and 8). The lower units, however, display a complex structural pattern due to the interference between the E-W to NNE-SSW faults and the N-S trending thrust (Figs. 7 and 9).

The syn-folding sequence displays a gentler geometry, characterized by thinning towards the crest of the anticline and upwards decrease in folding intensity (Figs. 7, 8 and 9). The first depositional sequence (as defined by Millán et al., 1994) does not reach the crest of the anticline and onlaps onto both flanks. The upper depositional sequences progressively cover the top of the Guara Fm (Figs. 7 and 8).

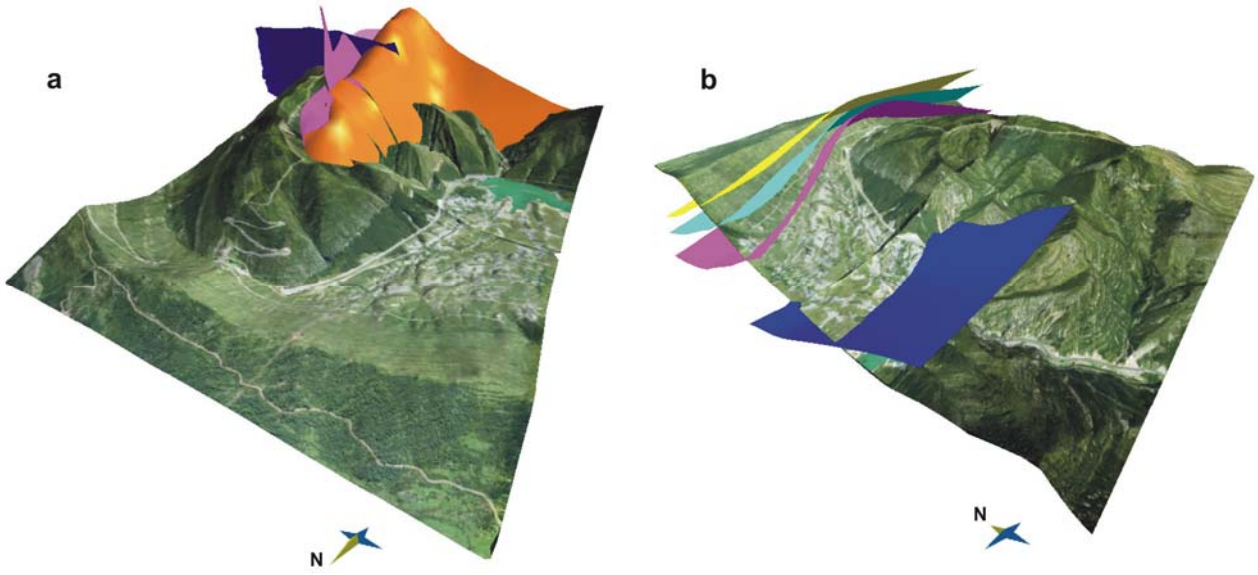

Fig. 9. Oblique images of The Pico del Águila anticline. (a) shows the interference between the anticline (Garumnian horizon in orange), the set of NNE-SSW to E-W faults (dark blue), and the N-S internal thrust (pink); (b) shows the geometry of the growth strata (sequences I to IV) intersecting the topography and thinning towards the periclinal closure defined by the Guara limestones.

3D RESTORATION OF THE PICO DEL ÁGUILA ANTICLINE

Methodology. Geomechanical restoration of structures in 3D

The sequential restoration of The Pico del Águila anticline was carried out using Dynel3D (igeoss. Maerten and Maerten, 2006). Dynel3D is a mechanical, continuum, elastic code based on the finite element method (FEM). Although strictly elastic, the program is suitable to model the development and behaviour of complex geological structures such as folds and faults (Maerten and Maerten, 2006).

In Dynel3D, the stratigraphic units are discretized with tetrahedral elements that are assigned elastic properties. Faults are represented by contact surfaces. The tetrahedral elements deform elastically in response to constraints such as applied and/or internal forces, displacements, and interface contact regions (faults). Dynel3D uses an iterative, explicit solver that allows forces to be transmitted from node to node through the entire system until equilibrium is reached. This formulation is well suited to model complex geological scenarios that comprise several stages, such as structural restoration. In addition, the explicit solution scheme is efficient and stable (Maerten and Maerten, 2006). There are indeed limitations associated to the use of elasticity to restore large, non-recoverable strain. In Dynel3D, these limitations are overcome by restoring and summing small increments of deformation, and including the effect of faults, décollements and flexural slip. In this way, each volume is required to restore elastically but on the whole, the model experiences finite, permanent strains that are manifested by fault, décollement and flexural slip offsets (Maerten and Maerten, 2006, and Guzofski et al., 2009 who use a similar restoration technique).

Initial setup, boundary conditions and experimental parameters

The 3D reconstruction of the Pico del Águila anticline was taken as the deformed stage to restore. As we stated before, the reconstructed growth strata are key to constrain the restoration sequentially and obtain a reliable deformation path.

One of the characteristics of the FEM algorithm in Dynel3D is that it needs strong, closed boundary conditions. A closed boundary or *bounding box* must be defined previous to the volume generation (Fig. 10 a), in such a way that all surfaces have the same XY extent and all calculations are restricted to the bounding box. The size of the tetrahedral elements used to discretize the stratigraphic units is defined by the user. The smaller the size of the elements the higher the model's resolution but also the time and memory needed for the computation. Therefore, a balance must be kept between the resolution of the model, the amount of allocated memory and the solution time. For a kilometre-scale structure such as the Pico del Águila anticline, with nearly 2 km of stratigraphic thickness (including the growth strata), we used an average side length of 310 m, which reproduces reliably the geometry of the anticline and does not exceed the memory allocation threshold allowed by a regular personal computer.

The construction of the tetrahedra may become problematic in volumes highly segmented by small-scale, closely separated faults. These faults may give rise to dramatic changes in shape and thickness that would need a larger amount of tetrahedra to be reproduced. The eight faults affecting the pre-folding sequence are characterized by a heave that barely exceeds several tens of meters, introducing local perturbations that do not affect the regional structure. Therefore, they were not included in the restoration. For the same reason, since the stratigraphic thickness of both the Upper Cretaceous and the Garumnian units is below the average side length of the tetrahedra, these units were merged into a unique mechanical unit called *Garumnian-Cretaceous*, with mechanical properties corresponding to the average of the former units.

The physical-based restoration algorithm run in Dynel3D needs several rock mechanical properties to be set up. These properties include the Young's modulus, Poisson's ratio, density and porosity (this last one used only if decompaction is considered). As these mechanical properties vary with lithology along the stratigraphic sequence,

different values were established with regard to the predominant lithology of each unit. These values are listed in Table 1, and are average values of each lithology listed in charts of rock mechanical properties derived from laboratory experiments. Using these values implies certain overestimation of the mechanical properties of the rocks described in the field: fresh intact decimetre-scale laboratory samples have larger strength values than fractured, heterogeneous kilometric-scale rock masses described in the field (Schultz, 1996). However, the relative values between the different modelled units keep a similar ratio as if field-described mechanical properties were used, providing good insight on how the spatial distribution of rock mechanical properties influences fold evolution.

Table 1. Mechanical properties used to restore the Pico del Águila anticline

Unit	Predominant Lithology	Young's Modulus (Pa)	Poisson's ratio	Density (Kg/m3)
GS-IV*	Sandstone	2.2 e+10	0.24	2480
GS-III*	Marlish Sandstones	2.2 e+10	0.24	2480
GS-II*	Marls	2.8 e+10	0.14	2530
GS-I*	Marls	2.8 e+10	0.14	2530
Guara	Limestones	4.8 e+10	0.25	2500
Garumnian-Cretaceous	Mudstones-Limestones	2.8 e+10	0.14	2530
Triassic	Dolomitic Limestones	4.8 e+10	0.25	2500

These are average values for each rock type, and partially based on field indications
* GS: Growth strata; Arguis and Belsué-Atarés Fms.

The method allows us to model the behaviour of the contact between units, setting it up in such a way that the algorithm allows or prohibits layer-parallel displacement between the units (*i.e.* flexural slip). In the case of the Pico del Águila, the type of interface contact between units is summarized in Table 2. The contact between a stratigraphic horizon and a fault surface is set to slip by default, although the user can set it up to be fixed as if the horizon and the fault were attached. No constraints were applied to the sides of the bounding box. This allowed us to investigate the rotation of the model throughout the restoration.

Results: 3D restoration of the Pico del Águila anticline

Once the 3D reconstruction of the Pico del Águila anticline was completed, a sequential restoration was carried out back to the initial non-deformed state of the Guara Formation top surface. To do so, five restoration stages were considered. These stages follow the reconstruction of the bounding surfaces of the four growth depositional sequences and the top

of the Guara Formation (Figs. 10 and 11). The distribution of average shear strain (abbreviated as *strain* from now on) corresponding to each restoration step was also plotted in order to track the evolution of the deformation (Fig. 12). Due to the limitations of the elastic model the computed shear strain is likely to be lower when compared to other numerical methods (e.g. Discrete Element Models). For this reason, we are mostly interested in investigating strain patterns rather than absolute strain magnitudes.

Table 2. Units showing evidence or absence of layer parallel slip

Unit	Predominant Lithology	Slip/Stick*
GS-IV*	Sandstone	Stick
GS-III*	Marlish Sandstones	Stick
GS-II*	Marls	Slip
GS-I*	Marls	Slip
Guara	Limestones	Stick
Garumnian-Cretaceous	Mudstones-Limestones	Slip
Triassic	Dolomitic Limestones	Slip

* Slip: evidence of layer-parallel slip
Stick: absence of layer-parallel slip

Restoration of the top of the growth sequence IV (36.6 Myr) to the horizontal removes most of the tilting effect associated to the emplacement of the South-Pyrenean frontal thrust, decreasing significantly the northwards plunge of the anticline in the underlying units (Fig. 10 a and b). A gentle vertical axis clockwise rotation is observed (*ca.* 15º; Fig. 11 a and b). The fold geometry changes from nearly symmetrical to a markedly asymmetrical E-SE verging fold due to layer parallel slip between units (Fig. 10 a and b). Strain is distributed heterogeneously throughout the model, each unit exhibiting different strain according to their mechanical properties (Fig. 12 b). Growth sequence IV displays moderate to high strain: minimum values are distributed around the associated synclines, and progressively increase towards the anticline. Higher strain values correspond to the hinge and eastern limb of the anticline, coinciding with areas in which sequence IV has minimum stratigraphic thickness (Fig. 12 b). Due to the layer parallel slip described in the syn-kinematic rocks, the rest of the growth sequences display low to moderate strain, with the highest strain values in the hinge area of the associated synclines. Within the pre-folding sequence, the Garumnian-Cretaceous exhibits the highest strain, with maximum values in the hinge areas of the anticline and the synclines, and moderate to high strain along the fold limbs. Similarly, the Triassic displays moderate to high strain in the anticline and synclines hinges, and moderate strain along the flanks. The Guara Formation displays low to moderate strain along both fold flanks, and high strain in the hinge of the synclines (Fig. 12 b).

Sequence III (37.17 Myr) is the first restored growth unit that does not cover all the

anticline. Restoration of this sequence results in little variation of fold geometry with respect to the previous step, with a decrease in the plunge of the anticline of barely 4º (Fig. 10 c) and a clockwise rotation of 2º (Fig 11 c). The associated strain (Fig. 12 c) is not particularly high with respect to the other restoration steps (Fig. 12), with low to moderate strain in sequence III (moderate strain is concentrated in the hinge of the anticline) and low strain in the rest of the growth sequence. At this stage, the highest strain is accommodated by the pre-folding units, particularly the Guara Formation, in the eastern syncline and along the western limb (Fig. 12 c). The Garum-Cetaceous displays moderate to high strain, relatively homogeneous throughout the unit, and pronounced layer-parallel slip with respect to the units above and below. The Triassic exhibits moderate to high strain, more concentrated in the middle sequence of the synclines and anticline hinges. Low to moderate strain is observed all along the interface between the Triassic and Garum-Cretaceous (Fig. 12 c).

After restoring growth sequence II (37.74 Myr), the structural style remains similar to the previous stages, even though the northwards plunge of the anticline has almost disappeared (Fig. 10 d) and the structure has rotated clockwise *ca.* 10º additional degrees (Fig. 11 d). The associated strain (Fig. 12 d) is higher than in the previous stage, with a maximum located around the periclinal closure of the anticline. As in previous stages, the minimum strain is located around the hinge area of the associated synclines. The Guara Formation accommodates moderate strain in the western limb and the crest of the anticline, and high strain in the hinge of the eastern syncline (Fig. 12 d). The Garum-Cretaceous displays high strain, except in the crest of the anticline where strain markedly decreases. The Triassic displays a very heterogeneous strain distribution, varying from moderate to high in all structural domains across the unit (Fig. 12 d).

The restoration of growth sequence I (40.04 Myr) unveils the Guara Formation in the crest of the structure and causes a small decrease in the plunge of the anticline (Fig. 10 e). After restoring growth sequence I, a large amount of deformation is still observed in the pre-folding units, which display a well-developed anticline (Fig. 10 e). No significant vertical axis rotation is observed (Fig. 11 e). Strain in sequence I is heterogeneously distributed, displaying low to moderate high strain around the hinge of the synclines and along the flanks onlapping the Guara Formation (Fig. 12 e). The pre-folding units display a very different behaviour with respect to each other: The Guara Formation exhibits low strain in the crest of the anticline and moderate strain in the periclinal closure and along the flanks. The Garumnian-Cretaceous shows moderate to high strain, particularly high in the hinge of the anticline and along the flanks. And the Triassic displays moderate to high strain in the synclines, moderate to high strain along the décollement, and low strain in the crest of the anticline (Fig. 12 e).

Finally, the restoration of the Guara Formation (41.52 Myr) to a flat horizontal configuration causes unfolding of the pre-folding sequence and additional clockwise rotation of *ca.* 6º (Figs. 10 f and 11 f). The vertical axis rotation varies through the pre-folding units, displaying a slight larger rotation of each unit with respect to the unit immediately below (Fig. 10 f). The strain associated to the restoration of the Guara Formation ranges from very low to very high,

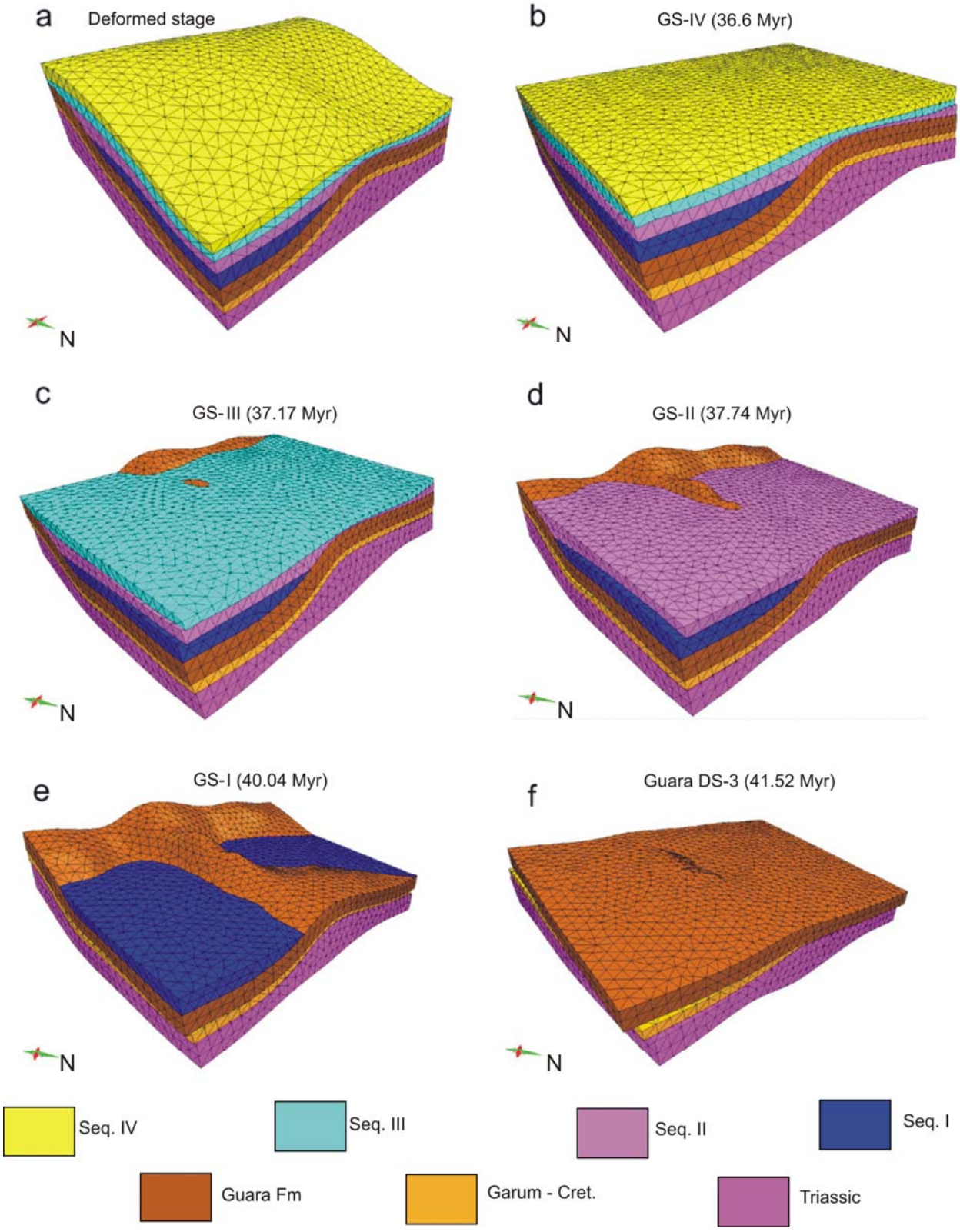

Fig. 10. Sequential, geomechanical restoration of The Pico del Águila anticline. (a) Deformed stage; (b) restoration of growth sequence IV (36.6 Myr); (c) restoration of growth sequence III (37.17 Myr); (d) restoration of growth sequence II (37.74 Myr); (e) restoration of growth sequence I (40.04 Myr); and (f) restoration of Guara Formation (41.52 Myr).

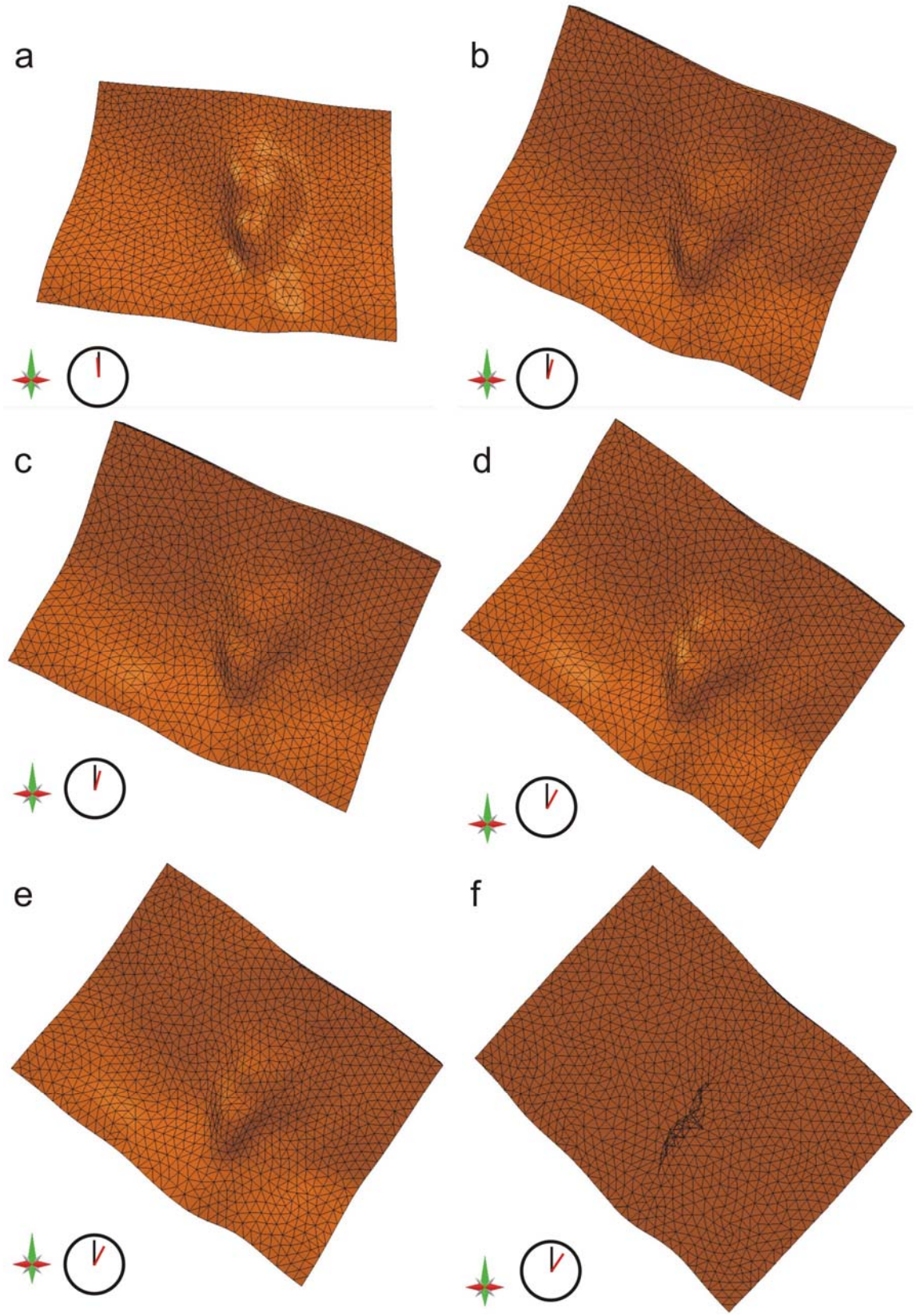

Fig. 11. Geometry of the top of the Guara Formation in map view through the different restoration stages, illustrating the progressive rotation of the anticline. Notice the clock next to each stage: the black hand points towards the N whereas the red hand indicates the axial trend of the structure at each stage. a) Deformed stage; (b) restoration of growth sequence IV (36.6 Myr); (c) restoration of growth sequence III (37.17 Myr); (d) restoration of growth sequence II (37.74 Myr); (e) restoration of growth sequence I (40.04 Myr); and (f) restoration of Guara Formation (41.52 Myr).

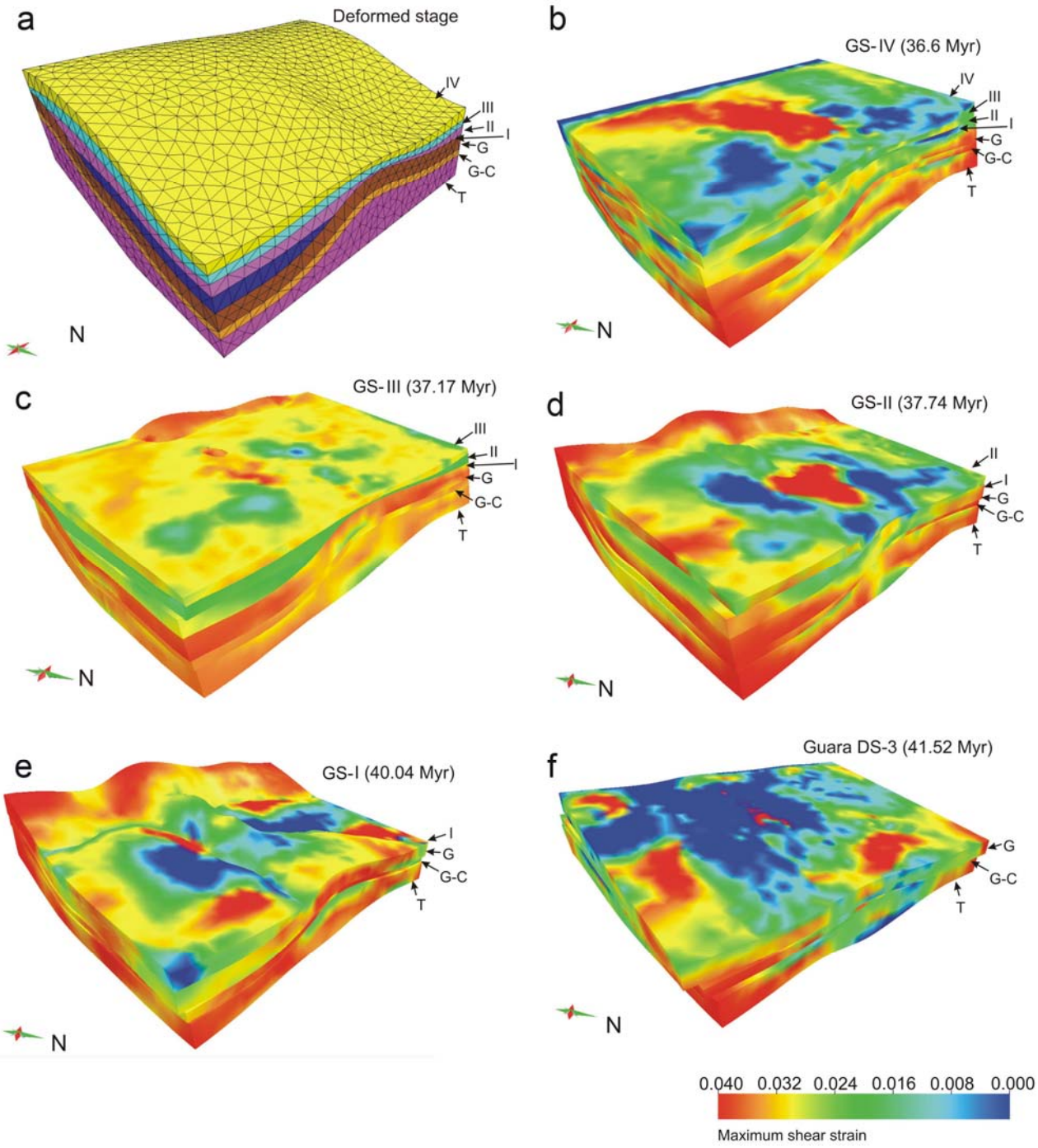

Fig. 12. Average shear strain between the restoration steps of Fig. 10. a) Deformed stage geometry for reference; (b) restoration of growth sequence IV (36.6 Myr); (c) restoration of growth sequence III (37.17 Myr); (d) restoration of growth sequence II (37.74 Myr); (e) restoration of growth sequence I (40.04 Myr); and (f) restoration of Guara Formation (41.52 Myr). T: Triassic; G-C: Garumnian Cretaceous; G: Guara; I: Growth sequence 1; II: Growth sequence 2; III: Growth sequence 3; IV: Growth sequence 4.

with low to moderate values throughout the model, and maximum values in the hinge of the synclines and locally in the crest of the anticline (Fig. 12 f). The Garumnian-Cretaceous and Triassic display larger strain values, particularly concentrated in the hinge of the synclines. In both units, the crest of the anticline and the periclinal closure are characterized by low to moderate strain values (Fig. 12 f). The top and bottom of the units display slightly lower strain values along their contacts, with significant layer-parallel slip between them.

DISCUSSION

3D reconstruction and restoration of the Pico del Águila anticline provides new insights into the structural evolution of the Central External Sierras (CES).

The three-dimensional model allows us to visualize the complex interference pattern of the anticline, as well as the geometry of the growth strata. Although the anticline is tilted by the emergence of the South Pyrenean thrust, the 3D reconstruction shows that both periclinal closures are in the hangingwall of the South Pyrenean thrust. The southern closure of Pico del Águila shows a slight plunge towards the South (around 10º), and the bedding of the Guara Formation shows an orogen-parallel E-W attitude along the thrust front. This suggests that the Pico del Águila (and possibly other N-S anticlines of the External Sierras) were not truncated by the Santo Domingo thrusts system.

Concerning the continuity of the fold to the north, it has been proposed that the anticline continues plunging to the north and might be buried under the sediments of the Jaca piggy-back basin. However, the 3D reconstruction displays a much gentler fold in the northern termination of the model (Figs. 7 A-A' and 8), suggesting that the Pico del Águila anticline dies out shortly to the north of the model.

Vertical axis rotation is a determining factor in the structural evolution of the N-S anticlines in the CES (Hogan and Burbank, 1996; Pueyo et al., 2002 and 2003; Oliva-Urcía and Pueyo, 2007; Rodríguez-Pintó et al., 2008, among others). This rotation is considered to be nearly rigid (negligible differential rotation between flanks; Pueyo et al., 2002) and variable through time. The sequential restoration presented in this work reproduces naturally this process, reporting values which are in accordance with previous works on the kinematics of the CES (Fig. 11). The restoration gives a maximum rotation value of 33º, without imposing any particular, ad-hoc kinematics to the model. This rotation value is lower than the maximum value reported in Pueyo et al. (2002) (40º in the base of the Arguis Formation and higher in the underlying Guara Fm), but within the value span reported in more recent publications (*ca.* 21º in Rodríguez-Pintó et al., 2008, and 28º in Vidal-Royo et al., 2009), which seems to fit better the reprocessed and newly acquired paleomagnetic data (Rodríguez-Pintó et al., 2008 and E.L. Pueyo, personal communication). Table 3 summarizes the incremental and cumulative rotation values obtained from the restoration. An average rotation rate of 5.5º/Myr is calculated for the deposition of the entire growth sequence consisting of the Arguis and Belsué-Atarés Formations, which is in accordance with the approximately 7º/Myr rotation rate reported by paleomagnetic data (Rodríguez-Pintó et al., 2008).

The restoration suggests counter clockwise rotation from the initial non-deformed to the present configuration (Fig. 11). This is in contradiction with the sense of rotation reported by paleomagnetic data (Pueyo et al., 2002; Rodríguez-Pintó et al., 2008). Paleomagnetism provides strong kinematic criteria to constrain the sense of rotation of the magnetic vectors through time. Many paleomagnetic sites have been measured along

both limbs of the Pico del Águila, indicating a regional clockwise rotation of the CES through its geological history. The rotation observed in the restoration results from not constraining the sides of the bounding box. The model, hence, was able to move freely and unconstrained. Based on the geometry of the initial configuration (deformed stage), the contrasts in mechanical properties, and the different layer parallel slip between units, the algorithm solved the system and revealed a 33º vertical axis rotation as the mechanically most stable solution to restore the anticline. In this sense, the geomechanical restoration validates the rotational kinematics of the anticline as well as the magnitude of the rotation reported by paleomagnetic techniques. The geomechanical restoration provides insight about the rotational kinematics and rotation magnitude of the Pico del Águila, but not about the relative rotation in a regional reference frame.

Table 3. Rotation of the anticline according to the 3D restoration

Unit	Age (in Myr) *	Interval Rotation (º)	Cumulative Rotation (º)
GS-IV*	36.6	15	15
GS-III*	37.17	2	17
GS-II*	37.74	10	27
GS-I*	40.04	0	27
Guara	41.52	6	33

* Age refers to the top surfaces. Extracted from Millán *et al.* (1994) and Pueyo *et al.* (2002)

The maximum incremental and cumulative thicknesses and uplifts, sedimentation and uplift ratios from the restoration are summarized in Table 4. Incremental thicknesses were measured from the stratigraphic logs published in Millán et al. (1994) and Millán (1995). Incremental uplifts were calculated extracting from the model the maximum Z increase among the deformed and the restored stage of each unit. To calculate the sedimentation and uplift rates, we considered the incremental uplift and sedimentation values, as well as the age interval between the depositions of two consecutive surfaces. Compaction was not considered. During the deposition of growth sequence I, the structure was characterized by a large uplift rate and a moderately low sedimentation rate (line slopes in Fig. 13 a and c). This is evidenced by the restoration of the growth strata, which shows that the pre-folding sequence still accommodates a large amount of deformation after restoring growth sequence I (Figs. 10 e and 12 e). In spite of the large deformation accommodated by the growth strata, the largest uplift and the lowest sedimentation took place during the early stages of deformation (before and during sedimentation of growth sequence I; Fig. 13 a and c). Large uplift, the creation of space available for sedimentation, and the transgressive cycle that characterized the deposition of the Guara and Arguis Formations (Millán et al., 1994; Castelltort et al., 2003), controlled the change of sedimentary facies from the Guara shallow marine limestones to the Arguis slope marls. Similar to our work, the uplift evolution predicted by Poblet and Hardy (1995) and Poblet et al. (1997) based on

kinematic modelling, indicates a steep uplift ratio in the early stages of deformation, decreasing progressively as shortening advanced (line slopes in Fig. 13 b). These previous works, however, assumed a nearly constant sedimentation rate (line slopes in Fig. 13 d), which our work does not support. The geomechanical restoration suggests increasingly higher sedimentation rates until the deposition of growth sequence II, and nearly constant rates until the end of deformation (line slopes Fig. 13 c). This evolution is observed in both flanks of the structure, although there is a small difference between the flanks: both the uplift and the sedimentation rates are larger in the eastern limb of the anticline than in the western one (Fig. 13 a and c). The ratio between sedimentation and uplift rates during the development of the structure, however, is comparable and within the same order of magnitude in both flanks (Table 4).

Table 4. Kinematic parameters obtained from the 3D reconstruction and restoration of the Pico del Águila anticline, for Eastern and Western limbs.

Eastern Limb								
Unit	Age (Myr)*	IT (m)**	CT (m)	IU (m)	CU (m)	R_s (m/Myr)	R_U (m/Myr)	$R_{U/S}$
Guara (DS3)	41.52	100	100	< 100	< 100	-	-	-
GS-I	40.04	384	484	1360	1360	259.46	918.92	3.54
GS-II	37.74	550	1034	94	1454	239.13	40.87	0.17
GS-III	37.17	440	1474	152	1606	771.93	266.67	0.35
GS-IV	36.6	320	1794	100	1706	561.4	175.44	0.31
Western Limb								
Unit	Age (Myr)*	IT (m)**	CT (m)	IU (m)	CU (m)	R_s (m/Myr)	R_U (m/Myr)	$R_{U/S}$
Guara (DS3)	41.52	100	100	< 100	< 100	-	-	-
GS-I	40.04	225	325	1168	1168	152.03	789.19	5.19
GS-II	37.74	690	1015	138	1306	300	60	0.2
GS-III	37.17	375	1390	125	1431	657.89	219.3	0.33
GS-IV	36.6	340	1730	105	1536	596.49	184.21	0.31

Age refers to the top surfaces; IT: Incremental Thickness; CT: Cumulative thickness; IU: Incremental uplift; CU: Cumulative Uplift; R_S: Sedimentation rate; R_U: Uplift rate; $R_{U/S}$: Uplift/Sedimentation ratio
* Values taken from Millán et al. (1994) and Pueyo et al. (2002); ** Values taken from Millán (1995)

Several works shed light on the folding mechanisms that contributed to the formation of the Pico del Águila anticline. Poblet and Hardy (1995) considered a progressive rotation of the western limb, based on inverse kinematic modeling and analysis of the growth record. Novoa et al. (2000) found a certain component of kink band migration in addition to the progressive limb rotation, based on an inclined-shear restoration of the cross-section presented in Poblet and Hardy (1995). Finally, Vidal-Royo et al. (2010) stated that limb lengthening was the predominant mechanism in the upper units of the pre-folding sequence, whereas

pervasive reverse faulting and limb rotation were the main processes in the lower units of the fold. However, the folding mechanisms are difficult to ascertain with such simplistic kinematic assumptions, given that the mechanisms are closely related to the mechanical properties and behaviour of each unit (Vidal-Royo et al., 2010). Natural folds often deviate from the end-member kinematic models, specifically in cases where large strength contrasts localize strains and influence deformation kinematics (Guzofski et al., 2009). In the case of The Pico del Águila anticline, the complexity of the geological setting is of particular relevance: the vertical-axis rotation, the mechanical interlayering of the stratigraphy, and the interference pattern between N-S and E-W structures led to multiple folding mechanisms that acted simultaneously through the different units and structural domains. The geomechanical restoration shows evidences of complex kinematics, with several folding mechanisms interacting in 3D: In the Guara Formation, a limb lengthening folding mechanism dominates in the periclinal closure, whereas limb rotation is the main mechanism along the N-S oriented part of the limbs. Kink band migration predominates in the hinge of the associated synclines, and a combination of limb lengthening and limb rotation occurs along the E-W oriented limbs. Such differences in the folding mechanisms necessarily imply a differential distribution of strain throughout the structure. As shown by the restoration, strain is distributed differentially depending on the mechanical properties of each unit, on the structural domain, and consequently on the folding mechanisms (Figs. 12 and 14). The partitioning and differences in folding mechanisms and strain across the Pico del Águila were predicted by Vidal-Royo et al. (2010) using 2D Discrete Element models (DEM) of complex mechanical stratigraphy plus growth strata. A comparison between the DEM and a series of cross sections at different stages of the 3D restoration is presented in Fig. 14. The stratigraphy modelled in the DEM consisted of two weak levels characterized by very low internal breaking strength (i.e. allowing flexural flow to occur; purple and orange units in Fig. 14) bounded by stronger units with larger breaking strength. During deformation, syn-kinematic sedimentation was added, characterized by sediments of very low breaking strength (Fig. 14).

There are fundamental differences between the geomechanical restoration (a 3D, inverse, continuum, elastic technique highly affected by predefined discontinuities such as faults and interlayer slip), and the DEM (a 2D, forward, discontinuum technique in which discontinuities arise spontaneously in the model). Due to the limitations of the geomechanical, elastic restoration, strain magnitudes are lower in the restoration than in the DEM (Fig. 14). In the DEM strain is two-dimensional and fully contained in the plane of the model. On the contrary, the cross sections from the restoration display 3D strain in 2D, and represent an average shear strain that is not necessarily contained in the plane of the cross section. In addition, the restoration displays the effect of layer-parallel slip (i.e. contact surfaces), which is not included in the DEM. Layer-parallel slip in the restoration adds local perturbations to the strain field at the contact between units (Fig. 14). Despite these differences, a general comparison between the restoration and the DEM points out interesting resemblances regarding geometry and strain evolution.

In the initial stage (Fig. 14 a), the 3D restoration displays some relict deformation in the lower pre-folding units of the cross-section (Triassic and Garuminan-Cretaceous). This deformation is explained by the fact that the top of the Guara Formation was deposited during the first stages of anticlinal growth, with the underlying units already presenting evidences of incipient fold activity. During the first stages of

deformation and in both, the 3D restoration and DEM, strain preferably concentrates in the hinges of the anticline and synclines suggesting rotation of both limbs (Fig. 14 b and c). Moderately high strain is observed along both limbs, indicating a certain component of limb lengthening, particularly in the NW flank. In the 3D restoration and DEM, the early stage growth strata accommodate deformation mainly in the crest of the anticline rather than in the synclines (Fig. 14 b). In the 3D restoration and DEM, after the maximum strain is reached (coinciding with the beginning of activity of the internal thrust; Fig. 14 c), the kinematics changes, and kink band migration of the synclines (active synclinal axis) is the main

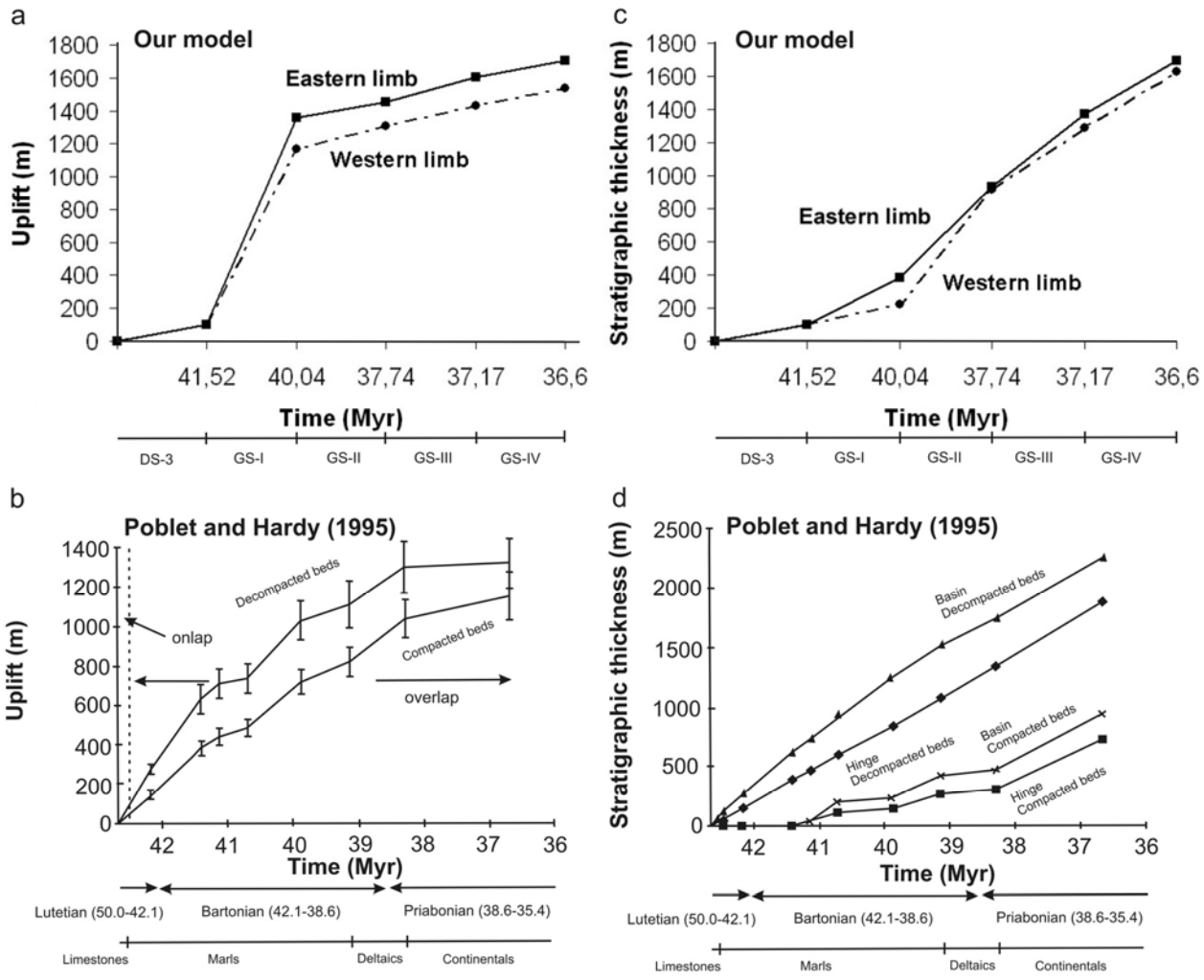

Fig. 13. Comparison of uplift and sedimentation in the Pico del Águila anticline through the deposition of the growth strata: a) uplift calculated for both limbs from the 3D reconstruction and restoration; b) uplift predicted by Poblet and Hardy (1995) using inverse kinematical modelling; c) sedimentation calculated for both limbs from the 3D reconstruction and restoration (decompaction was not considered); d) sedimentation predicted by Poblet and Hardy (1995) from inverse kinematic modeling. In a to d, rates are given by line slopes.

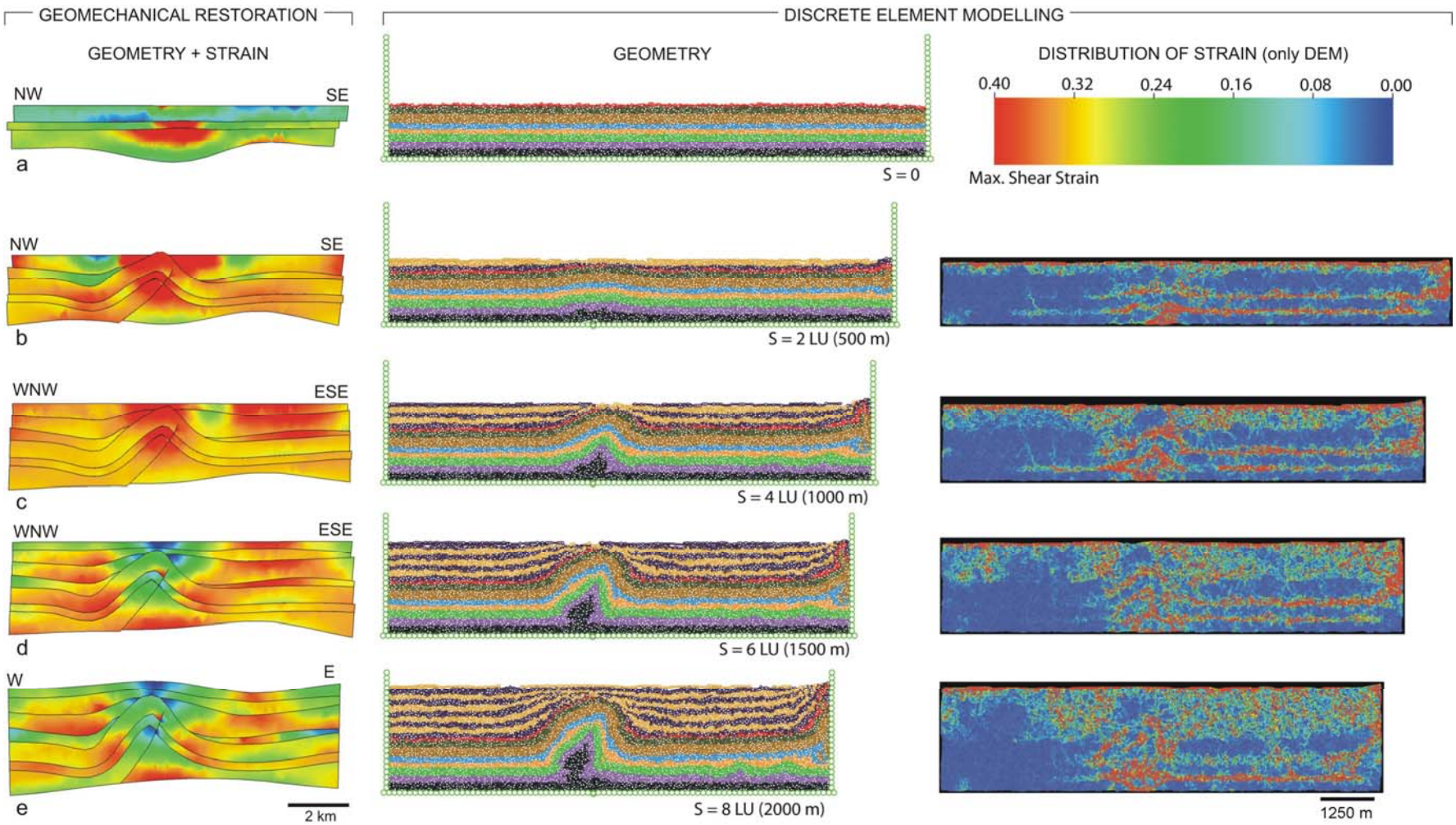

Fig. 14. Comparison of the structural evolution predicted by sections taken from different stages across 3D restoration and 2D Discrete Element Modelling (DEM. Vidal-Royo et al., 2010). Strain in cross sections of 3D restoration (see Fig. 12 for scale) and DEM model is strain between restoration/model steps. a) Initial stage; b) after deposition of growth sequence II and 500 m of shortening in the DEM; c) after deposition of growth sequence III and 1000 m of shortening in the DEM; d) after deposition of growth sequence IV and 1500 m of shortening in DEM; and e) after deforming sequence IV and 2000 m of shortening in the DEM. Strain in the DEM was computed using the program SSPX (Cardozo and Allmendinger, 2009).

mechanism observed within the growth package (Fig. 14 d and e). Similarly, in the pre-folding sequence strain concentrates in the hinges of the synclines, and along the limbs, due to fold growth dominated by limb lengthening rather than rotation. The hinge of the anticline is released from strain, with only local maximums registered near the tip line of the internal thrust (Fig. 14 d and e). As in the 3D restoration, the DEM shows the footwall of the internal thrust displaying a strain maximum at the base of the Triassic (black unit in the DEM). The Garumnian-Cretaceous (equivalent to the orange-green sequence in the DEM) accommodates the maximum strain along the limbs and the hinges of the associated synclines.

CONCLUSIONS

A consideration of the rock mechanical properties of the Pico del Águila anticline allows us to reconstruct the complex fold kinematics of the structure. The 3D reconstruction and geomechanical restoration of the anticline suggest a rotation value of 33º, with a calculated rotation velocity of *ca.* 5.5º/Myr. These values are in accordance with previous works on the kinematics of the structure (Pueyo et al., 2002; Rodríguez-Pintó et al., 2008; Huyghe et al., 2009). Uplift and sedimentation rates varied through time. The uplift rate was much larger than the sedimentation rate in the first stages of deformation (uplift/sedimentation rates ratio of 3.54 in the eastern and 5.19 in the western limb). In the late stages of deformation this relation was inverted (uplift/sedimentation ratio of 0.31 in both flanks). The Pico del Águila anticline displays a large amount of deformation during the deposition of growth sequence I. The creation of space available for deposition of later sequences II, III and IV was due to the emplacement of the South Pyrenean thrust, which developed synchronously to the formation of The Pico del Águila anticline (although it started after the deposition of growth sequence I and continued until Early Miocene). In contrast to previous works (Millán et al., 1995; Pueyo et al., 2002), we believe that the Pico del Águila anticline was not truncated by the emplacement of the Santo Domingo thrust, since the southern closure of the fold is visible in the hangingwall of the South Pyrenean thrust, although it is affected by the interference between N-S and E-W structures.

The 3D reconstruction and restoration of the Pico del Águila anticline suggest that the growth of detachment folds cannot be explained by simplistic kinematics and geometrical assumptions. Common features are observed and convenient folding mechanisms have been described in previous kinematic models such as Poblet and Hardy (1995) and Poblet et al. (1997). However, as suggested by DEM (Vidal-Royo et al., 2010) and geomechanical modelling (Guzofski et al., 2009 and this work), fold kinematics and evolution strongly depend on the spatial distribution of rock mechanical properties and competence contrasts. Therefore, different folding mechanisms may occur simultaneously depending on the mechanical behaviour and brittle-ductile coupling of the stratigraphic units involved in the detachment fold. In addition, the geomechanical restoration demonstrates that multiple folding mechanisms are observed within a given stratigraphic unit depending on the structural domain of the fold. Consequently, the development of a detachment fold in 3D is characterized by a combination of multiple folding mechanisms that occur simultaneously in different units and structural domains during the formation of the anticline. Thus, the understanding of fold kinematics should take into account the mechanical behaviour of the rocks involved in the structure. This is of great importance in petroleum structural geology, specifically for defining the 3D evolution of hydrocarbon traps,

and predicting the 3D strain, fractures, and petrophysical properties distributions of faulted and folded natural reservoirs.

ACKNOWLEDGEMENTS

The authors wish to thank IGEOSS, Paradigm™, and Midland Valley Exploration for providing academic licenses of their software Dynel3D, Gocad, and Move, respectively. This work is an initiative of the Group of Geodynamics and Basin Analysis (GGAC, 2009 SGR 1198) at Universitat de Barcelona. Special thanks to Dr. E. L. Pueyo for fruitful discussions, opinions and critical review of this study. This research was supported by StatoilHydro, the Geomod 3D project (CGL2004-05816-C02-01/BTE), the MODES-4D project (CGL2007-66431-C02-01/BTE) and the Geomodels Institute Consortium. O. Vidal-Royo also acknowledges the Agència de Gestió d'Ajuts Universitaris i a la Recerca (AGAUR) for providing a PhD grant (2005 FI 00200) and additional funds (2008 BE-1 00348) for a 3-month stay at the Center for Integrated Petroleum Research (CIPR), and the Department of Petroleum Engineering at The University of Stavanger (UiS) (Norway). We also wish to thank CIPR and UiS for their logistic support during this period.

REFERENCES

ALMELA, A. & RÍOS, J.M. (1951) *Mapa geológico de España 1:50000 serie Antigua, 248 (Apiés).* 50 pp + map. IGME Ed. Madrid.

ANASTASIO, D.J. (1992) Structural Evolution of the External Sierras, Southern Pyrenees, Spain. In: *Structural Geology of Fold and Thrust Belts* (Ed. by S. Mitra and G.W. Fisher), pp 239-251. Johns Hopkins University Press, Baltimore.

ANASTASIO, D.J. & HOLL, J.E. (2001) Transverse fold evolution in the External Sierras, Southern Pyrenees, Spain. *Journal of Structural Geology*, 23 (2-3), 379-392.

BISTACCHI, A., MASSIRONI, M., DAL PIAZ G. V., DAL PIAZ, G., MONOPOLI, B., SCHIAVO, A. & TOFFOLON, G. (2008) 3D fold and fault reconstruction with an uncertainty model: An example from an Alpine tunnel case study. *Computers and Geosciences*, 34 (4), 351-372.

BORRACCINI, F., DE DONATIS, M., DI BUCCI, D. & MAZZOLI, S. (2002) 3D Model of the active extensional fault system of the high Agri River valley, Southern Apennines, Italy. In: *General Contributions* (Ed. by M. J. Jessell). Journal of the Virtual Explorer, 6, 1-6.

BRAATHEN, A., TVERANGER, J., FOSSEN, H., SKAR, T., CARDOZO, N., SEMSHAUG, S.E., BASTESEN E. & SVERDRUP E. (2009) Fault Facies and its applications to sandstone reservoirs. *American Association of Petroleum Geologists Bulletin,* 93 (7), 891-917.

CARDOZO, N. & ALLMENDINGER, R.W. (2009) SSPX: A program to compute strain from displacement/velocity data. *Computers and Geosciences*, 35, 1343-1357.

CASTELLTORT, S., GUILLOCHEAU, F., ROBIN, C., ROUBY, D., NALPAS. T., LAFONT, F. & ECHARD, R. (2003) Fold control on the stratigraphic record: a quantified sequence stratigraphic study of the Pico del Aguila anticline in the south-western Pyrenees (Spain). *Basin Research*, 15, 527-551.

FALIVENE, O. (2007) *Testing three-dimensional facies reconstruction and modelling techniques applied to cored and outcropping analogues. Examples from swamp coal zones to alluvial fans and marine turbidite sequences*. PhD Thesis. Universidad de Barcelona. Departament d'

Estratigrafia, Paleontologia i Geociencies Marines y Departament de Geodinamica i Geofisica.

FERNÁNDEZ, O., MUÑOZ, J.A., ARBUÉS. P., FALIVENE, O. & MARZO, M. (2004). Three-dimensional reconstruction of geological surfaces: An example of growth strata and turbidite systems from the Ainsa basin (Pyrenees, Spain). *American Association of Petroleum Geologists Bulletin*, 88 (8), 1049-1068.

FERNÁNDEZ, O. (2004) *Reconstruction of geological structures in 3D: An Example from the southern Pyrenees.* PhD Thesis, Departament de Geodinàmica i Geofísica, Universitat de Barcelona, Barcelona, Spain.

FERNÁNDEZ, O. (2005) Obtaining a best fitting plane through 3D georeferenced data. *Journal of Structural Geology*, 27, 855-858.

FORD, M., LE CARLIER DE VESLUD, C. & BOURGEOIS, O. (2007). Kinematic and geometric analysis of fault-related folds in a rift setting: The Dannemarie basin, Upper Rhine Graben, France. *Journal of Structural Geology*, 29, 1811-1830.

GRANDO, G.,SCHLEDER, Z., SHACKLETON, R., SEED, G., BUDDIN, T., MCCLAY, K. & BORRACCINI, F. (2009) 3D structural evolution and kinematics of the Frampton growth fold system, Western Mississippi Fan Fold Belt, deep-water Gulf of Mexico. *Search and Discovery Article* # 50161.

GUZOFSKI, C.A., MUELLER, J.P., SHAW, J.H., MURON, P., MEDWEDEFF, D.A., BILOTTI, F. & RIVERO, C. (2009) Insights into the mechanisms of fault-related folding provided by volumetric structural restorations using spatially varying mechanical constraints. *American Association of Petroleum Geologists Bulletin*, 93 (4), 479-502.

HOGAN P.J. & BURBANK, D.W. (1996) Evolution of the Jaca Piggyback basin and emergence of External Sierras, Southern Pyrenees. In: *Tertiary Basins of Spain* (Ed. by P.F. Friend and C.J. Dabrio), pp. 153-160. Cambridge University Press.

HOLL, J.E. & ANASTASIO, D.J. (1993) Paleomagnetically derived folding rates, southern Pyrenees, Spain. *Geology*, 21 (3), 271-274.

HUYGHE, D., MOUTHEREAU, F., CASTELLTORT, S., FILLEAUDEAU. P.Y. & EMMANUEL, L. (2009) Paleogene propagation of the southern Pyrenean thrust wedge revealed by finite strain analysis in frontal thrust sheets: Implications for mountain building. *Earth and Planetary Science Letters*, doi:10.1016/j.epsl.2009.10.002.

IGME. (1992) *Mapa Geológico de España, Hoja 248, Apiés.* Unpublished 36 pp report + 1:50000 map. Instituto Geológico y Minero de España, Madrid.

MAERTEN, L. & MAERTEN, F. (2006) Chronologic modeling of faulted and fractured reservoirs using geomechanically based restoration: Technique and industry applications. American *Association of Petroleum Geologists Bulletin*, 90 (8), 1201-1226.

MAERTEN, L., GILLESPIE, P. & DANIEL, J.M. (2006) Three-dimensional geomechanical modeling for constraint of subseismic fault simulation. *American Association of Petroleum Geologists Bulletin*, 90 (9), 1337-1358.

MAERTEN, L. (2007) Geomechanics to solve structure related issues in petroleum reservoirs. *AAPG-ER Newsletter*, September 2007.

MALLADA, L. (1878) *Geología de la provincial de Huesca. Mem. Com.* Mapa geológico de España, Madrid. 559 pp.

MILLÁN, H., AURELL, M. & MELÉNDEZ, A. (1994) Synchronous detachment folds and coeval sedimentation in the Prepyrenean External Sierras (Spain): a case

study for a tectonic origin of sequences and system tracts. *Sedimentology*, 41 (5), 1001-1024.

MILLÁN, H. (1995) *Estructura y Cinemática del frente de cabalgamiento surpirenaico en las Sierras Exteriores Aragonesas*. PhD Thesis, Departamento de Ciencias de la Tierra, Universidad de Zaragoza, Zaragoza.

MITRA, S. (2003) A unified kinematic model for the evolution of detachment folds. *Journal of Structural Geology*, 25, 1659-1673.

MORETTI, I. (2008) Working in complex areas: New restoration workflow based on quality control, 2D and 3D restorations. *Marine and Petroleum Geology*, 25, 205-218.

NOVOA, E., SUPPE, J. & SHAW, J.H. (2000) Inclined-Shear Restoration of Growth Folds. *American Association of Petroleum Geologists Bulletin*, 84 (6), 787-804.

OLIVA-URCÍA, B. & PUEYO, E.L. (2007) Gradient of shortening and vertical-axis rotations in the Southern Pyrenees (Spain), insights from a synthesis of paleomagnetic data. *Revista de la Sociedad Geológica de España*, 20 (1-2), 105-118.

POBLET, J. & HARDY, S. (1995). Reverse modelling of detachment folds; application to the Pico del Aguila anticline in the South Central Pyrenees (Spain). *Journal of Structural Geology*, 17 (12), 1707-1724.

POBLET, J., MCCLAY, K.R., STORTI, F. & MUÑOZ, J.A. (1997) Geometries of syntectonic sediments associated with single-layer detachment folds. *Journal of Structural Geology*, 19 (3-4), 369-381.

PUEYO, E.L. (2000) *Rotaciones Paleomagnéticas en Sistemas de Pliegues y Cabalgamientos. Tipos, Causas, Significado y Aplicaciones (Ejemplos de las Sierras Exteriores y Cuenca de Jaca, Pirineo Aragonés).* PhD Thesis, Departamento de Ciencias de la Tierra, Universidad de Zaragoza, Zaragoza.

PUEYO, E.L., MILLÁN, H. & POCOVÍ, A. (2002) Rotation velocity of a thrust: a paleomagnetic study in the External Sierras (Southern Pyrenees). *Sedimentary Geology*, 146 (1), 191-208.

PUEYO, E.L., POCOVÍ, A, PARÉS, J.M., MILLÁN, H. & LARRASOAÑA, J.C. (2003) Thrust ramp geometry and spurious rotations of paleomagnetic vectors. *Studia Geophysica Geodetica*, 47, 331-357.

PUIGDEFÀBREGAS, C. (1975) La Sedimentación Molásica en la Cuenca de Jaca. *Monografías del Instituto de Estudios Pirenaicos. Número Extraordinario de Revista Pirineos*, 104, Instituto de Estudios Pirenaicos, Jaca.

RODRIGUEZ-PINTÓ, A., PUEYO, E.L., POCOVÍ, A. & BARNOLAS, A. (2008) Cronología de la actividad rotacional en el sector central del frente de cabalgamiento de Sierras Exteriores (Pirineo Occidental). *Geotemas*, 10, 1207-1210.

ROUBY, D. & COBBOLD, P.R. (1996) Kinematic analysis of a growth fault system in the Niger Delta from restoration in map view. *Marine and Petroleum Geology*, 13 (5), 565-580.

SANDERS, C., BONORA, M., RICHARDS, D., KOZLOWSKI, E., SYLWAN, C. & COHEN, M. (2004) Kinematic structural restorations and discrete fracture modeling of a thrust trap: a case study from the Tarija Basin, Argentina. *Marine and Petroleum Geology*, 21, 845-855.

SCHULTZ, R.A. (1996) Relative scale and the strength and deformability of rock masses. *Journal of Structural Geology*, 18 (9), 1139-1149.

SELZER. G. (1948) Geología de las sierras surpirenaicas del Alto Aragón. (Translated from the original version, "Geologie der sudpyrenäische Sierren in Oberaragonien", Berlin, 1934). *Publicación Extraordinaria Geol. España. C.S.I.C.*, 185-231.

SOLER, M. & PUIGDEFÀBREGAS, C. (1970) Líneas generales de la geología del Alto Aragón Occidental. *Pirineos*, 96, 5-20.

TANNER, D.C., BERHMANN, J.H. & DRESMANN, H. (2003) Three-dimensional retro-deformation of the Lechtal Nappe, Northern Calcareous Alps. *Journal of Structural Geology*, 25, 737-748.

VIDAL-ROYO, O., KOYI, H.A. & MUÑOZ, J.A. (2009) Formation of orogen-perpendicular thrusts due to mechanical constrasts in the basal décollement in the Central External Sierras (Southern Pyrenees, Spain). *Journal of Structural Geology*, 31, 523-539.

VIDAL-ROYO, O., HARDY, S. & MUÑOZ, J.A. (2010) The roles of complex mechanical stratigraphy and syn-kinematic sedimentation in fold development: Insights from discrete-element modelling and application to the Pico del Águila anticline (External Sierras, Southern Pyrenees). In: *Kinematic Evolution and Structural Styles of Fold-and-Thrust Belts* (Ed. by J. Poblet and R.J. Lisle), Special Publication of the Geological Society, *accepted*.

ZANCHI, A., SALVI, F., ZANCHETTA, S., STERLACCHINI, S., & GUERRA, G. (2009) 3D reconstruction of complex geological bodies: Examples from the Alps. *Computers and Geosciences*, 35, 49-69

CHAPTER V

Results and General Discussion: Integration of modelling techniques

In this chapter we present a summary of the results presented in previous sections and discuss the validation and integration of these results in order to construct a unified conceptual model of evolution for the Pico del Águila anticline. Since this part of the Thesis addresses the benefits, drawbacks, limitations and whole integration of the results presented in the previous chapters, a general discussion about the modelling techniques, their results, suitability and applications is also offered. This integrated work, general discussion and model of evolution for the Pico del Águila anticline has been carried out as the fourth scientific publication of this Thesis. As in the previous chapters, an abridged summary in Catalan is presented firstly, followed by the abridged abstract in English and the publication itself. The work has been submitted to the journal *Geologica Acta* and is cited as follows:

Vidal-Royo, O., Muñoz, J.A., Hardy, S., Koyi, H.A., Cardozo, N., (submitted). Integration of modelling techniques in the understanding of the structural evolution of the Pico del Águila anticline (External Sierras, Southern Pyrenees). Submitted to Geologica Acta.

5.1 RESUM DEL CAPÍTOL (Summary in Catalan)

Presentem en aquest capítol un resum dels resultats exposats en els capítols anteriors d'aquesta Tesi, així com una discussió general sobre la validació i integració d'aquests resultats per tal d'elaborar un model conceptual unificat d'evolució per l'anticlinal del Pico del Águila. Atès que aquesta part de la Tesi versa sobre els beneficis, desavantatges i limitacions dels models i la integració general dels resultats presentats en els capítols previs, s'ofereix també una discussió general sobre les tècniques de modelització emprades, els resultats obtinguts, la seva escaiença i les seves aplicacions.

L'anticlinal del Pico del Águila és un conegut exemple de plec de desenganxament amb sedimentació marina a fluvio-deltaica associada, amb una tendència estructural N-S, paral·lela a la direcció de transport tectònic dels Pirineus Meridionals.

Basat en observacions de camp que indiquen una distribució heterogènia del nivell de desenganxament Triàsic, els models analògics mostren el procés de generació d'estructures perpendiculars al sistema orogènic que poden donar lloc als anticlinals N-S descrits a les Sierras Exteriores Aragonesas.

Els models numèrics investiguen l'efecte d'una estratigrafia mecànica complexa, caracteritzada per una intercalació d'unitats competents i incomptetents (amb marcades diferències en el grau de competència, per tant) i de la sedimentació sin-cinemàtica en el creixement i evolució de l'anticlinal.

Basat en dades de camp i interpretacions de perfils sísmics s'ha portat a terme una reconstrucció i restitució geomecànica tridimensional de l'anticlinal del Pico del Águila. D'aquestes se'n deriva la coexistència de de múltiples mecanismes de plegament actuant simultàniament en diferents unitats i dominis estructurals, la qual implica al seu torn un patró i distribució de la deformació que no poden ser avaluats mitjançant aproximacions o tècniques de modelització cinemàtiques o/i bidimensionals.

S'integren també els resultats obtinguts a partir de les esmentades tècniques de modelització amb les dades i coneixements previs de la regió, es

discuteixen els beneficis, desavantatges i limitacions de cadascuna d'aquestes tècniques de modelització, i es presenta un model integrat d'evolució estructural del Pico del Águila. Aquest anàlisi crític dels resultats i aquest esforç d'integració porten sense dubte cap a una millor comprensió de l'estructura i dels processos que menaren l'evolució dels plecs de desenganxament N-S de les Sierras Exteriores Aragonesas dels Pirineus Meridionals.

5.2 ABRIDGED SUMMARY

This paper reports on the integration of different modelling techniques to construct a unified and better constrained conceptual model of structural evolution of the Pico del Águila anticline (External Sierras, Southern Pyrenees, Spain). The structure is a well-known example of detachment fold, which exhibits a N-S structural trend, parallel to the direction of tectonic transport in the Southern Pyrenees. Based on field observations of an unevenly distributed Triassic décollement, analogue modelling show how to generate orogen-perpendicular structures which may result in transverse anticlines. Numerical models investigate the effect of a complex mechanical stratigraphy, characterized by an interlayering of competent and incompetent layers, plus syn-kinematic sedimentation in the fold growth. Based on field data and seismic interpretations, a 3D reconstruction and sequential geomechanical restoration of the Pico del Águila anticline reports the coexistence of multiple folding mechanisms occurring simultaneously in different units and structural domains of the fold, leading to a complex strain pattern that can not be assessed by simplistic kinematic 2D approaches. By integrating the presented models with the previous data in the region, we discuss about the benefits and drawbacks of each modelling technique and present an integrated model of structural evolution for the Pico del Águila anticline. This brings a better comprehension of the structure as well as the processes that drove the evolution of the N-S detachment anticlines in the External Sierras of the Southern Pyrenees.

Structural evolution of the Pico del Águila anticline (External Sierras, Southern Pyrenees) derived from sandbox, numerical and 3D modelling techniques

O. VIDAL-ROYO [1]*, J.A. MUÑOZ [1], S. HARDY [1, 2], H. KOYI [3] and N. CARDOZO [4]

[1] Geomodels Institute. GGAC, Departament de Geodinàmica i Geofísica, Universitat de Barcelona
Facultat de Geologia. C/ Martí i Franquès s/n, 08028, Barcelona, Spain

[2] ICREA (Institució Catalana de Recerca i Estudis Avançats), Catalonia, Spain

[3] Hans Ramberg Tectonic Laboratory, Department of Earth Sciences, Uppsala University
Villavägen 16, SE-752 36, Uppsala, Sweden

[4] Department of Petroleum Engineering, University of Stavanger
PC 4036 Stavanger, Norway
*Corresponding author: oskarvidal@ub.edu (O. Vidal-Royo)

ABSTRACT

This paper reports on the integration of different modelling techniques to construct a unified and better constrained conceptual model of structural evolution of the Pico del Águila anticline (External Sierras, Southern Pyrenees, Spain). The structure is a well-known example of detachment fold, which exhibits a N-S structural trend, parallel to the direction of tectonic transport in the Southern Pyrenees. Based on field observations of an unevenly distributed Triassic décollement, analogue modelling show how to generate orogen-perpendicular structures which may result in transverse anticlines. Numerical models investigate the effect of a complex mechanical stratigraphy, characterized by an interlayering of competent and incompetent layers, plus syn-kinematic sedimentation in the fold growth. Based on field data and seismic interpretations, a 3D reconstruction and sequential geomechanical restoration of the Pico del Águila anticline suggests the coexistence of multiple folding mechanisms occurring simultaneously in different units and structural domains of the fold, leading to a complex strain pattern that can not be assessed by simplistic kinematic 2D approaches. By integrating the models with previous data in the region, we discuss the benefits and drawbacks of each modelling technique and present an integrated model of structural evolution for the Pico del Águila anticline. This allows us a better comprehension of the structure as well as the processes that drove the evolution of the N-S detachment anticlines in the External Sierras of the Southern Pyrenees.

KEYWORDS | Analogue modelling, Numerical modelling, 3D model, restoration, detachment, Pico del Águila.

INTRODUCTION

Geological models in Earth Sciences provide explanations and improve the understanding of the geological processes that may take place in the planet. In most cases, they should not purport to be a direct replica of nature but a way to simulate and represent geological processes in a feasible timescale for human-beings.

Structural geology has a long history in the use of modelling as a tool to better understand the generation and evolution of structures. Since the first attempts in sandbox experiments (Hall, 1815; Daudre, 1879; Cadell, 1888; among others), a wide variety of modelling techniques have arisen and developed as a result of geoscientists' needs to solve new concerns. Analogue models have become more sophisticated, incorporating elements and devices that produce more quantitative results to compare with nature (Koyi, 1997). With the rise and spread of computers, numerical models have been developed contributing with mathematical algorithms that brought great advances in the understanding of geological processes (Krumbein and Graybill, 1965; Agterberg, 1967; Harbaugh and Merriam, 1968). In this sense, numerical models added a quantitative control of the laws and parameters that govern natural processes.

Despite all these advances, each modelling technique usually has its particular strengths, weaknesses and limitations, which results in a relatively simplified or incomplete representation of nature. This makes each approach suitable for certain purposes, keeping in mind that knowing the limitations of the technique is essential to correctly understand what a model is delivering. For this reason, behind each model there should be feasible parameters to test and/or observable processes to unveil, rather than an attempt to make a detailed replica of a natural case.

In this study we present three different modelling approaches to better understand the structural evolution of the N-S anticlines in the External Sierras of the Southern Pyrenees (Spain). Among them, we selected the Pico del Águila anticline as a target structure, since it is a world-class example of detachment anticline, easily accessible, and exhibits good exposure and a geological map that can be understood as a down-plunge section of the anticline. The N-S transverse anticlines are characterized by the interference pattern with the E-W Pyrenean-trend structures. The N-S anticlines show a high degree of preservation of the entire growth strata record, which allows us to constrain the timing of deformation. The structure is well-known and has been reported in a plethora of publications of multiple disciplines. New insights about the kinematics and structural evolution of the Pico del Águila have been derived from sedimentological analysis (Millán et al., 1994; Castelltort et al., 2003), paleomagnetism (Pueyo et al., 2002; Rodríguez-Pintó et al., 2008), analogue modelling (Nalpas et al., 1999, 2003), 2D kinematical models (Poblet and Hardy, 1995; Poblet et al., 1997), restoration of cross sections (Novoa et al., 2000) and other multidisciplinary approaches (Huyghe, et al., 2009). Despite this plethora of multidisciplinary works, there is a lack of integrated studies gathering the insights

provided by different modelling techniques to complement and validate each other.

All these reasons make the Pico del Águila anticline an ideal structure to reconstruct in 3D. In our study we first present a 3D reconstruction of the Pico del Águila, from which the geometry of the interference pattern between N-S and E-W structures is unveiled. Rather than providing answers about the structural evolution, the 3D model poses new questions about the geological processes that took place in the generation and evolution of the anticline. These questions were tackled by using different modelling techniques, which are presented after the 3D model. In this sense, our study aims to present a unified and better constrained model of structural evolution based on the integration of results from analogue modelling (Vidal-Royo et al., 2009), 2D mechanical models (Vidal-Royo et al., 2010) and 3D geomechanical restoration of the Pico del Águila anticline (Vidal-Royo et al., *submitted*). The presented analogue models show how orogen-perpendicular structures can be generated in a single event of shortening due to strong mechanical contrasts in the basal décollement level. The numerical models evaluate the importance of mechanical stratigraphy and syn-kinematic sedimentation in the growth of a detachment anticline such as the Pico del Águila. Finally, the 3D geomechanical restoration shows the complexity of the interference pattern in the Pico del Águila anticline, its sequential evolution through time as well as the combination of multiple folding mechanisms acting simultaneously during the fold growth.

GEOLOGICAL SETTING

The geology of the External Sierras is widely known and reported in many studies through the years. A detailed discussion of the geological aspects of the area is beyond the scope of this work. The interested reader will find accurate descriptions of the field geology in key publications as Puigdefàbregas (1975), Millán et al. (1994), and Pueyo et al. (2002). However, a general overview is offered for completeness.

The Pico del Águila anticline is located in the External Sierras ("Sierras Exteriores Aragonesas") of the Southern Pyrenees. The External Sierras consists of several imbricated thrust sheets detached on evaporitic, calcareous and dolomitic facies of the Middle and Upper Triassic (Muschelkalk and Keuper facies) (Soler and Puigdefàbregas, 1970; IGME, 1992; Millán et al. 1994; Millán, 1995; Pueyo et al., 2002). It constitutes the frontal emerging part of the South-Pyrenean thrust sheet and is displaced southwards over the Tertiary sediments of the Ebro foreland basin.

One of the peculiarities of the Central External Sierras (CES from now on) is the presence of a set of N-S to NW-SE anticlines. These structures are perpendicular to the general structural trend of the Pyrenees (E-W; tectonic transport towards the south) and create a complex interference pattern (Fig. 1). The N-S anticlines become younger and smaller westwards (Millán et al., 1994; Millán, 1995) and their growth was synchronous with the deposition of Middle Eocene to Oligocene sediments (Fig. 2) and

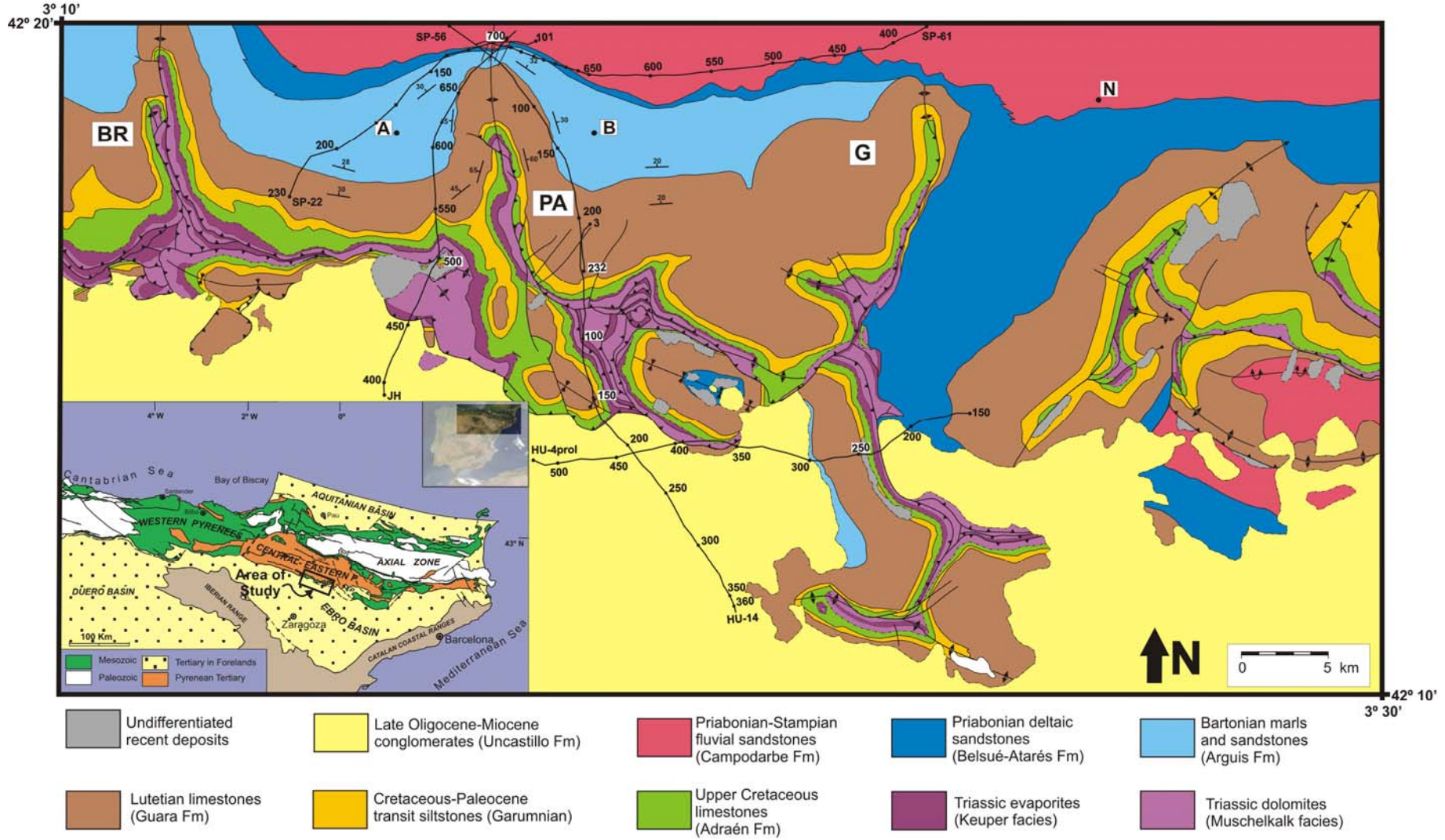

FIGURE 1 | **Geological map of the Central External Sierras (modified from IGME, 1992). BR: Bentué de Rasal anticline; PA: Pico del Águila anticline; G: Gabardiella anticline complex; A: Arguis Village; B: Belsué Village. Inset shows the location and the regional tectonic setting of the study area. Black lines indicate the seismic profiles used to reconstruct the morphology of the Pico del Águila at depth.**

the development of the South-Pyrenean thrust front (active until Early Miocene times; Puigdefàbregas, 1975; Holl and Anastasio, 1993; Millán et al., 1994; Millán, 1995).

The Pico del Águila is one of the most studied N-S anticlines of the CES. It grew from 42.67 ± 0.02 Ma (Upper Lutetian) to 34.8 ± 1.72 Ma (Lower Priabonian) (Poblet and Hardy, 1995) and displays a spectacular growth strata record (Figs. 3 and 4) (Millán et al., 1994; Millán, 1995, Poblet and Hardy, 1995; Pueyo et al., 2002; Castelltort et al., 2003; Vidal-Royo et al., 2010).

The stratigraphic record of the CES is an interlayered sequence of competent and incompetent units (Millán et al., 1994), each of them showing a different mechanical response to deformation (Vidal-Royo et al., 2010). The stratigraphy of the area consists of a few hundred metres thick Mesozoic succession covered by a thicker Paleogene sequence (Fig. 2). The Mesozoic consists of Triassic limestones, dolomites and gypsum-bearing clays, and Upper Cretaceous shallow marine limestones. The Paleogene comprises continental sandstones, siltstones and lacustrine limestones of the Cretaceous-Paleocene transition (Garumnian facies), shallow marine platform limestones of the Guara Formation (Lutetian), shallow marine and transitional marls, limestones and deltaic sandstones of the Arguis and Belsué-Atarés Formations (Upper Lutetian to Middle Priabonian), and fluvial clays, sandstones and conglomerates of the Campodarbe Formation (Middle Priabonian to Middle Oligocene).

The pre-folding sequence comprises Triassic to Lutetian rocks with the upper limit atop of the depositional sequence 2 of the Guara Formation. Within the Triassic décollement, field observations and geological mapping (IGME, 1992) indicate that Muschelkalk limestones and dolomites (Middle Triassic rocks) are the oldest materials outcropping in the core of the anticline (Fig. 1) and are internally thrusted, showing high internal deformation. On the other hand, although Keuper clays and evaporites (Upper Triassic rocks) outline the geometry of the fold as the rest of the upper Mesozoic sequence do, important decrease of thickness is observed towards the inner part, where it is nearly absent in the core of the anticline (Fig. 1). In such a way, Keuper facies are thicker and better exposed in the areas between, rather than in the core of the N-S anticlines, where the frontal South-Pyrenean thrust emerges. The syn-folding sequence comprises the depositional sequence 3 of the Guara Formation (Fig. 3) and the shallowing upwards sequence formed by the Arguis, the Belsué-Atarés and the base of the Campodarbe Formations. The base of the Arguis Formation defines a regional unconformity, indicating a steep change to slope depositional environments (Figs. 2 and 4). Millán et al. (1994) defined four major depositional sequences within the Arguis and Belsué-Atarés Formations. Sequence I (named GS-I herein) is made of Late Lutetian to Early Bartonian blue marls and sandy glauconite-bearing marls. This sequence thins towards the crest of the anti-

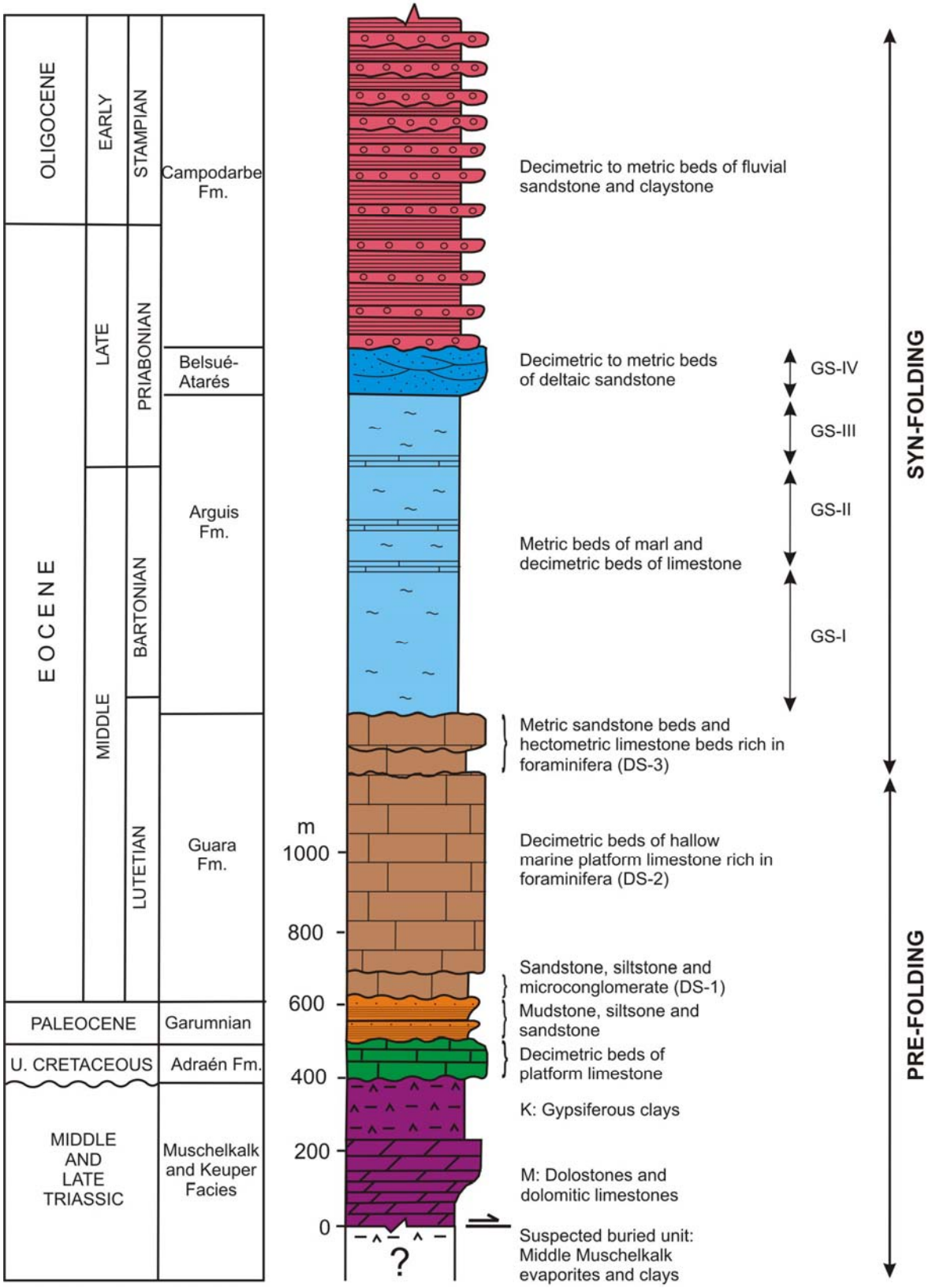

FIGURE 2 | Stratigraphic column describing the lithologies and average thicknesses of the materials involved in the Central External Sierras. M: Muschelkalk facies; K: Keuper facies. DS: Depositional sequences within Guara Fm. GS: Depositional sequences within the growth strata (Arguis and Belsué-Atarés Fms.). Modified after Millán et al., 1994.

cline and is not existent at the hinge area (Fig. 4). Sequence II (named GS-II herein) is Middle to Late Bartonian in age, and comprises barely bioturbated blue marls. Sequence III (named GS-III herein) is a pectinid platform of Early Priabonian age formed by barely bioturbated blue marls rich in marine fossil content. Sequence IV (named GS-IV herein) is formed by Early Priabonian deltaic sandy marls and pure siliciclastic levels formed by deltaic progradation. The lower limit of this sequence is equivalent to the contact between the Arguis and Belsué-Atarés Formations. The upper limit is a regional unconformity, recognizable all along the South-Pyrenean basin, and corresponding to the contact between the Belsué-Atarés and Campodarbe Formations (Fig. 2). This unconformity represents a sharp transition to continental depositional environments.

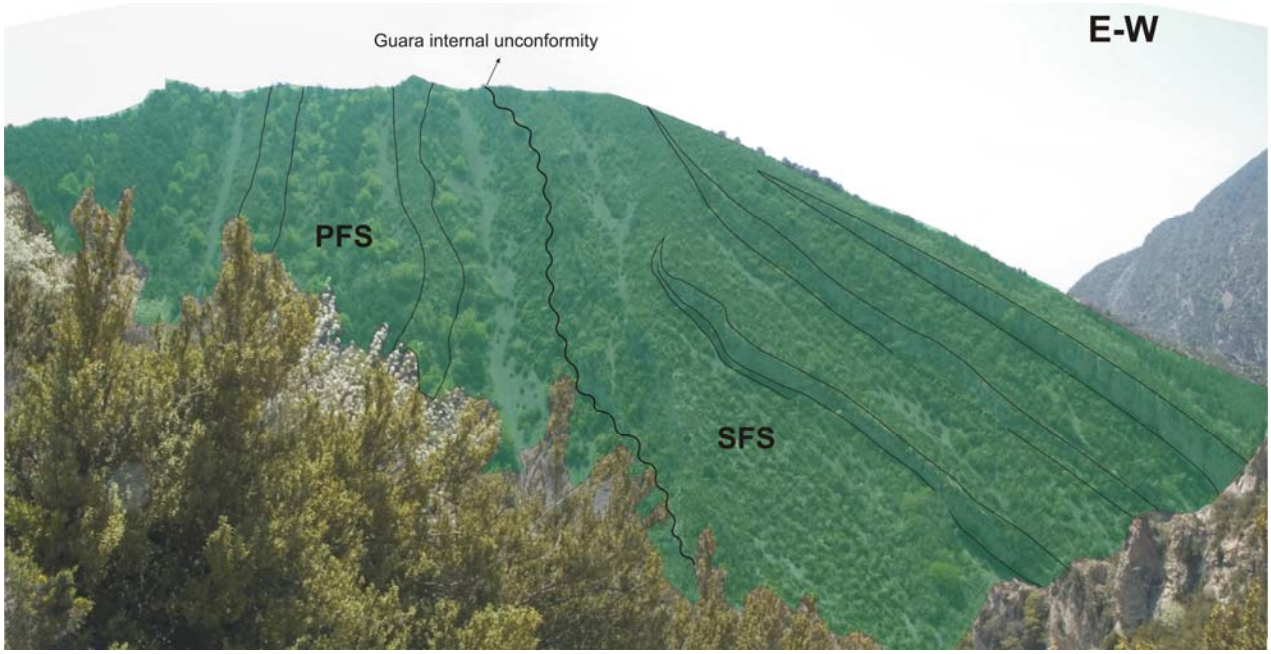

FIGURE 3 **Oblique photograph of the uppermost part of the western limb. It shows an internal unconformity of Guara limestone Fm that separates the Pre-Folding Sequence (PFS) and the Syn-Folding Sequence (SFS). See how the horizons of the SFS clearly thin towards the E.**

3D-RECONSTRUCTION OF THE PICO DEL ÁGUILA ANTICLINE

Methodology of reconstruction

The reconstruction of the Pico del Águila anticline is based on surface and subsurface data, which have been integrated in a 3D GIS framework. This results in a better constrained model that honours all the available data. The acquired data at surface comprise dip measurements, fault and fracture traces and measurement, and a detailed field mapping of bedding traces within the growth strata record. These data were positioned in 3D onto a Digital Terrain

Model of the area with resolution ± 2.5 m (Fig. 5). The Pico del Águila anticline was reconstructed by applying the *Dip Domain Method* (Fernández et al., 2004 a and b), which states that geometries can be simplified to volumes in which bedding attitude is constant (Fig. 6).

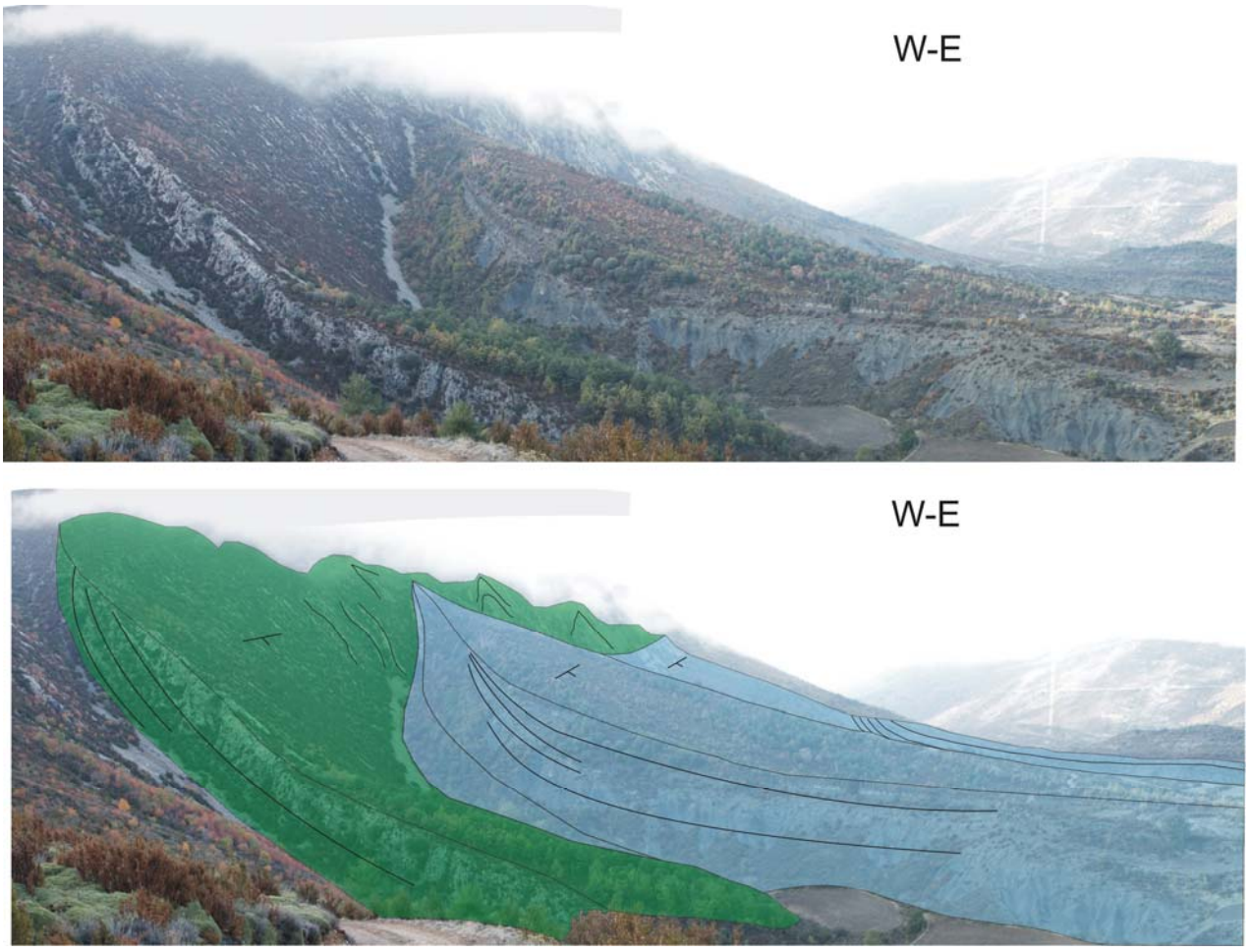

FIGURE 4 | Oblique photograph of the eastern limb of Pico del Águila anticline. One can clearly observe the onlap of Arguis marls (in blue) thinning towards the Guara limestones (in green).

To apply the dip-domain method, a comprehensive geometrical model must be established from the available data. This geometrical model must include: 1) a definition of dip domains (average bedding attitude of the domain and polarity, position, and extent of boundaries); and 2) a definition of 3D stratigraphic geometries (a model of stratigraphic separations between different horizons). A totality of 91 dip domains have been defined for the top of the Guara Formation, assuming ± 5º in strike direction and ± 3º in dip value as a tolerance limit between domains. By intersecting the

adjacent dip domains, the map of structural contours is obtained. From this, the interpolation of the structural contours was easily performed in GOCAD (Paradigm™), obtaining a smoother geometry of the reference surface that honours all the input data. The rest of the pre-folding surfaces were reconstructed using a tool in 3DMove (Midland Valley Exploration) that allows creating new folded surfaces from an existing one, for parallel and similar folds. Since the Pico del Águila is considered a kilometric-scale parallel fold (Millán, 1995), the parallel fold tool was used to reconstruct the geometry of the Triassic, Upper Cretaceous and Garumnian top surfaces. The syn-folding surfaces were constructed individually applying the Dip Domain Method. To control the variation in thickness we have benefited from the excellent exposure of the growth strata and the stratigraphic logs taken from Millán et al. (1994).

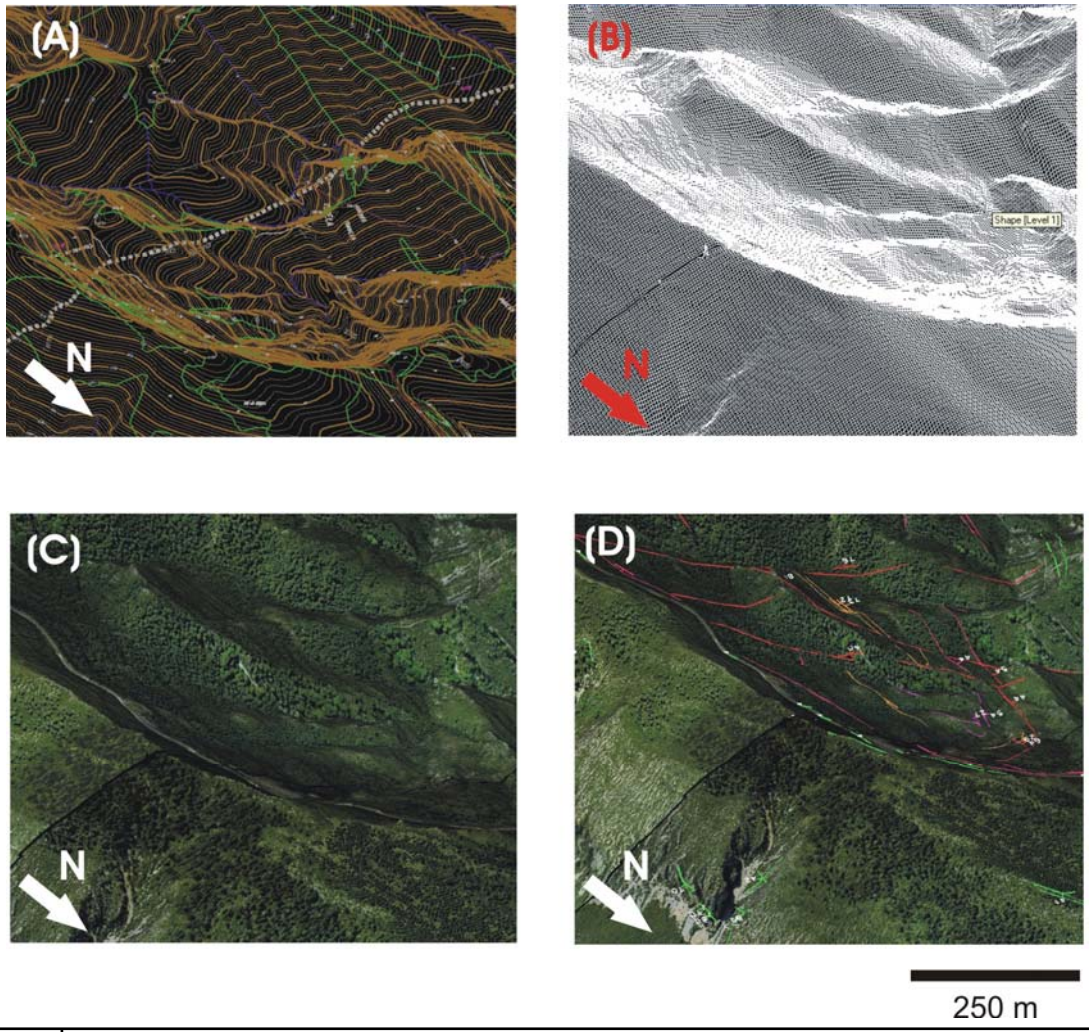

FIGURE 5 | **Different steps of the DTM construction and digitization of the acquired data. (A) 1:5000 Digital Topographical map, from which a XYZ elevation model is extracted. After that, a triangulation is carried out, creating a net made of triangles. From this one, a 5 x 5 m regular lattice is created (B), in which the corresponding ortophotograph is upholstered (C). Once the DTM is ready, digitalization process can be carried out, placing all the available data (D).**

Subsurface data consist of several seismic profiles which have been interpreted to understand the structure in depth and validate the field interpretations. Due to the poor quality of the seimic data, only the general features of the pre-folding sequence were interpreted, as well as the geometry of the South-Pyrenean frontal thrust. The seismic interpretation was then converted to depth using the interval velocity of each unit as deduced from an exploratory well outside the area and the Common Depth Points (CDP's) of the seismic profiles. This information was brought to the reference 3D framework, in order to correlate between the different profiles. A map of structural contours in 3D was then created for each fault/horizon. In case of the pre-folding stratigraphic horizons, the new data was attached as control points in depth to the corresponding contour map.

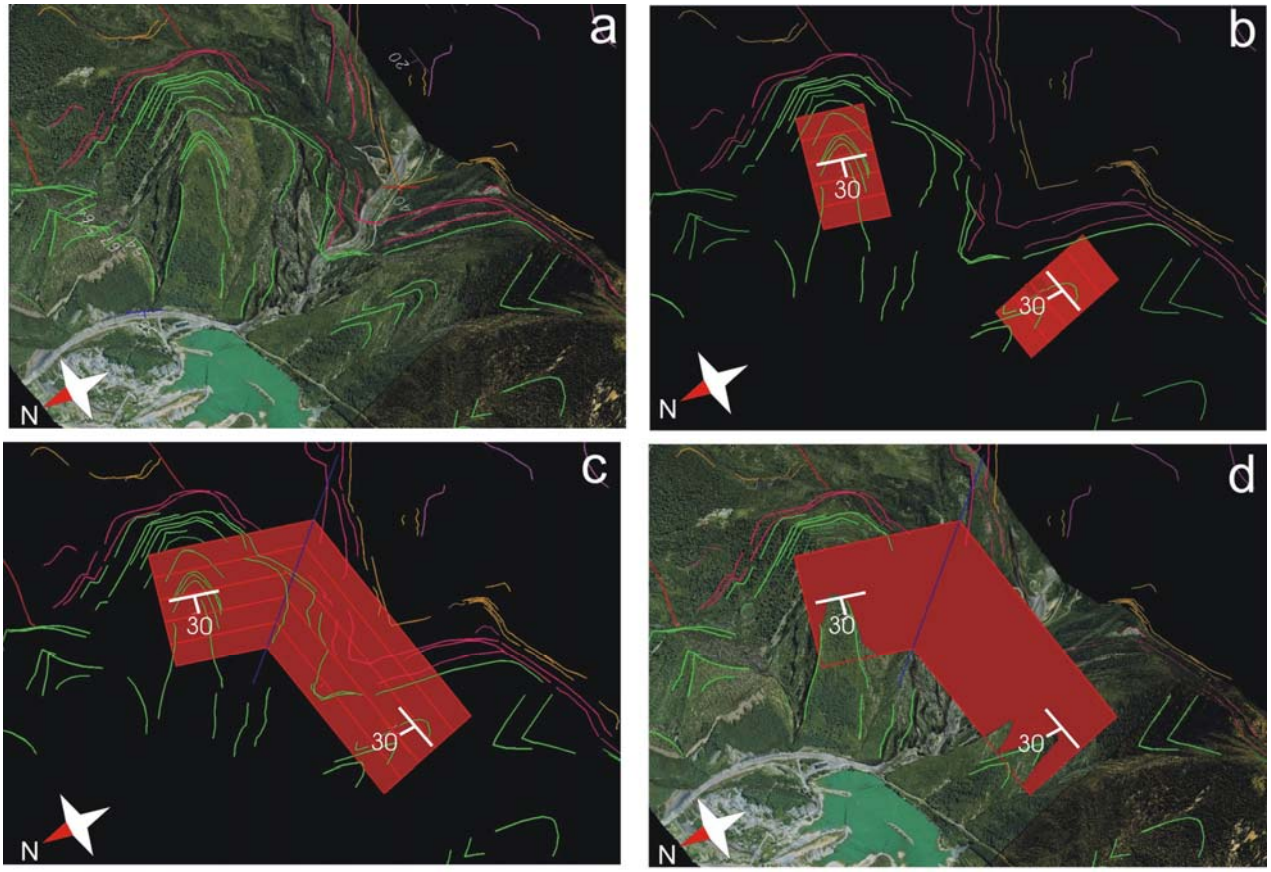

FIGURE 6 **Sketches summarizing the procedure followed in the creation of the 3D reconstruction: positioning of the dip data (a), creation of the dip domains (b), definition of the extension, intersection of the dip domains, and generation of the map of structural contours (c), and generation of the surface (d).**

Results

Eight stratigraphic horizons and nine faults were reconstructed. For the pre-folding sequence, the reconstructed top horizons are (Fig. 7): 1) the Guara Formation (reference surface of the fold); 2) the Garumnian facies (Cretaceous-Tertiary transition); 3) the Upper Cretaceous; and 4) the Triassic rocks. Eight fault surfaces and an internal N-S thrust as well as the geometry of the South-Pyrenean frontal thrust were reconstructed. Regarding the syn-folding sequence, the top of the four main depositional sequences within the Arguis and Belsué-Atarés Formations were reconstructed (GS-I to IV; Figs. 8 and 9).

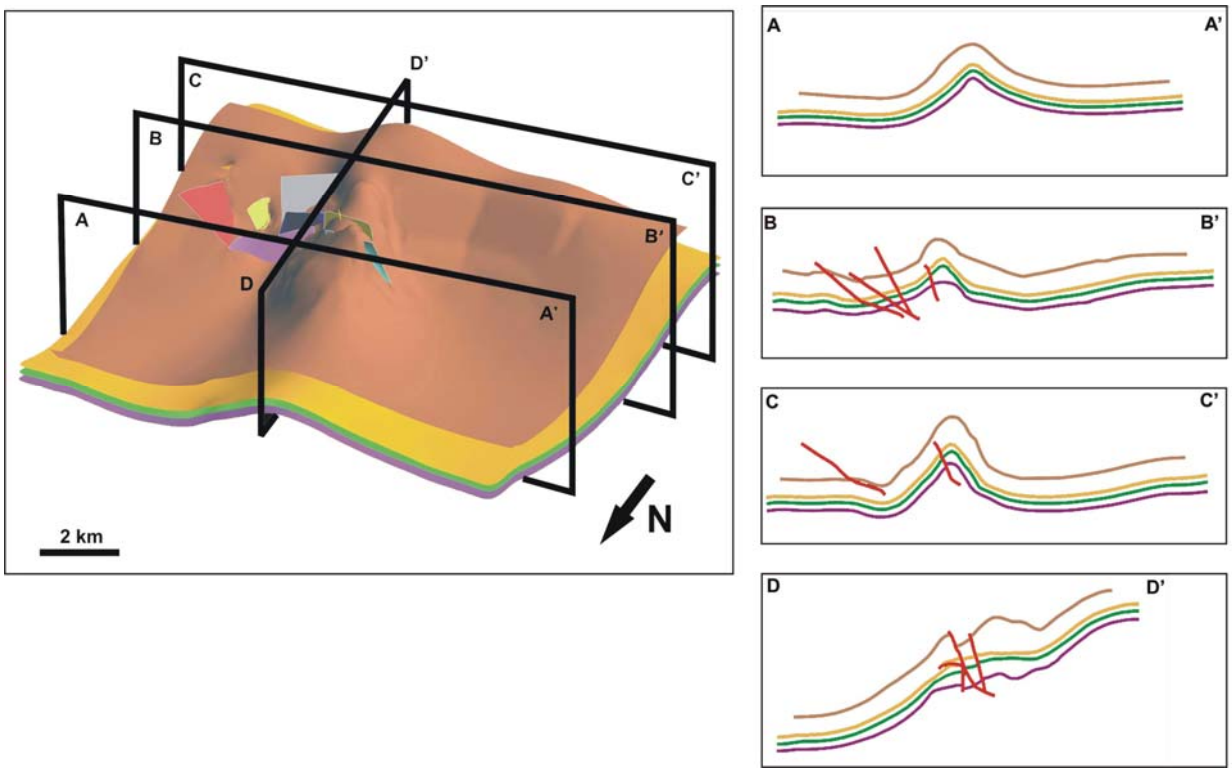

FIGURE 7 **Several cross-sections of the Pico del Águila anticline showing the structure of the pre-folding sequence . Brown: Top of Guara Fm.; Yellow: Top of Garum facies; Green: Top of Upper Cretaceous; Purple: Top of Triassic materials; Diverse colours (red in the cross sections): internal faults affecting the structure.**

The geometry of the South-Pyrenean frontal thrust surface consists of a ramp that dips towards the N, ranging from 15º in the rear part to 37º in the frontal emerging zone, and a sub-horizontal flat extending to the north. The top of the Guara Fm is barely affected by the set of faults and unconformably overlies the N-S thrust. The

lower units, however, display a complex structural pattern due to the interference between the faults (E-W to NNE-SSW in azimuth) and the N-S trending thrust (Figs. 7 and 10a).

The syn-folding sequence displays a gentler geometry, characterized by thinning towards the crest of the anticline and upwards decrease in the intensity of deformation (Figs. 8, 9 and 10b). GS-I does not reach the crest of the anticline and onlaps onto both flanks. The upper depositional sequences progressively cover the top of the Guara Fm (Figs. 8 and 9).

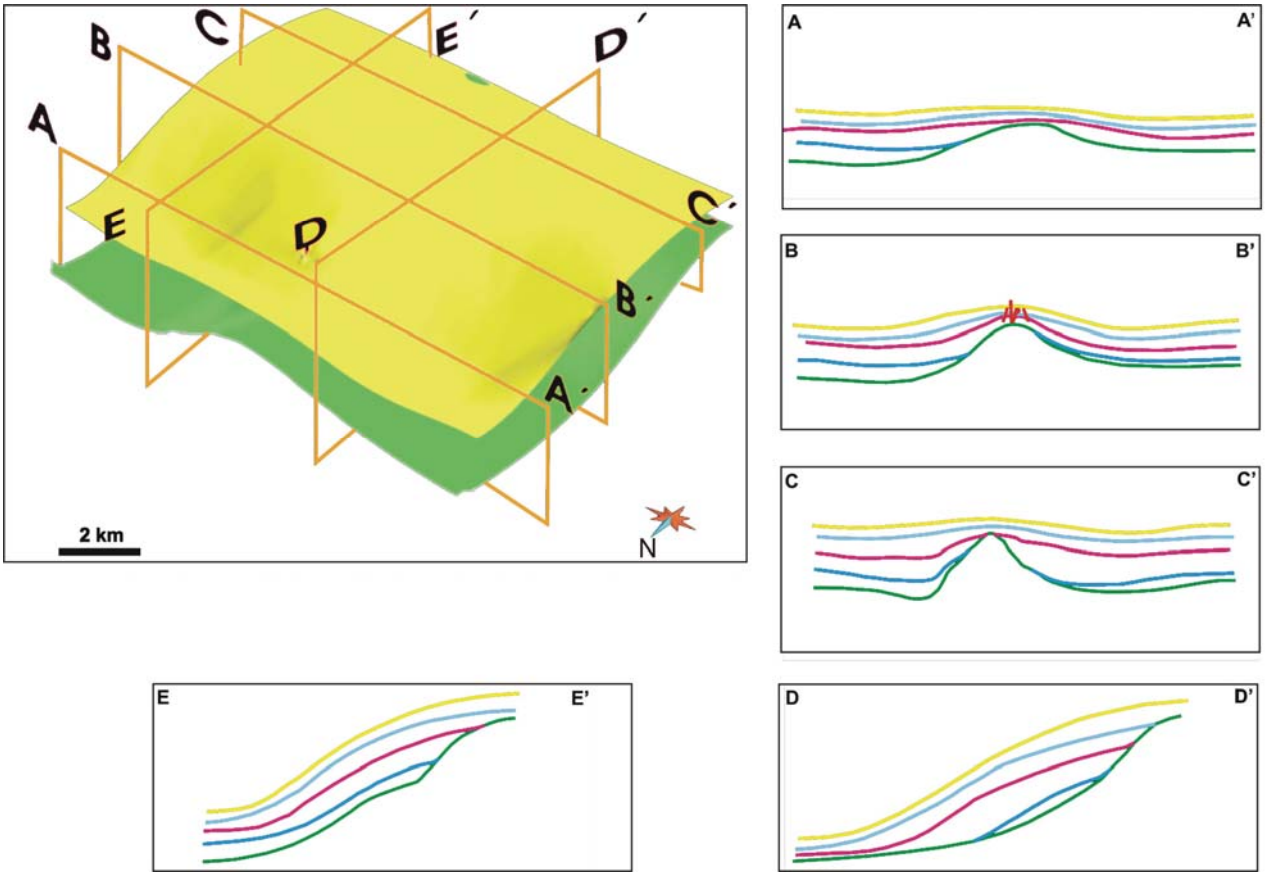

FIGURE 8 | **Cross sections along and across the 3D model, showing the geometry of the reconstructed syn-folding units (top of the four major deposicional sequences described in the area). Notice how the units thin towards the crest of the anticline and how the first depositional sequence do not reach the anticline's crest. Guara Fm. is shown in green for reference.**

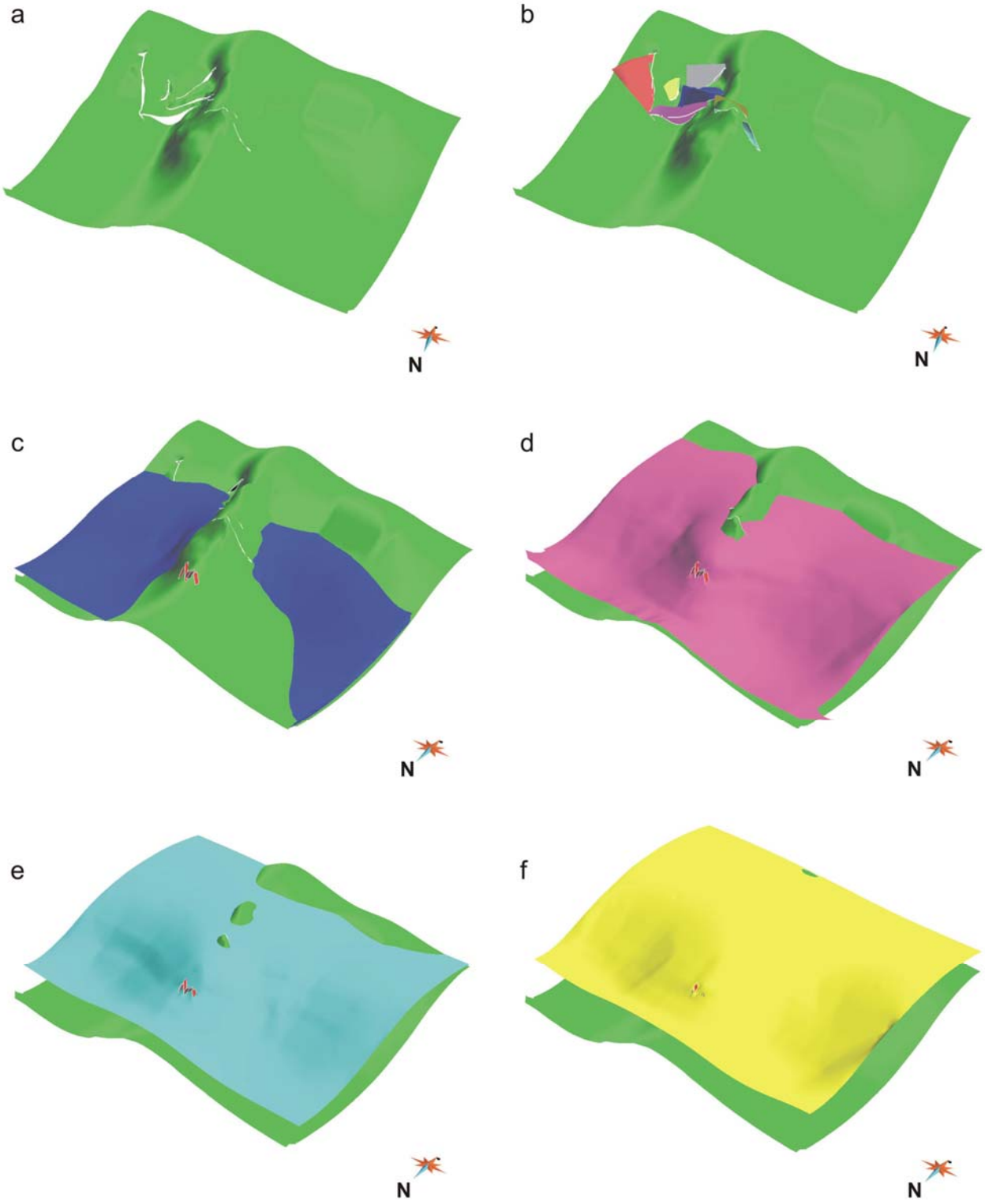

FIGURE 9 | **3D views of the reconstructed syn-folding depositional sequences. a) Top of Guara Fm (reference surface; in brown in Fig. 7) for reference; b) Top of Guara Fm. plus the inner reconstructed faults; c) Top of Guara Fm covered by the Depositional Sequence 1; d) Top of Guara Fm covered by the Depositional Sequence 2; e) Top of Guara Fm covered by the Depositional Sequence 3; and f) Top of Guara Fm covered by the Depositional Sequence 4.**

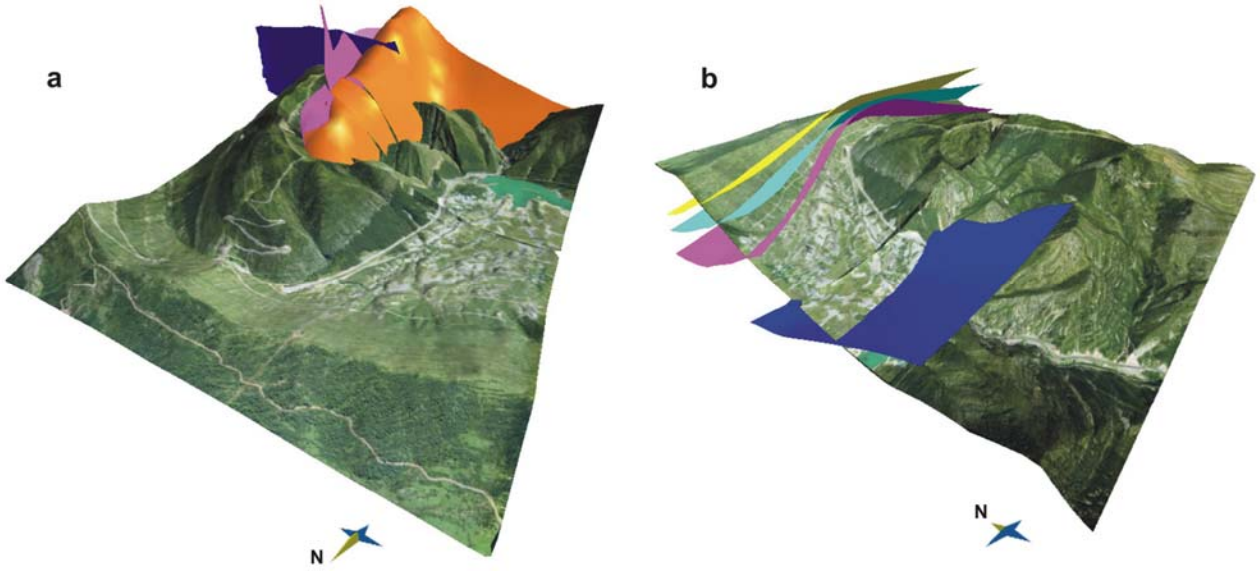

FIGURE 10 | **Oblique images of The Pico del Águila anticline. (a) shows the interference between the anticline (Garumnian horizon in orange), the set of NNE-SSW to E-W faults (dark blue), and the N-S internal thrust (pink); (b) shows the geometry of the growth strata (sequences I to IV) intersecting the topography and thinning towards the periclinal closure defined by the Guara limestones.**

ANALOGUE MODELLING: GENERATION OF OROGEN-PERPENDICULAR THRUSTS

The analogue models presented in this work aim to test the initial geometry of the basal décollement as a factor controlling the generation of orogen-oblique and orogen-transverse structures such as the ones observed in the CES. The experimental design is based on field observations which indicate a nearly absence of Keuper facies in the core of the transverse anticlines (e.g. Pico del Águila and Gabardiella anticlines, Fig. 1), and a thicker presence of these materials in between, where the orogen-parallel structures develop (e.g. South-Pyrenean thrust front). The aim of this irregularly distributed detachment level was to test how lateral contrasts in friction were able to cause the generation of arcuate, oblique and even transverse structures regardless of the orientation of the shortening.

Initial setup, materials and modelling strategy

The initial setup is constituted by a colour inter-layered sequence of sand covering an uneven basal level made of three transparent silicone patches adjacent to pure brittle sand (Fig. 11). Dry quartz sand with a density of 1700 kg m^{-3}, cohesive strength C of ca. 140 Pa and sieved to an average grain size of 35 μm was used to simulate the brittle sedimentary cover of Upper Cretaceous to Lutetian rocks. The Triassic irregular detachment level was simulated by means of the Newtonian viscous silicone putty SGM36

(density of 987 kg m^{-3} and effective viscosity η of 5 x 10^4 Pa s at room temperature, manufactured by Dow Corning Ltd.) adjacent to dry quartz sand.

The deformation rig sat upon a glued-sand aluminium plate. The model had a fixed width of 45 cm, an initial length of 60 cm, and a constant detachment thickness of 8 mm (Fig. 11). Our intention by gluing sand onto the basal plate was to force high friction behaviour in the basement in order to accentuate the contrast between the ductile décollement (silicone layers) and the frictional décollement (sand). Compression was applied at a rate of 2 cm/h (5.56 x 10-6 m/s) from one side using a motor-driven worm screw (Fig. 11). The model was shortened by up to 20% during 6 h.

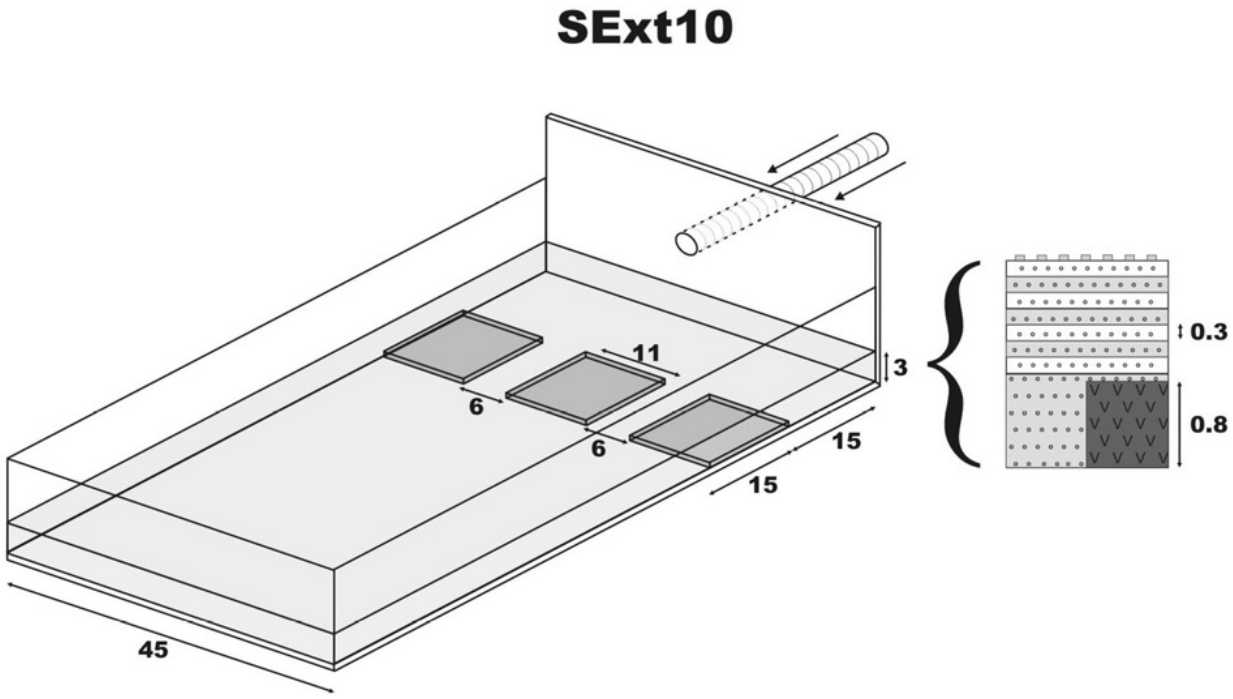

FIGURE 11 | **Initial setup of the analogue model SExt10 presented in this work, showing the distribution of ductile (SGM-36) and brittle (sand) décollements and the shortening orientation. The stratigraphic sequence of each model is presented aside. All the values are in cm.**

Results from Analogue models

Shortening of the models caused deformation in both the sand and the silicone layers. As described below, the deformation pattern was different between areas detached on the frictional décollement (sand detachment; HF areas) and areas detached on the ductile décollement (silicone detachment; LF areas). Deformation starts developing three frontward thrusts, since deformation front has not reached yet the silicon patches. After 9% of shortening (Fig. 12b), deformation reaches the silicon patches, creating a clear differential advance between areas detaching on silicon and areas detaching on sand. The HF areas show additional uplift

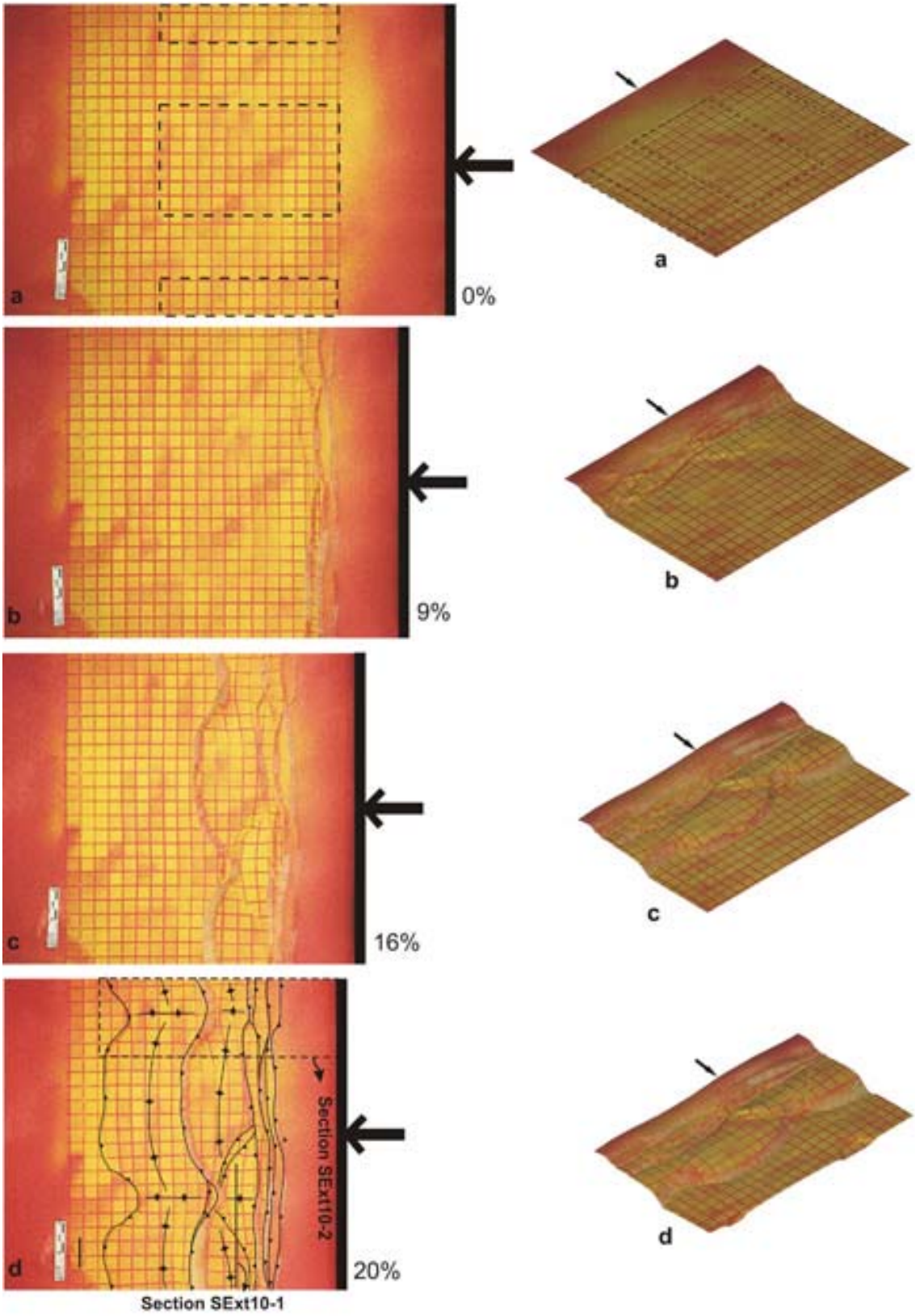

FIGURE 12 **Top and 3D views of the analogue modelling experiment at different stages: a) non-deformed stage; b) after 9% of shortening; c) after 16% of shortening; d) after 20% of shortening. The arrows indicate the orientation and sense of shortening.**

than the LF areas, occasionally expressed via some local oblique thrusts that merge with the main straight frontal thrusts in the rear part of the model. After 16% of shortening (Fig. 12c), structures are not able to assimilate more deformation and the front migrates frontwards. Consequently, a second generation of parallel-to-shortening structures is formed. Nevertheless, the location of the thrust front in the LF areas coincides with the frontal tip line of the silicon patches. After 20% of shortening (Fig. 12d) the HF areas do not advance as far as the LF areas do, creating a structural pattern constituted by wavy thrusts that transport further the areas detached on silicone than the areas detached on sand.

The deformation of ductile layers by flow, ductile thickening and folding is laterally transferred to HF areas, where lateral thrust ramps climb up section from the ductile layers at their lateral pinch-outs. These lateral ramps merge in the core of the HF areas, uplifting and gently deforming the units above, and highly faulting the units below (Fig. 13a and b). This results in a lateral migration of ductile layers towards HF areas and the thickening along the HF/LF boundary where the lateral ramps detach (Fig. 13a and b). In horizontal sections, where the internal geometry of the layers is shown at depth, the layers show general foreland-directed thrusts in which lower units are thrusted and upper units are gently folded. Only a periclinal closure is observed in the orogen-side of the transverse structures (Fig. 13c). This indicates that these structures slightly plunge towards the hinterland ought to the tilting created by the emplacement of the frontal foreland-directed thrust.

Therefore, areas detaching on sand partially assimilate the deformation by an additional uplift with regard to areas detaching on silicon, developing gentle transverse anticlines in the hangingwall of the thrusts. The localization of their crest fits almost exactly with the centre of the HF areas. This indicates that the contrast in friction between silicon and sand along the shortening direction has acted as a buttress, nucleating the thrust generation in the tip line of the silicon patches.

NUMERICAL MODELLING: ROLE OF MECHANICAL STRATIGRAPHY AND SYN-KINEMATIC SEDIMENTATION

This section presents results from a numerical model that has been used to better understand the role of a non-trivial mechanical stratigraphy and syn-kinematic sedimentation in the growth of the Pico del Águila anticline. A two-dimensional Discrete Element Modelling technique (2DDEM) has been used.

This method treats a rock mass as an assemblage of circular elements connected in pairs by breakable springs or bonds (Hardy and Finch, 2005, 2007). Thus, it is possible to model different mechanical properties (e.g. a stratigraphic sequence) by assigning different values of breaking threshold to each pair of elements (cf. Hardy and Finch, 2005). This allows us to test the effect of a given mechanical stratigraphy on geometry, fold kinematics and folding mechanisms. As such,

the method provides more information than previous kinematic modelling approaches. Furthermore, it allows for easy monitoring of displacement/location of the elements through time. In this way, the displacement path, the kinematic evolution and the strain distribution within the body can be easily tracked at any stage of the modelling. Given the competent/incompetent interlayering that characterizes the stratigraphic record (Fig. 2), we believe it an ideal method with which to model the Pico del Águila anticline.

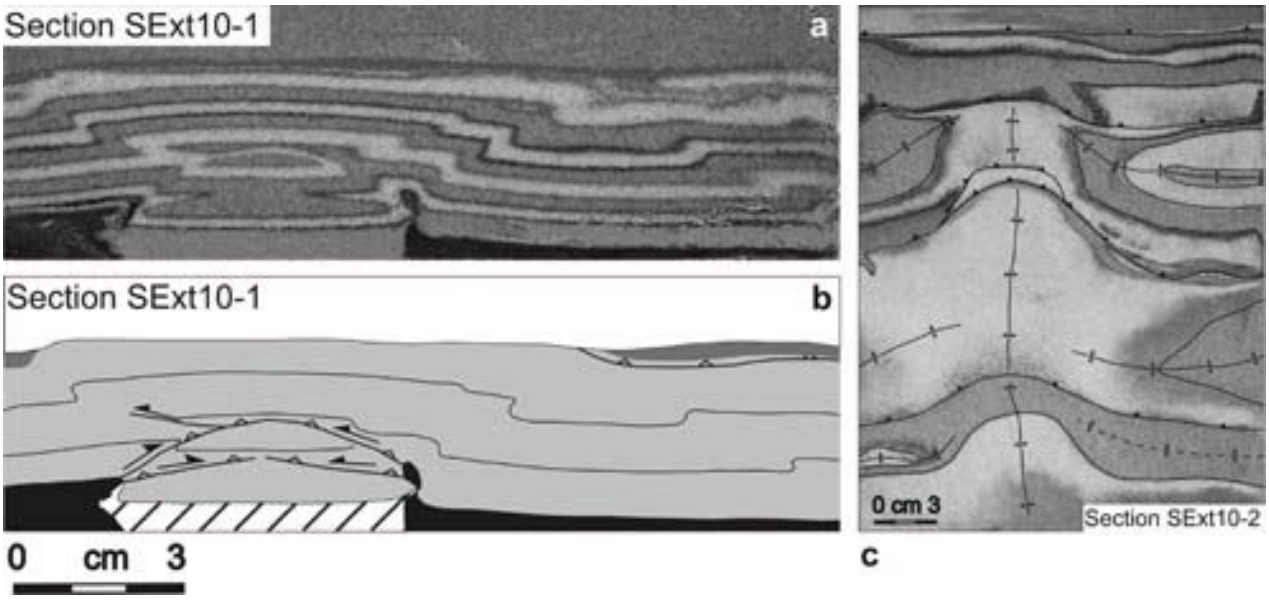

FIGURE 13 | **Pictures and line-drawings of perpendicular-to-shortening and horizontal sections of model SExt10 (see Fig. 12 for location). Section SExt10-1 shows the additional uplift of HF areas with regard to LF areas. Deformation is assimilated by high faulting in the lower units and by gentle folding and small oblique reverse faults in the upper units (the small faults caused for the pure brittle behaviour of loose dry sand). Notice the thickening of ductile layers towards HF areas, and how lateral ramps detach on LF/HF limits and merge in the core of the structure, uplifting the upper units. Section SExt10-2 shows the interference structural pattern between orogen-parallel and transverse structures. This provides valuable information since allows to observe how units modify their geometry when changing the behaviour of the basal décollement.**

As explained previously, the Pico del Águila provides a well-exposed down-plunge view of a fold down to the Triassic core, along with a well described mechanical stratigraphy and spectacular growth strata that record the fold development. This provides an excellent basis to compare how the mechanical stratigraphy behaved in the natural fold vs. the model, and how the syn-kinematic sedimentation influenced the fold evolution.

Initial setup and experimental parameters

The behaviour of the simulated rock mass is broadly elasto-plastic and frictionless (Place

and Mora, 2001; Finch et al., 2003, 2004; Hardy and Finch, 2005, 2007), an approach used in previous studies to model the brittle deformation in sedimentary rocks in the upper crust. Deformation of the modelled sedimentary sequence occurs in response to shortening at a subduction slot at the base of the model (a common configuration in sandbox experiments). A velocity discontinuity is created at the subduction slot in the central basal part of the box, in which the right half of the model moves leftwards at a continuous rate of 0.001 m per time step (Fig. 14). A homogeneous rock density of 2500 kg m^{-3} has been used, a typical value of upper-crustal sedimentary rocks. A value of 5.5 x 10^9 N m^{-2} is used for the elastic constant (K) in the experiments. The experiment was run for 2,000,000 time steps with output of the assembly every 100,000 steps (i.e. every 100 m shortening). This provided a precise control on the structural evolution and variation of the strain distribution and a well constrained geometry of the syn-kinematic sedimentation. The total displacement was 2 km.

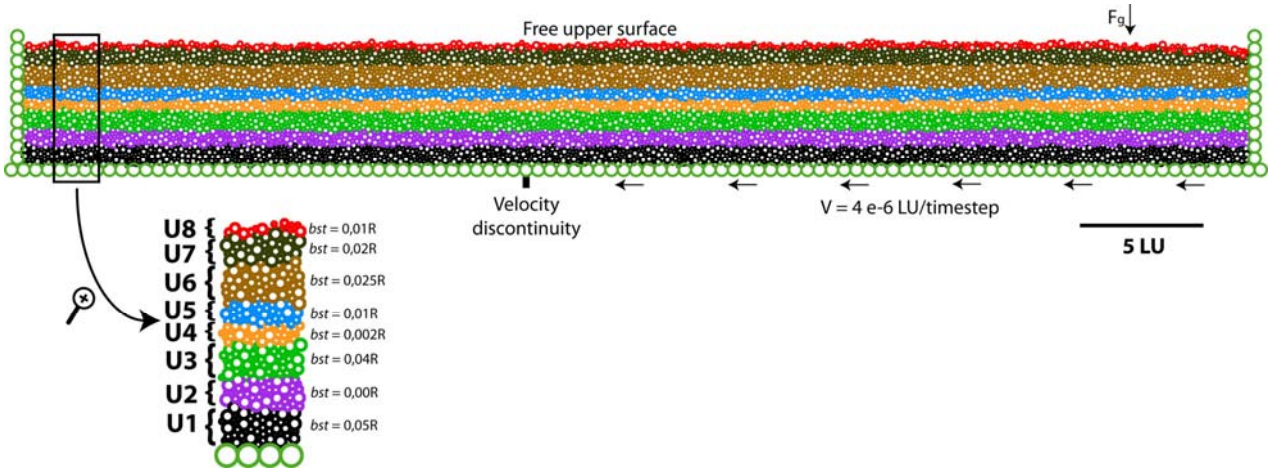

FIGURE 14 | Initial setup and boundary conditions applied in the DEM experiment. The initial assembly contains 10245 elements with radii of 31.25, 25, 18.75, and 12.5 m, positioned at random in a box that measures 12.5 x 1.25 km. The assemblage is composed of 32 flat-lying layers that are later grouped in eight units with different mechanical properties. Displacement is increased at 0.001 m/time-step. Fg corresponds to the force of gravity.

Within the modelling framework, one lattice unit (LU) corresponds to 250 metres. The initial particle assembly contains 10245 elements with four different radii of 0.125, 0.1, 0.075 and 0.05 LU (i.e. 31.25, 25, 18.75 and 12.5 m, respectively) distributed at random in an enclosed rectangular box. We believe these dimensions are suitable, since they provide enough resolution to model a kilometric-scale structure like the Pico del Águila anticline, avoiding the generation of preferred planes of weakness and allowing a non-predefined localisation of deformation that a homogeneous particle size would imply. After initial generation, the elements are allowed to relax to a stable equilibrium

and are left to settle under gravity for ~2,000,000 time steps to obtain a stable, well-packed initial assemblage and to further minimise void space. The resulting initial assembly is 12.5 km long and ca. 1.25 km thick, simulating a continuous rock mass that can deform by progressive bond breakage (fracturing/faulting) and bulk motion of unbroken pairs of elements (folding). The syn-kinematic sedimentary sequence was modelled by adding incrementally a total of 11708 elements. The initial particle assembly was composed of 32 flat layers grouped into units with different mechanical properties to create a complex mechanical stratigraphy (Fig. 14).

Results from Numerical models

The geometrical and shear strain evolution of this model are shown in Fig. 15.

After 4% bulk shortening (500 m; Fig. 15b) a small, low amplitude structure has started to grow above the velocity discontinuity as a perturbation with layer-parallel geometry. The incompetent units U2 and U4 exhibit high shear strain in both the structure itself and some distance across the model. Competent unit U1 shows high shear strain and is complexly deformed in the core of the anticline. The other pre-kinematic units only exhibit low shear strain which is slightly accentuated in the fold (Fig. 15b). The growth strata show high but variable amounts of shear strain. However, two types of strain within the growth strata package must be distinguished. Firstly, the shear strain due to the recent deposition and ongoing compaction of the recently deposited units (essentially restricted to the uppermost two layers of the assembly; i.e. the thin horizontal red area at the top of the strain distribution maps; Fig. 15). Secondly, the shear strain exhibited by the growth pile due to shortening and consequent fold development. A border-effect is generated at the right-hand edge of the model due to the displacement of this wall towards the left. After 8% bulk shortening (1000 m; Fig. 15c), the central structure has grown significantly, its limbs have steepened and now it verges slightly towards the right. Disharmonic folding is observed. Below U4 minor folds have developed, particularly in U2-U4 towards the right-hand edge of the model, and the core of the structure is now becoming complexly deformed in U1. Above U4, the pre-kinematic units define a gentler fold geometry. The syn-kinematic sequence shows marked thickness variations producing flanking sedimentary wedges which thin towards the crest of the anticline. Within the growth strata package, moderate to high shear strain is observed and a distinct contrast in shear strain is observed at the base of the growth strata package. After 12% bulk shortening (1500 m; Fig. 15d), thickening of the incompetent units is seen in the hinge of both flanking synclines and the core of the fold becomes highly deformed. In particular, U1 starts to become dramatically deformed, displaying bottle-neck geometry. Small folds continue to grow in U2 between the anticline and the right-hand model border. Disharmonic folding is observed in the hinge of the anticline, with large differences in folding style above and below U4. Shear strain continues to be concentrated within the

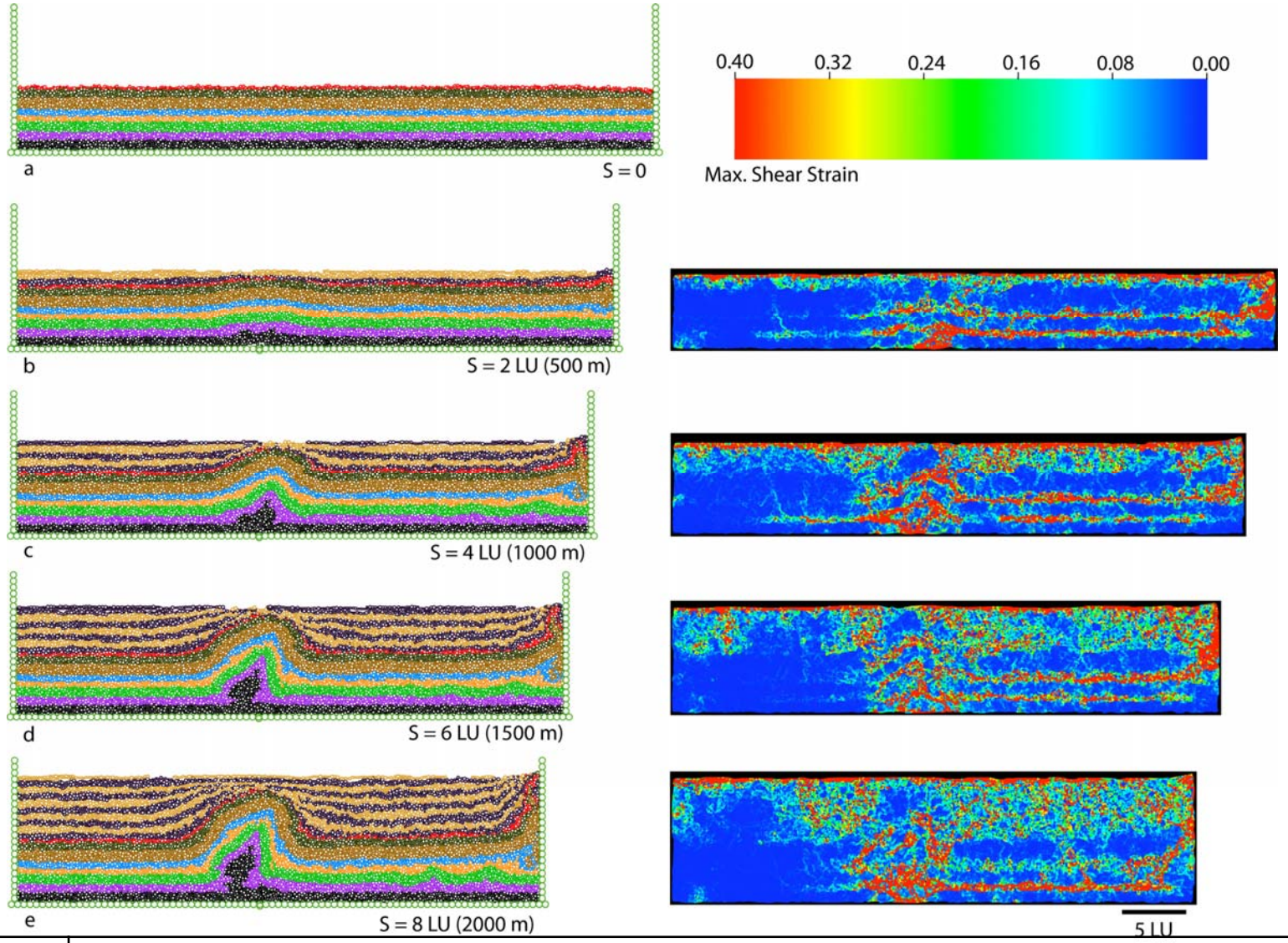

FIGURE 15 **Evolution of the DEM model shown at: a) 0 m; b) 500 m; c) 1000 m; d) 1500 m; and e) 2000 m. The left column illustrates the geometrical evolution of the model as shortening goes on. The right column shows the distribution of the shear strain at the reported stages. Scale at the top-right of the figure illustrates the range of shear strain considered.**

incompetent units. Growth strata rotate and thin against the growing structure displaying much internal shear strain. At 16% bulk shortening (2000 m; Fig. 15e) the upwards growth of the anticline appears to cease (growth strata overlap the structure) with the fold tightening by limb rotation. However, the model shows a shift in the distribution of shortening from the central fold to the right edge, manifested by propagation of folding from the right edge, and giving rise to small décollement folds detached on U2. In the main fold, shear strain is still concentrated in the core, as well as in the limbs particularly in U4 and U5. In the core, U1 is further "pinched" into a bottle-neck structure. At this stage, the growth strata package is about 1.2 km thick, similar to the one observed in nature at the Pico del Águila.

3D GEOMECHANICAL RESTORATION OF THE PICO DEL ÁGUILA ANTICLINE

The restoration has been done using a Finite Element Modelling algorithm which considers measurable mechanical properties of the rocks (what has been called *geomechanical* restoration) rather than any imposed kinematical criteria. In most cases the kinematics of a structure are unknown or not precisely quantified, and the geomechanical restoration delivers a mechanically stable result based on the geometry of the deformed stage and the mechanical properties of the rocks (such as density, Young modulus, Poisson's ratio or porosity, among others; Maerten and Maerten, 2006; Guzofski et al., 2009).

Methodology and initial setup

The sequential restoration of The Pico del Águila anticline was done using Dynel3D (igeoss. Maerten and Maerten, 2006). The code implemented in Dynel3D is based on the finite element method (FEM), a continuum technique that allows the study of natural deformation based on the mechanical properties of rocks. Although strictly elastic, the program is suitable to model the development and behaviour of complex geological structures such as folds and faults (Maerten and Maerten, 2006). The stratigraphic units are discretized with tetrahedral elements that are assigned elastic properties. Faults are represented by contact surfaces. The tetrahedral elements deform elastically in response to constraints such as applied and/or internal forces, displacements, and interface contact regions (faults). Dynel3D uses an iterative, explicit solver that allows forces to be transmitted from node to node through the entire system until equilibrium is reached. This formulation is well suited to model complex geological scenarios that comprise several stages, such as structural restoration. In addition, the explicit solution scheme is efficient and stable (Maerten and Maerten, 2006).

The 3D reconstruction of the Pico del Águila anticline was taken as the deformed stage to restore. The reconstructed growth strata were key to constrain the timing of the restoration. The average side length of the tetrahedra was 310 m, a reasonable balance to represent a kilometre-scale structure without exceeding the memory allocation threshold allowed by a regular computer. This average side length implies that bodies with

dimensions below the threshold are not represented, being simplified in bodies of larger dimensions. That is the case of the Garumnian and the Upper Cretaceous (thickness below the average side length), which were merged into a unique mechanical unit named *Garumnian-Cretaceous*, with averaged mechanical properties. Similarly, the eight internal faults exhibit a heave that barely exceeds several tens of meters. Thus, they were not included in the restoration. As said, the algorithm run in Dynel3D needs several rock mechanical properties to be set up (Young's modulus, Poisson's ratio and density). As these properties vary with lithology along the stratigraphic sequence, different values were established with regard to the predominant lithology of each unit. These values are listed in Table 1.

Table 1. Mechanical properties used to restore the Pico del Águila anticline

Unit	Predominant Lithology	Young's Modulus (Pa)	Poisson's ratio	Density (Kg/m3)
GS-IV*	Sandstone	2.2 e+10	0.24	2480
GS-III*	Marlish Sandstones	2.2 e+10	0.24	2480
GS-II*	Marls	2.8 e+10	0.14	2530
GS-I*	Marls	2.8 e+10	0.14	2530
Guara	Limestones	4.8 e+10	0.25	2500
Garumnian-Cretaceous	Mudstones-Limestones	2.8 e+10	0.14	2530
Triassic	Dolomitic Limestones	4.8 e+10	0.25	2500

These are average values for each rock type, and partially based on field indications
* GS: Growth strata; Arguis and Belsué-Atarés Fms.

Results

Five restoration stages were considered, following the reconstruction of the four top bounding surfaces of the growth depositional sequences (GS-I to IV) and the top of the Guara Formation (Fig. 16). The distribution of average shear strain (abbreviated as *strain* from now on) for each restoration step was also plotted to track the evolution of the deformation (Fig. 17).

Restoration of the top of the GS-IV (36.6 Myr) removes most of the tilting associated to the emplacement of the South-Pyrenean frontal thrust (Fig. 16 a and b). A *ca.* 15º vertical axis clockwise rotation is observed. Strain is distributed heterogeneously throughout the model (Fig. 17 b). GS-IV displays moderate to high strain distributed around the associated synclines, increasing progressively towards the anticline (higher strain values coinciding with areas in which GS-IV is thinner; Fig. 17 b). The rest

of the growth sequences display high strain in the hinge area of the synclines. Within the pre-folding sequence, the Garumnian-Cretaceous and Triassic exhibit high strain in the hinge areas of the anticline and the synclines. The Guara Formation displays low to moderate strain along both fold flanks, and high strain in the hinge of the synclines (Fig. 17 b).

The GS-III (37.17 Myr) is the first restored growth unit that does not cover all the anticline. Restoration of this sequence results in a plunge decrease of barely 4º (Fig. 16 c) and a clockwise rotation of 2º. Low to moderate strain in the hinge of the anticline at GS-III and low strain in the rest of the growth sequences is observed. The highest strain is accommodated by the Guara Formation in the eastern syncline and along the western limb (Fig. 17 c). The Garum-Cretaceous displays moderate to high strain and pronounced layer-parallel slip with respect to the units above and below. The Triassic exhibits moderate to high strain, more concentrated in the middle sequence of the synclines and anticline hinges.

After restoring GS-II (37.74 Myr), the plunge almost disappeared (Fig. 16 d) and the structure rotated *ca*. 10º additional degrees. The strain (Fig. 17 d) is higher than in the previous stage, particularly at the periclinal closure of the anticline. The Guara Formation accommodated moderate strain in the western limb and the crest of the anticline, and high strain in the hinge of the eastern syncline (Fig. 17 d). The Garum-Cretaceous displays high strain, excepting in the anticline crest. The Triassic displays moderate to high strain.

The restoration of GS-I (40.04 Myr) unveils the Guara Formation in the crest of the structure (Fig. 16 e). Large deformation is observed in the pre-folding units, displaying a well-developed anticline (Fig. 16 e). No significant vertical axis rotation is observed. Strain in GS-I is heterogeneously distributed, displaying low to moderate high strain around the hinge of the synclines and along the flanks onlapping the Guara Formation (Fig. 17 e). The Guara Formation exhibits low strain in the anticline crest and moderate strain in the periclinal closure and along the flanks. The Garumnian-Cretaceous shows particularly high in the hinge of the anticline and along the flanks. The Triassic displays moderate to high strain in the synclines and along the décollement, and low strain in the crest of the anticline (Fig. 17 e).

Finally, the restoration of the Guara Formation (41.52 Myr) causes unfolding of the pre-folding sequence and additional rotation of *ca.* 6º (Fig. 16 f). The vertical axis rotation varies through the pre-folding units, displaying a slight larger rotation of each unit with respect to the unit immediately below (Fig. 16 f). The strain ranges from very low to very high, with low to moderate values throughout the model, and maximum values in the hinge of the synclines and locally in the crest of the anticline (Fig. 17 f). The Garumnian-Cretaceous and Triassic display larger strain values in the hinge of the synclines (Fig. 17 f). The top and bottom of the units display slightly lower strain values along their contacts, with significant layer-parallel slip between them.

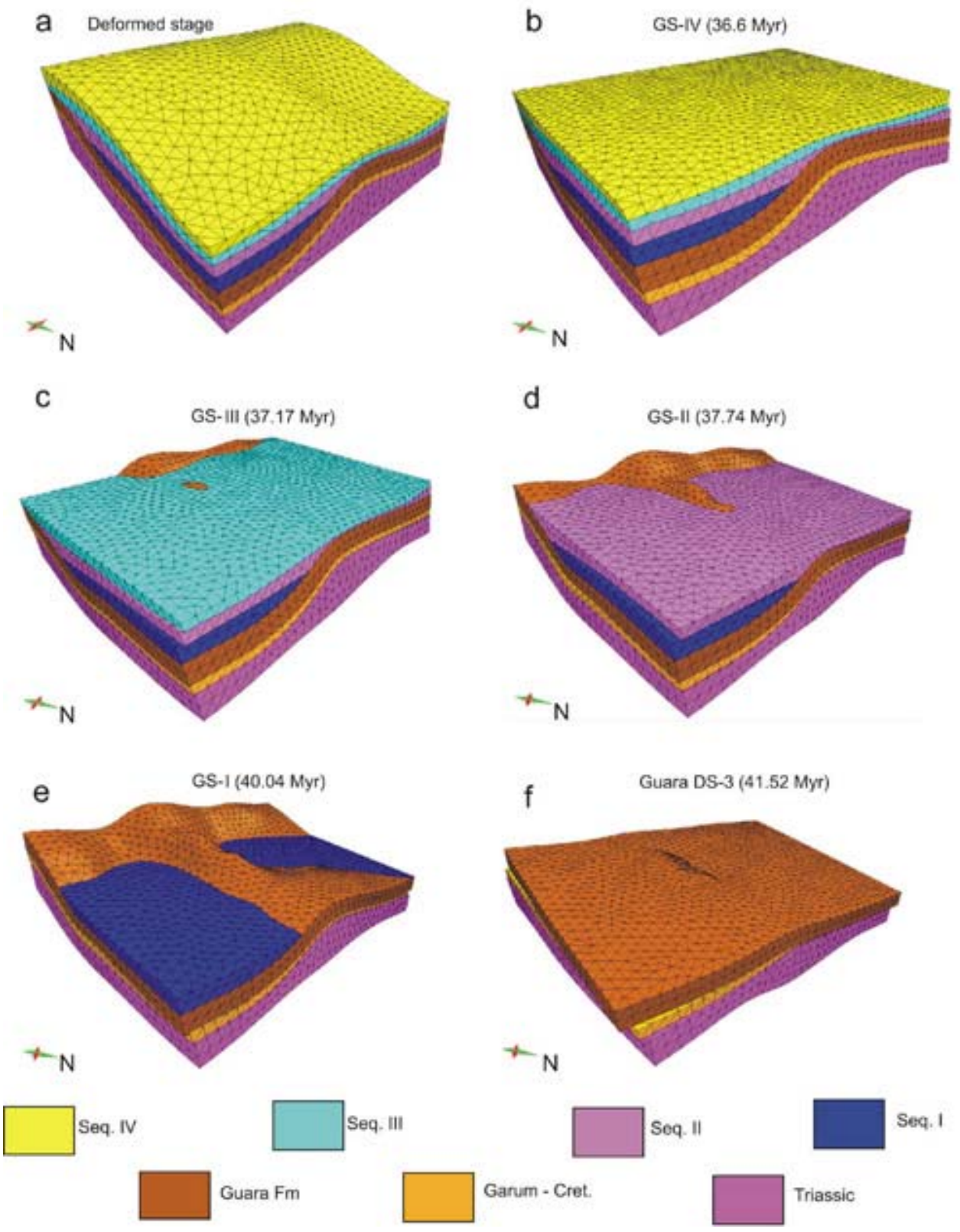

FIGURE 16 | Sequential, geomechanical restoration of The Pico del Águila anticline. (a) Deformed stage; (b) restoration of GS-IV (36.6 Myr); (c) restoration of GS-III (37.17 Myr); (d) restoration of GS-II (37.74 Myr); (e) restoration of GS-I (40.04 Myr); and (f) restoration of Guara Formation (41.52 Myr).

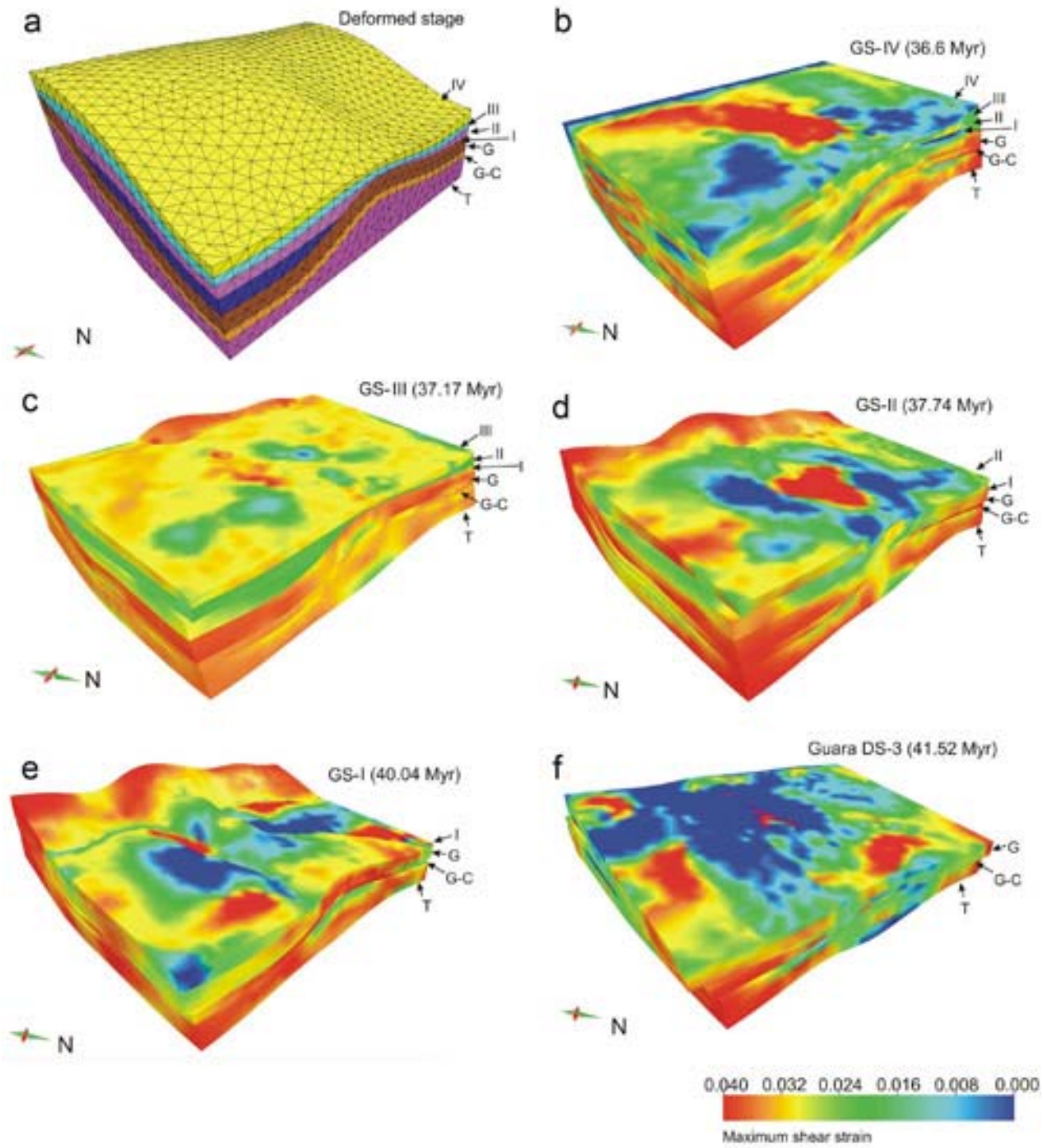

FIGURE 17 | Average shear strain between the restoration steps shown in Fig. 16: a) Deformed stage geometry for reference; (b) restoration of GS-IV (36.6 Myr); (c) restoration of GS-III (37.17 Myr); (d) restoration of GS-II (37.74 Myr); (e) restoration of GS-I (40.04 Myr); and (f) restoration of Guara Formation (41.52 Myr). T: Triassic; G-C: Garumnian Cretaceous; G: Guara; I: GS-I; II: GS-II; III: GS-III; IV: GS-IV.

DISCUSSION

On the benefits and drawbacks of each technique

Each of the presented models delivers new insights on the structural evolution of the Pico del Águila anticline, improving in such a way the geological knowledge of the External Sierras. Each of them was specifically designed to test certain parameters observed in the field, incorporating the contributions to the model of structural evolution. However, recalling the limitations of each technique is essential to choose the most appropriate method for a given purpose. In such a way, one can evaluate the outcome of the model and extract the net contribution of the whole results.

In this sense, sandbox modelling was a good technique to model the heterogeneities of the basal décollement at a regional scale: it allowed an easy visualization in 3D of the model response to deformation in terms of differential advance/uplift of the overburden, structural style and relief across the different domains. Given the important changes of structural style in 3D, the analogue models represent the structural features at a regional scale. The mechanical contrast between loose sand and silicon putty was suitable to model the effect of lateral changes between Keuper and Muschelkalk facies in the Triassic décollement. It effectively reproduced a larger N-S uplift (*i.e.* parallel to shortening direction) in the areas detached on high friction décollement (HF areas) and a larger advance of the deformation front in areas detached on ductile décollement (LF areas). On the contrary, working with loose sand and silicon do not provide enough accuracy to model the internal complexity of the overburden: high contrasts in mechanical behaviour are described in the field along the stratigraphic sequence, in which inner ductile units are present and have great influence in the growth of the structure (Figs. 2 and 15). To model this, a wide diversity of analogue materials would be needed, and even then, the available mechanical properties would be limited to the number of different materials used in the modelling. For this reason, we found more suitable to assess the role of the mechanical stratigraphy in the fold growth by means of numerical modelling.

The scaling of parameters has always been a key issue in sandbox modelling: the dimensions of the field structure, the stratigraphic thickness of units and the mechanical properties of the materials must be rescaled to accomplish similar processes in a smaller by far timescale. Although not discussed herein, the suitability of the analogue materials, the rescaling factor of their physical properties and the dimensions of the experimental apparatus versus the thickness of the model units are factors that must be considered accurately when designing the initial setup of the model. For the models presented in this work, these aspects were discussed in more detail in Vidal-Royo et al. (2009), based on many other works such as Weijemars, 1986; Bonini, 2003; Cagnard et al., 2006 or Amilibia et al., 2005, among others.

On the technical aspects, the morphological and structural changes of the model can be captured in real time and

observed physically (Fig. 12), the advance/uplift contrasts can be easily illustrated with a simple photo camera (Fig. 18), and a qualitative distribution of strain across the different structural domains can be derived by comparing a series of top views. However, in analogue modelling all the data must be extracted and well documented during the model run and sectioning, and the repeatability is usually much more time-consuming and less accurate than in numerical models.

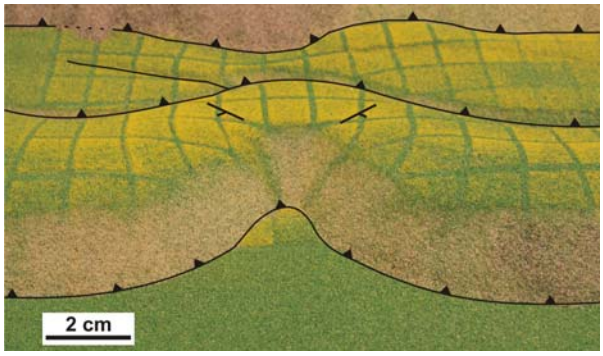

FIGURE 18 | Detailed photograph of an orogen-perpendicular structure formed in model SExt13 (not discussed in this work). The thrust front is characterized by a wavy morphology in which the overburden generates transverse anticlines above the HF areas (detached on sand).

The mechanical properties of the overburden, as well as the effect of the growth strata in the distribution of the strain during the fold growth can be better controlled if modelled numerically. The Discrete Element Modelling (DEM) permits a precise control of the mechanical response of each modelled unit, hence, to set up a highly complex mechanical stratigraphy with which to model a plethora of geological scenarios. This makes the DEM an ideal method to explore in detail the evolution of the N-S detachment anticlines of the CES. The method allows us to track every single particle of the model and its associated physical information (displacement, velocity and acceleration vectors, instant position etc.) from which the distribution of strain through time is easily derived. The DEM models presented in this work have contributed with new insights on how the deformation is differentially accommodated depending on the mechanical behaviour of each unit, leading to large contrasts in structural style between adjacent units within the sedimentary cover of the Pico del Águila anticline. The numerical models allow a precise control of the parameters introduced in the model. It is important to have control of the thickness of the pre-folding units (constant thickness, set up before running the model), and even more in the case of the growth strata, to model a geological setting as described in the field. However, there is no superimposed kinematics to the model. The DEM is a forward modelling technique in which the physical properties of the particles, the initial dimensions of the bounding box and the stratigraphic thicknesses are the only introduced parameters. In this sense the DEM keeps similarities with the classical sandbox models, but allows major control of the mechanical properties and instantaneous monitoring of the kinematic parameters and strain distribution of any/all particle(s) of the assembly. On the other hand, the presented DEM models are strictly 2D, providing a partial representation of the modelled structure (comparable to an E-W cross section of the anticline). Although 3D DEM

experiments are already in development (Carmona et al., 2008) they still are very expensive in terms of time consumption, especially to model complex geological settings such as the N-S anticlines of the CES. For this reason, a 2D DEM approach has been suitable to understand the role of the mechanical stratigraphy plus growth strata in a single structure, since the sandbox experiments already shed light on the generation of the N-S structures in 3D at a regional scale. Technically, the DEM experiments represent one step further in the modelling applied to structural geology. By calculations based on field observations of the mechanical response of rocks in nature a mechanical complex interlayering can be modelled, improving the validation between model and nature with regard to more simplistic approaches such as analogue models or kinematic models that need superimposed constraints to be run. In addition, the method outputs as many intermediate steps as the modeller decides. The outcome files are stored and can be accessed later in the future for further analysis or comparisons. The repeatability of the experiments is better than in sandbox modelling.

The Pico del Águila anticline is a truly 3D structure with excellent preservation of the growth strata record. The interference pattern between the N-S anticline and the E-W South Pyrenean thrust creates a structure with a complex kinematic evolution that is difficult to represent properly by means of 2D approaches. All these factors permitted the three-dimensional reconstruction of the structure plus growth strata with which to assess a time-constrained model of evolution. The good degree of exposure, outcropping conditions and the easy accessibility made it an ideal case to carry out field data acquisition and detailed mapping of geological traces. This led to a reconstruction of the pre-folding units and growth strata in 3D, which allowed the understanding of the geometry and served as a basis to carry out the restoration. Based on the mechanical response of rocks to deformation, the geomechanical-based algorithm of Dynel3D presented an alternative to perform a sequential time-constrained restoration in 3D without invoking the complex and not precisely quantified kinematics of the structure. Thus, the major benefit of a geomechanical restoration is that it allows us to restore a structure by introducing real, measurable properties of the rocks without imposing any kinematic criteria. Density, Young Modulus, Poison's ratio or porosity can be measured in strength tests in the laboratory, or alternatively, general values can be found in published charts of mechanical properties for different materials. In any case, measurable or easily accessible values are used to perform a restoration that returns a physically-based result in accordance with the kinematics derived from a diversity of disciplines. The algorithm solves the system and delivers the mechanically most stable solution, letting the model move freely and unconstrained in the XYZ directions. The main drawbacks of this method, so far, link directly with the technical limitations of computer calculations. The algorithm implemented in Dynel3D may need to allocate a large amount of the computer's memory, depending on the desired resolution

of the model (i.e. the size of the tetrahedra). This means that for a few kilometre scale structure as the Pico del Águila, a regular computer can stand up to a resolution of few hundreds of meters. This makes the method unsuitable to study in detail and at this scale geological features which are below the resolution threshold. The algorithm is based on the use of elasticity laws to restore large, non-recoverable (inelastic) deformation. This implies certain limitations indeed. Particularly on the magnitude of strain, the use of elasticity laws return strain values which are notably lower than the predicted by other modelling techniques (e.g. DEM) and the values obtained in field/laboratory experiments. Therefore, the method is suitable to realize strain patterns/distributions, folding mechanisms and potential fractured domains rather than predict strain magnitudes and/or mesoscale fracture patterns/ orientations within the structure.

On the validation and integration of modelling techniques

All the experiments presented in this work have been, in a way or another, based on observations, descriptions and data acquired in the field. Once we are aware of the advantages and limitations of each modelling technique we should have a better image of what each model delivers, and be able to give feasible explanation to the question that motivated its use. Validating and integrating the results from different approaches means, hence, gather the contributions of each modelling tool to construct a unified model of structural evolution, but also cover the gaps that each modelling leaves, complementing one to each other.

In this sense the analogue models provided new insights at regional scale, giving explanation about the processes that led to the generation of those initially arcuate, oblique thrusts, which finally ended up in the N-S anticlines of the External Sierras. The modelling was based on field observations of a nearly absence of Keuper facies in the core of the N-S anticlines, and replicated many features of the natural case: larger N-S uplift associated to the emplacement of an E-W foreland-directed thrust in areas with little or no presence of ductile layer (Keuper facies), larger advance of the deformation front in areas between the transverse structures, N-S anticlines located at the hangingwall of the frontal thrust and plunging towards the hinterland, vertical axis rotation of the hangingwall in the N-S anticlines and wavy (non-straight) morphology of the foreland-directed thrusts (Figs. 12, and 18). However, the analogue models did not investigate neither the internal complexity of the sedimentary cover nor the effect of the syn-kinematic sedimentation in the fold growth. Loose sand itself is not a suitable material to model the tight steep structure of the N-S anticlines of the CES, characterized by a complex interlayering in which the mechanical properties vary along with the stratigraphic sequence (Figs. 2 and 14). Instead, the DEM fulfilled this gap and reproduced the structural style of the Pico del Águila anticline after setting up a mechanical stratigraphy that modelled the one described in the field. The different way in which each unit accommodated deformation was

replicated by the DEM experiments: pervasive faulting and high internal deformation of the lower units cohabited with gentle folding in the upper units, at the same time that growth strata accommodated large amount of deformation and equilibrated the anticline against gravitational instabilities (Fig. 15). The internal décollement level acted as a barrier, allowing the upper units to gently fold whereas the lower ones concentrated more deformation by means of fracturing and folding. This gave us new insight about how the stratigraphy of the CES responded to shortening, and how multiple folding mechanisms acted simultaneously depending on the mechanical properties of each unit. Despite this, the 2D framework of DEM did not inform about other important kinematic features that imply the three-dimensionality (e.g. the clockwise rotation of the N-S anticline, its relationship with the E-W South Pyrenean thrust and associated interference structures) neither the effect of flexural slip, which has been described in the field. This major limitation has been overcome by the 3D reconstruction and geomechanical restoration of the Pico del Águila (mostly based in field "hard" data), which added the third dimension, validated and improved the structural evolution and mechanical response predicted by the analogue and numerical models. The restoration reproduced naturally a vertical-axis rotation of 33º without imposing any kinematic constrain, in such a way that validates the rotation reported by paleomagnetic measurements (Pueyo et al., 2002; Rodríguez-Pintó et al., 2008) and analogue models (Vidal-Royo et al., 2009); it also reported a different evolution of sedimentation and uplift between flanks and a layer parallel slip as described in the field (Fig. 16). As it was already suggested by the DEM experiments, multiple folding mechanisms were observed acting simultaneously in different units, depending on the mechanical behaviour of each of them. In addition, the restoration pointed out that multiple folding mechanisms acted synchronously also within a given unit, depending on the structural domain of the fold. This combination of folding mechanisms obviously gives rise to a complex distribution of strain through time, in which deformation preferably concentrates in a different structural domain depending on the mechanical properties of each unit (Fig. 17). On the other hand, we have already mentioned the limitations and drawbacks of the geomechanical restoration performed in Dynel3D. The lack of information associated to the limit of the resolution of tetrahedra is partially overcome by the DEM, which reports a different mechanical response by every single unit. The limitations associated to the use of elastic laws to recover large, non-recoverable deformation are overcome by restoring and summing small increments of deformation, and including the effect of faults, décollements and flexural slip. In this way, each volume is required to restore elastically but on the whole, the model experiences finite, permanent strains that are manifested by fault, décollement and flexural slip offsets (Maerten and Maerten, 2006, and Guzofski et al., 2009 who use a similar restoration technique).

In general, each modelling technique presented in this work tackles new questions

on the structural evolution of the N-S anticlines of the CES, provides new insights in accordance to observations in nature, and takes one step further the aspects that remained uncovered by other modelling approaches. In other words, the presented modelling techniques contribute with new aspects on the geology of the CES; validate the results obtained by the other modelling and integrates part of a unified and better constrained geological history of the Central External Sierras (Fig. 19).

The Pico del Águila anticline: integrated model of structural evolution

The different modelling results presented in this work combined with the previous studies of the area in many different disciplines allow us to present an integrated model of evolution for the Pico del Águila anticline.

The Pico del Águila is a décollement anticline detached on a complex interplaying of Muschelkalk and Keuper facies (Middle and Upper Triassic). Prior to the deposition of the Cretaceous-Tertiary cover, the area already had a complex structure and a long geological history. According to paleogeographic reconstructions (López-Gómez et al., 2002; Castillo-Herrador, 1974; Jurado, 1990; Salvany, 1990) the region was located in a high of the Triassic extensional basin, in which little sedimentation took place during Upper Triassic times. This structural position influenced the low and irregular stratigraphic thickness of the Keuper facies (red clays and gypsum-bearing clays) observed in the area and the complex interfingering with the pre and syn-extensional Middle Triassic Muschelkalk facies (M2: clays and evaporites, M3: dolomites and dolomitic limestones) (Fig. 19 a). In addition, the structural pattern at that time was likely to be complex, and the present-day observed pervasive fracturing partially inherited from Triassic times. This complex structural setting resulted in a mechanically heterogeneous, unevenly distributed Triassic substratum on top of which the Cretaceous-Tertiary sedimentary cover was deposited.

It was 42.67 ± 0.02 Ma ago (Upper Lutetian) (Poblet and Hardy, 1995) when the Pico del Águila anticline started to grow. Given the mechanical heterogeneities in the Triassic décollement, the anticline generated at high angle (between 69º and 57º depending on which value of total rotation is taken) with respect to the E-W regional structural trend (Fig. 19 b). The sedimentary cover experienced a larger NNW-SSE uplift in areas with less presence of Keuper facies (lower cover/ductile décollement ratio), at low angle with the direction of tectonic transport (ca. N-S). These large mechanical contrasts in the basal décollement level also drove the clockwise rotation process, influencing the deformation front to advance at a different velocity depending on the mechanic nature of the décollement at different areas. Given the mechanical complexity of the sedimentary cover, along which a heterogeneous mechanical response is described, N-S shortening was accommodated by folding instead of generating an oblique thrust ramp, forming an

incipient detachment anticline at the same time that carbonatic shallow marine platform sedimentation (Guara DS-3) was depositing. At ca. 41.52 Ma ago a sharp transition from carbonate platform to slope depositional settings took place, beginning the deposition of the azoic glauconite-bearing marls (GS-I of the Arguis Formation). The deposition of this sequence was characterized by a great uplift of the anticline, larger than the sedimentation rate. This resulted in a thinning and onlapping of GS-I onto the flanks of the Pico del Águila, which remained uncovered by the sediments of the GS-I (Fig. 19 c). This large uplift, the creation of space available for sedimentation, and the transgressive cycle that characterized the deposition of the Guara and Arguis Formations (Millán et al., 1994; Castelltort et al., 2003), controlled the change of sedimentary facies from the Guara shallow marine limestones to the Arguis slope marls. At this time and unitl ca. 40.04 Ma an increasingly higher sedimentation rate was described. The South Pyrenean thrust front started to generate, adding a slight northwards tilting to the anticline (Fig. 19 c). At ca. 40.04 Ma there was a change in the depositional environment that led to the end of deposition of GS-I. Different folding mechanisms characterized the evolution at this early stage: in GS-I kink band migration predominates in the hinge of the associated synclines, and a combination of limb lengthening and limb rotation occurs along the E-W oriented limbs, whereas in Guara Fm limb lengthening dominates in the periclinal closure and limb rotation is the main mechanism along the N-S oriented part of the limbs (Fig. 19 d). This complex interplay between different folding mechanisms in different units and structural domains characterizes the entire fold growth, and lead to the contrasts in structural style that are described in the field: an internal thrust parallel to the fold trend affects the faulted and complexly deformed Muschelkalk-middle Guara sequence whereas the overlying upper Guara-Campodarbe sequence is more simply folded. With further shortening the emplacement of the South Pyrenean thrust ramp increases the plunge of the anticline at the same time that the progressive rotation takes place (Fig. 19 d). At ca. 37.74 Ma the depositional setting changed slightly and the presence of benthic foraminifera, bryozoans, bivalves and echinoids is described (Millán et al., 1994). On the whole, the anticline had already rotated ca. 6º at this time from the beginning of deformation. However, as shown by the restoration, flexural slip accentuates the rotation of the upper layers with respect to the lower ones, since a slight additional rotation is observed in the upper units. The anticline, therefore, did not rotate as a rigid block: the mechanical contrasts in the basal décollement drove the general rotation of the structure as the South Pyrenean thrust advanced but flexural slip between units allowed additional rotation of each unit as one move upwards in the stratigraphic sequence. According to Millán et al. (1994), after deposition of GS-III at ca. 37.17 Ma the depositional setting changed to a low angle carbonate ramp which consist on marly facies (outer ramp facies) interlayered with carbonate facies (middle ramp facies) rich in benthic pectinid community. A significant rotation of ca. 10º was observed with respect to the previous stage as well as an increase of about 4º in the northwards plunge of the anticline. Both

increments indicate a larger activity in the emplacement of the South Pyrenean thrust during this period. Deposition of GS-IV (Belsué-Atarés Fm., ca. 36.6 Ma), in contrast, did not imply a significant increase in the rotation (barely 2º) and plunge (about 4º) of the anticline. This was the first depositional sequence that covered all the anticline (Fig. 19 e), and implied a change in the depositional setting to deltaic lobes prograding on to prodelta marls, made up by coarsening upward sequences of sandstones and thin marly sequences (Millán et al., 1994). Due to the layer parallel slip described in the syn-kinematic rocks, growth sequences accommodated low to moderate strain, with high strain concentrated in the pre-folding sequence, mainly due to the emplacement of the South Pyrenean thrust ramp underneath. Finally, from top of GS-IV until the cease of deformation (estimated at 34.8 ± 1.72 Ma according to Poblet and Hardy, 1995) the depositional setting changed from fluviodeltaic to fluvial environments, characterized by the sandstones, clays and conglomerates of the Campodarbe Fm. The registered rotation was important, of ca. 15º with respect to the previous stage, and the increment in plunge of about 18º (Fig. 19 e). This indicates that the emplacement of the South Pyrenean thrust ramp had the most intense activity during this time elapse. The layer parallel slip led to a differential folding and rotation of the units that generated the asymmetry described in the present-day geometry. Also during this last stage of deformation normal faulting in the crest of the anticline was described within the entire growth strata, mostly due to outer arc stretching and crestal instabilities.

CONCLUSIONS

Three different modelling techniques have been presented and integrated in order to better understand the structural evolution of the Pico del Águila anticline and, hence, the N-S anticlines of the External Sierras (Southern Pyrenees, Spain).

Analogue models provide new insights on the evolution of the oblique and transverse structures of the Central External Sierras. Based on the uneven distribution of the Triassic detachment level, models simulate the characteristics of the N-S trending anticlines of Central External Sierras: generation synchronous with the emplacement of the South-Pyrenean frontal thrust, higher structural relief compared to orogen-parallel structures, absence of a representative ductile décollement in the core, faulting of lower units and folding of upper ones, plunge towards the hinterland, and foreland-side closure not thrusted by the frontal emerging South-Pyrenean thrust.

FIGURE 19 | (NEXT PAGE) Different sketches summarizing the structural evolution of the Pico del Águila as derived from the presented modelling techniques and the 3D reconstruction of the anticline: a) pre-deformed stage (Middle Lutetian); b) Upper Lutetian, beginning of the deformation; c) Middle Bartonian, deposition of GS-I; d) Upper Bartonian, deposition of GS-II; e) Middle Priabonian, deposition of Campodarbe Fm (post-kinematic) and cease of deformation.

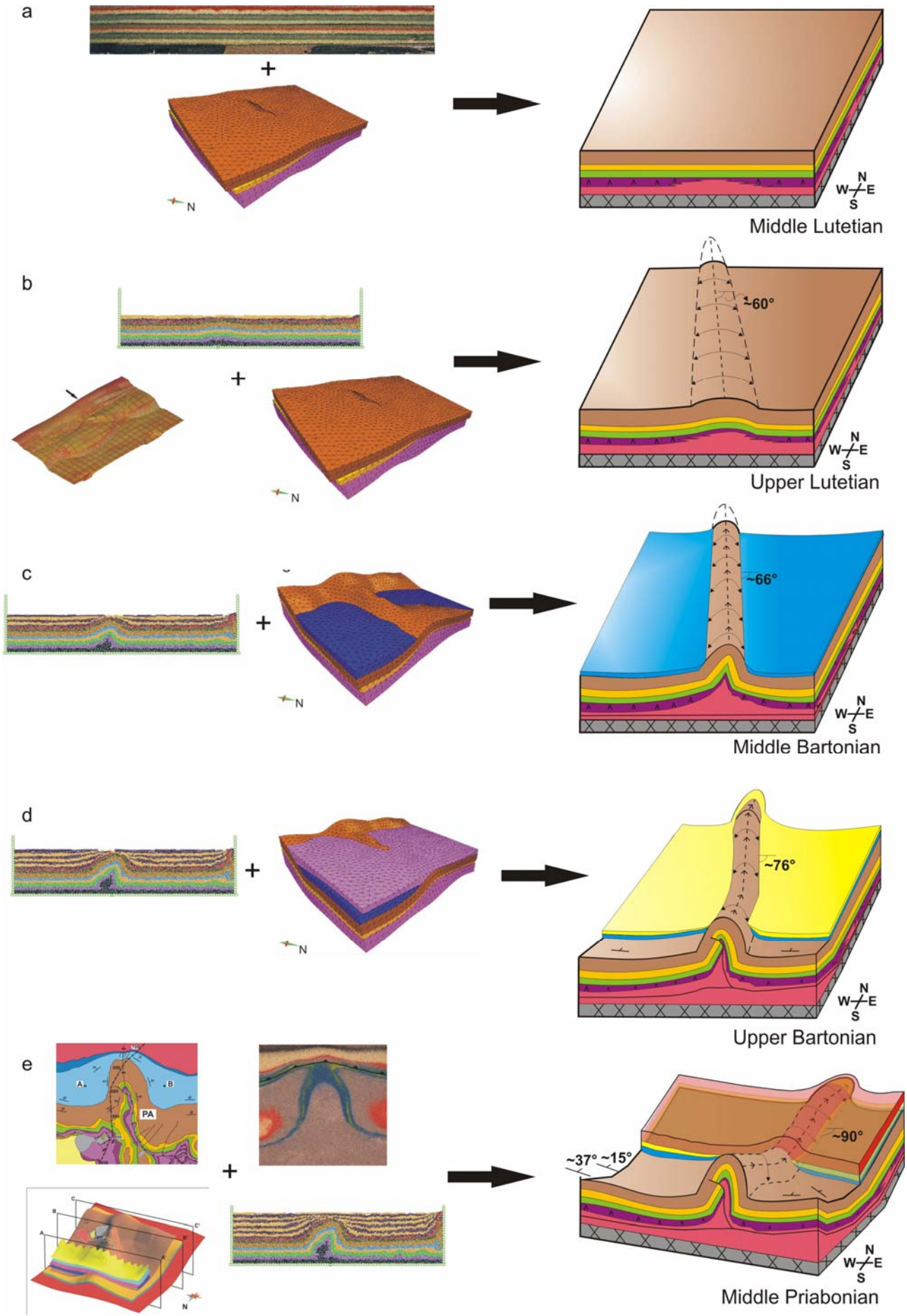
a
N
W
E
S
Middle Lutetian
b
~60°
N
W
E
S
Upper Lutetian
c
~66°
N
W
E
S
Middle Bartonian
d
~76°
N
W
E
S
Upper Bartonian
e
A
B
PA
~90°
~37°
~15°
N
W
E
S
Middle Priabonian

The Discrete-Element models have been used to test the influence of complex competent/incompetent interlayering and the presence of growth strata in the generation and development of the Pico del Águila anticline. The mechanical interlayering leads to high shear strain and complex deformation within the incompetent units, whereas the competent units are subject to more distributed shear strain and simple folding. As a result of the differing mechanical responses to shortening, it is difficult to explain the evolution of such a structure in terms of simple kinematic models. The addition of growth strata reduces the effects of stretching, extensional faulting and gravitational instabilities on the crest of the anticline, and the load of the syn-kinematic package also led the deformation to be more confined to the core of the structure, which is thus tighter than in the absence of growth strata.

The 3D reconstruction and restoration of the Pico del Águila anticline also suggest that the development of a detachment fold in 3D is characterized by a combination of multiple folding mechanisms that occur simultaneously in different units and structural domains during the formation of the anticline, depending on the mechanical properties of the involved materials. Thus, the understanding of fold kinematics should not skip the mechanical behaviour of the rocks to have a better understanding of the evolution of a structure.

The proper integration of different modelling techniques deals with the insights that each approach delivers, but also with the limitations of each particular modelling. In this sense, we present a model of evolution for the Pico del Águila anticline based on the integration of the analogue and numerical modelling and 3D geomechanical restoration of the structure, plus the insights provided by key previous works in the region. Combining multidisciplinary modelling techniques, hence, brings a better understanding of the evolution of this structure as well as the processes that drove the evolution of the N-S detachment anticlines in the External Sierras of the Southern Pyrenees.

ACKNOWLEDGEMENTS

The authors wish to thank IGEOSS, Paradigm™, and Midland Valley Exploration for providing academic licenses of their software Dynel3D, Gocad, and Move, respectively. This work is an initiative of the Group of Geodynamics and Basin Analysis (GGAC, 2009 SGR 1198) at Universitat de Barcelona. This research was supported by StatoilHydro, the Geomod 3D project (CGL2004-05816-C02-01/BTE), MODES-4D project (CGL2007-66431-C02-01/BTE) and the Geomodels Institute Consortium. O. Vidal-Royo also acknowledges the Agència de Gestió d'Ajuts Universitaris i a la Recerca (AGAUR) for providing a PhD grant (2005 FI 00200) and additional funds (2006 BE-2 00095 and 2008 BE-1 00348) to stay during several months at the Hans Ramberg Tectonic Laboratory of Uppsala University (Sweden), the Center for Integrated Petroleum Research (CIPR) at University of Bergen (UiB), and the Department of Petroleum Engineering at the University of Stavanger (UiS) (Norway). We also wish to thank Uppsala University, CIPR and UiS for their logistic support during

those periods. H.A. Koyi is funded by the Swedish Research Council (VR).

REFERENCES

Agterberg, F.P., 1967. Computer techniques in geology. Earth-Science Reviews, 3, 47-77.

Amilibia, A., McClay, K.R., Sàbat, F., Muñoz, J.A., Roca, E., 2005. Analogue Modelling of Inverted Oblique Rift Systems. Geologica Acta, 3 (3), 251-271.

Bonini, M., 2003. Detachment folding, fold amplification, and diapirism in thrust wedge experiments. Tectonics, 22(6), 1065, doi:10.1029/2002TC001458.

Borraccini, F., De Donatis, M., Di Bucci, D., Mazzoli, S., 2002. 3D Model of the active extensional fault system of the high Agri River valley, Southern Apennines, Italy. In: Jessell, M. J. (ed.). General Contributions: 2002. Journal of the Virtual Explorer, 6, 1-6.

Cadell, H.M., 1888. Experimental Researches in mountain building. Royal Society of Edinburgh Transactions, 35, 337-360.

Cagnard, F., Brun, J.P., Gapais, D., 2006. Modes of thickening of analogue weak litospheres. Tectonophysics, 421 (1-2), 145-160.

Carmona, A., Clavera, R., Gratacós, O., Hardy, S., 2008. Combining Discrete Element Modelling and process-based models: initial results. Bolletino di Geofisica teorica ed applicata, 49, 358-364.

Carrera, N., Muñoz, J.A., Roca, E., 2009. 3D reconstruction of geological surfaces by the equivalent dip-domain method: An example from field data of the Cerro Bayo Anticline (Cordillera Oriental, NW Argentine Andes). Journal of Structural Geology, 31, 1573-1585.

Castelltort, S., Guillocheau, F., Robin, C., Rouby, D., Nalpas. T., Lafont, F., Echard, R., 2003. Fold control on the stratigraphic record: a quantified sequence stratigraphic study of the Pico del Aguila anticline in the south-western Pyrenees (Spain). Basin Research, 15, 527-551.

Castillo-Herrador, F., 1974. Le Trias évaporitique des basins de la Vallée de l'Ebre et de Cuenca. Bulletin de la Societé Géologique de France, 16, 49-63.

Daudre, A., 1879. Etudes Synthétiques de Géologie Expérimentale, pt. 1. Paris, Dunod, 828 p.

Felleman, J., 1990. There's a GIS in your future. Government Information Quarterly, 7 (3), 261-267.

Fernández, O., Muñoz, J.A., Arbués. P., Falivene, O., Marzo, M., 2004a . Three-dimensional reconstruction of geological surfaces: An example of growth strata and turbidite systems from the Ainsa basin (Pyrenees, Spain). American Association of Petroleum Geologists Bulletin, 88 (8), 1049-1068.

Fernández, O., 2004b. Reconstruction of geological structures in 3D: An Example from the southern Pyrenees. Doctoral Thesis, Departament de Geodinàmica i Geofísica, Universitat de Barcelona, Barcelona, Spain, 376 pp.

Finch, E., Hardy, S., Gawthorpe, R.L., 2003. Discrete element modelling of contractional fault-propagation folding above rigid basement blocks. Journal of Structural Geology, 25, 515-528.

Finch, E., Hardy, S., Gawthorpe, R.L., 2004. Discrete element modelling of extensional fault-propagation folding above rigid basement fault blocks. Basin Research, 16, 489-506.

Ford, M., Le Carlier de Veslud, C., Bourgeois, O., 2007. Kinematic and geometric analysis of fault-related folds in a rift setting: The Dannemarie basin, Upper Rhine Graben, France. Journal of Structural Geology, 29, 1811-1830.

Gente, P., Auzende, J.M., Renard, V., Fouquet, Y., Bideau, D., 1986. Detailed geological mapping by

submersible of the East Pacific Rise axial graben near 13º N. Earth and Planetary Science Letters, 78 (2-3), 224-236.

Guzofski, C.A., Mueller, J.P., Shaw, J.H., Muron, P., Medwedeff, D.A., Bilotti, F., Rivero, C., 2009. Insights into the mechanisms of fault-related folding provided by volumetric structural restorations using spatially varying mechanical constraints. American Association of Petroleum Geologists Bulletin, 93 (4), 479-502.

Hall, J. Sir, 1815. On the vertical position and convolutions of certain strata and their relation with granite. Royal Society of Edinburgh Transactions, 7, 79-108.

Harbaugh, J.W., Merriam, D.F., 1968. Computer applications in stratigraphic analysis. John Wiley Sons Inc., New York, USA, 282 p.

Hardy, S., Finch, E., 2005. Discrete-element modelling of detachment folding. Basin Research, 17, 507-520.

Hardy, S., Finch, E., 2007. Mechanical stratigraphy and the transition from trishear to kink-band fault-propagation fold forms above blind basement thrust faults: A discrete-element study. Marine and Petroleum Geology, 24, 75-90.

Holl, J.E., Anastasio, D.J., 1993. Paleomagnetically derived folding rates, southern Pyrenees, Spain. Geology, 21 (3), 271-274.

Huyghe, D., Mouthereau, F., Castelltort, S., Filleaudeau. P.Y., Emmanuel, L., 2009. Paleogene propagation of the southern Pyrenean thrust wedge revealed by finite strain analysis in frontal thrust sheets: Implications for mountain building. Earth and Planetary Science Letters, doi:10.1016/j.epsl.2009.10.002.

IGME, 1992. Mapa Geológico de España. Hoja 248, Apiés. Instituto Geológico y Minero de España, Madrid, Unpublished 36 pp report + 1:50000 map.

Jurado, M.J., 1990. El Triásico y el Liásico basal evaporíticos del subsuelo de la cuenca del Ebro. In: Ortí, F., Salvany, J.M. Formaciones evaporíticas de la Cuenca del Ebro y cadenas periféricas, y de la zona de Levante. Enresa, Madrid, 21-28.

Koyi, H.A., 1997. Analogue modelling: from a qualitative to a quantitative technique – a historical perspective. Journal of Petroleum Geology, 20, 223-238.

Krumbein, W.C., Graybill, F.A., 1965. Application of the general linear model to Map Analysis. An Introduction to Statistical Models in Geology, McGraw-Hill, New York, 319-357.

López-Gómez, K., Arche, A., Pérez-López, A., 2002. Permian and Triassic. In: Gibbons, W., Moreno, T. (eds.). The Geology of Spain. The Geological Society of London, 185-212.

Maerten, L., Maerten, F., 2006. Chronologic modeling of faulted and fractured reservoirs using geomechanically based restoration: Technique and industry applications. American Association of Petroleum Geologists Bulletin, 90 (8), 1201-1226.

Millán, H., Aurell, M., Meléndez, A., 1994. Synchronous detachment folds and coeval sedimentation in the Prepyrenean External Sierras (Spain): a case study for a tectonic origin of sequences and system tracts. Sedimentology, 41 (5), 1001-1024.

Millán, H., 1995. Estructura y Cinemática del frente de cabalgamiento surpirenaico en las Sierras Exteriores Aragonesas. Doctoral Thesis, Departamento de Ciencias de la Tierra, Universidad de Zaragoza, Zaragoza, 330 pp + annex.

Nalpas, T., Györfi, I., Guillocheau, F., Lafont, F., Homewood, P., 1999. Influence de la charge sédimentaire sur le développement d'anticlinaux synsédimentaires. Modélisation analogique et exemple du terrain (bordure sud du basin de Jaca). Bulletin de la Societé Géologique de France, 170 (5), 733-740.

Nalpas, T., Gapais, D., Vergés, J., Barrier, L., Gestain, V., Leroux, G., Rouby, D., Kermarrec, J.J., 2003. Effects of rate and nature of synkinematic sedimentation on the growth of compressive structures constrained by analogue models and field examples. In: McCant, T., Saintot, A. (eds.). Tracing Tectonic Deformation Using the Sedimentary Record. Geological Society, London, Special Publications 208, 307-319.

Novoa, E., Suppe, J., Shaw, J.H., 2000. Inclined-Shear Restoration of Growth Folds. American Association of Petroleum Geologists Bulletin, 84 (6), 787-804.

Place, D., Mora, P., 2001. A random lattice solid model for simulation of fault zone dynamics and fracture processes. In: Mulhaus, H.B., Dyskin, A.V., Pasternak, E. (eds.). Bifurcation and Localisation Theory for Soils and Rocks '99. A.A. Balkema, Rotterdam/Brookfield.

Poblet, J., Hardy, S., 1995. Reverse modelling of detachment folds, application to the Pico del Aguila anticline in the South Central Pyrenees (Spain). Journal of Structural Geology, 17, 1707-1724.

Poblet, J., McClay, K.R., Storti, F., Muñoz, J.A., 1997. Geometries of syntectonic sediments associated with single-layer detachment folds. Journal of Structural Geology, 19 (3-4), 369-381.

Pueyo, E.L., Millán, H., Pocoví, A., 2002. Rotation velocity of a thrust: a paleomagnetic study in the External Sierras (Southern Pyrenees). Sedimentary Geology, 146 (1), 191-208.

Puigdefàbregas, C., 1975. La Sedimentación Molásica en la Cuenca de Jaca. Monografias del Instituto de Estudios Pirenaicos. Número Extraordinario de Revista Pirineos, 104, Instituto de Estudios Pirrenaicos, Jaca, 153 pp + annexes.

Rodriguez-Pintó, A., Pueyo, E.L., Pocoví, A., Barnolas, A., 2008. Cronología de la actividad rotacional en el sector central del frente de cabalgamiento de Sierras Exteriores (Pirineo Occidental). Geotemas, 10, 1207-1210.

Salvany, J.M., 1990. Introducción a las evaporitas triásicas de las cadenas periféricas de la cuenca del Ebro: Catalánides, Pirineo y Región Cantábrica. In: Ortí, F., Salvany, J.M. (eds.). Formaciones evaporíticas de la Cuenca del Ebro y cadenas periféricas, y de la zona de Levante. Enresa, Madrid, 21-28.

Scheck, M., Bayer, U., 1999. Evolution of the Northeast German Basin – inferences from a 3D structural model and subsidence analysis. Tectonophysics, 313, 145-169.

Soler, M. , Puigdefàbregas, C., 1970. Líneas generales de la geología del Alto Aragón Occidental. Pirineos, 96, 5-20.

Tanner, D.C., Berhmann, J.H., Dresmann, H., 2003. Three-dimensional retro-deformation of the Lechtal Nappe, Northern Calcareous Alps. Journal of Structural Geology, 25, 737-748.

Vidal-Royo, O., Koyi, H.A., Muñoz, J.A., 2009. Formation of orogen-perpendicular thrusts due to mechanical constrasts in the basal décollement in the Central External Sierras (Southern Pyrenees, Spain). Journal of Structural Geology, 31, 523-539.

Vidal-Royo, O., Hardy, S., Muñoz, J.A., 2010. The roles of complex mechanical stratigraphy and syn-kinematic sedimentation in fold development: Insights from discrete-element modelling and application to the Pico del Águila anticline (External Sierras, Southern Pyrenees). In: Poblet, J., Lisle, R.J. (eds.). Kinematic Evolution and Structural Styles of Fold-and-Thrust Belts, Special Publication of the Geological Society, accepted.

Vidal-Royo, O., Cardozo, N., Muñoz, J.A., Hardy, S., Maerten, L., 2010. Multiple mechanisms driving detachment folding as deduced from 3D reconstruction and geomechanical restoration: The

Pico del Águila anticline (External Sierras, Southern Pyrenees). Basin Research, submitted.

Weijermars, R., 1986. Flow behaviour and physical chemistry of bouncing putties and related polymers in view of tectonic laboratory applications. Tectonophysics, 124, 325-358.

Wilsher, W.A., de Wit, M.J., Marrao, E., 1989. A GIS solution for Gondwana geoscientific data. Journal of African Earth Sciences, 9 (2), 371-374.

Zanchi, A., Salvi, F., Zanchetta, S., Sterlacchini, S., Guerra, G., 2009. 3D reconstruction of complex geological bodies: Examples from the Alps. Computers and Geosciences, 35, 49-69.

CHAPTER VI

Final Remarks and Perspectives of Advance

6.1 FINAL REMARKS

The different modelling techniques presented in this Thesis have been applied to unveil the geological processes that drove the formation and evolution of the transverse anticlines of the External Sierras. Besides this, they have also contributed to improve a methodology with which to tackle the study of other geological structures, characterized by less favorable conditions of outcrop and accessibility. In this sense, the integration of modelling techniques presented in this memoir has been valuable in two main different aspects: the geological and the methodological aspects.

6·1·1 GEOLOGICAL ASPECTS

From a purely geological point of view, the knowledge of the geology of the Central External Sierras has benefited from the work presented in this Thesis. New insights have been pointed out by applying new and up to date modelling techniques to a geological setting that has been broadly studied since many years ago.

As said, three different modelling techniques have been presented and integrated in order to better understand the structural evolution of the Pico del Águila anticline and, hence, the N-S anticlines of the External Sierras.

Analogue models provided new insights on the evolution of the oblique and transverse structures of the Central External Sierras. Based on the uneven distribution of the Triassic detachment level, models simulate the characteristics of the N-S trending anticlines of Central External Sierras: generation synchronous with the emplacement of the South-Pyrenean frontal thrust, higher structural relief compared to orogen-parallel structures, absence of a representative ductile décollement in the core, faulting of lower units and folding of upper ones, plunge towards the hinterland, and foreland-side closure not thrusted by the frontal emerging South-Pyrenean thrust.

The Discrete-Element models have been used to test the influence of complex competent/incompetent interlayering and the presence of growth strata in the generation and development of the Pico del Águila anticline. The mechanical interlayering leads to high shear strain and complex deformation within the incompetent units, whereas the competent units are subject to more distributed shear strain and simple folding. As a result of the differing mechanical responses to shortening, it is difficult to explain the evolution of such a structure in terms of simple kinematic models. The addition of growth strata reduces the effects of stretching, extensional faulting and gravitational instabilities on the crest of the anticline, and the load of the syn-kinematic package also led the deformation to be more confined to the core of the structure, which is thus tighter than in the absence of growth strata.

The 3D reconstruction and restoration of the Pico del Águila anticline also suggest that the development of a detachment fold in 3D is characterized by a combination of multiple folding mechanisms that occur simultaneously in different units and structural domains during the formation of the anticline, depending on the mechanical properties of the involved materials. Thus, the understanding of fold kinematics should not skip the mechanical behaviour of the rocks to have a better understanding of the evolution of a structure.

6·1·2 METHODOLOGICAL ASPECTS

The multidisciplinary approach in which this Thesis is based has also taught us how important is to guide the structural modelling by field observations, in an attempt of understanding what is going on in nature, rather than trying to reproduce in detail a given geometry. Geological modelling is about understanding the geological processes that take part in nature, and models are nothing else but tools that help the geoscientists to overcome their own limitations as human-beings. Hence, models should never go beyond what is observed in nature, and should not be used to make unfounded assumptions in the absence of natural indicators.

Working with different modelling techniques requires an additional effort to gather the contributions from the different approaches, be aware of the net result of each model, take into account the presence of undesired features such as border effects, rule out fake results and be able to integrate all the individual results in a global conceptual model. However, in the end, a better constrained result is obtained, since it must be in accordance with all the models, the geological features observed in nature and the knowledge that other workers provided previously. Far from being disruptive in terms of understanding, working from such a multidisciplinary approach gives a better global picture of the interaction of the processes and mechanisms that govern natural deformation.

The proper integration of different modelling techniques deals with the insights that each approach delivers, but also with the limitations of each particular modelling. In this sense, we presented a model of evolution for the Pico del Águila anticline based on the integration of the analogue and numerical modelling and 3D geomechanical restoration of the structure, plus the insights provided by key previous works in the region. Combining multidisciplinary modelling techniques, hence, brings a better understanding of the evolution of this structure as well as the processes that drove the evolution of the N-S detachment anticlines in the External Sierras of the Southern Pyrenees. However, a similar workflow could be followed to study any other structure worldwide. In this sense, a multidisciplinary approach aims to use the most

suitable methods for each case-study, and the modelling integration presented in this Thesis is no exception to this. Paying special attention to the mechanical response of the materials to deformation will undoubtedly result in a better understanding of the structural evolution of a given structure, being able to derive its kinematics without invoking any superimposed criteria to it.

6.2 PERSPECTIVES OF ADVANCE

After several years working in the N-S anticlines of the External Sierras many questions, challenges and concerns have arisen, some of which have been finally solved, but some of which still remain unanswered. In addition, there are parallel investigations that have been put aside due to lack of time, human resources or simply because did not find the way to link them with the main global objective of this Thesis. Once the big job is finished, it will be perhaps the time to get back and pay more attention to them. These issues are:

a) The 3D reconstruction and sequential restoration of the Pico del Águila neighboring N-S structures such as the Bentué de Rasal and Gabardiella detachment anticlines. Carrying out this exercise in neighboring structures would provide a better picture of the clockwise rotation of the N-S anticlines at a more regional scale, giving tools to compare the evolution of the deformation along the trace of the South-Pyrenean thrust front.

b) An accurate fracture analysis in the field. Manoel Valcárcel already did a Bachelor's degree work on the analysis of the fractures associated to the growth of the Pico del Águila, reaching promising results with which to compare the strain pattern derived from the restoration and the numerical models. However, a more intense study would be of great interest, investing a longer period and more resources to gain more measurement stations and, hence, a better control on how fractures distribute throughout the anticline.

c) An automated tool to reconstruct growth strata geometries. The growth strata sequences reconstructed in the Pico del Águila anticline were carried

out by applying the dip domain method individually for each horizon. However, this method is largely time consuming and may become tedious if a large number (hundreds or thousands) of dip data are available. Benefiting from the excellent outcrop conditions and accessibility, the reconstructed growth strata may become an excellent basis to develop an automated method to reconstruct growth strata geometries from physically measurable parameters of the rocks.

d) Reprocessing of the seismic lines available in the area. The seismic surveys that provided the profiles available in the area were carried out during the 1960's. As a result, the seismic lines of the area are of poor quality, and do not allow accurate interpretations of the geometry of the units, particularly in the shallower levels of the growth strata. This is a major limitation to correctly understand the geometry of the External Sierras at depth. Although it is partially overcome by magnificent outcropping conditions, an up to date reprocessing of the seismic lines would greatly improve the interpretation and understanding of the N-S anticlines at depth.

REFERENCES

List of References cited throughout the Thesis memoir

Agterberg, F.P., 1967. Computer techniques in geology. Earth-Science Reviews, 3, 47-77.

Almela, A. & Ríos, J.M.; 1951. Mapa geológico de España 1:50000 serie Antigua, 248 (Apiés). IGME Ed. Madrid, 50 pp + map.

Amilibia, A., McClay, K.R., Sàbat, F., Muñoz, J.A., Roca, E., 2005. Analogue Modelling of Inverted Oblique Rift Systems. Geologica Acta, 3 (3), 251-271.

Anastasio, D.J. & Holl, J.E.; 2001. Transverse fold evolution in the External Sierras, Southern Pyrenees, Spain; Journal of Structural Geology, 23 (2-3), pp 379-392.

Anastasio, D.J.; 1992. Structural Evolution of the External Sierras, Southern Pyrenees, Spain; In: Mitra, S.; Fisher, G.W. (Eds.), Structural Geology of Fold and Thrust Belts. Johns Hopkins University Press, Baltimore, pp 239-251.

Atkinson, P.A. & Wallace, W.K. 2003. Competent unit thicknesses in detachment folds in the Northeastern Brooks Range, Alaska: geometric analysis and a conceptual model. Journal of Structural Geology, 25, 1751-1771.

Bahroudi, A. & Koyi, H.A.; 2003. Effect of spatial distribution of Hormuz salt on deformation style in the Zagros fold and thrust belt: an analogue modeling approach. Journal of the Geological Society, 160, 719-733.

Beaumont, C.; Muñoz, J.A.; Hamilton, J.; Fullsack, P.; 2000. Factors controlling the Alpine evolution of the central Pyrenees inferred from a comparison of observations and geodynamical models. Journal of Geophysical Research, 105, 8121-8145.

Bentham, P. & Burbank, D.W.; 1996. Chronology of Eocene foreland basin evolution along the western oblique margin of the South-Central Pyrenees. In: Friend, P.F.; Dabrio, C.J. (eds), Tertiary Basins of Spain. Cambridge University Press, Cambridge, 144-152.

Bistacchi, A., Massironi, M., Dal Piaz G. V., Dal Piaz, G., Monopoli, B., Schiavo, A. & Toffolon, G. (2008) 3D fold and fault reconstruction with an uncertainty model: An example from an Alpine tunnel case study.

Computers and Geosciences, 34 (4), 351-372.

Bonini, M., 2003. Detachment folding, fold amplification, and diapirism in thrust wedge experiments. Tectonics, 22(6), 1065, doi:10.1029/2002TC001458.

Bonini, M.; 2007. Deformation patterns and structural vergence in brittle-ductile thrust wedges: An additional analogue modelling perspective. Journal of Structural Geology, 29, 141-158.

Borraccini, F., De Donatis, M., Di Bucci, D., Mazzoli, S., 2002. 3D Model of the active extensional fault system of the high Agri River valley, Southern Apennines, Italy. In: Jessell, M. J. (ed.). General Contributions: 2002. Journal of the Virtual Explorer, 6, 1-6.

Braathen, A., Tveranger, J., Fossen, H., Skar, T., Cardozo, N., Semshaug, S.E., Bastesen E. & Sverdrup E. (2009) Fault Facies and its applications to sandstone reservoirs. American Association of Petroleum Geologists Bulletin, 93 (7), 891-917.

Cadell, H.M., 1888. Experimental Researches in mountain building. Royal Society of Edinburgh Transactions, 35, 337-360.

Cagnard, F., Brun, J.P., Gapais, D., 2006. Modes of thickening of analogue weak litospheres. Tectonophysics, 421 (1-2), 145-160.

Camborde, F., Mariotti, C. & Donzé, F.V. 2000. Numerical study of rock and concrete behaviour by discrete element modelling. Computers and Geotechnics, 27 (4), 225-247.

Camerlo, R.H., Benson, E.F., 2006. Geometric and seismic interpretation of the Perdido fold belt: Northwestern deep-water Gulf of Mexico. American Association of Petroleum Geologists Bulletin, 90 (3), 363-386.

Cardozo, N. & Allmendinger, R.W. 2009. SSPX: A program to compute strain from displacement/velocity data. Computers and Geosciences, 35 (6), 1343-1357.

Carmona, A., Clavera, R., Gratacós, O., Hardy, S., 2008. Combining Discrete Element Modelling and process-based models: initial results. Bolletino di Geofisica teorica ed applicata, 49, 358-364.

Carrera, N., Muñoz, J.A., Roca, E., 2009. 3D reconstruction of geological surfaces by the equivalent dip-domain method: An example from field data of the Cerro Bayo Anticline (Cordillera Oriental, NW Argentine Andes). Journal of Structural Geology, 31, 1573-1585.

Casas-Sainz, A.M., Soto-Marín, R., González, A. & Villalaín, J.J. 2005. Folded onlap geometries: implications for recognition of syn-sedimentary folds. Journal of Structural Geology, 27, 1644-1657.

Castelltort, S., Guillocheau, F., Robin, C., Rouby, D., Nalpas. T., Lafont, F., Echard, R., 2003. Fold control on the stratigraphic record: a quantified sequence stratigraphic study of the Pico del Aguila anticline in the south-western Pyrenees (Spain). Basin Research, 15, 527-551.

Castillo-Herrador, F.; 1974. Le Trias évaporitique des basins de la Vallée de l'Ebre et de Cuenca. Bulletin

de la Societé Géologique de France, 16, 49-63.

Cobbold, P.R.; Rosello, E.A.; Vendeville, B.C.; 1989. Some experiments on interacting sedimentation and deformation above salt horizons. Bulletin de la Societé Géologique de France, 8, 453-460.

Costa, E. & Vendeville, B.C.; 2002. Experimental insights on the geometry and kinematics of fold-and-thrust belt above weak, viscous evaporitic décollement. Journal of Structural Geology, 24, 1729-1739.

Cotton, J.T. & Koyi, H.A.; 2000. Modelling of thrust fronts above ductile and frictional detachments: Application to structures in the Salt Range and Potwar Plateau, Pakistan. Geological Society of America Bulletin, 112, 351-363.

Crespo-Blanc, A.; 2008. Recess drawn by the internal zone outer boundary and oblique structures in the paleomargin-derived units (Subbetic Domain, central Betics): An analogue modeling approach. Journal of Structural Geology, 30, 65-80.

Daudre, A., 1879. Etudes Synthétiques de Géologie Expérimentale, pt. 1. Paris, Dunod, 828 p.

Davis, D.M. & Engelder, T.; 1985. The role of salt in fold-and-thrust belts. Tectonophysics, 119, 67-88.

Dinarés, J.; McClelland, E.; Santanach, P.; 1992. Contrasting rotations within thrust sheets and kinematics of thrust tectonics as derived from paleomagnetic data: an example from the Southern Pyrenees. In: McClay, K.R. (Ed.), Thrust Tectonics. Chapman & Hall, London, 265-276.

Donzé, F., Magnier, S.A. & Bouchez, J. 1996. Numerical modelling of a highly explosive source in an elastic-brittle rock mass. Journal of Geophysical Research, 101 (2), 3103-3112.

Dooley, T.P.; Jackson, M.P.A.; Hudec, M.R.; 2007. Initiation and growth of salt-based thrust belts on passive margins: results from physical models. Basin Research, 19, 165-177.

Falivene, O. (2007). Testing three-dimensional facies reconstruction and modelling techniques applied to cored and outcropping analogues. Examples from swamp coal zones to alluvial fans and marine turbidite sequences. PhD Thesis. Universidad de Barcelona. Departament d' Estratigrafia, Paleontologia i Geociencies Marines y Departament de Geodinamica i Geofisica.

Felleman, J., 1990. There's a GIS in your future. Government Information Quarterly, 7 (3), 261-267.

Fernández, O. (2005) Obtaining a best fitting plane through 3D georeferenced data. Journal of Structural Geology, 27, 855-858.

Fernández, O., 2004b. Reconstruction of geological structures in 3D: An Example from the southern Pyrenees. Doctoral Thesis, Departament de Geodinàmica i Geofísica, Universitat de Barcelona, Barcelona, Spain, 376 pp.

Fernández, O., Muñoz, J.A., Arbués. P., Falivene, O., Marzo, M., 2004a . Three-dimensional reconstruction of geological surfaces: An example of growth strata and turbidite systems from the Ainsa basin (Pyrenees, Spain). American

Association of Petroleum Geologists Bulletin, 88 (8), 1049-1068.

Finch, E., Hardy, S. & Gawthorpe, R.L. 2003. Discrete element modelling of contractional fault-propagation folding above rigid basement blocks. Journal of Structural Geology, 25, 515-528.

Finch, E., Hardy, S. & Gawthorpe, R.L. 2004. Discrete element modelling of extensional fault-propagation folding above rigid basement fault blocks. Basin Research, 16, 489-506.

Ford, M., Le Carlier de Veslud, C., Bourgeois, O., 2007. Kinematic and geometric analysis of fault-related folds in a rift setting: The Dannemarie basin, Upper Rhine Graben, France. Journal of Structural Geology, 29, 1811-1830.

Gente, P., Auzende, J.M., Renard, V., Fouquet, Y., Bideau, D., 1986. Detailed geological mapping by submersible of the East Pacific Rise axial graben near 13º N. Earth and Planetary Science Letters, 78 (2-3), 224-236.

Grando, G. & McClay, K.R. 2007. Morphotectonics domains and structural styles in the Makran accretionary prism, offshore Iran. Sedimentary Geology, 196, 157-179.

Grando, G.,Schleder, Z., Shackleton, R., Seed, G., Buddin, T., McClay, K. & Borraccini, F. (2009) 3D structural evolution and kinematics of the Frampton growth fold system, Western Mississippi Fan Fold Belt, deep-water Gulf of Mexico. Search and Discovery Article # 50161.

Grelaud, S.; Nalpas, T.; Vergés, J.; Karpuz, R.; 2002. Role of décollement levels in thrust systems: field examples and analogue modelling. Bolletino di Geofisica teorica ed applicata, 42 N. ½ supplement, 178-180.

Guzofski, C.A., Mueller, J.P., Shaw, J.H., Muron, P., Medwedeff, D.A., Bilotti, F., Rivero, C., 2009. Insights into the mechanisms of fault-related folding provided by volumetric structural restorations using spatially varying mechanical constraints. American Association of Petroleum Geologists Bulletin, 93 (4), 479-502.

Hall, J. Sir, 1815. On the vertical position and convolutions of certain strata and their relation with granite. Royal Society of Edinburgh Transactions, 7, 79-108.

Harbaugh, J.W., Merriam, D.F., 1968. Computer applications in stratigraphic analysis. John Wiley Sons Inc., New York, USA, 282 p.

Hardy, S & Finch, E. 2005. Discrete-element modelling of detachment folding. Basin Research, 17, 507-520.

Hardy, S & Finch, E. 2007. Mechanical stratigraphy and the transition from trishear to kink-band fault-propagation fold forms above blind basement thrust faults: A discrete-element study. Marine and Petroleum Geology, 24, 75-90.

Hardy, S., McClay, K.R. & Muñoz, J.A. 2009. Deformation and fault activity in space and time in high resolution numerical models of doubly vergent thrust wedges. Marine and Petroleum Geology, 26, 232-248.

Harrison, J.C.; 1995. Tectonics and Kinematics of a foreland folded belt influenced by salt, Arctic Canada. In: Jackson, M.P.A.; Roberts, D.G. and Snelson, S. (eds), Salt Tectonics:

A Global Perspective. AAPG Memoirs, 65, 379-412.

Hill, K.C., 1991. Structure of the Papuan Fold Belt, Papua New Guinea. American Association of Petroleum Geologists Bulletin, 74 (5), 857-872.

Hogan P.J. & Burbank, D.W.; 1996. Evolution of the Jaca Piggyback basin and emergence of External Sierras, Southern Pyrenees. In: Friend, P.F.; Dabrio, C.J. (Eds.), Tertiary Basins of Spain. Cambridge University Press, pp. 153-160.

Holl, J.E., Anastasio, D.J., 1993. Paleomagnetically derived folding rates, southern Pyrenees, Spain. Geology, 21 (3), 271-274.

Homza, T.X. & Wallace, W.K. 1995. Geometric and kinematic models for detachment folds with fixed and variable detachment depths. Journal of Structural Geology, 17, 475-488.

Homza, T.X. & Wallace, W.K. 1997. Detachment folds with fixed hinges and variable detachment depth, Northeastern Brooks Range. Journal of Structural Geology, 19, 337-354.

Huyghe, D., Mouthereau, F., Castelltort, S., Filleaudeau. P.Y., Emmanuel, L., 2009. Paleogene propagation of the southern Pyrenean thrust wedge revealed by finite strain analysis in frontal thrust sheets: Implications for mountain building. Earth and Planetary Science Letters, doi:10.1016/j.epsl.2009.10.002.

IGME. 1987. Contribución de la exploración petrolífera al conocimiento de la geología de España. Instituto Geológico y Minero de España. Published report plus maps.

IGME; 1992. Mapa Geológico de España; Hoja 248, Apiés; Instituto Geológico y Minero de España, Madrid, Unpublished 36 pp report + 1:50000 map.

Jurado, M.J.; 1990. El Triásico y el Liásico basal evaporíticos del subsuelo de la cuenca del Ebro. In: Ortí, F. and Salvany, J.M. Formaciones evaporíticas de la Cuenca del Ebro y cadenas periféricas, y de la zona de Levante. Enresa, Madrid, 21-28.

Koyi, H.A. & Cotton, J.; 2004. Experimental insights on the geometry and kinematics of fold-and-thrust belts above weak, viscous evaporitic décollement; a discussion. Journal of Structural Geology, 26, 2139-2141.

Koyi, H.A. & Sans, M.; 2006. Deformation transfer in viscous detachments: comparison of sandbox models to the South Pyrenean Triangle Zone. Geological Society, London, Special Publications, January 1, 2006; 253(1): 117 - 134.

Koyi, H.A. & Vendeville, C.B.; 2003. The effect of décollement dip on geometry and kinematics of model accretionary wedges. Journal of Structural Geology, 25, 1445-1450.

Koyi, H.A., 1997. Analogue modelling: from a qualitative to a quantitative technique - a historical perspective. Journal of Petroleum Geology, 20, 223-238.

Koyi, H.A.; 1988. Experimental modeling of role of gravity and lateral shortening in Zagros mountain belt. AAPG Bulletin, 72, 1381-1394.

Koyi, H.A.; 1995. Mode of internal deformation in sand wedges. Journal of Structural Geology, 17, 293-300.

Krumbein, W.C., Graybill, F.A., 1965. Application of the general linear model to Map Analysis. An Introduction to Statistical Models in Geology, McGraw-Hill, New York, 319-357.

Kuhn, M.R. 1999. Structured deformation in granular materials. Mechanics of Materials, 31, 407-429.

Larrasoaña, J.C.; Parés, J.M.; Pueyo, E.L. 2001. Stable Eocene Magnetization Carried by Magnetite and Iron Sulphides in Marine Marls (Pamplona-Arguis Formation, Southern Pyrenees, Northern Spain); Studia Geophysica et Geodaetica, 47 (2), pp 237-254.

Letouzey, J.; Colletta, B.; Vially, R.; Chermette, J.C.; 1995. Evolution of salt-related structures in compressional settings. In: Jackson, M.P.A.; Roberts, D.G.; Snelson, S. (eds), Salt tectonics: A Global perspective. American Association of Petroleum Geologists Memoir, 65, 41-60.

Liu, H.; McClay, K.R.; Powell, D.; 1992. Physical models of thrust wedges. In: McClay, K.R. (Ed.), Thrust Tectonics. Chapman & Hall, 71-81.

Lohrmann, J.; Kukowski, N.; Adam, J.; Oncken, O.; 2003. The impact of analogue material properties on the geometry, kinematics and dynamics of convergent sand wedges. Journal of Structural Geology, 25, 1691-1711.

López-Gómez, K.; Arche, A.; Pérez-López, A.; 2002. Permian and Triassic. In: Gibbons, W. And Moreno, T. (eds), The Geology of Spain. The Geological Society of London, 185-212.

Luján, M.; Storti, F.; Balanyá, J.C.; Crespo-Blanc, A.; Rosetti, F.; 2003. Role of décollement material with different rheological properties in the structure of the Aljibe thrust imbricate (Flysch Trough, Gibraltar Arc): an analogue modelling approach. Journal of Structural Geology, 25, 867-881.

Maerten, L. (2007) Geomechanics to solve structure related issues in petroleum reservoirs. AAPG-ER Newsletter, September 2007.

Maerten, L., Gillespie, P. & Daniel, J.M. (2006) Three-dimensional geomechanical modeling for constraint of subseismic fault simulation. American Association of Petroleum Geologists Bulletin, 90 (9), 1337-1358.

Maerten, L., Maerten, F., 2006. Chronologic modeling of faulted and fractured reservoirs using geomechanically based restoration: Technique and industry applications. American Association of Petroleum Geologists Bulletin, 90 (8), 1201-1226.

Mallada, L.; 1878. Geología de la provincial de Huesca. Mem. Com. Mapa geológico de España, Madrid. 559 pp.

Massoli, D.; Koyi, H.A.; Barchi. M.R.; 2006. Structural evolution of a fold and thrust belt generated by multiple décollements: analogue models and natural examples from Northern Apennines (Italy). Journal of Structural Geology, 28, 185-199.

McClay, K.R. & Whitehouse, P.; 2004. Analogue Modelling of doubly vergent thrust wedges. In: McClay, K.R. (ed) Thrust Tectonics and Hydrocarbon Systems. American Association of Petroleum Geologists, Memoir 82, 372-399.

McClay, K.R.; Whitehouse, P.S.; Dooley, T.; Richards, M.; 2004. 3D evolution of fold and thrust belts formed by oblique convergence. Marine and Petroleum Geology, 21, 857-877.

McElroy. R. 1990. Thrust kinematics and syntectonic sedimentation: the Pyrenean frontal ramp, Huesca, Spain. PhD Thesis, University of Cambridge.

Millán, H., 1995. Estructura y Cinemática del frente de cabalgamiento surpirenaico en las Sierras Exteriores Aragonesas. Doctoral Thesis, Departamento de Ciencias de la Tierra, Universidad de Zaragoza, Zaragoza, 330 pp + annex.

Millán, H., Aurell, M., Meléndez, A., 1994. Synchronous detachment folds and coeval sedimentation in the Prepyrenean External Sierras (Spain): a case study for a tectonic origin of sequences and system tracts. Sedimentology, 41 (5), 1001-1024.

Mitra, S. 2003. A unified kinematic model for the evolution of detachment folds. Journal of Structural Geology, 25, 1659-1673.

Mitra, S., 2002. Structural Models of Faulted Detachment Folds. American Association of Petroleum Geologists Bulletin, 86 (9), 1673-1694.

Mora, P. & Place, D. 1993. A lattice solid model for the non-linear dynamics of earthquakes. International Journal of Modern Physics C, 4 (6), 1059-1074.

Moretti, I. (2008) Working in complex areas: New restoration workflow based on quality control, 2D and 3D restorations. Marine and Petroleum Geology, 25, 205-218.

Mulugeta, G. & Koyi, H., 1992. Episodic accretion and strain partitioning in a model sand wedge. Tectonophysics, 202, 319-333.

Mulugeta, G. & Koyi, H.A; 1987. Three-dimensional geometry and kinematics of experimental piggy-back thrusting. Geology, 15, 1052-1056.

Mulugeta, G.; 1988. Modelling the geometry of Coulomb thrust wedges. Journal of Structural Geology, 10, 847-859.

Muñoz, J.A.; 1992. Evolution of a continental collision belt: ECORS-Pyrenees crustal balanced cross-section. In: McClay, K.R. (Ed.), Thrust Tectonics. Chapman & Hall. Pp 235-246.

Nalpas, T., Gapais, D., Vergés, J., Barrier, L., Gestain, V., Leroux, G., Rouby, D., Kermarrec, J.J., 2003. Effects of rate and nature of synkinematic sedimentation on the growth of compressive structures constrained by analogue models and field examples. In: McCant, T., Saintot, A. (eds.). Tracing Tectonic Deformation Using the Sedimentary Record. Geological Society, London, Special Publications 208, 307-319.

Nalpas, T., Györfi, I., Guillocheau, F., Lafont, F., Homewood, P., 1999. Influence de la charge sédimentaire sur le développement d'anticlinaux synsédimentaires. Modélisation analogique et exemple du terrain (bordure sud du basin de Jaca). Bulletin de la Societé Géologique de France, 170 (5), 733-740.

Nigro, F. & Renda, P. 2004. Growth patterns of underlithified strata during thrust-related folding. Journal of Structural Geology, 26, 1913-1930.

Nilforoushan, F.; Koyi, H.A.; Swantesson, J.O.H.; Talbot, C.J.; 2008. Effect of basal friction on surface and volumetric strain in models of convergent settings measured by laser scanner. Journal of Structural Geology, 30, 366-379.

Novoa, E., Suppe, J., Shaw, J.H., 2000. Inclined-Shear Restoration of Growth Folds. American Association of Petroleum Geologists Bulletin, 84 (6), 787-804.

Oliva, B.; Millán, H.; Pocoví, A.; Casas, A.M.; 1996; Estructura de la Cuenca de Jaca en el sector occidental de las Sierras Exteriores Aragonesas. Geogaceta, 20 (4), 800-802.

Oliva-Urcía, B. & Pueyo, E.L.; 2007. Gradient of shortening and vertical-axis rotations in the Southern Pyrenees (Spain), insights from a synthesis of paleomagnetic data. Revista de la Sociedad Geológica de España, 20 (1-2), 105-118.

Place, D., Mora, P., 2001. A random lattice solid model for simulation of fault zone dynamics and fracture processes. In: Mulhaus, H.B., Dyskin, A.V., Pasternak, E. (eds.). Bifurcation and Localisation Theory for Soils and Rocks '99. A.A. Balkema, Rotterdam/Brookfield.

Poblet, J., Hardy, S., 1995. Reverse modelling of detachment folds, application to the Pico del Aguila anticline in the South Central Pyrenees (Spain). Journal of Structural Geology, 17, 1707-1724.

Poblet, J.; McClay, K.R.; Storti, F.; Muñoz, J.A.; 1997. Geometries of syntectonic sediments associated with single-layer detachment folds; Journal of Structural Geology, 19 (3-4), pp 369-381.

Pocoví, A.J.; 1979. Estudio geológico de las Sierras Marginales Catalanas (Prepirineo de Lérida). Acta Geológica Hispánica, 13, 73-79.

Pueyo, E.L. (2000) Rotaciones Paleomagnéticas en Sistemas de Pliegues y Cabalgamientos. Tipos, Causas, Significado y Aplicaciones (Ejemplos de las Sierras Exteriores y Cuenca de Jaca, Pirineo Aragonés). PhD Thesis, Departamento de Ciencias de la Tierra, Universidad de Zaragoza, Zaragoza.

Pueyo, E.L., Millán, H., Pocoví, A., 2002. Rotation velocity of a thrust: a paleomagnetic study in the External Sierras (Southern Pyrenees). Sedimentary Geology, 146 (1), 191-208.

Pueyo, E.L.; 2000. Rotaciones Paleomagnéticas en Sistemas de Pliegues y Cabalgamientos. Tipos, Causas, Significado y Aplicaciones (Ejemplos de las Sierras Exteriores y Cuenca de Jaca, Pirineo Aragonés); PhD Thesis, Departamento de Ciencias de la Tierra, Universidad de Zaragoza, Zaragoza, 300 pp + annex.

Pueyo, E.L.; Millán, H.; Pocoví, A.; Parés, J.M.; 1997. Determination of the folding mechanism by AMS data: study of the relation between shortening and magnetic anisotropy in the Pico del Águila anticline (Southern Pyrenees). Physics and Chemistry of the Earth, 22 (1-2), 195-201.

Pueyo, E.L.; Millán, H.; Pocoví, A.; Parés, J.M.; 2000. Cinemática rotacional del cabalgamiento basal surpirenaico en as Sierras Exteriores Aragonesas: datos magnetotectónicos. Acta Geológica Hispánica, 32 (3-4), 119-137.

Pueyo, E.L.; Parés, J.M.; Millán, H.; Pocoví, A.; 2003b. Conical folds and apparent rotations in paleomagnetism (a case study in the Southern Pyrenees). Tectonophysics, 362, 345-366.

Pueyo, E.L.; Pocoví, A; Parés, J.M.; Millán, H.; Larrasoaña, J.C.; 2003a. Thrust ramp geometry and spurious rotations of paleomagnetic vectors. Studia Geophysica Geodetica, 47, 331-357.

Puigdefàbregas, C.; 1975. La Sedimentación Molásica en la Cuenca de Jaca; Monografias del Instituto de Estudios Pirenaicos. Número Extraordinario de Revista Pirineos, 104, Instituto de Estudios Pirrenaicos, Jaca, 153 pp + annexes.

Rodriguez-Pintó, A., Pueyo, E.L., Pocoví, A., Barnolas, A., 2008. Cronología de la actividad rotacional en el sector central del frente de cabalgamiento de Sierras Exteriores (Pirineo Occidental). Geotemas, 10, 1207-1210.

Rouby, D. & Cobbold, P.R. (1996) Kinematic analysis of a growth fault system in the Niger Delta from restoration in map view. Marine and Petroleum Geology, 13 (5), 565-580.

Salvany, J.M.; 1990. Introducción a las evaporitas triásicas de las cadenas periféricas de la cuenca del Ebro: Catalánides, Pirineo y Región Cantábrica. In: Ortí, F. and Salvany, J.M. Formaciones evaporíticas de la Cuenca del Ebro y cadenas periféricas, y de la zona de Levante. Enresa, Madrid, 21-28.

Sanders, C., Bonora, M., Richards, D., Kozlowski, E., Sylwan, C. & Cohen, M. (2004) Kinematic structural restorations and discrete fracture modeling of a thrust trap: a case study from the Tarija Basin, Argentina. Marine and Petroleum Geology, 21, 845-855.

Scheck, M., Bayer, U., 1999. Evolution of the Northeast German Basin - inferences from a 3D structural model and subsidence analysis. Tectonophysics, 313, 145-169.

Schreurs, G; Hänni, R; Vock, P.; 2002. Analogue modeling of transfer zones in fold and thrust belts: a 4-D analysis. Journal of the Virtual Explorer, 6, 43-49.

Schultz, R.A. (1996) Relative scale and the strength and deformability of rock masses. Journal of Structural Geology, 18 (9), 1139-1149.

Selzer. G.; 1948. Geología de las sierras surpirenaicas del Alto Aragón. (Translated from the original version, "Geologie der sudpyrenäische Sierren in Oberaragonien", Berlin, 1934). Publicación Extraordinaria Geol. España. C.S.I.C.; Madrid, IV, 185-231.

Smit, J.H.W.; Brun, J.P.; Sokoutis, D.; 2003. Deformation of brittle-ductile thrust wedges in experiments and nature. Journal of Geophysical Research, 108 (B10), 2480, doi:10.1029/2002JB002190.

Soler, M. , Puigdefàbregas, C., 1970. Líneas generales de la geología del Alto Aragón Occidental. Pirineos, 96, 5-20.

Soto, R.; Casas, A.M.; Storti, F.; Faccena, C.; 2002. Role of lateral thickness variations on the development of oblique structures at the Western end of the South Pyrenean Central Unit. Tectonophysics, 350, 215-235.

Soto, R.; Casas-Sainz, A.M.; Pueyo, E.L.; 2006. Along-strike variation of orogenic wedges associated with vertical axis rotations. Journal of Geophysical Research, 111, B10402, doi: 10.1029/2005JB004201.

Storti, F. & Poblet, J. 1997. Growth stratal architectures associated to décollement folds and fault-propagation folds. Inferences on fold kinematics. Tectonophysics, 282, 353-373.

Storti, F.; Soto-Marin, R; Faccena, C.; Casas-Sainz, A.; 2001. Role of the backstop-to-cover thickness ratio on vergence partitioning in experimental thrust wedges. Terra Nova, 13 (6), 413-417.

Storti, F.; Soto-Marin, R; Rossetti, F..; Casas-Sainz, A.; 2007. Evolution of experimental thrust wedges accreted from along-strike tapered, silicone-floored multilayers. Journal of the Geological Society of London, 164, 73-85.

Strayer, L.M., Erickson, S. G. & Suppe, J. 2004. Influence of growth strata on the evolution of fault-related folds: Distinct-element models. In: McClay, K. (ed), Thrust Tectonics and Hydrocarbon Systems. American Association of Petroleum Geologists Memoir, 82, 413-437.

Swantesson, J.O.H.; 2005. Weathering and erosion of rock carvings in Sweden during the period 1994-2003. In: Micro Mapping with laser scanner for Assessment of Breakdown rates, 29. Karlstad University Studies, 99.

Swantesson, J.O.H.; Moses, C.A.; Berg, G.E.; Jansson, M.J.; 2006. Methods for measuring shore platform micro erosion: A comparison of the micro-erosion meter and laser scanner. Zeitschrift für Geomorphologie N.F. Vol. 144 (Supplement), 1-17.

Talbot, C.J.; 1992. Centrifuge models of Gulf of Mexico profiles. Marine and Petroleum Geology, 9, 412-432.

Tanner, D.C., Berhmann, J.H., Dresmann, H., 2003. Three-dimensional retro-deformation of the Lechtal Nappe, Northern Calcareous Alps. Journal of Structural Geology, 25, 737-748.

Tavani, S., Storti, F. & Salvini, F. 2007. Modelling growth stratal architectures associated with double edge fault-propagation folding. Sedimentary Geology, 196, 119-132.

Teixell, A. & García-Sansegundo, J.; 1995. Estructura del sector central de la Cuenca de Jaca (Pirineos Meridionales). Revista de la Sociedad Geológica de España, 8(3), 215-228.

Teixell, A. & Koyi, H.A., 2003, Experimental and field study of the effects of lithological contrasts on thrust-related deformation. Tectonics, 22, 1054, doi:10.1029/2002TC001407.

Vidal-Royo, O., Cardozo, N., Muñoz, J.A., Hardy, S., Maerten, L., 2010. Multiple mechanisms driving detachment folding as deduced from 3D reconstruction and geomechanical restoration: The Pico del Águila anticline (External Sierras, Southern Pyrenees). Basin Research, submitted.

Vidal-Royo, O., Hardy, S., Muñoz, J.A., 2010. The roles of complex mechanical stratigraphy and syn-kinematic sedimentation in fold development: Insights from discrete-element modelling and application to the Pico del Águila anticline (External

Sierras, Southern Pyrenees). In: Poblet, J., Lisle, R.J. (eds.). Kinematic Evolution and Structural Styles of Fold-and-Thrust Belts, Special Publication of the Geological Society, accepted.

Vidal-Royo, O., Koyi, H.A., Muñoz, J.A., 2009. Formation of orogen-perpendicular thrusts due to mechanical constrasts in the basal décollement in the Central External Sierras (Southern Pyrenees, Spain). Journal of Structural Geology, 31, 523-539.

Weijermars, R. & Schmeling, H.; 1986. Scaling of Newtonian and non-Newtonian fluid dynamics without inertia for quantitative modelling of rock flow due to gravity (including the concept of rheological similarity). Physics of the Earth and Planetary Interiors, 43, 316-330.

Weijermars, R.; 1986. Flow behaviour and physical chemistry of bouncing putties and related polymers in view of tectonic laboratory applications. Tectonophysics, 124, 325-358.

Williams, R.B.G.; Swantesson, J.O.H.; Robinson, D.A.; 2000. Measuring rates of surface downwearing and mapping microtopography: The use of micro-erosion meters and laser scanners in rock weathering studies. Zeitschrift für Geomorphologie N.F. Vol. 120 (Supplement), 51-66.

Wilsher, W.A., de Wit, M.J., Marrao, E., 1989. A GIS solution for Gondwana geoscientific data. Journal of African Earth Sciences, 9 (2), 371-374.

Zanchi, A., Salvi, F., Zanchetta, S., Sterlacchini, S., Guerra, G., 2009. 3D reconstruction of complex geological bodies: Examples from the Alps. Computers and Geosciences, 35, 49-69.